

2016

Seismic performance of unbonded post-tensioned precast wall systems subjected to shake table testing

Maryam Nazari
Iowa State University

Follow this and additional works at: <https://lib.dr.iastate.edu/etd>

Recommended Citation

Nazari, Maryam, "Seismic performance of unbonded post-tensioned precast wall systems subjected to shake table testing" (2016).
Graduate Theses and Dissertations. 15233.
<https://lib.dr.iastate.edu/etd/15233>

This Dissertation is brought to you for free and open access by the Iowa State University Capstones, Theses and Dissertations at Iowa State University Digital Repository. It has been accepted for inclusion in Graduate Theses and Dissertations by an authorized administrator of Iowa State University Digital Repository. For more information, please contact digirep@iastate.edu.

**Seismic performance of unbonded post-tensioned precast wall systems
subjected to shake table testing**

by

Maryam Nazari

A dissertation submitted to the graduate faculty
in partial fulfillment of the requirements for the degree of
DOCTOR OF PHILOSOPHY

Major: Civil Engineering (Structural Engineering)

Program of Study Committee:
Sri Sritharan, Major Professor
Simon Laflamme
Jay Shen Jiehua
Igor Beresnev
Wei Hong

Iowa State University

Ames, Iowa

2016

Copyright © Maryam Nazari, 2016. All rights reserved.

TABLE OF CONTENTS

LIST OF FIGURES	vii
LIST OF TABLES	xiii
LIST OF NOTATIONS	xiv
UNIT CONVERSIONS	xvii
ACKNOWLEDGEMENTS	xviii
ABSTRACT	xix
CHAPTER 1 INTRODUCTION	1
1.1. Overview	1
1.2. Seismic Resilient Concrete Structures.....	5
1.2.1. Seismic energy dissipation capacity	7
1.2.2. Seismic design approach.....	10
1.3. Research Scope and Objectives.....	14
1.4. Thesis Layout	16
1.5. References	17
CHAPTER 2 EXAMINATION OF THE CURRENT STATE OF THE ART	19
2.1. Historical Perspective	19
2.2. Experimental Large-scale Testing	26
2.2.1. Quasi-static loading	27
2.2.2. Dynamic loading.....	33
2.3. Dynamic Response Characterization.....	39
2.3.1. Fiber models and Finite Element models.....	40
2.3.2. Lumped plasticity and multi-spring models	43
2.4. Codification	50
2.5. References	51

CHAPTER 3 SINGLE PRECAST CONCRETE ROCKING WALLS AS EARTHQUAKE FORCE-RESISTING ELEMENTS	57
3.1. Abstract.....	57
3.2. Introduction	58
3.3. Experimental Program.....	60
3.3.1. Prototype structure	60
3.3.2. Test matrix	61
3.3.3. Seismic test set-up and instrumentation.....	64
3.3.4. Load protocol.....	65
3.4. Analytical Model	68
3.5. Testing and Results.....	69
3.5.1. Observations	70
3.5.2. Characteristic response	71
3.5.3. Influence of prestressing.....	74
3.5.4. Damping components	75
3.5.5. Performance-based seismic evaluation.....	78
3.6. Comparison with Analytical Results	81
3.7. Use of SRW in Seismic Design.....	82
3.7.1. Base shear vs. damping.....	83
3.7.2. R-factor	84
3.8. Conclusions	85
3.9. Acknowledgments	87
3.10. References	87
CHAPTER 4 DYNAMIC EVALUATION OF PREWEC SYSTEMS WITH VARYING HYSTERETIC ENERGY DISSIPATION	90
4.1. Abstract.....	90
4.2. Introduction	91
4.3. Test Program	92
4.3.1. Prototype structure	92
4.3.2. Test units.....	93

4.3.3.	Test set-up and loading protocol.....	98
4.4.	Analytical Modeling in OpenSees.....	101
4.5.	Test Observations and Key Results.....	102
4.5.1.	Test observations.....	103
4.5.2.	Lateral load response.....	105
4.5.3.	Post-tensioning behavior.....	106
4.5.4.	Wall uplift.....	108
4.5.5.	Behavior of O-connector.....	109
4.5.6.	Equivalent damping ratio.....	110
4.5.7.	Residual drift and self-centering capability.....	113
4.6.	Analytical Comparisons with Experimental Results.....	114
4.7.	Seismic Applicability of PreWEC Systems.....	116
4.7.1.	Performance-based seismic assessment.....	116
4.7.2.	Shear resistance vs. damping.....	121
4.7.3.	R-factor.....	122
4.7.4.	Design recommendations.....	123
4.8.	Conclusions.....	124
4.9.	Acknowledgements.....	126
4.10.	References.....	127
 CHAPTER 5 INTERACTION OF DIFFERENT DAMPING COMPONENTS ON DYNAMIC RESPONSE OF ROCKING WALLS.....		129
5.1.	Abstract.....	129
5.2.	Introduction.....	130
5.3.	Energy Dissipation Mechanisms for Seismic Protection of Rocking Systems ..	132
5.4.	Summary of Experimental Investigation.....	135
5.5.	Participation of Different Energy Dissipation Components.....	139
5.6.	Effect of Supplementary Hysteretic Dampers on Seismic Rocking Response ..	141
5.6.1.	Maximum of response.....	142
5.6.2.	Decay of response.....	144
5.7.	Single Rocking Walls with Limited Hysteretic Damping.....	145

5.7.1.	Rate of input energy input into a SDOF system	146
5.7.2.	Negative rate of energy input into SRWs	147
5.8.	Conclusions	149
5.9.	Acknowledgments	151
5.10.	References	151
 CHAPTER 6 STRENGTH REDUCTION FACTORS FOR SEISMIC DESIGN OF PRECAST CONCRETE ROCKING WALL SYSTEMS AND VERIFICATION		153
6.1.	Abstract.....	153
6.2.	Introduction	154
6.3.	Rocking Wall Systems.....	156
6.4.	Current Design Practice.....	157
6.5.	Recommended New R-factors.....	159
6.6.	Proposed Design Approach	160
6.7.	Parametric Study.....	162
6.7.1.	Design of the buildings	162
6.7.2.	Example of design of the buildings with SRWs	163
6.7.3.	Example of design of the buildings with PreWECs.....	165
6.8.	Selection and Scaling of Ground Motions.....	167
6.9.	Analytical Model	171
6.10.	Dynamic Results.....	173
6.10.1.	Lateral drift	173
6.10.2.	Absolute acceleration and residual drift	176
6.11.	Cost-effective Design of Rocking Wall Systems	177
6.12.	Conclusions	179
6.13.	Acknowledgments	181
6.14.	References	181
 CHAPTER 7 CONCLUSIONS AND RECOMMENDATIONS		184
7.1.	Introduction	184
7.2.	Summary of Results and Conclusions.....	185

7.3. Recommended Research	195
7.4. References	196

LIST OF FIGURES

Figure 1-1. Typical brittle wall failures in 2011 Christchurch earthquake (Sritharan et al. 2014).....	3
Figure 1-2. Damage in plastic hinge region, 2011 Christchurch earthquake (Sritharan et al. 2014)	3
Figure 1-3. Idealized hysteresis behavior of traditional and self-centering systems (Henry 2011).....	6
Figure 1-4. Typical details of rocking walls with and without supplementary energy dissipaters.....	7
Figure 1-5. Idealized energy content during a rocking cycle (Ma 2009).....	9
Figure 1-6. Housner rocking block (Housner 1963).....	9
Figure 1-7. R-factor as used in force-based design approach (Carrillo et al. 2013).....	11
Figure 1-8. Fundamentals of Direct Displacement-Based Design (Priestley 2000).....	12
Figure 1-9. Equivalent damping for bilinear and rigid-perfectly-plastic (R-P-P) loop (Dwairi et al. 2007).....	13
Figure 1-10. Seismic performance objectives for buildings (SEAOC 1999)	14
Figure 2-1. Different types of connectors to be used with PreWEC (Henry 2011).....	23
Figure 2-2. Force-displacement behavior of J- and O-connectors (Henry 2011).....	23
Figure 2-3. Experimentally verification of the measured response of O-connectors (Henry 2011).....	24
Figure 2-4. Different failure and fracture types in O-connectors (Twigden and Henry 2015).....	25
Figure 2-5. Paramount building with hybrid moment-resisting frames (Englekirk 2002)	26
Figure 2-6. Negligible observed damage to the Southern Cross Hospital designed with a rocking-dissipative solution during the Christchurch earthquake (Pampanin et al. 2011).....	26

Figure 2-7. Schematic representation of the test set-up reported by Rahman and Restrepo (2000).....	27
Figure 2-8. Cyclic response and damage state of a hybrid wall (a) vs. SRW (b) (Rahman and Restrepo, 2000).....	28
Figure 2-9. Measured cyclic load response of SRWs tested by Perez et al. (2004)	29
Figure 2-10. The test set-up and cyclic loading applied to PreWECs (Sritharan et al. 2015)	30
Figure 2-11. Comparison of the observed damage in PreWEC and RC wall (Sritharan et al. 2015)	30
Figure 2-12. Cyclic response of the PreWEC from experimental data and SA method (a) along with the associated equivalent viscous damping (b) (Sritharan et al. 2015).....	31
Figure 2-13. Damage to the wall toes during quasi-static testing of SRWs and PreWECs (Twigden 2016).....	31
Figure 2-14. Measured force-displacement response of SRWs and PreWECs (Twigden 2016).....	32
Figure 2-15. Measured EVD of SRW and PreWECs from cyclic hysteresis loops (Twigden 2016).....	33
Figure 2-16. Pseudo-dynamic testing of jointed walls in PRESSS building (Priestly et al. 1999).....	34
Figure 2-17. The 5% damped multiple-level acceleration response spectra, suggested for soil type Sc in high seismic zone (SEOAC 1999).....	35
Figure 2-18. Successful seismic performance of the jointed walls (Priestly et al. 1999).....	35
Figure 2-19. Shake table test of precast concrete building at UCSD (Fleischman et al. 2005).....	36
Figure 2-20. Energy dissipation capacity of rocking walls with and without externally mounted dampers (Marriot 2009).....	37

Figure 2-21. Comparison between DDBD method and shake table test results of SRW test unit with different damping ratios (Twigden 2016)	39
Figure 2-22. Fiber model used for modelling precast concrete walls (Kurama et al. 1999)	41
Figure 2-23. Fiber model and Finite Element model (Belleri et al. 2013).....	42
Figure 2-24. Lumped plasticity model with two parallel rotational springs (Marriot et al. 2009).....	44
Figure 2-25. Analytical model for the five-story building with the jointed wall system (Rahman and Sritharan 2006).....	45
Figure 2-26. Single degree of freedom model as shown in Twigden (2016)	45
Figure 2-27. Two-spring model of jointed walls in PRESSS building (Conley et al. 1999).....	47
Figure 2-28. Multi-spring model with contact damping included (Marriot et al. 2009)	48
Figure 2-29. Viscous and friction dampers representing 2.4% contact damping (Marriot et al. 2009).....	48
Figure 2-30. Multi-spring model developed by Watkins et al. (2013) using modified concrete springs	49
Figure 3-1. (a) Precast concrete wall with unbonded PT (b) wall uplift due to base excitation, and (c) moment resisting mechanism during rocking	59
Figure 3-2. Details of the prototype building (1 m = 3.28 ft).....	61
Figure 3-3. Elevation (a and b) and cross sections (c) of SRW1 (1 m = 3.28 ft)	63
Figure 3-4. Experimental set-up used for the shake table testing.....	65
Figure 3-5. Spectral acceleration of scaled ground motions selected for the shake table testing	68
Figure 3-6. OpenSees model for a rocking wall (1 m = 3.28 ft; 1 kip = 4.45 kN)	69

Figure 3-7. Typical condition of wall base region after experiencing EQ-III level motions..	70
Figure 3-8. Impact of armoring the wall base using a steel channel as evidenced for EQ-IV level motions (1 m = 3.28 ft)	71
Figure 3-9. Global and local behavior of SRW2 using experimental data and the SA method (1 m = 3.28 ft; 1 kip = 4.45 kN).....	73
Figure 3-10. Influence of initial prestress force on the global behavior of test walls.....	75
Figure 3-11. Estimation of equivalent viscous damping ratio of rocking walls using the experimental data	78
Figure 3-12. Ratio of the maximum wall demands to the allowable limits.....	80
Figure 3-13. Comparison between analytical results and experimental data (1 kip = 4.45 kN).....	82
Figure 3-14. Assessment of shear resistance of test walls using DDBD approach (1 kip = 4.45 kN; 1 m = 3.28 ft).....	84
Figure 3-15. R-factor for design of the scaled prototype wall (FBD solution).....	85
Figure 4-1. Details of the prototype building (1 m = 3.28 ft; 1 kip = 4.45 kN).....	93
Figure 4-2. Prototype building, details of the test unit and test set-up (1 m = 3.28 ft; 1 kip = 4.45 kN).....	95
Figure 4-3. Testing of O-connectors and the cyclic response (1 m = 3.28 ft; 1 kip = 4.45 kN).....	96
Figure 4-4. Configuration of PreWEC and PreWEC-s test units.....	98
Figure 4-5. Experimental set-up used for the shake table testing	99
Figure 4-6. Opensees model for a PreWEC system (1 m = 3.28 ft; 1 kip = 4.45 kN).....	102
Figure 4-7. Impact of armoring the wall base using a steel channel (1 m = 3.28 ft).....	104
Figure 4-8. Lateral response of test units (1 kip = 4.45 kN).....	106

Figure 4-9. Post-tensioning force response: variation and loss vs. lateral drift (1 kip = 4.45 kN).....	107
Figure 4-10. Deflected shape and wall uplift response (1 m = 3.28 ft)	109
Figure 4-11. Response of O-connectors (1 m = 3.28 ft; 1 kip = 4.45 kN).....	110
Figure 4-12. Equivalent viscous damping ratio of test units (1 m = 3.28 ft; 1 kip = 4.45 kN).....	113
Figure 4-13. Residual drift of test units	114
Figure 4-14. Comparison between analytical results and the experimental data (1 kip = 4.45 kN).....	116
Figure 4-15. Ratio of the maximum system demands to the allowable limits.....	120
Figure 4-16. Observed vs. DDBD design shear forces of the test units (1 kip = 4.45 kN) ..	122
Figure 4-17. R-factors for design of the PreWEC systems with varying damping ratios (1 kip = 4.45 kN).....	123
Figure 5-1. Rocking response and the associated energy terms	134
Figure 5-2. Details of the prototype building (1 m = 3.28 ft).....	137
Figure 5-3. Experimental set-up used for the shake table testing	137
Figure 5-4. Selected spectral acceleration of scaled ground motions.....	138
Figure 5-5. Participation of different damping terms to dissipate the seismic energy input into the rocking systems	140
Figure 5-6. Time history drift response of SRW vs. PreWEC from group A.....	142
Figure 5-7. Forced and free phases of response of SRW2 during $0.8 \times E_q$ -4s.....	142
Figure 5-8. Impact of added hysteretic damping on the peak drift during multiple-level motions.....	144
Figure 5-9. Impact of added hysteretic damping on decay of response for EQ-III and EQ-IV events	145

Figure 5-10. Energy input into a SDOF system during sinusoidal motions of different frequencies	147
Figure 5-11. Rate of energy input into the rocking walls of group A during $1.4 \times T_{akatori}$.	148
Figure 5-12. Negative rate of input energy at the time of impacts of SRW2	149
Figure 6-1. Rocking wall systems.....	156
Figure 6-2. Dimensions (a) and corresponding force-displacement behavior (b) of an O-connector used in PreWEC (1 m = 3.28 ft; 1 kip = 4.45 kN)	157
Figure 6-3. Plan view and elevations of the buildings (1 m = 3.28 ft)	163
Figure 6-4. Spectral acceleration of scaled NF and FF ground motions selected for analysis.....	171
Figure 6-5. OpenSees model for a rocking wall (1 m = 3.28 ft; 1 kip = 4.45 kN)	172
Figure 6-6. Experimental verification of the analytical results (Nazari et al. 2016)	173
Figure 6-7. Ratio of the maximum drift to the allowable limit (d_{max}).....	174
Figure 6-8. Average ratio of the maximum drift to the allowable limit	175
Figure 6-9. Impact of additional hysteretic damping on the drift time history response.....	176
Figure 6-10. Average ratio of the maximum absolute acceleration (a) and residual drift (b) to the allowable limits	177
Figure 6-11. Normalized cost index for different case studies	179

LIST OF TABLES

Table 3-1. Test matrix (1 m = 3.28 ft; 1 ksi = 6.9 MPa; 1 kip = 4.45 kN)	64
Table 3-2. List of input motions used for shake table testing of SRWs	67
Table 4-1. Summary of design parameters and capacities for the prototype PreWEC and the scaled test unit (1 m = 3.28 ft; 1 kip = 4.45 kN)	96
Table 4-2. Test matrix (1 m = 3.28 ft; 1 kip = 4.45 kN; 1 ksi = 6.9 MPa)	97
Table 4-3. List of ground motions	100
Table 4-4. Typical condition of the wall base region and connectors after experiencing EQ-III level motions (1 m = 3.28 ft).....	103
Table 4-5. Seismic acceptance criteria of test units according to ACI ITG-5.1 (2008) (1 m = 3.28 ft; 1 kip=4.45 kN).....	117
Table 4-6. Design forces obtained from DDBD approach (Priestley 2000) (1 m = 3.28 ft; 1 kips = 4.45 kN)	121
Table 5-1. List of ground motions	138
Table 5-2. Test matrix.....	139
Table 6-1. Design of the buildings with SRWs (1 m = 3.28 ft; 1 ksi = 6.9 MPa; 1 kip = 4.45 kN).....	168
Table 6-2a. Design of the buildings with PreWECs – Wall panel (1 m = 3.28 ft; 1 ksi = 6.9 MPa; 1 kip = 4.45 kN)	168
Table 6-2b. Design of the buildings with PreWECs – connectors and end columns (1 m = 3.28 ft; 1 ksi = 6.9 MPa)	169
Table 6-2c. Design of the buildings with PreWECs – force deformation properties of O- connectors (1 m = 3.28 ft; 1 kip = 4.45 kN)	169

LIST OF NOTATIONS

α = cost of material per foot of post-tensioning tendon

a_{max} = maximum of wall absolute acceleration

A_p = area of post-tensioning tendon in wall panel

$A_{p,col}$ = area of post-tensioning tendon in end column

β = cost of labor per foot of post-tensioning tendon

β_h = relative energy dissipation ratio

$\Delta_{c,D\%}$ = displacement of connectors at $D\%$ wall lateral drift

$\Delta_{c,y}$ = displacement of connectors at yield

Δ_d = wall design drift

Δ_F = wall drift at fracture of connectors

Δ_T = wall target drift

ΔE_I = rate of seismic input energy

ΔE_k = kinetic energy loss that occurs immediately before and immediately after an impact

$\Delta E_{k,ACC}$ = accumulated kinetic energy loss due to impacts during an earthquake

ΔE_{link} = energy dissipated by the link beam force to displace the wall during impacts

d_{ave} = average of wall lateral drift

d_b = diameter of the rebar

d_{max} = maximum of wall lateral drift

d_r = wall residual drift

d_{res} = average of wall residual drift

d_{RES} = maximum possible wall residual drift

D_N = Normalized average maximum drift

ξ_{area} = area-based equivalent viscous damping

ξ_{el} = elastic damping

ξ_{eq} = total equivalent viscous damping ratio

$\xi_{hys,D\%}$ = hysteretic damping ratio at $D\%$ wall lateral drift

ξ_{imp} = equivalent viscous damping ratio due to impacts

ξ_{vis} = inherent viscous damping ratio

E_{es} = recoverable elastic strain energy

E_{hys} = hysteretic energy dissipation

E_{imp} = continuous equivalent viscous energy dissipation due to impacts

E_I = seismic input energy introduced to the system during base excitation

E_k = kinetic energy

E_{vis} = viscous energy dissipation

f_a = nonlinear restoring forces generated by the hysteretic characteristics of structural elements

f_D = elastic viscous damping force

f_I = inertia force provided by the external mass-rig

f_{pi} = initial stress of post-tensioning tendon in wall panel

$f_{pi,col}$ = initial stress of post-tensioning tendon in end column

f_{py} = yield strength of post-tensioning tendon

f_{pu} = ultimate strength of post-tensioning tendon

f_s = total resisting force of the system with the corresponding energy term of E_s

$F_{c,ave}$ = average of connector forces at yield and $D\%$ wall lateral drift

$F_{c,D\%}$ = force of connectors at $D\%$ wall lateral drift

$F_{c,y}$ = force of connectors at yield

γ = cost of material per O-connector

H_{eff} = effective height of an equivalent single degree of freedom system

H_s = seismic height

k_e = effective stiffness

μ = ductility of the system

m_{eff} = effective mass of an equivalent single degree of freedom system

M_s = seismic mass

M/V = base moment to base shear ratio

$N_{conn.}$ = total number of O-connectors

N_{wall} = number of wall systems per building

P_{cost} = cost index

P_{crane} = crane charges

P_D = gravity load transferred through the wall panel

P_{embeds} = installation cost for member bracing and embeds

P_i = initial prestress force in the wall panel

P_N = Normalized amplitude of drift peak

$PT_{L,col}$ = Length of PT tendons in end column

$PT_{L,W}$ = Length of PT tendons in wall panel

R -factor = strength reduction factor

u_{es} = elastic deformation

u_{hys} = inelastic deformation

V_d = design-level base shear

$V_{D\%}$ = shear resistance at $D\%$ wall lateral drift

V_e = base shear force corresponding to the elastic response of the system

UNIT CONVERSIONS

Measurement	From Metric Units	Conversion Factor	To English Units
Length	millimeter (mm)	0.03937	inches (in.)
Length	millimeter (mm)	0.00328	feet (ft)
Length	meter (m)	39.37	inches (in.)
Length	meter (m)	3.281	feet (ft)
Force	kilonewtons (kN)	224.81	pound-force (lbf)
Pressure	megapascal (MPa)	145.04	pound per square in (psi)

ACKNOWLEDGEMENTS

First and foremost, I would like to acknowledge the immense support from my supervisor Dr. Sri Sritahran. His valued input and guidance throughout my doctoral study were essential to the completion of this dissertation. Without his encouragement, I would never have made this achievement.

The research presented in this dissertation was based upon the NEES Rocking Wall project supported by the National Science Foundation (NSF) Grant Number CMMI-1041650 and Dr. Joy Pauschke served as the program director for this grant. The financial support by this organization is gratefully acknowledged. All shake table tests were conducted using the NEES shared facility at the University of Nevada, Reno (UNR). The test units were donated by Clark Pacific and MidState Precast through coordination by PCI West. Materials provided by Sumiden Wire, GTI, Hayes Industries and help provided by ironworker local 118 with post-tensioning of specimens are also gratefully acknowledged.

I greatly appreciate all the help from the laboratory personnel of UNR, Dr. Sriram Aaleti, Doug Wood, and Owen Steffens of Iowa State structural laboratory for their assistance in conducting the experimental research reported in this dissertation. A sincere thank you is also extended to Dr. Catherine French at University of Minnesota and Susie Nakaki at KPFF Consulting Engineers for their guidance throughout the design and testing of specimens.

I would like to express my thanks to Dr. Wei Hong, Dr. Simon Laflamme, Dr. Jay Shen Jiehua, and Dr. Igor Beresnev for serving on my Ph.D. program committee.

Last but not least, I would like to thank my parents and siblings for their continuous love and support. I would not have made it through if it were not for them.

ABSTRACT

The research in this dissertation was conducted with the primary aim of understanding the seismic response of unbonded post-tensioned precast concrete rocking walls both with and without additional hysteretic energy dissipaters. These wall systems dissipate the seismic input energy mainly through impacts of the wall on top of the foundation during rocking as well as the external hysteretic damping. The behavior of these walls are largely investigated based on experimental tests using quasi-static loading and few numerical studies. A systematic seismic design approach for their application in high seismic regions is still lacking. To date, there are limited large-scale studies that have evaluated the lateral response of these rocking walls using earthquake ground motions of different intensities and there is little published data on quantification of their different energy dissipation components.

To address the main objective of overcoming the aforementioned limitations, a series of large-scale experimental shake table tests were conducted on four unbonded post-tensioned precast Single Rocking Walls (SRWs) and four Precast Wall with End Columns (PreWEC) systems by subjecting them to a set of earthquake excitations with varying intensities. These walls were designed by varying key design parameters such as: (i) the initial prestress force, P_i , (ii) base moment to base shear ratio, and (iii) the number and location of additional hysteretic dampers in PreWECs, namely O-connectors.

Minimal wall base damage was observed as these wall systems were subjected to the design-level ground motions. As intended, all walls provided the self-centering behavior during ground motions of different intensities and the additional O-connectors started to yield and dissipate the seismic energy at 0.6% wall drifts. The rocking wall tests generally indicated the

satisfactorily seismic performance of SRWs and PreWECs in terms of the lateral drift, absolute acceleration, and residual drift during design-level and greater earthquakes; however, it was found that walls with reduced resistance responded beyond the allowable limits during such strong ground motions. Further studies were experimentally conducted to evaluate equivalent viscous damping ratios of SRWs and PreWECs and apply them to achieve desirable seismic design forces that ensure their promising seismic response. Participation of different damping components of the walls with and without external hysteretic dampers in energy dissipation of the system was also evaluated. The results revealed the potential of SRWs to remove a part of the seismic energy and dissipate the rest relying on their limited damping capacity. It was highlighted that the additional hysteretic damping provided in PreWECs reduced the maximum drift and decay of the response.

An investigation was performed using a simplified single degree of freedom analytical model to emulate the seismic response of SRWs and PreWECs. The nonlinear dynamic analysis results calculated from this model were then verified using the shake table test results.

Lastly, the seismic forces recommended for the design of rocking walls with different damping ratios, as prescribed in the preliminary stages of this research, were validated by conducting an extensive numerically based case-study. For this purpose, six, nine, and twelve story buildings were designed using SRWs and PreWECs and the responses were evaluated during a set of near-field and far-field ground motions scaled to represent design-level and maximum considered events. In addition to an excellent performance of both systems designed following the recommendations of this dissertation, PreWECs were shown to be the most economical rocking wall solution for the design of these seismic-resilient buildings.

CHAPTER 1

INTRODUCTION

1.1. Overview

Numerous past earthquakes around the world have progressively assisted with understanding the performance of reinforced concrete buildings and improving the seismic design standards.

In the pre-1970s era, an elastic design method was commonly promoted with an intention of making the structure strong enough so that it would respond elastically when subjected to an earthquake input motion. In this case, the induced stresses in the structure were expected to remain below the allowable elastic limits chosen for the expected earthquake forces. Extensive damage caused to structures until the mid-1970s (e.g., 1971 San Fernando earthquake) revealed significant deficiencies of the elastic design approach such as underestimation of design forces and deflections, formation of plastic actions at arbitrary locations, and evidence of non-ductile failure modes (e.g., shear failure). Following this event, a shift in design philosophy began to take place.

To overcome the challenges associated with the elastic design method, the capacity design principle was developed in the 1970s (Park and Paulay 1975), which paved the way to significantly improve the seismic design approach that has been widely adopted in design standards. According to this philosophy, special detailing of longitudinal and confinement reinforcement in critical regions of structures, namely plastic hinge regions, is provided to allow for ductile flexural yielding rather than them experiencing brittle failure modes. The intentional formation of plastic hinges, which is designed to develop at certain locations of a building, such as wall base, behaves as an energy dissipating region to protect the rest of the structure from unexpected failures. This

method should allow the structures to respond inelastically to large displacements without experiencing significant strength degradation. As a result, the structure will be designed for a reduced design force than required by the elastic method, making the structure less sensitive to the expected input ground motion. While some design standards aim to achieve ductile wall response by adopting the capacity design philosophy (e.g., NZS 3101 2006; CEN 2004), others attempt to achieve the same behavior without explicitly implementing this design philosophy (e.g., ACI 318-11 2011).

The 2011 Christchurch Earthquake in New Zealand ($M_w = 6.2$) has confirmed the improved seismic performance of modern structures resulting from the use of the capacity design philosophy by achieving their life-safety design objectives. However, a number of concrete walls were identified with severe damage. As reported by Sritharan et al. (2014) and shown in Figure 1-1, the desired inelastic deformations did not fully develop in some reinforced concrete (RC) walls; this was suspected to be due to design flaws such as inadequate amount of longitudinal bars experiencing fracture in the wall end regions, poor anchorage of horizontal reinforcement, poor detailing of lap splice regions, inappropriate detailing of horizontal (or shear) reinforcement, and/or lack of adequate ties between the two layers of reinforcement in the web region.

Sritharan et al. (2014) also observed a significant damage in the plastic hinge regions in walls that appeared to have good reinforcement details, as indicated in Figure 1-2. While further investigation is required, this damage was mostly attributed to the walls with lightly reinforced web regions. They indicated that large tensile strain demand on the longitudinal reinforcement caused local buckling of the wall in the potential plastic hinge region.



Figure 1-1. Typical brittle wall failures in 2011 Christchurch earthquake (Sritharan et al. 2014)



Figure 1-2. Damage in plastic hinge region, 2011 Christchurch earthquake (Sritharan et al. 2014)

According to these observations, most of concrete structural walls, which were designed following the principles of design by capacity, provided a satisfactory global behavior by providing life safety when buildings were subjected to large lateral displacements. However, severe damage was occurred due to potential undesirable failure modes in plastic hinge regions.

In addition to the observations from 2011 Christchurch earthquake, some damage to the plastic hinge regions of RC structural walls, which were designed to develop ductile behavior, is predictable; large residual drifts and wide residual cracks are expected, as the walls dissipate seismic energy by subjecting the longitudinal reinforcement in plastic hinge regions to large inelastic strains.

Consequently, a new design approach, known as the performance-based design method, has been developed to minimize damage, thereby economic losses due to downtime, as well as to prevent collapse and ensuring life safety of the structures subjected to design-level earthquakes. Initiating with the idea of constructing seismic resilient precast structures in early 2000, a new technique was developed for improving seismic performance of structures. Using unbonded post-tensioning as the primary reinforcement of precast concrete walls presented a seismic resilient system, which was not only aimed at preventing collapse of the structure, but also its re-centering capability resulted from elastic behavior of the post-tensioning tendons helped to mitigate the sustained damage (this topic will be further discussed in the following section). Since the concept of self-centering precast concrete walls was recently applied in structural systems, their seismic performance was not much assessed by earthquake input motions. As a result, a comprehensive investigation is expected to elevate the confidence of practicing engineers on using these innovative and economical precast structural systems in seismic regions.

In this study, performance of a series of scaled precast concrete walls will be evaluated by conducting shake table tests, using multiple-level ground motions. Consequently, this study will help to develop a systematic approach for seismic design of these structural systems. The remainder of this introductory chapter focuses on different types of precast concrete walls and their

energy dissipation sources. A brief description of the current seismic design methods will be presented, followed by the scope of research and the thesis layout.

1.2. Seismic Resilient Concrete Structures

The cast-in-place (CIP) RC walls are frequently used as the primary lateral load resisting system in buildings to resist both gravity loads and lateral forces generated by earthquakes. This type of construction has been practiced in urban regions for medium- to high-rise buildings. Traditionally, concrete structural walls are continuous throughout the building height. To simplify the construction process, the longitudinal reinforcement of walls near the base is spliced to the bars extended from the footing using either lap splices or mechanical couplers.

With widespread applications of precast members in structural construction, the idea of utilizing unbonded post-tensioning tendons for assembling precast concrete walls has been developed. Appreciating both precast and prestressed concrete technology, the newly developed lateral resisting elements, namely unbonded post-tensioned precast concrete walls improved the seismic performance of structures. The simplest form of this system, consists of a single precast wall tied down to the foundation with unbonded post-tensioning (PT). PT tendons are designed as the primary reinforcement of these walls to provide sufficient lateral strength for the system. In addition, these tendons are designed to remain elastic during design-level earthquakes, thereby enabling self-centering behavior when the wall uplifts and rocks. However, they may undergo yielding and experience some prestressing loss at higher seismic drifts. The restoring force provided by the PT tendons re-center the wall back to its original position when the lateral force is removed. As a result, minimal structural damage is expected, resulting in superior seismic performance when compared to the extensive damage that would be expected for a reinforced

concrete wall due to the formation of plastic hinging at the wall base. The inelastic action generated in these resilient self-centering walls to resist the earthquake forces is limited. Unlike the conventional RC walls, with a degrading stiffness hysteresis behavior, as shown in Figure 1-3a, a Single Rocking Wall (SRW) exhibits a bilinear elastic behavior with minimal energy dissipation capacity (see Figure 1-3b). The softening in the slope of the lateral load response is identified by the beginning of a gap opening at the wall base panel and non-linear behavior of concrete in compression. As a result of this elastic bilinear behavior, external energy dissipating elements have been incorporated for additional hysteretic energy dissipation capacity of these self-centering walls. A flag-shape hysteretic behavior is defined to idealize the developed integrated system, as shown in Figure 1-3c. A schematic of the unbonded post-tensioned precast concrete rocking walls without (Figure 1-4a) and with different types of external energy dissipaters (Figures 1-4b to 1-4d) are shown in Figure 1-4. These systems will be further discussed in Chapter 2.

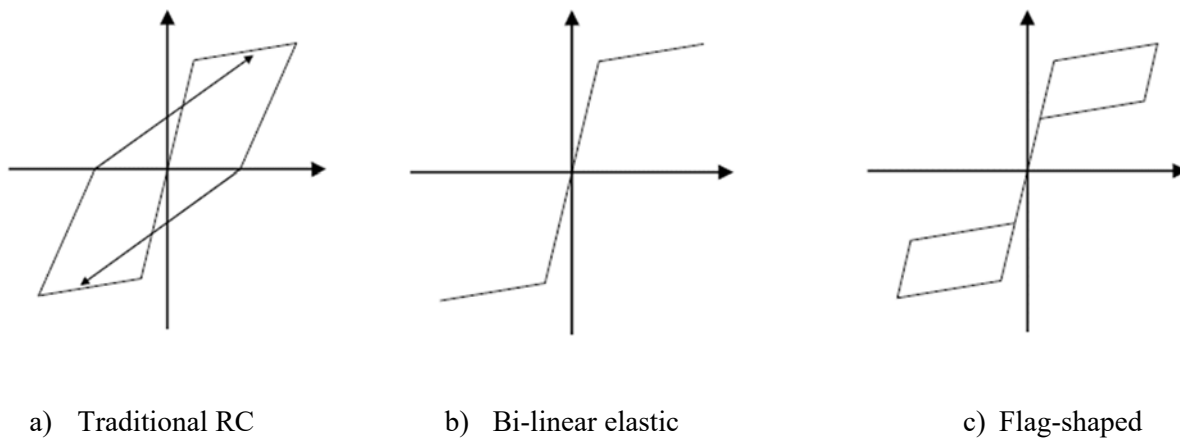


Figure 1-3. Idealized hysteresis behavior of traditional and self-centering systems (Henry 2011)

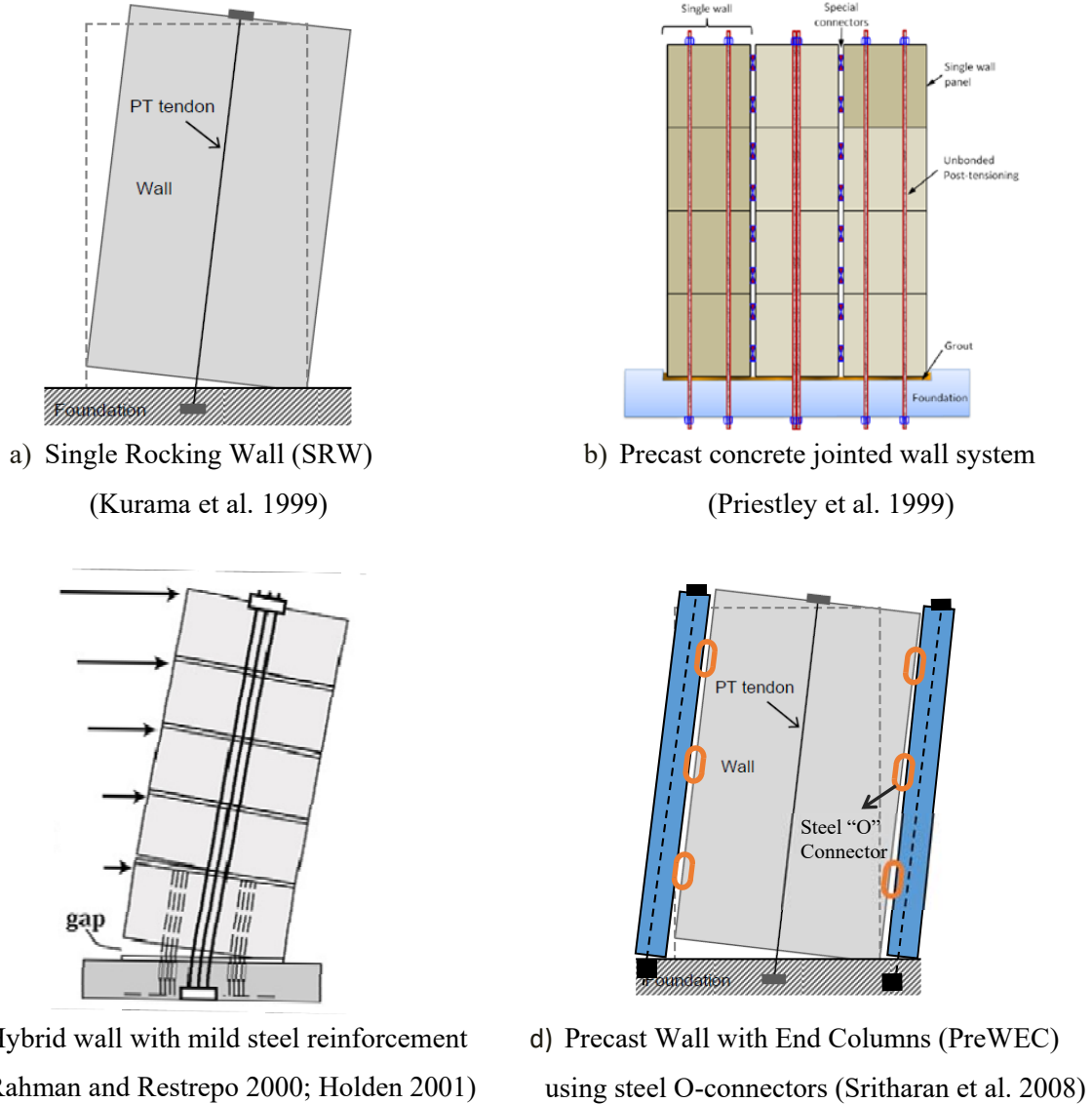


Figure 1-4. Typical details of rocking walls with and without supplementary energy dissipaters

1.2.1. Seismic energy dissipation capacity

The main source of seismic energy imparted by earthquake excitations into traditionally reinforced concrete walls is dissipated through inelastic action in the plastic hinge regions. Closely-spaced transverse reinforcement as well as a minimum amount of longitudinal bars provide a ductile member with the ability to undergo large inelastic deformation with negligible

flexural strength degradation. In the unbonded post-tensioned concrete rocking walls, this form of damping is mainly provided by inelastic deformations of the supplementary hysteretic energy dissipaters. Precast concrete walls without additional dampers (i.e., SRW) also provide limited hysteresis damping due to material nonlinearity of concrete at wall toes as well as the PT tendons if they experience yielding. Accordingly, their measured response does not follow the idealized bilinear-elastic hysteresis rule of Figure 1-3b. This was observed by Perez et al. (2004) through monotonic and cyclic testing of five precast concrete walls; yet, the amount of this damping has not been quantified and considered for seismic design of SRWs.

The rocking walls also dissipate the energy imparted to a structure during an earthquake through impacts of the rocking body on top of the footing. When subjected to a lateral load, a wall panel secured with unbonded post-tensioning rocks on top of the foundation, with a single gap opening and closing at its base. During contact of the colliding concrete bodies, kinetic energy of relative motion is transformed into internal energy of deformation known as strain energy by the contact force. An elastic part of this internal energy is reconverted into kinetic energy when two bodies drive apart; however, the rest is dissipated from the system in the form of radiation damping through each impact. Consequently, the wall starts to rotate from one corner to the opposite corner with a smaller kinetic energy, as shown in Figure 1-5. As presented by Housner (1963), the ratio of kinetic energy immediately after and immediately before an impact is called coefficient of restitution (c.o.r or r) and is used as a measure of the energy loss due to impacts (Equation 1-1).

$$c.o.r = r = \left(\frac{\dot{\theta}_{after}}{\dot{\theta}_{before}} \right)^2 \quad \text{(Equation 1-1)}$$

where $\dot{\theta}_{after}$ and $\dot{\theta}_{before}$ are angular velocities of the rocking wall after and before an impact.

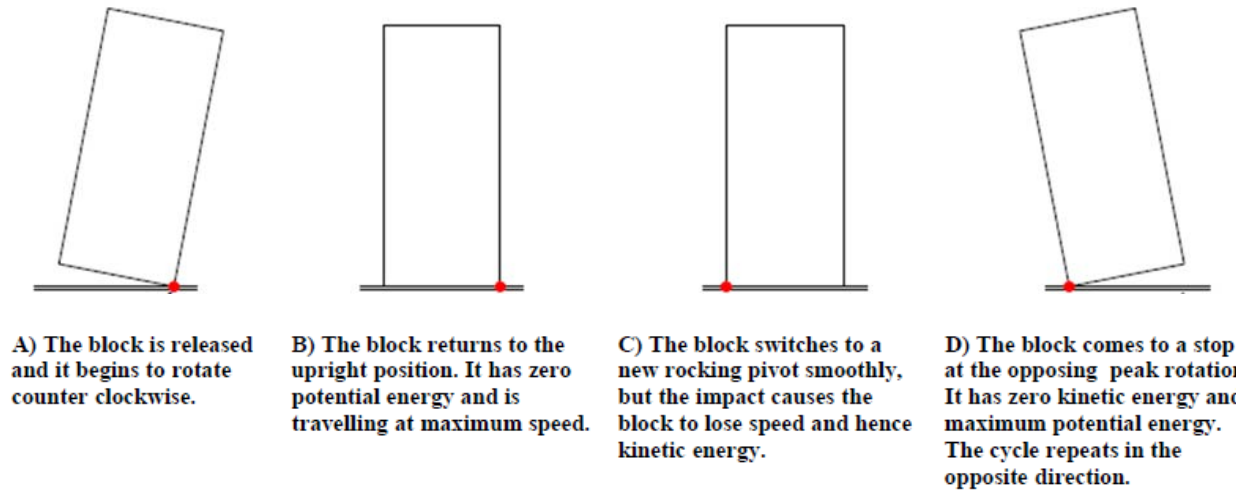


Figure 1-5. Idealized energy content during a rocking cycle (Ma 2009)

Presuming the angular momentum about the point of impending impact is conserved (because no external force is applied to the system), Housner (1963) showed that this ratio could be related to the geometry of the block, by the expression defined as Equation 1-2:

$$r = \left[1 - \frac{mR^2}{I_o}(1 - \cos 2\alpha)\right]^2 \quad (\text{Equation 1-2})$$

where I_o is the moment of inertia of the rocking wall about point O (see Figure 1-6) and other parameters are shown in Figure 1-6.

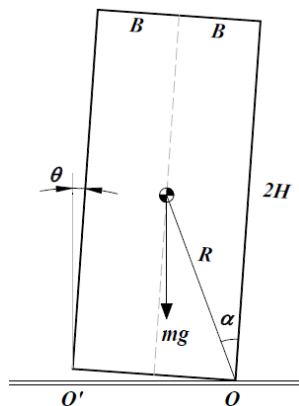


Figure 1-6. Housner rocking block (Housner 1963)

When a rocking wall is subjected to an earthquake excitation, Equation 1-2 is not valid anymore, since the angular momentum is not conserved, but the energy loss could be estimated using the fundamental equation (i.e., Equation 1-1). It is worth noting that depending on the direction of the earthquake acceleration and the wall relative velocity, the rate of energy input due to horizontal ground motion could be positive or negative. When energy is added to the rocking system due to earthquake excitation, the observed kinetic energy right after the impact may even increase, indicating a coefficient of restitution greater than one. Therefore, this coefficient may not thoroughly represent the energy loss due to impacts during an earthquake loading. An accurate prediction of this form of damping is required to implement it in seismic design of rocking walls.

1.2.2. Seismic design approach

Two main approaches are widely used in current codes for lateral design of structures subjected to a design-level or greater earthquake. The design base shear, estimated from the traditional Force-Based approach (FBD), is determined from multiplication of effective seismic weight of the structure by a seismic response coefficient (S_a/g). A spectral response acceleration factor (S_a) is defined based on the period of the system using standard design elastic response spectrum (e.g., IBC 2009; ASCE 7-05 2005). This spectrum is defined based on a damping ratio of 5% and is different for site classes of A to F. A response modification factor of R is applied in current design codes following the force-based approach to take into account ductility capacity of the structure (see Figure 1-7). Due to lack of research, the current practice recommends an R-factor of 5 for designing the structures using precast concrete rocking walls, similar to what is applied for the traditional CIP walls.

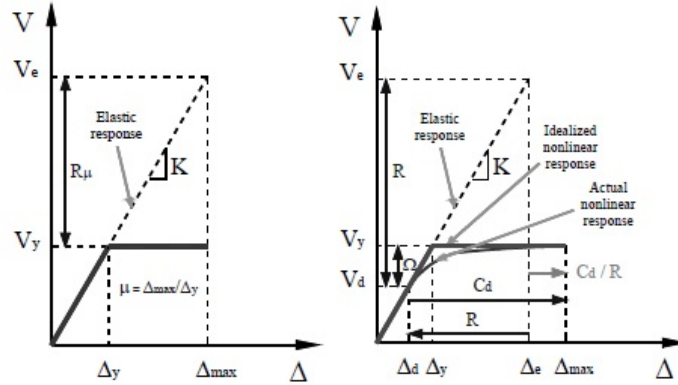


Figure 1-7. R-factor as used in force-based design approach (Carrillo et al. 2013)

It has been realized that it is the lateral displacements that correlate to the structural damage, rather than the forces. As a result, researchers began to focus on the idea of reaching a target displacement for a given earthquake (Priestley 2000). In the new approach, which is known as the Direct Displacement-Based Design (DDBD), the structure is allowed to reach a certain amount of displacement/drift to ensure the acceptable performance level under an assumed design earthquake. The design base shear is obtained from the product between the target lateral displacement and effective stiffness (k_e) of a substitute linear viscoelastic single degree of freedom (SDOF) system, as shown in Figure 1-8a and Figure 1-8b. The determination of an appropriate level of damping of the structure, as shown in Figure 1-8c, based on the desired displacement ductility and type of the structure, can be used to estimate the effective period of the system (T_e) for the design displacement of Δ_d (see Figure 1-8d). Accordingly, to design precast concrete walls with and without additional hysteretic energy dissipaters following DDBD approach, an exact estimation of their damping components are required.

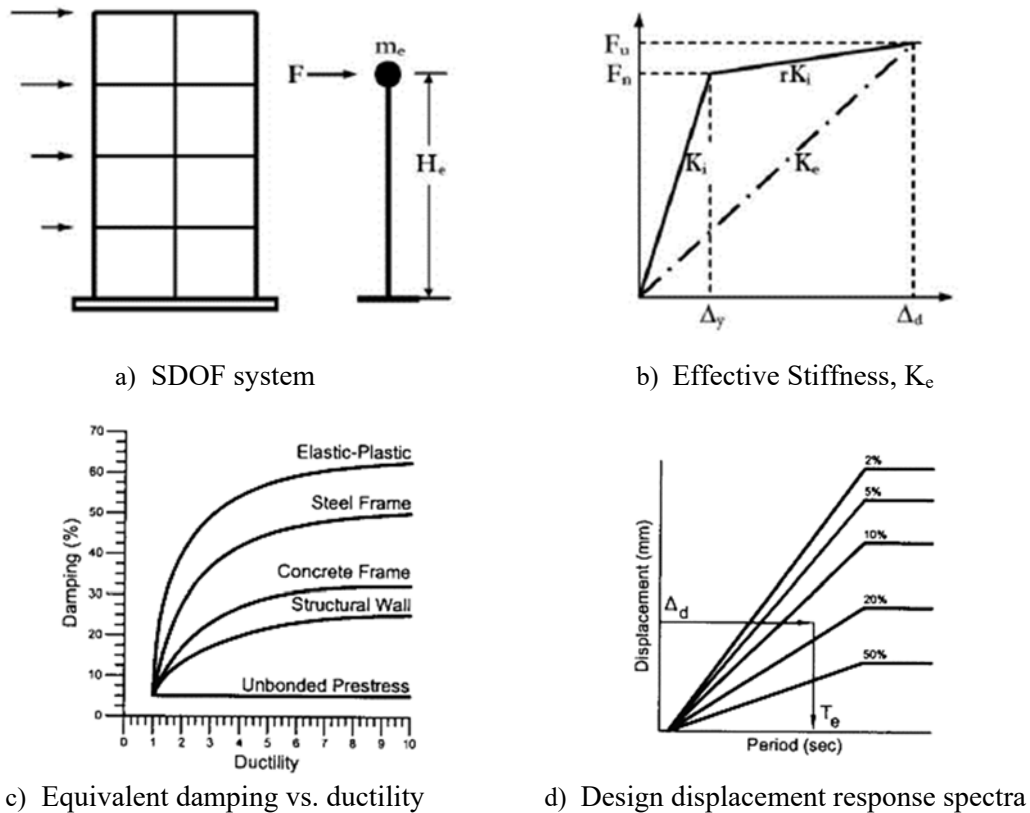


Figure 1-8. Fundamentals of Direct Displacement-Based Design (Priestley 2000)

As discussed in Priestley (2000), estimation of an equivalent viscous damping ratio (ξ_{eq}) is required to represent all damping components of the system as applied in the DDBD procedure. This damping term is determined as a combination of an elastic component (ξ_{el}) and a hysteretic part (ξ_{hys}). ξ_{el} is usually included in time history analysis to account for damping that is not captured by the hysteretic model. This damping is related to the secant stiffness to design displacement of the substitute SDOF system as shown in Figure 1-8a and Figure 1-8b (Priestley 2000). The following equation is defined to relate the initial and/or tangent elastic damping to a secant stiffness based damping ratio (Priestley et al. 2005)

$$\xi_{eq} = \kappa \xi_{el} + \xi_{hys} \quad (\text{Equation 1-3})$$

where $\kappa = \mu^{\hat{\lambda}}$ and $\hat{\lambda}$ is the secant stiffness factor defined in Priestley et al. (2005).

While different equations are introduced to estimate ξ_{hys} , Jacobsen's Damping Secant Stiffness (JDSS) approach as suggested by Dwairi et al. (2007) is used as shown in Figure 1-9 and presented by Eq. 1-4:

$$\xi_{hys} = \frac{2 A_1}{\pi A_2} = \frac{A_1}{2\pi F_{max} \Delta_{max}} \quad (\text{Equation 1-4})$$

where, A_1 is the area enclosed by a hysteresis loop at a given drift of Δ_{max} and lateral force of F_{max} . A_2 is the area of the rectangle circumscribing the hysteresis loop.

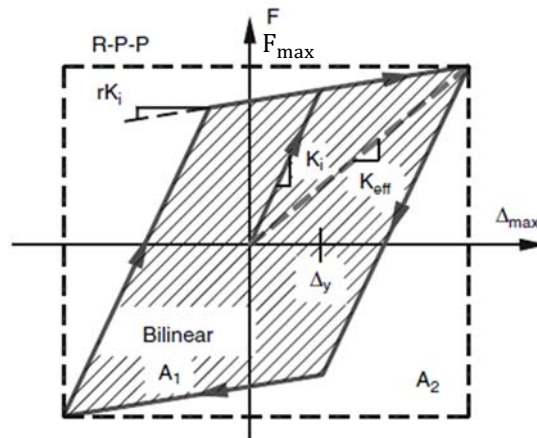


Figure 1-9. Equivalent damping for bilinear and rigid-perfectly-plastic (R-P-P) loop
(Dwairi et al. 2007)

The concepts defined in DDBD method allowed for creating a standardized approach for performance-based seismic evaluation of structures while subjected to multiple-level intensities of ground motions. Following this philosophy, different structural and non-structural performance levels are defined to ensure acceptable performance when the structure is subjected to ground motions varying from frequent (EQ-I) to the maximum considered earthquakes (EQ-IV). As

outlined by Priestley (2000) and the performance-based design appendix of the SEAOC blue book (see Figure 1-10), the design philosophy (i.e., Basic Objective, Enhanced Objective 1 or 2) should target appropriate performance levels (i.e., Immediate Occupancy to Near Collapse) for four levels of seismic hazard (i.e., EQ-I to EQ-IV). A multiple-level performance-based seismic evaluation of post-tensioned precast rocking systems designed following either FBD or DDBD solution is required to allow for their application in regions of high seismicity.

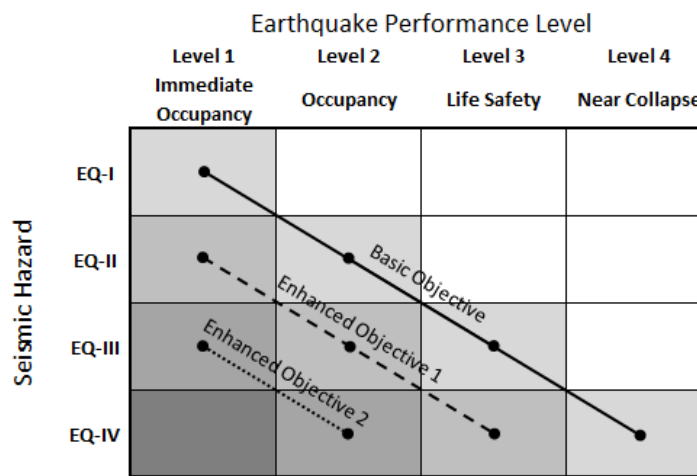


Figure 1-10. Seismic performance objectives for buildings (SEAOC 1999)

1.3. Research Scope and Objectives

Extensive research into characterizing the local and global behavior of unbonded post-tensioned precast concrete rocking walls has been completed over the last two decades, but implementation of these components into building practice has been limited. This is due to the fact that much work on rocking walls has focused on quasi-static testing of these systems and the existing knowledge about their seismic response when subjected to ground motions of various intensities is insufficient. The scope of this research is to provide better understanding on seismic response of rocking precast concrete walls designed with unbonded post-tensioning using two

different systems: Single Rocking Walls (SRWs) and Precast Walls with End Columns (PreWECs). To successfully achieve the scope, a shake table test investigation was used to test a number of rocking walls with varying quantities of post-tensioning (PT) and hysteretic energy dissipation using a suite of input ground motions and a multiple-level seismic performance evaluation method. The project scope is fulfilled by achieving the following objectives:

1. Investigate the local and global lateral resisting behavior of rocking walls through scaled shake table tests. Attention is given to examine the influence of different design variables such as post-tensioning parameters and energy dissipation capacities.
2. Establish a simplified analytical model in OpenSees (McKenna et al. 2000) to predict the complex rocking response and verify this model using experimental data.
3. Examine the performance-based seismic response of unbonded post-tensioned precast SRWs, when subjected to earthquakes of different intensities and evaluate the influence of additional energy dissipaters, as provided in PreWECs, on mitigating multiple-level seismic performance of rocking wall systems.
4. Quantify different components of damping associated with the rocking of concrete precast walls both with and without additional hysteretic energy dissipating elements and evaluate participation ratio of individual damping terms in energy dissipation of rocking walls.
5. Introduce equivalent viscous damping ratio and strength Reduction (or R) factor for seismic design of rocking walls, following the Direct Displacement-Based Design (DDBD) and the Force-Based Design (FBD) approaches, respectively.
6. Develop systematic approach for the seismic design of unbonded post-tensioned precast concrete rocking walls.

1.4. Thesis Layout

The thesis will comprise of seven chapters including the general introduction presented in this chapter. Following the introductory chapter, Chapter 2 reviews the available literature on previous experimental investigations as well as analysis and design procedures relevant to the unbonded post-tensioned precast rocking walls with and without external energy dissipaters. Chapter 3 presents the seismic performance of single rocking walls through a set of shake table testing conducted on four test walls (i.e., SRW1-4) and an experimentally verified analytical model. The acceptability of SRWs in seismic design is investigated through the performance-based evaluation of these four test walls during multiple-level intensity input motions. Next, the equivalent viscous damping ratio representing different energy dissipation components of SRWs and the corresponding R-factor for the seismic design of these walls are evaluated. In Chapter 4 the impact of external energy dissipaters on the seismic response of SRWs was evaluated, by studying the behavior of four PreWEC systems while these test units were subjected to multiple-level input ground motions. To design PreWECs following an FBD solution, a new set of R-factors as a function of damping ratio is suggested. Finally, recommendations for seismic design of precast concrete rocking walls with different energy dissipation ratios are summarized in Chapter 4. The analytical model as used for SRWs is also updated and experimentally verified for PreWEC systems. Chapter 5 indicates the experimental investigation, examining and comparing different energy dissipation components of all test walls including, SRWs and PreWEC systems, during different earthquake excitations. The results from this chapter reveal how SRWs relying on negligible hysteretic damping can perform well during large earthquakes. The sixth chapter looks specifically at verification of the developed R-factors for seismic design of unbonded post-tensioned precast concrete rocking walls. In this chapter, six, nine, and twelve story high full-scale

precast post-tensioned wall system buildings were designed to the suggested approaches as previously presented in Chapters 3 and 4. Using the experimentally verified analytical model, seismic performance of these buildings will be presented during design-level and maximum considered earthquakes. The closing chapter will contain conclusions derived from this research, along with recommendations for any possible future research to pave the way for designing structures that conserve their functionality after severe ground motions.

1.5. References

- ACI 318-11 (2011) Building code requirements for structural concrete. Farmington Hills, MI.
- ASCE 7-05 (2005) Minimum design loads for buildings and other structures, ASCE/SEI 7-05.
- Carrillo, J., Blandón-Valencia, J., Rubiano, A. (2013) A review of conceptual transparency in US and Colombian seismic design building codes, *Ingeniería e Investigación*. **33**(2), 24 - 29.
- Henry, R.S., (2011) Self-centering Precast Concrete Walls for Buildings in Regions with Low to High Seismicity, PhD Thesis. University of Auckland.
- Holden, T. J. (2001) A comparison of the Seismic Performance of Precast Wall Construction: Emulation and Hybrid Approaches. Research Report 2001-04, University of Canterbury, Christchurch.
- Housner, G. (1963) The behavior of inverted pendulum structures during earthquake excitations. *Bull. Seismol. Soc. Am.*, **53** (2), 403-417.
- IBC I (2009) International Code Council. International Building Code.
- Kurama, Y., Sause, R., Pessiki, S., and Lu, L.-W. (1999) Lateral load behavior and seismic design of unbonded post-tensioned precast concrete walls. *ACI Structural Journal*, **96**(4), 622-632.
- Ma, Q. (2009) The mechanics of rocking structures subjected to ground motion. PhD Thesis, Department of CEE, The University of Auckland, New Zealand.

- McKenna, F., Fenves, G., and Scott, M. (2000) Open system for earthquake engineering simulation. University of California, Berkeley, CA.
- NZS 3101-06 (2006) Concrete structures standards. Standards New Zealand, Wellington, New Zealand.
- Park, R. and Paulay, T. (1975) Reinforced Concrete Structures, *John Wiley & Sons. New York*, 769 p.
- Perez, F. J., Pessiki, S., and Sause, R. (2004) Experimental and analytical lateral load response of unbonded post-tensioned precast concrete walls. ATLSS Report No. 04-11, Lehigh University, Bethlehem, PA.
- Priestley, M. J. N., Sritharan, S., Conley, J. R., and Pampanin, S. (1999) Preliminary results and conclusions from the PRESSS five-story precast concrete test building. *PCI Journal*, **44**(6), 42-67.
- Priestley, M. J. N. (2000) Performance Based Seismic Design. 12th World Conference on Earthquake Engineering, Auckland, New Zealand, 2000.
- Rahman, A. M. and Restrepo, J. I. (2000) Earthquake resistant precast concrete buildings: seismic performance of cantilever walls prestressed using unbonded tendons. Research Report 2000-5, University of Canterbury, Christchurch.
- Seismology Committee (1999) Recommended lateral force requirements and commentary (Blue book), Structural Engineers Association of California, SEAOC, Calif., 327–421.
- Sritharan, S., Beyer, K., Henry, R. S., Chai, Y.H., and Kowalsky, M. (2014) Understanding Poor Seismic Performance of Concrete Walls and Design Implications. *Earthquake Spectra*, **30**(1), 307–334.
- Sritharan, S., Aaleti, S., Henry, R. S., Liu, K. Y., and Tsai, K. C. (2008) Introduction to PreWEC and key results of a proof of concept test. *M. J. Nigel Priestley Symposium*, North Tahoe, California, IUSS Press, Pavia, Italy, 95-106.

CHAPTER 2

EXAMINATION OF THE CURRENT STATE OF THE ART

An extensive review of literature related to unbonded post-tensioned precast concrete rocking walls was undertaken as part of this study. This chapter first traces the development of rocking walls over the past few decades and describes implementation of these systems in some buildings around the world. Then a summary of several experimental and numerical investigations performed for the development of concrete rocking walls as well as current seismic design guidelines and code provisions are given. The chapter highlights shake table testing on self-centering walls with dynamic results that provide estimations of their damping components.

2.1. Historical Perspective

In response to an organized need to construct seismic-resilient precast structures, a joint US-Japan research program entitled PREcast Seismic Structural Systems (PRESSSS) was initiated in the early 1990's. In one of the earlier tests carried out by the National Institute of Standards and Technology (NIST), as part of the inter-program coordination of the US. PRESSSS program, cyclic lateral force behavior of a precast concrete beam-column joint subassembly with fully-grouted post-tensioned tendons was investigated (Cheok and Lew 1991). Because significant stiffness degradation, pinching, and thereby unreliable energy dissipation were observed in the response, Priestley and Tao (1993), after an analytical investigation, suggested the application of unbonded post-tensioning (PT) to tie precast components into building frames. This type of connection reduced tendon strains and provided self-centering behavior by designing the PTs so as to remain elastic during an earthquake. Their consequent limited energy dissipation capacity was modified

by using special spiral reinforcements at the beam end regions. Inter-program coordination of the PRESSSS research program supported experimental testing of several (i.e., bonded, partially debonded, and fully unbonded) post-tensioned precast beam-column joint subassemblies to examine their superior performance compared to traditional cast-in-place connections (e.g., Stone et al. 1995; Priestley and MacRae 1996; and Stanton et al. 1997). In addition to these investigations undertaken on self-centering prestressed frame connections during the PRESSSS program, researchers at Lehigh University analytically investigated this concept for application to precast concrete walls, leading to the development of unbonded post-tensioned precast concrete rocking walls (Kurama et al. 1999). Such walls were conceived to have relatively little energy dissipation, because their PT tendons were designed not to yield during a design-level earthquake event. This, however, led to uncertainties associated with their possibly unreliable performance in high-seismicity areas.

To overcome such limitations, jointed (or coupled) walls were developed by Priestley et al. (1999) as part of the final phase of the PRESSSS program. They consisted of two or more unbonded post-tensioned precast concrete walls connected through U-shaped Flexural Plates (UFP); this in turn increased energy dissipation of the system in comparison to that of a single rocking wall, because the connectors experience large inelastic deformations as the walls rock when subjected to moderate to large earthquake loads. Although they performed satisfactorily, such systems were not often applied in buildings as substitutes for equivalent cast-in-place walls because they exhibited lower moment resistance and required expensive connectors which had unpredictable behavior (Sritharan et al. 2015). In consideration of these two points, several researchers have suggested the implementation of different configurations of external energy dissipaters in precast rocking walls.

The alternative hybrid wall concept was developed subsequent to the application of hybrid beam-column connections developed during the PRESSS program. In particular, researchers at the University of Canterbury (Rahman and Restrepo 2000; Holden et al. 2001) carried out several tests on precast walls connected to foundations using both post-tensioning tendons and grouted mild steel reinforcement. While the former was mostly capable of providing moment resistance and self-centering behavior of the wall, the latter provided additional hysteretic energy dissipation. These bars were usually debonded over a short length to reduce the strain demand and prevent fracture of the mild steel when subjected to the design-level earthquake loading. Because of their placement within the wall, these bars cannot be easily replaced as a consequence of any possible fracture during a strong earthquake.

Researchers have proceeded on to investigate other sources of external dampers for precast concrete walls. Kurama et al. (2000 and 2001) introduced the application of unbonded post-tensioned walls utilizing friction devices and linear viscous supplementary energy dissipaters. Although they were successful in reducing drift levels compared to a wall with no additional dampers, these devices were expensive in terms of both material and installation cost. Marriot et al. (2008) continued research in the area of application of supplemental dampers by using externally-mounted tension-compression yielding steel dampers on unbonded precast concrete walls. This new configuration of energy dissipaters was prone to buckling if dampers were not carefully designed. Recent examples of research into hybrid technology include a series of experimental testing of self-centering concrete walls with distributed friction devices (Tong et al. 2014) and passive supplemental damping devices combined with unbonded post-tensioned concrete rocking walls (Nicknam and Filiatrault 2015).

Originating from the idea of jointed walls in PRESS program, Precast concrete Wall with End Columns (PreWEC) was developed by Sritharan et al. (2008). In that system, the wall panel was not divided into several separate panels; it was instead connected to end columns (e.g., steel, concrete filled steel tubes, or precast concrete) using easily-replaceable oval-shaped mild steel connectors called O-connectors. As reported by Henry (2011), flexural yielding was considered to be the most desirable mechanism for designing these connectors. This was because the shear connectors, as tested by Shultz and Magana (1996) to be used for jointed walls, were required to be manufactured from stainless steel, since they were subjected to large strain demands while providing energy dissipation capacity. Instead, for PreWECs, connectors were constructed from grade A50 mild steel and expected to yield as they underwent relative vertical deformations at the wall-column joint, during rocking of the system. In that way, in addition to providing an external source of energy dissipation, the forces developed in the connectors contribute to the systems' moment capacity. Accordingly, this new wall concept promoted use of precast systems by: (1) increasing the resistance of the wall system by increasing the lever moment arm between the post-tensioning tendons and the compression block in the wall toe, as well as, incorporating the participation of O-connectors, and (2) using inexpensive energy dissipaters that can be easily inspected and/or replaced following an earthquake.

As connectors were to be constructed from flexurally deforming plates, Henry (2011) performed a series of analytical studies to investigate the performance of different configurations of connectors, as shown in Figure 2-1. When force-deformation behavior of Slotted Flexural Plates (SFP), flexural plates with holes, J-shaped flexural plates (J-connector), and Oval-shaped flexural plates (O-connector) were compared, O-connectors appeared to be best-suited for the PreWEC

system. Figure 2-2 shows satisfactory force-displacement response of O-connectors, their large displacement capacity, and reliable energy dissipation capacity when compared to J-connectors.

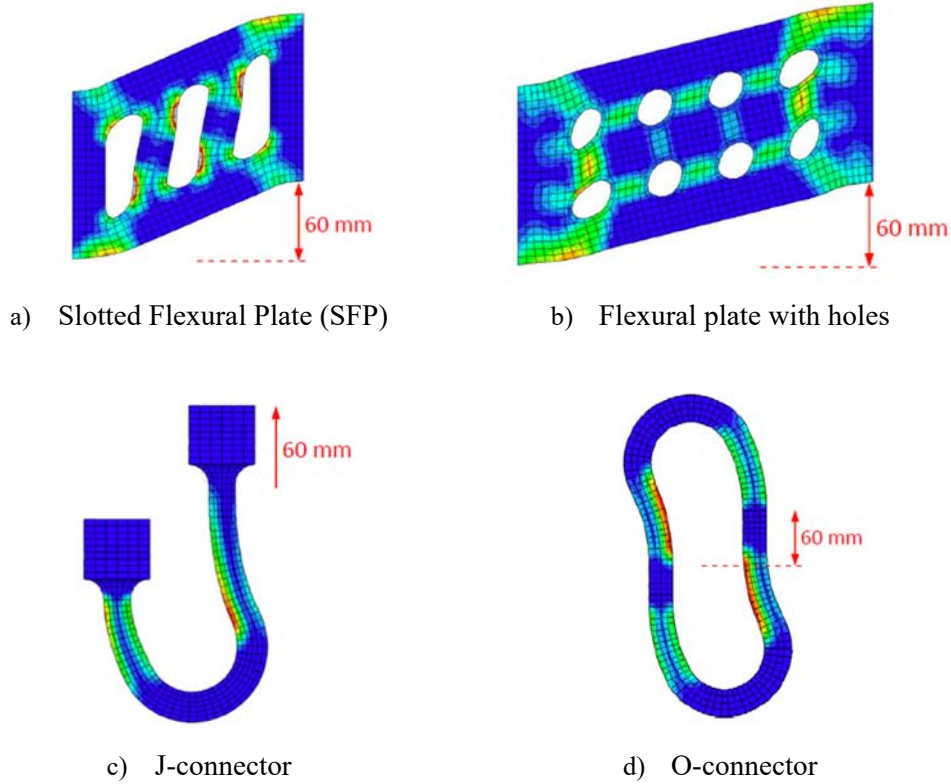


Figure 2-1. Different types of connectors to be used with PreWEC (Henry 2011)

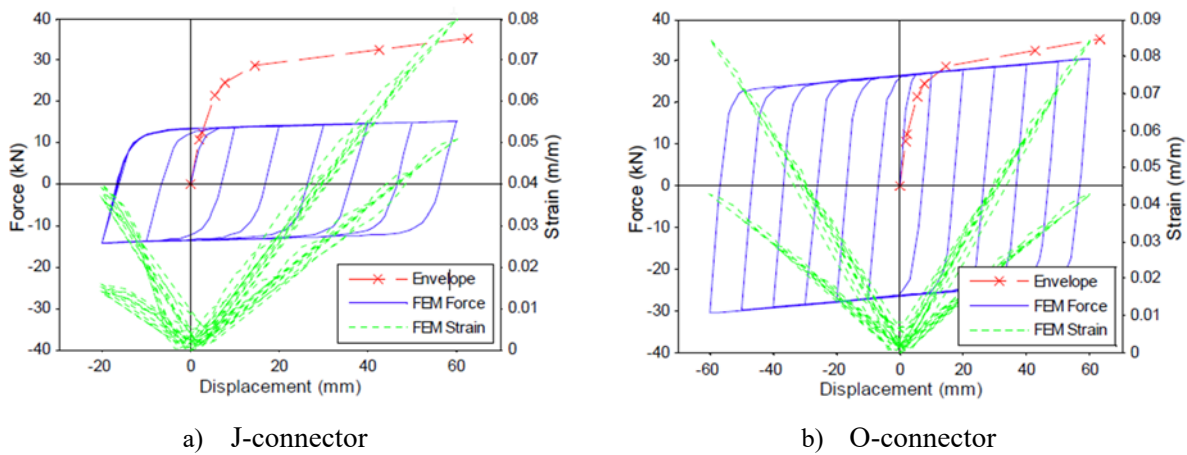
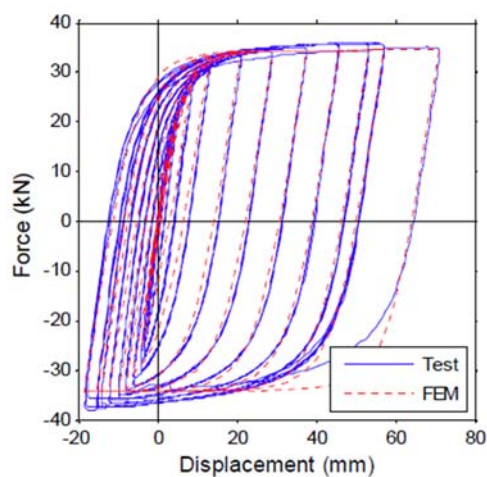
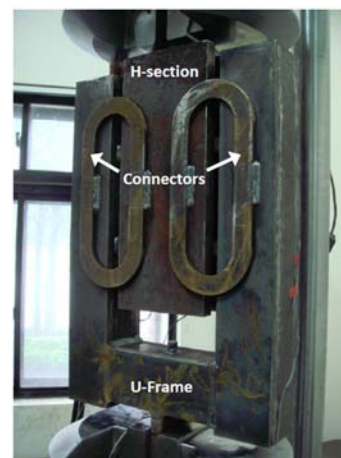


Figure 2-2. Force-displacement behavior of J- and O-connectors (Henry 2011)

Figure 2-3a shows easily-predictable behavior of O-connectors, as their expected analytical response closely matched the data observed from the experimental testing (see the test-set up in Figure 2-3b).



a) Comparison of measured and calculated response



b) Test set-up

Figure 2-3. Experimentally verification of the measured response of O-connectors (Henry 2011)

Twigden and Henry (2015) demonstrated different failure types of O-connectors (i.e., fracture of connector leg, distributed cracking, and out-of-plane buckling), as shown in Figure 2-4. They implied that a reduction in the connector length-to-thickness ratio can prevent their observed out-of-plane buckling. This study also made recommendations regarding the welding process for a preferred ductile failure of connector leg away from the edge of the weld (e.g., preventing type 1 failure as shown in Figure 2-4).

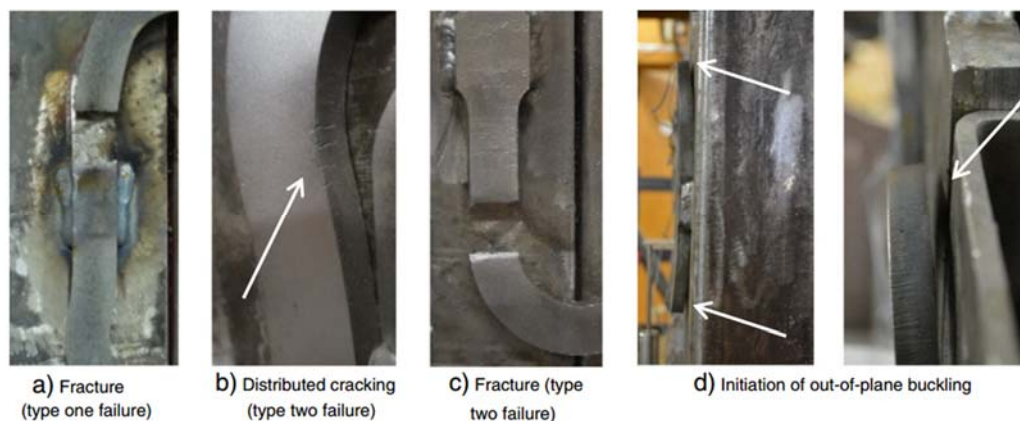


Figure 2-4. Different failure and fracture types in O-connectors (Twigden and Henry 2015)

Since the development of rocking walls with additional hysteretic dampers, several buildings have been constructed using such systems. A number of on-site implementations of PRESSS technology buildings have been applied in high seismic regions around the world. Those built in New Zealand were even tested under real earthquake shaking during the 2011 Christchurch event.

One of the first and tallest buildings designed with a self-centering hybrid moment-resisting frame was the 39-story Paramount building (see Figure 2-5) located in San Francisco, California (Englekirk 2002). In New Zealand, different types of concrete, masonry, and timber rocking structures have been constructed. One of those buildings was the Southern Cross Hospital located in Christchurch that resisted the 2011 earthquake using the post-tensioned hybrid walls coupled with U-shape flexural plate dissipaters. As shown in Figure 2-6, negligible damage was observed to both structural and non-structural components of that building (Pampanin et al. 2011).

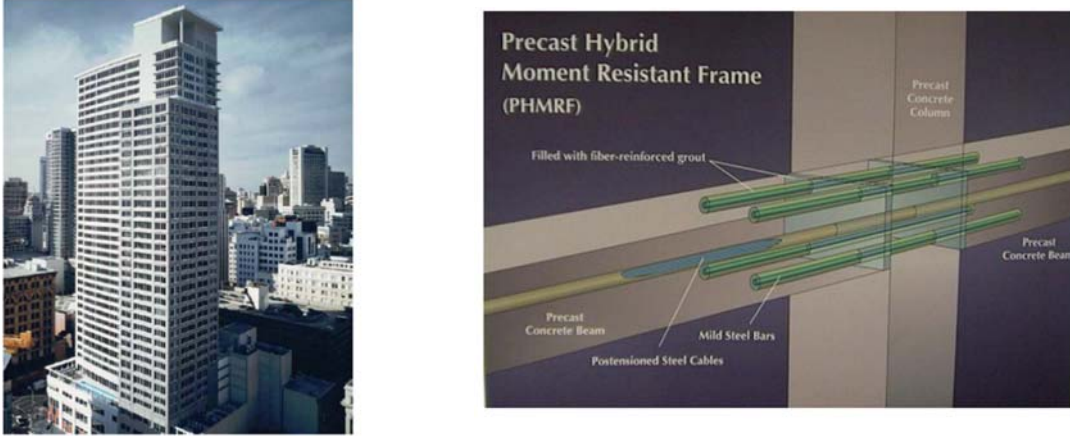


Figure 2-5. Paramount building with hybrid moment-resisting frames (Englekirk 2002)



Figure 2-6. Negligible observed damage to the Southern Cross Hospital designed with a rocking-dissipative solution during the Christchurch earthquake (Pampanin et al. 2011)

2.2. Experimental Large-scale Testing

An extensive literature review is presented in this section to describe experimental large-scale studies conducted on precast concrete walls both with and without additional energy dissipaters, using quasi-static loading. Also, their dynamic response based on a few experimental research studies using free vibration and shake table testing was discussed.

2.2.1. Quasi-static loading

Following development of the hybrid wall concept, Rahman and Restrepo (2000) tested three half-scaled post-tensioned walls, including two systems equipped with mild steel reinforcing bars as external energy dissipaters (see Figure 2-7).

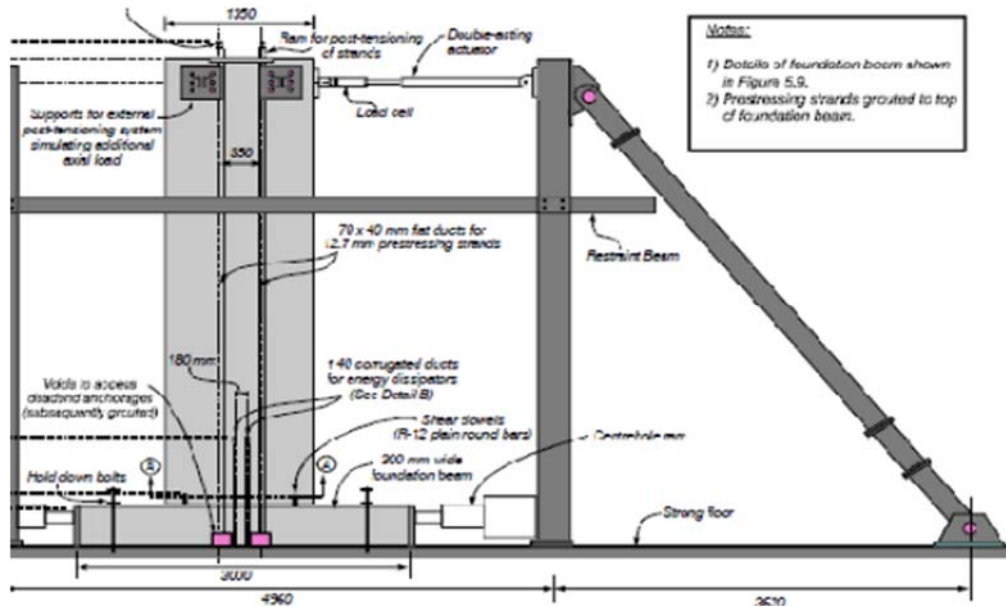


Figure 2-7. Schematic representation of the test set-up reported by Rahman and Restrepo (2000)

Quasi-static reverse cyclic lateral loading on these walls demonstrated: (1) satisfactory lateral response of the hybrid walls without strength degradation with lateral drifts of up to 3 to 4%, as shown in Figure 2-8, and (2) an equivalent viscous damping ratio of up to 14% due to yielding of the mild steel reinforcement in both tension and compression; Figure 2-8 shows the increased area enclosed by the hysteresis loops when additional damping has been provided through a standard reinforcing bar placed across the wall-to-foundation interface.

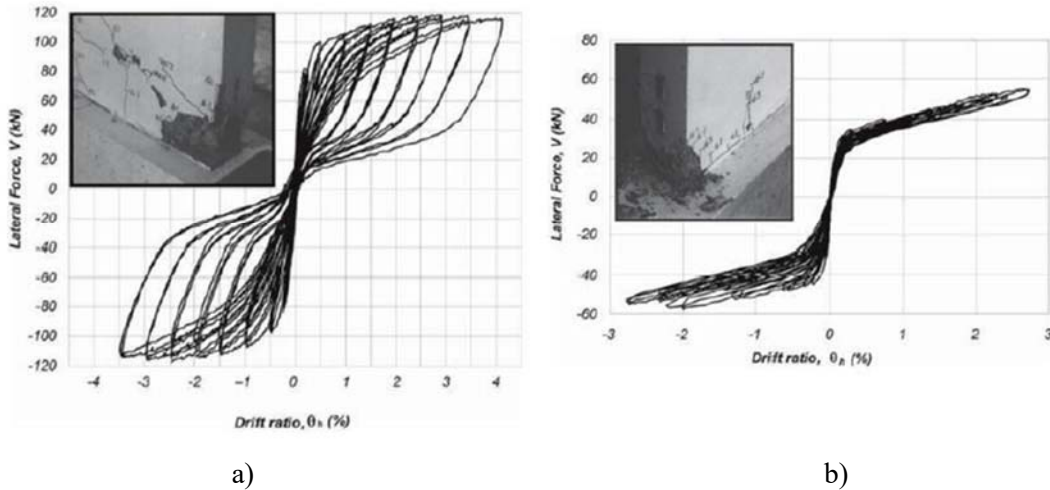


Figure 2-8. Cyclic response and damage state of a hybrid wall (a) vs. SRW (b)
(Rahman and Restrepo, 2000)

Holden et al. (2001) subjected two identical hybrid and traditional cast-in-place concrete walls to pseudo-static reverse cyclic loading and observed no visible damage in the precast wall. The conventional wall, however, sustained flexural cracking close to the wall base and therefore exhibited larger energy dissipation capacity compared to that provided by the mild steel reinforcement in the hybrid wall.

The majority of experimental testing on unbonded post-tensioned SRWs was performed by Perez et al. (2002). Those Lehigh University researchers attempted to evaluate and compare the monotonic and cyclic lateral response of five test walls designed with different parameters, including areas of post-tensioning tendons, initial prestressing, initial stress in concrete due to post-tensioning, and confining reinforcement details provided in the wall toe. Results of the pseudo-static testing performed by Perez et al. (2002) revealed some hysteretic energy dissipation involved in their nearly nonlinear elastic force-deformation response, as shown in Figure 2-9. This was reported as mainly due to material nonlinearity of concrete at wall toes and the PT tendons if they experienced yielding (Perez et al. 2004).

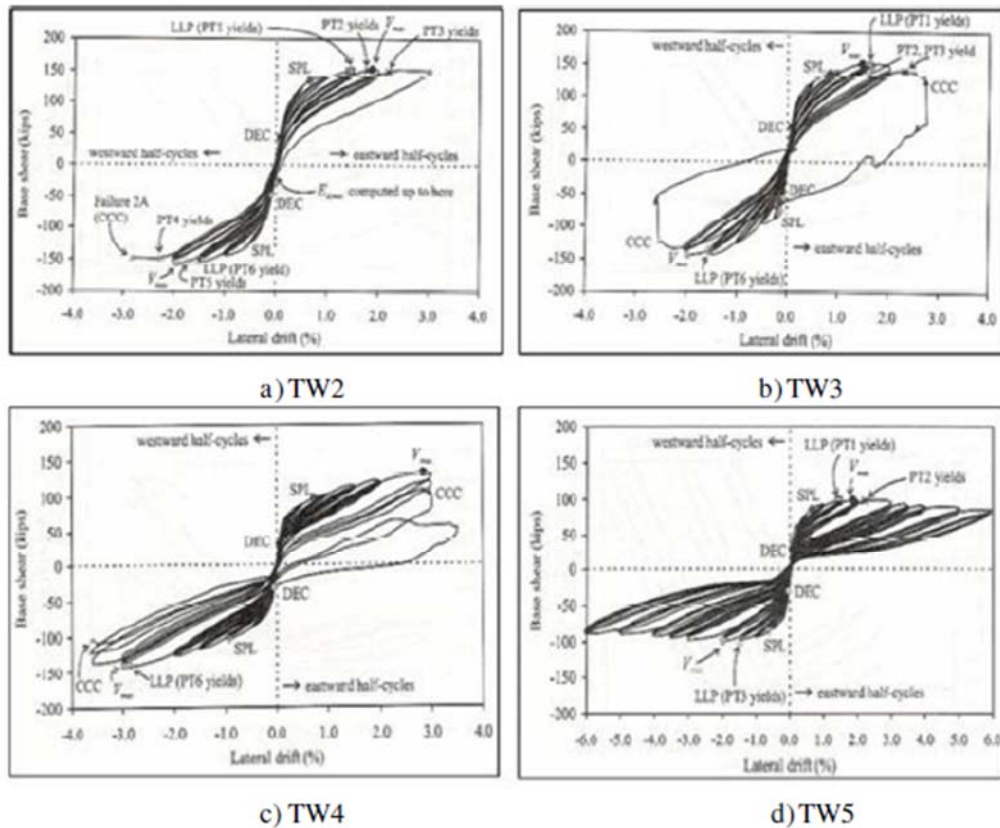


Figure 2-9. Measured cyclic load response of SRWs tested by Perez et al. (2004)

The PerWEC system has been experimentally validated with large scale pseudo-static cyclic testing (Sritharan et al. 2015); its performance was compared to that of an emulated reinforced concrete wall, namely RWN. Figure 2-10 presents the test set-up, instrumentation, and the load protocol. Based on the test observations, the RC wall experienced significant damage and required more extensive repair compared to the PreWEC (see Figure 2-11). The results from this study were also used to verify the accuracy of the Simplified Analysis (SA) method developed by Aaleti and Sritharan (2009) to predict both global and local responses of the PreWEC system. Both measured and expected force-displacement response of the PreWEC system is presented in Figure 2-12 along with a comparison of its hysteretic energy dissipation capacity compared to the RC

wall. It was shown that the PreWEC generally provided lower damping compared to the traditional concrete wall. As reported by these researchers, however, addition of each O-connector added about 0.4% of equivalent viscous damping ratio and increased the lateral resistance by 1.5% during drift cycles of 1 to 3%. These values can be increased by adjusting the dimensions and/or number of O-connectors.

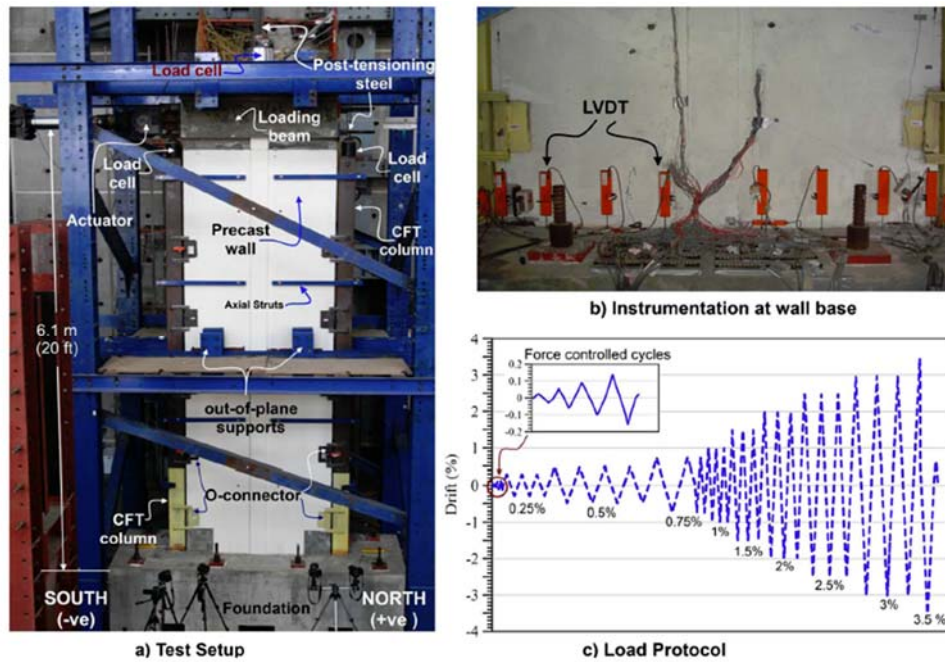


Figure 2-10. The test set-up and cyclic loading applied to PreWECs (Sritharan et al. 2015)

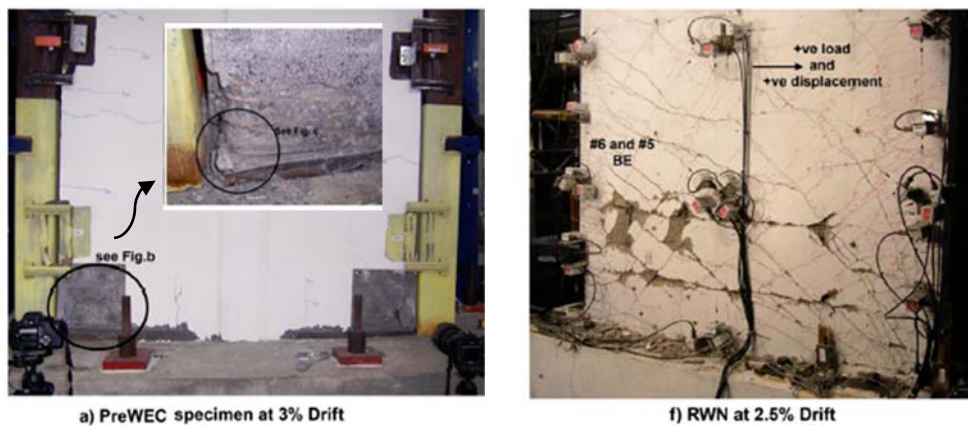


Figure 2-11. Comparison of the observed damage in PreWEC and RC wall (Sritharan et al. 2015)

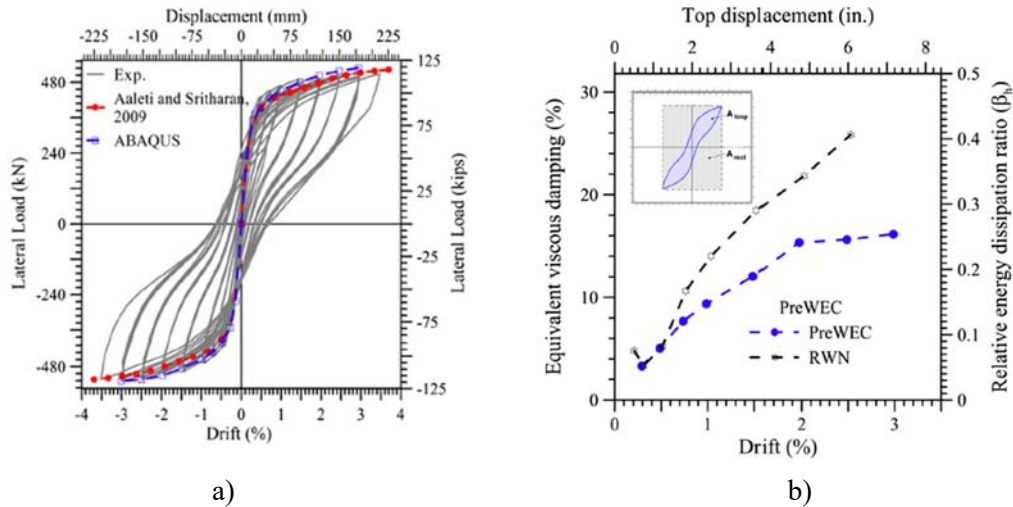


Figure 2-12. Cyclic response of the PreWEC from experimental data and SA method (a) along with the associated equivalent viscous damping (b) (Sritharan et al. 2015)

Twigden (2016) investigated the performance of two SRWs and two PreWECs through five pseudo-static cyclic tests. Four and six O-connectors were laser cut out of 2.54 in. thick mild steel plate and used to join the wall panels to the end columns. Test observations, as shown in Figure 2-13, confirmed insignificant damage to the wall toes.

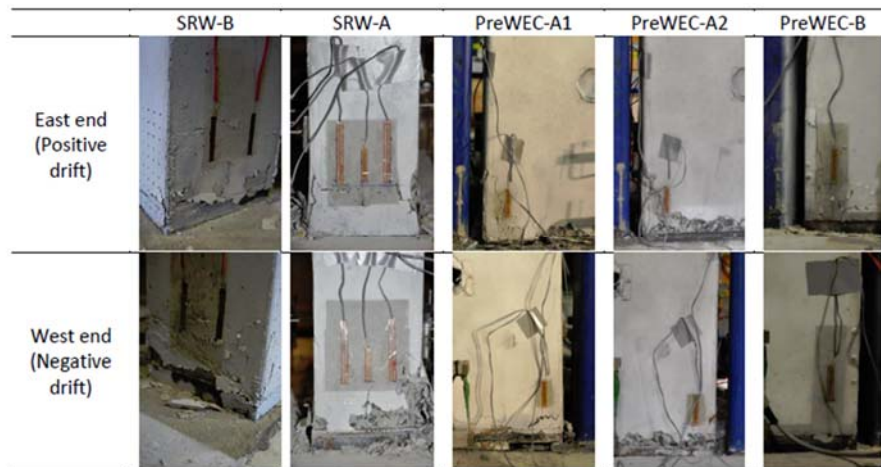


Figure 2-13. Damage to the wall toes during quasi-static testing of SRWs and PreWECs (Twigden 2016)

Accuracy of the SA method proposed by Aaleti and Sritharan (2009) was also certified as shown in Figure 2-14 by comparing the experimental force-displacement response of the test walls with their calculated behavior, following the SA method (named A&S in this figure).

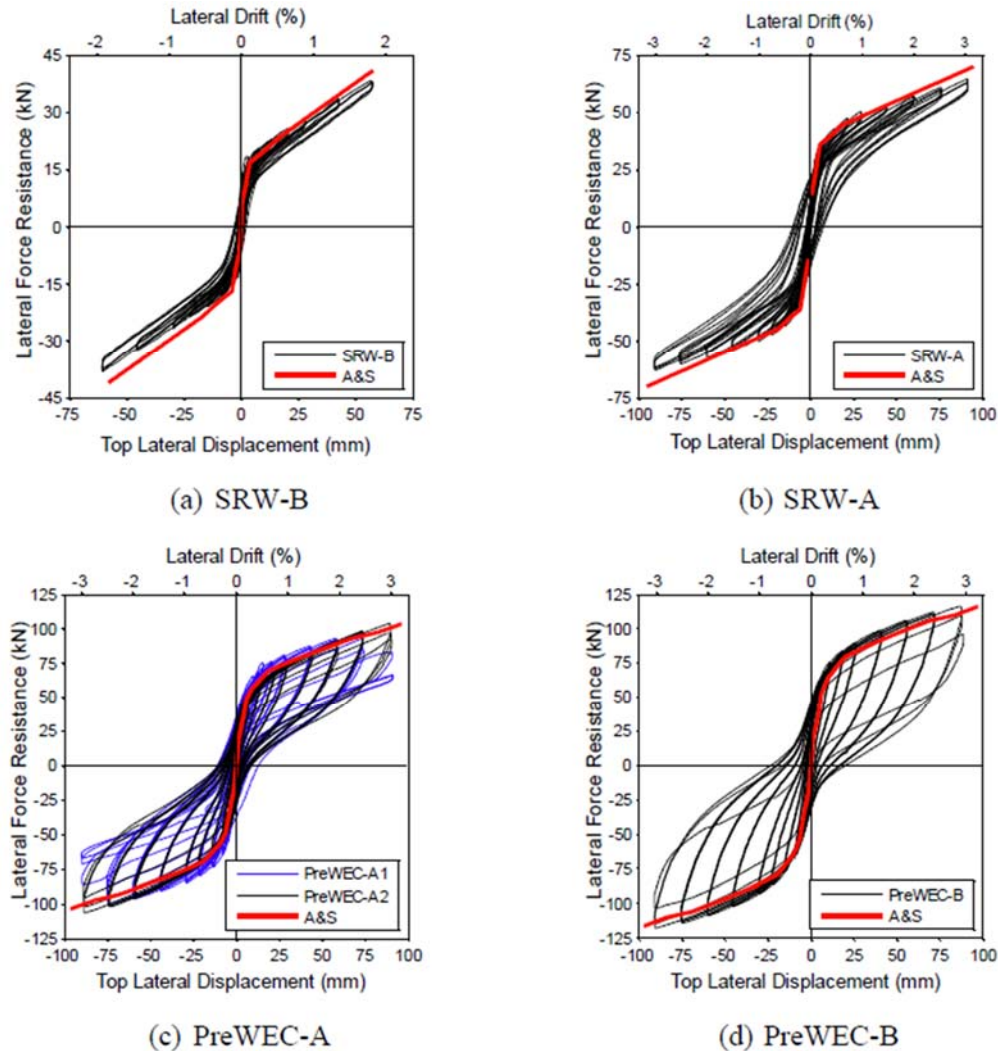


Figure 2-14. Measured force-displacement response of SRWs and PreWECs (Twigden 2016)

Based on measured hysteretic loops, an area-based equivalent viscous damping (EVD) ratio of 3 to 5% was reported for SRWs as well as 1.1 to 1.4% EVD per connector for PreWECs. Variation of the EVD of SRWs and PreWECs vs. lateral drift of the wall systems is illustrated in Figure 2-15. To measure the EVD, an equation presented in Chopra (2007) was used, in which A_1

is the area enclosed by the hysteresis loop (as plotted in Figure 2-14) defined by maximum force and displacement of F_{max} and Δ_{max} :

$$\xi_{area} = \frac{A_1}{2\pi F_m \Delta_m} \quad (\text{Equation 2-1})$$

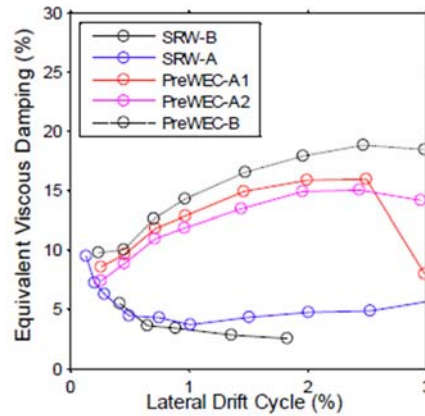


Figure 2-15. Measured EVD of SRW and PreWECs from cyclic hysteresis loops (Twigden 2016)

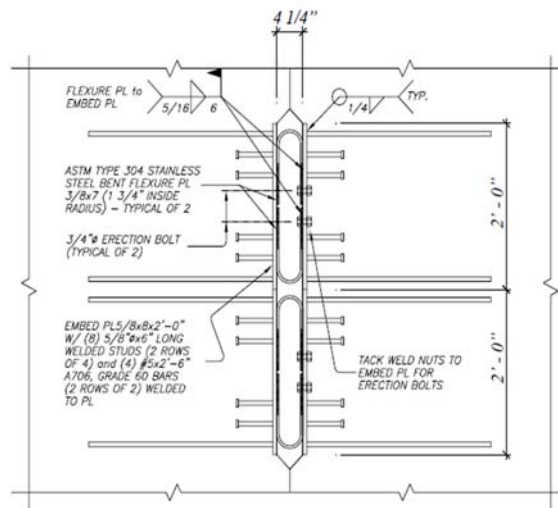
2.2.2. Dynamic loading

During the final phase of the PRESSS program, a 60% scale model of a five-story precast building was subjected to a series of pseudo-dynamic tests. The PRESSS building was designed to resist seismic loads using orthogonal moment-resisting frames and precast jointed walls. As shown in Figure 2-16, this coupled system consisted of four panels, each 2½ stories tall (18.75-ft) by 9-ft wide and 8-in. thick, and vertically jointed to form two walls attached horizontally using twenty UFP connectors (see Figure 2-16b). These wall were tested under simulated seismic loads, including short-duration ground motions, which were compatible with acceleration response spectra of 1.5 EQ-I, EQ-II and EQ-III as shown in Figure 2-17.

Figure 2-18 presents findings from this first test conducted on jointed walls. Exceptional performance of this rocking building was observed in Figure 2-18a; the jointed walls experienced minimal spalling of the cover concrete in the compressed toe of the panel after the building was subjected to a design-level earthquake with an intensity of EQ-III. Based on the observed moment-lateral displacement response of the PRESSS building (see Figure 2-18b), it was concluded that both the self-centering capability provided by the post-tensioning tendons and the energy dissipation capacity provided by the UFP connectors were excellent, while wall drifts were limited to a maximum of 1.85% during design-level simulated earthquakes.



a) Jointed walls in PRESSS building



b) UFP connectors

Figure 2-16. Pseudo-dynamic testing of jointed walls in PRESSS building (Priestly et al. 1999)

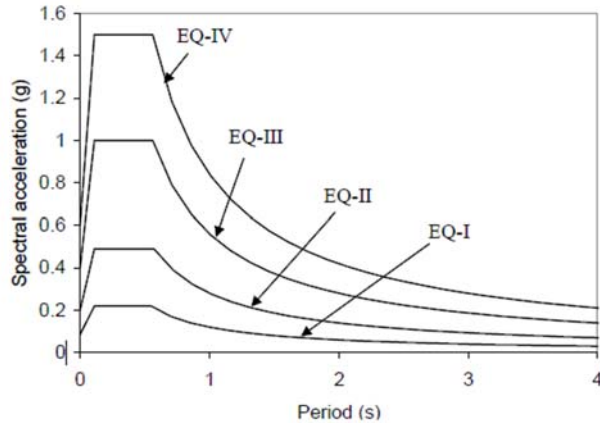
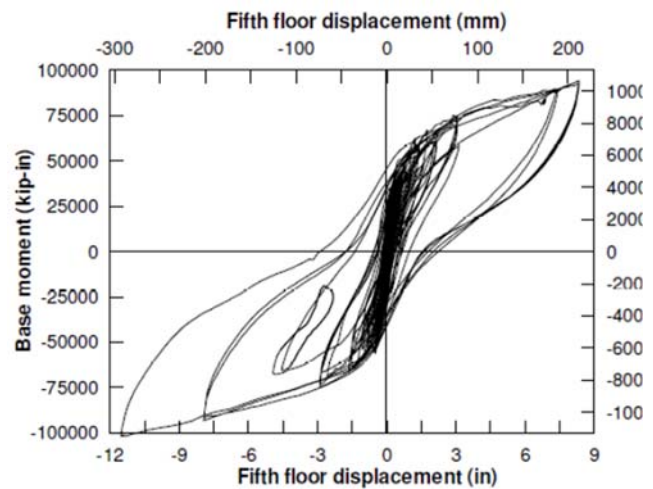


Figure 2-17. The 5% damped multiple-level acceleration response spectra, suggested for soil type Sc in high seismic zone (SEOAC 1999)



a) Negligible observed damage at the wall base



b) Stable and fat hysteresis loops

Figure 2-18. Successful seismic performance of the jointed walls (Priestly et al. 1999)

Hybrid walls were also tested under dynamic loading when they were used to design a prototype precast concrete parking structure at the University of California at San Diego (UCSD). This was done as part of a large collaborative project that involved shake table testing of a building system to establish a Diaphragm Seismic Design Methodology (DSDM). The building, shown in Figure 2-19, was subjected to extensive shake table testing on the NEES large high-performance

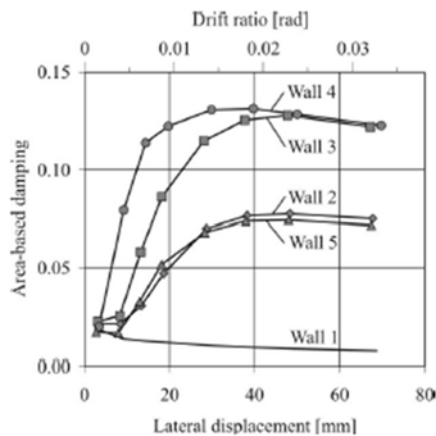
outdoor shake table. Although researchers (Fleischman et al. 2005) focused mainly on the interaction of the two hybrid walls with the surrounding building, their performance was evaluated when they were connected to the floor slabs using slotted insert shear connectors. The connectors, designed by IVI Inc., allowed for the vertical uplift of the wall as the building was subjected to different intensities of earthquakes. This detail, that excluded the walls from carrying gravitational forces, failed while transferring horizontal inertia forces between the floor and wall during the maximum considered input motions. This happened because uplift of the wall exceeded the slot capacity. Results from this testing were analytically evaluated by Belleri et al. (2014) and highlighted the overall excellent dynamic performance of this type of lateral force resisting system in the precast concrete building.



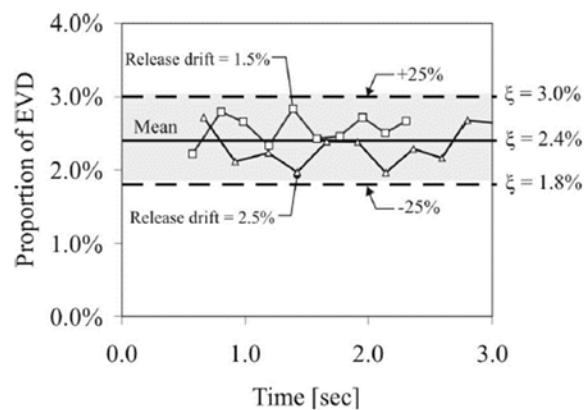
Figure 2-19. Shake table test of precast concrete building at UCSD (Fleischman et al. 2005)

Marriot (2009) reported on experimental shake table testing of a total of five post-tensioned walls, including one single precast wall and four walls with different configurations of external energy dissipaters with either fluid viscous dampers (FVD), tension-compression yielding mild

steel hysteretic dampers, or a combination of both. Using both near-field and far-field design level and maximum earthquake excitations, the performance of test walls was examined. All walls, including the SRW, provided satisfactory response, with the maximum drift reaching a value less than 1.5%, the target drift ratio. It was shown that hybrid walls incorporating tension-compression yielding dissipaters (Walls 3 and 4) were the most effective PT wall systems with respect to low peak floor-accelerations and peak displacements. These walls had the largest area-based hysteretic damping, as shown in Figure 2-20a. Hysteretic area-based damping due to nonlinear behavior of concrete was reported to be negligible for the SRW (Wall 1). To estimate the contact damping of the post-tensioned only wall, SRW was subjected to free-vibration testing with release drifts of 1.5% and 2.5%. Figure 2-20b shows the subsequent equivalent viscous damping ratio, on the order of 1 to 3%. This damping, proportional to the secant stiffness of the wall at release, would have included a combination of pure contact damping, material nonlinearity of the concrete at the rocking interface, and inherent viscous damping of the wall (Marriot 2009).



a) Area-based equivalent damping of walls with and without external energy dissipaters



b) Contact damping of SRW from free vibration testing

Figure 2-20. Energy dissipation capacity of rocking walls with and without externally mounted dampers (Marriot 2009)

Twigden (2016) also completed a series of snap-back and shake table testing on one SRW and two PreWEC systems. These test walls were designed with respective moment capacities of 149 (110), 195 (144), and 205 (151) kN.m (kip.ft) in conformance with the Direct Displacement-Based Design method (DDBD) (Priestley 2000) and were previously described as being tested during a series of quasi-static loading.

The results from the free-vibration testing were used to estimate the equivalent viscous damping (EVD) ratio of the walls following an adjusted logarithmic decrement energy method. Because of the nature of dynamic loading, EVD ratios of PreWECs were reported to be greater at high drifts and lower at low drifts compared to the results from the previously-performed quasi-static testing. For the SRW, this was decreased to a value of between 0.9-3.8% corresponding to drifts between 2-0% as compared to EVD ratios calculated from the cyclic tests.

During the shake table testing, a suite of seven spectrum-compatible ground motions were applied to each of the wall systems at up to four different intensity levels (i.e., EQ-I to EQ-IV). As reported by Twigden (2016), due to the increased moment capacity of PreWECs compared to the SRW, these wall systems were also tested to ground motions with higher intensities of $1.5 \times \text{EQ-IV}$ and $2 \times \text{EQ-IV}$. Because of the shake table limitations, all ground motions were scaled to contain the maximum velocity of 10.87 in./s (276 mm/s). Consequently, the input motions used for testing the wall systems did not comprise of near-field, forward directivity. After the completion of testing, Twigden (2016) reported negligible damage to both wall systems. The maximum lateral drift of 2.49% was observed for the SRW during design-level 1989 San Fernando earthquake, namely EQ-III:GM2 in this study; however this wall displaced to a lower value of 1.85% when it was subjected to the larger MCE level EQ-IV:GM2 input motion. This large difference in maximum lateral drift response of SRW was reported to be either due to unintended differences in

ground motion input or the natural frequency of the wall during the specific ground motion. It was shown that the 3.48% maximum drift of the SRW during EQ-IV level motions was decreased to almost half in both PreWECs. Increasing the number of connectors from four to six per joint slightly decreased the maximum drift response from a value of 1.79% to 1.61% during 2×EQ-IV:GM2. Following the recommendations of NZS 3101-06 (2006), Twigden (2016) used an equivalent viscous damping ratio of 5% for designing SRWs; however, as shown in Figure 2-21, this researcher suggested to increase the EVD of SRW to a value of 6.65% to limit the drifts to levels below the design value, within the framework of the DDBD method (Priestley, 2000).

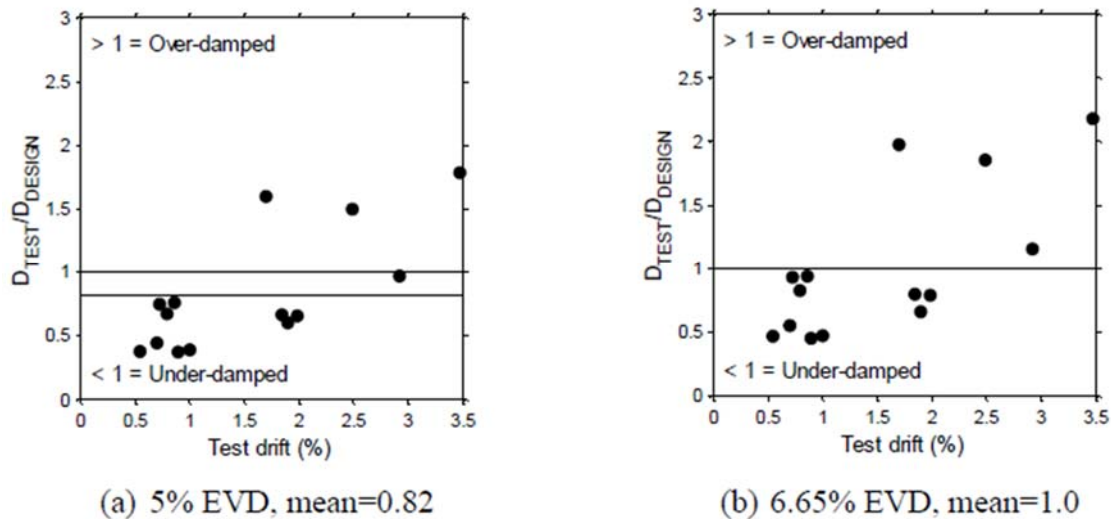


Figure 2-21. Comparison between DDBD method and shake table test results of SRW test unit with different damping ratios (Twigden 2016)

2.3. Dynamic Response Characterization

Several analytical approaches have been suggested for modeling the typical nonlinear response of rocking walls associated with base uplift. Damping due to impacts of the wall on top

of the foundation was one challenging aspect captured by the different models, as discussed in the following paragraphs.

2.3.1. Fiber models and Finite Element models

Fiber models were first developed by Kurama et al. (1999) to investigate both nonlinear static pushover and nonlinear dynamic time history response of a six-story unbonded post-tensioned concrete SRW. The fiber model, generated by a DRAIN-2DX program (1993), divided an element into different segments along its length; with each segment consisting of a number of discrete fiber layers representing concrete, steel, etc., and associated with appropriate uniaxial stress-strain relationships. In the model, the accuracy of the analysis increases with increasing the number of segments.

As shown in Figure 2-22, the wall panel was modeled with a number of fiber elements. Uniaxial compressive stress-strain concrete fibers with zero tensile strength and stiffness were used at the contact region to represent the gap opening. PT tendons were modeled with truss elements fixed at top and bottom representing the anchorage. An initial tensile force was applied to this truss element and equilibrated by compressive forces in concrete fiber elements. This fiber model in general accounts for axial-flexural interaction in the wall, gap opening at base, hysteretic behavior of PT steel, confined concrete near the ends of the wall base, and unconfined concrete (including concrete crushing and cracking).

Kurama et al. (1999) used this model to investigate the lateral load behavior of precast walls designed with varying parameters (e.g., number of PT tendons, wall length, location of tendons, and confinement details) and to study their effect on onset of softening, yielding of PT, and rupture of confinement reinforcement.

Using mass and stiffness proportional Rayleigh damping, Kurama et al. (1999) also conducted dynamic analysis on SRWs applying a 3% viscous damping ratio. The results from nonlinear time history analysis of unbonded precast concrete walls showed their larger displacement but lower residual drift compared to the cast-in-place (CIP) RC walls.

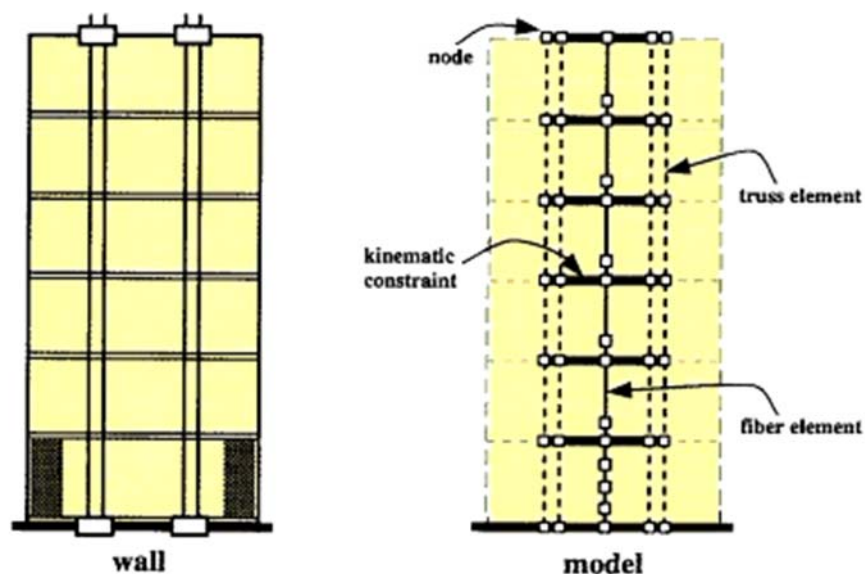


Figure 2-22. Fiber model used for modelling precast concrete walls (Kurama et al. 1999)

Kurama (2000) extended the fiber model for seismic design of unbonded post-tensioned precast concrete walls with external viscous fluid dampers connected to adjacent column braces. The supplementary viscous dampers were represented by truss elements with energy dissipation modeled with stiffness proportional damping. Using a 3% equivalent viscous damping as previously suggested by the researcher for an SRW, the nonlinear time history analysis of walls either with or without external dampers highlighted the impact of additional energy dissipation on a reduction in the maximum displacement of the precast walls.

The fiber model by Kurama (1999) has been used by other researchers to study the behavior of rocking walls. Erkman and Schultz (2009) used an extension of Kurama's model to designate

the self-centering behavior of precast walls with various PT configurations even though some PT tendons were allowed to yield. Belleri et al. (2013) used different rocking wall modeling techniques, including a fiber model (as shown in Figure 2-23a) to compare the calculated nonlinear time history response of precast walls adopted as lateral force resisting systems of the parking structure at UCSD (Fleischman et al. 2005). As they reported, the fiber elements used in all these model are based on a force formulation and on the assumption that plane sections remain plane, which is not true for regions of the wall immediately adjacent to the wall-foundation interface. They concluded therefore that the fiber model might be optimal to estimate the global response of the wall panels but not very accurate for predicting aspects of their local behavior such as contact length and strain distribution (Belleri et al. 2013).

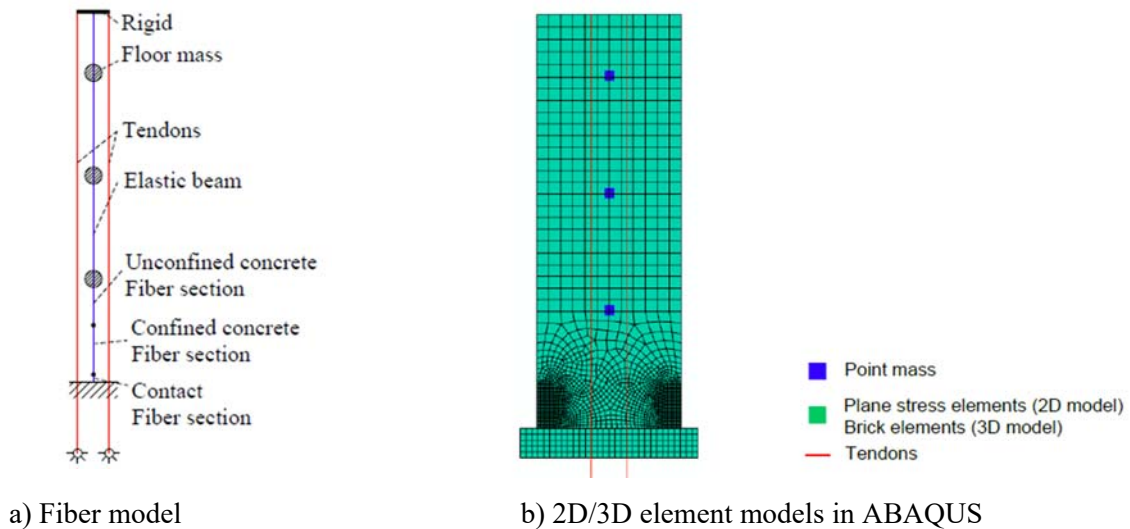


Figure 2-23. Fiber model and Finite Element model (Belleri et al. 2013)

More complicated models were therefore generated using finite element software ABAQUS (2011). This approach was first used by Kurama (2000) to validate the fiber model developed to capture the response of walls either with or without additional viscous dampers.

Henry (2011) also developed a finite element model using ABAQUS and the model exhibited excellent accuracy in capturing the cyclic response of SRWs and PreWECs. As presented in Figure 2-23b, Belleri et al. (2013) modeled the wall panel with either brick elements (3D model) or plane stress elements (2D model), while PT tendons were captured by truss elements. They modeled the contact surface using a “surface to surface contact” interaction, with “rough” tangential and “hard contact” normal behavior types and inelastic properties of concrete using a “concrete damaged plasticity” model available in software (ABAQUS 2011). An FEM was found out to be complex with respect to using detailed material behavior and sophisticated contact algorithm (Belleri et al. 2013) as well as not being very accurate in calculating the nonlinear dynamic response of the precast walls (Ma et al. 2006).

2.3.2. Lumped plasticity and multi-spring models

Lumped plasticity models, also called concentrated plasticity models, have been used by several researchers (e.g., Pampanin et al. 2001; Palermo et al. 2004) to model precast rocking walls, as these walls experience their main inelastic behavior at particular points such as wall-foundation interface. The resulting nonlinearity occurred due to the gap opening at the wall base is being modeled as a zero-length spring. Moment-rotation characteristics of this spring are usually assigned from the appropriate bilinear elastic hysteresis behavior at the base subsequent to section analysis or experimental results. By concentrating the plasticity of a rocking wall at its base, the wall panel could be modeled using elastic elements. If additional dampers were to be used to increase the energy dissipating capacity of wall systems, a parallel rotational spring with appropriate elasto-plastic hysteresis response should be incorporated as shown in Figure 2-24 (taken from Marriot et al. 2009). According to this figure and as recommended by Marriot et al.

(2009), the internally grouted mild steel reinforcement in hybrid walls can be modeled with Modified Takeda (Otani 1974) to account for bond degradation between steel and concrete. The measured hysteretic response of different types of externally-mounted dampers in precast wall systems can be directly used to capture moment-rotational behavior of this rotational spring.

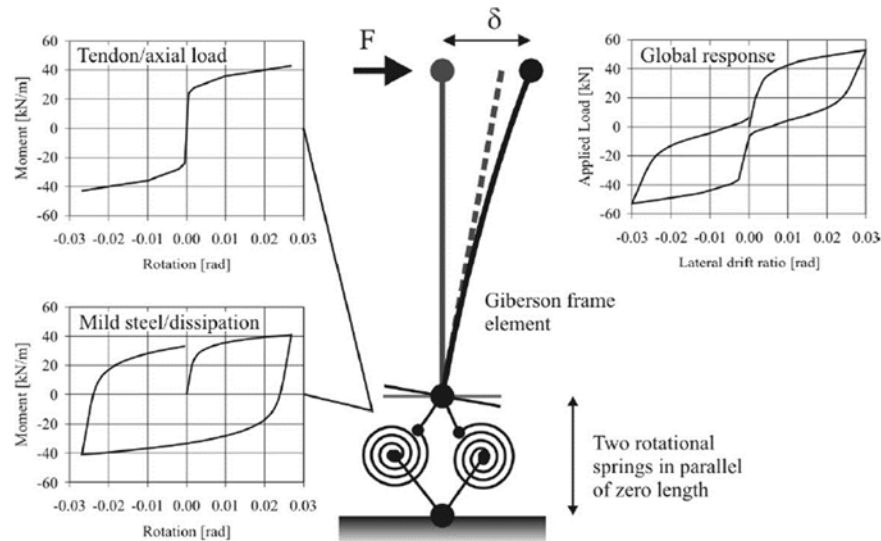


Figure 2-24. Lumped plasticity model with two parallel rotational springs (Marriot et al. 2009)

Rahman and Sritharan (2006) also conducted extensive nonlinear dynamic analysis on two five-story unbonded post-tensioned jointed precast wall systems at 60% scale, established as the Direct Displacement-Based (DDBD) and Force-Based (FBD) solutions for the prototype building used in the PRESSS program (Priestley et al. 1999). In this model, as shown in Figure 2-25, walls were modeled with elastic beam-column elements and the rocking interface was represented by a non-linear rotational spring at the base of each beam-column element. The vertical non-linear inelastic springs represent UFP connectors connected to rigid beam-column elements extending from the centerline of each wall toward the centerline of the jointed wall (Rahman and Sritharan, 2006). This study, mostly focused on multiple-level seismic performance evaluation of these

hybrid walls, showed that, when designed with DDBD, a significantly lower design base shear was achieved for the wall systems, leading to higher lateral drifts during strong motions. A modification in the DDBD approach was suggested to include higher ductility demands.

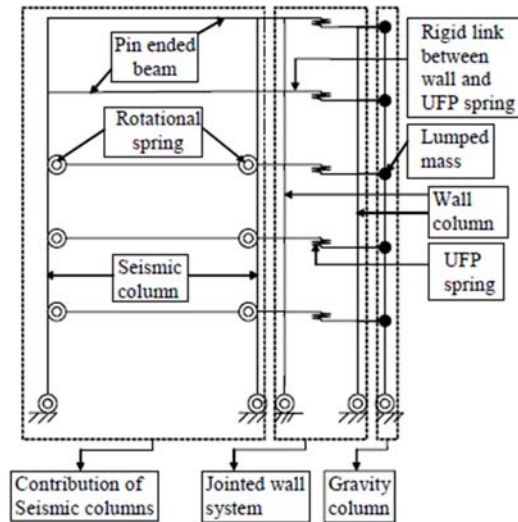


Figure 2-25. Analytical model for the five-story building with the jointed wall system (Rahman and Sritharan 2006)

The theory of lumped plasticity models was also used to idealize the wall with a single degree of freedom (SDOF) system, as shown in Figure 2-26, implementing a nonlinearly-elastic rotational base connection to solve its governing differential equation using numerical integration techniques.

$$m\ddot{u} + c\dot{u} + ku = -m\ddot{u}_g$$

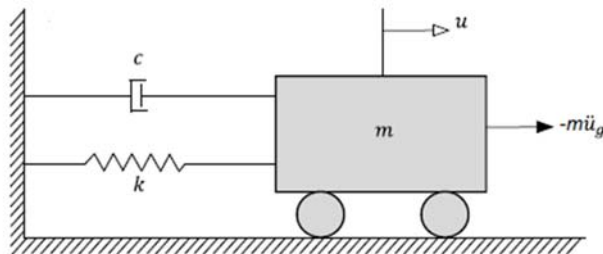


Figure 2-26. Single degree of freedom model as shown in Twigden (2016)

Ma et al. (2006) and Twigden (2016) used this SDOF model; they, however, applied two different approaches to capture the damping associated with the dynamic response of precast rocking walls. Ma et al. (2006) modeled damping of the rocking wall by applying the apparent coefficient of restitution (c.o.r) as estimated from an equation developed by Housner (1963) and previously presented in Chapter One (Equation 1-2). Using this approach, velocity of the rocking wall was reduced by a geometry-dependent and therefore constant c.o.r whenever the wall rotated through zero displacement. Ma et al. (2006) showed that damping greatly varies the response, and the equation developed by Housner (1963) may not be accurate during all impacts of the wall at the top of the foundation. As reported by Kalliontzis and Sritharan (2014), the rocking response was improved by using a c.o.r varying as a function of the angular displacement peak. In the SDOF model of rocking walls presented by Twigden (2016), an equivalent viscous damping ratio of 2% was suggested rather than controlling the velocity drop using a c.o.r. This tangential stiffness damping was shown to best emulate the shake table results of one SRW and two PreWECs in terms of displacement and acceleration. As reported by Twigden (2016), the SRW was modeled with a bilinear elasto-plastic spring with data measured during its cyclic testing. A second spring was also combined in parallel to represent the measured cyclic hysteretic behavior of O-connectors used for PreWECs.

The lumped plasticity models were not adequate to capture the exact response of the walls, because the rocking interface and the related damping due to rocking were not properly modeled. In addition, understanding the hysteretic cyclic response of spring elements is required for this model. For this purpose, more complicated multi-spring models were developed as introduced by Conley et al. (1999) to model the PRESSS building's post-tensioned rocking walls. He presented a two-spring model for the jointed walls, shown in Figure 2-27, in which two elastic compression-

only axial springs were positioned at either end of the wall at the center of the contact length. When the lateral load was applied, this model began to pivot about the springs and therefore captured the wall uplift.

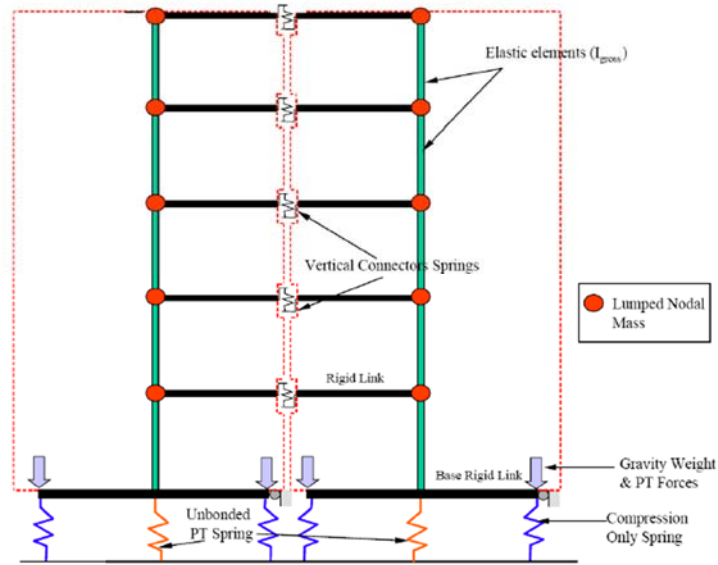


Figure 2-27. Two-spring model of jointed walls in PRESSS building (Conley et al. 1999)

The idea of using multiple springs at the rocking interface was extended by other researchers (e.g., Kim 2002; Palermo et al. 2004). Marriot et al. (2009) developed a multi-spring contact interface for modelling the rocking walls either with or without additional dampers, as shown in Figure 2-28. To analyze the systems under shake table dynamic loading, a contact viscous damping of 2.4%, previously estimated from free vibration testing of SRWs, was implemented in this model. Since the researchers related the contact damping to both displacement and velocity of the rocking system, this damping was modeled with a velocity-proportional damper (i.e., the viscous damper in Figure 2-28) and a displacement-proportional damper (i.e., the friction damper in Figure 2-28) at the effective height of the system. The damping coefficient and the friction damper force were constant and proportional to the secant stiffness to the maximum displacement

of the system to provide the required 2.4% contact damping, as shown in Figure 2-29. While this model was creative in terms of adding damping due to impact, the calculated results did not present a matching comparison for dynamic snap-back test results of the SRW.

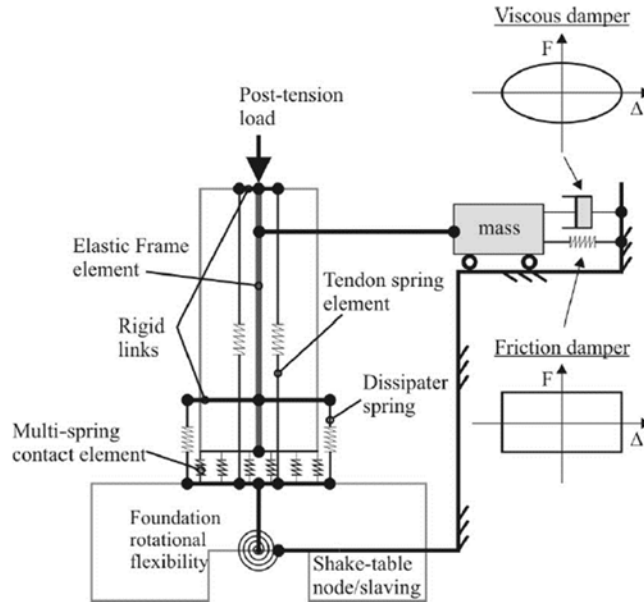


Figure 2-28. Multi-spring model with contact damping included (Marriot et al. 2009)

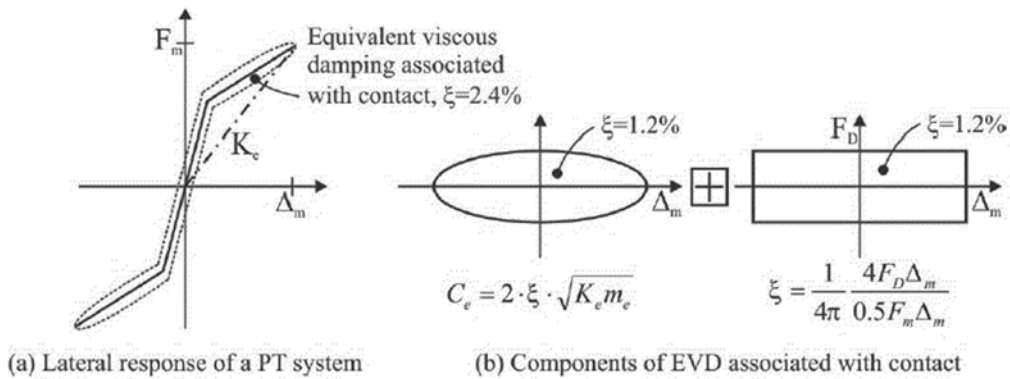


Figure 2-29. Viscous and friction dampers representing 2.4% contact damping (Marriot et al. 2009)

Watkins et al. (2013) suggested implementation of an improved uniaxial concrete stress-strain model for multi-springs of the wall-to-foundation interface (see Figure 2-30). These springs were modeled as a bed of truss elements at the wall base and were experimentally verified as providing better capture of wall lateral drifts at which crushing of concrete occurs. Comparison of the measured nonlinear cyclic response compared with the results of five tests on a SRW also reflected the accuracy of the model in capturing the residual displacement.

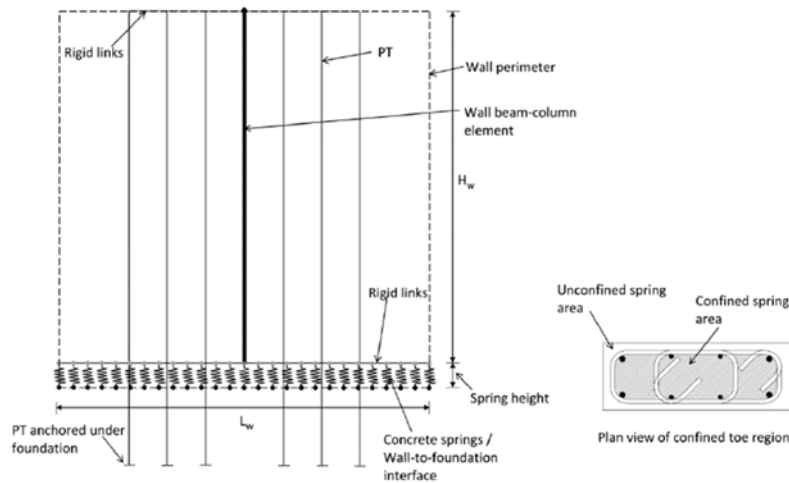


Figure 2-30. Multi-spring model developed by Watkins et al. (2013) using modified concrete springs

As summarized above, most of the aforementioned techniques for modelling the precast rocking walls were successful in capturing their static cyclic response, but accuracy of these models in emulating the dynamic test results was directly dependent on the assumed damping due to impact. Therefore, an accurate estimation of all energy dissipation components associated with rocking of the wall is required to produce more precise dynamic responses.

2.4. Codification

The findings from the experimental and numerical investigations with respect to the seismic behavior of self-centering concrete walls were used to develop appropriate design code provisions. For this purpose, the American Concrete Institute (ACI) set up Innovation Task Group 5 (ITG-5) to release two documents (i.e., ITG-5.1 2007; ITG-5.2 2009) based on the results from the PRESSS program (Priestley et al. 1999) and subsequent research on unbonded post-tensioned precast concrete walls (e.g., Kurama 2002; Stanton and Nakaki 2002). ITG-5.1 (2007) outlines seismic acceptance criteria for special unbonded post-tensioned precast concrete walls. According to this document, two separate experimental tests are required to successfully validate a new precast wall system and confirm that it meets requirements deemed by ACI ITG-5.1, including a minimum hysteretic damping ratio (i.e., about 8%) as well as system stiffness around zero drift (i.e., secant stiffness to the drift of ± 0.1 times the maximum applied drift should not be less than 0.1 times the initial stiffness) to control excessive displacements of the post-tensioned systems and low-cycle fatigue effects resulting from continuation of the system response following a major earthquake. To prevent slippage of a self-centering wall, this document limits the relative displacement between the wall base and the foundation to a value of 0.06 in. Jointed and hybrid walls satisfying the requirements of ITG-5.1 (2007) can be designed following the procedures outlined in ITG-5.2 (2009).

In 2006, appropriate design provisions for the application of unbonded PT precast concrete elements were also introduced into Appendix B of the New Zealand concrete design standard (i.e. NZS 3101-06 2006). Due to the direct correlation between damage and displacement, a DDBD approach (Priestley 2000), as described in Chapter 1, is applied in this document for use in seismic lateral force design of an unbonded PT system. Using this approach, NZS 3101-06 (2006) suggests

use of an equivalent viscous damping ratio of 5% for SRWs and the following weighted approach to calculate the equivalent viscous damping ratio of post-tensioned walls designed with additional dissipative systems.

$$\xi_{hys} = 5 + 30\left(1 - \frac{1}{\sqrt{\mu}}\right) \quad (\text{Equation 2-2})$$

where, μ is the ductility of the system and ξ_{hys} is the equivalent viscous damping ratio due to hysteretic action.

The New Zealand Concrete Society also detailed more specific design guidelines and design examples in their PRESSS Design Handbook (Pampanin et al. 2010). In this guideline, the equivalent viscous damping ratio used to design walls following a DDBD approach is defined by Equation 2-3, based on the moment contribution of additional hysteretic dampers.

$$\xi_{eq} = 5 + 30 \frac{\left(1 - \frac{1}{\sqrt{\mu}}\right)}{(\lambda + 1)} \quad (\text{Equation 2-3})$$

$$\lambda = \frac{M_{pt} + M_N}{M_s} \geq \alpha_o$$

where, M_{pt} , M_N , and M_s are the flexural strength contributions of the PT tendons, axial load, and energy dissipating devices, and α_o is the over-strength factor for the energy dissipating devices. The aforementioned equations do not include contact damping due to impacts of the wall on top of the foundation.

2.5. References

Aaleti, S. and Sritharan, S. A. (2009) simplified analysis method for characterizing unbonded post-tensioned precast wall systems. *Engineering Structures*; **31**(12): 2966–2975.

- ABAQUS (2011), User's manual version 6.8. Dassault Systèmes Simulia Corp.
- ACI 318-11 (2011) Building code requirements for structural concrete. Farmington Hills, MI.
- ACI Innovation Task Group 5.1. (2007). Acceptance criteria for special unbonded post-tensioned precast structural walls based on validation testing and commentary. American Concrete Institute, Farmington Hills, MI.
- ACI Innovation Task Group 5.2. (2009) Requirements for design of a special unbonded post-tensioned precast shear wall satisfying ACI ITG-5.1 and commentary (ACI ITG-5.2). American Concrete Institute, Farmington Hills, MI.
- Belleri, A., Torquati, M., and Riva, P. (2013) Finite element modelling of "rocking walls". *Proceedings of the 4th ECCOMAS Thematic Conference on Computational Methods in Structural Dynamics and Earthquake Engineering, Kos Island, Greece.*
- Belleri, A., Schoettler, M. J., Restrepo, J. I, and Fleischman, R. B. (2014) Dynamic Behavior of Rocking and Hybrid Cantilever Walls in a Precast Concrete Building (with Appendix). *ACI Journal*; **111**(3): 661-672.
- Cheok, G. S. and Lew, H. S. (1991) Performance of precast concrete beam-to-column connections subject to cyclic loading. *PCI Journal*, **36** (3), 56-67.
- Conley, J., Sritharan, S., and Priestley, M. J. N. (1999) Precast Seismic Structural Systems PRESS-3: The five story precast test building vol. 3-1: wall direction response. Report No. SSRP-99/19. Department of Structural Engineering, University of California, San Diego.
- Chopra, A. K. (2007) Dynamics of structures: Theory and applications to earthquake engineering. 3rd ed. Upper saddle river, NJ: Prentice Hall. Xxxiv, 876 p.
- Englekirk, R. E. (2002) Design-construction of the Paramount - A 39-story precast prestressed concrete apartment building. *PCI Journal*, **47**(4), 56-71.
- Erkmen, B. and Schultz, A.E. (2009) Self-centering behavior of unbonded post-tensioned precast concrete shear walls. *Journal of Earthquake Engineering*; **13**(7): 1047-1064.

- Fleischman, R. B., Naito, C., Restrepo, J., Sause, R., Ghosh, S. K., Wan, G., Schoettler, M., and Cao, L. (2005) precast Diaphragm Seismic Design Methodology (DSDM) project, part 2: research program. *PCI Journal*, **50**(6), 14-31.
- Henry, R.S. (2011) Self-centering Precast Concrete Walls for Buildings in Regions with Low to High Seismicity, PhD Thesis. University of Auckland.
- Holden, T. J. (2001) A Comparison of the seismic performance of precast wall construction: Emulation and hybrid approaches. Research Report 2001-04, University of Canterbury, Christchurch.
- Kalliontzis, D. and Sritharan, S. (2014) A finite element approach for modelling controlled rocking systems. *Proceedings of the 2nd European Conference on Earthquake Engineering and Seismology, Istanbul, Turkey*.
- Kim, J. (2002) Behavior of hybrid frames under seismic loading. University of Washington.
- Kurama, Y. C., Sause, R., Lu, L., and Pessiki, S. (1999) Seismic behavior and design of unbonded post-tensioned precast concrete walls. *PCI Journal*, **44**(3), 72-89.
- Kurama, Y. C., Sause, R., Pessiki, S., and Lu, L. (1999) Lateral load behavior and seismic design of unbonded post-tensioned precast concrete walls. *ACI Structural Journal*, **96**(4), 622-632.
- Kurama, Y. C. (2000) Seismic design of unbonded post-tensioned precast concrete walls with supplemental viscous damping. *ACI Structural Journal*; **97**(4): 648-658.
- Kurama, Y. C. (2001) Simplified seismic design approach for friction-damped unbonded post-tensioned precast precast concrete walls. *ACI Structural Journal*, **98**(5), 705-716.
- Kurama, Y. C. (2002) Hybrid post-tensioned precast concrete walls for use in seismic regions. *PCI Journal*; **47**(5): 36-59.
- Ma, Q. (2009) The mechanics of rocking structures subjected to ground motion, PhD Thesis. University of Auckland.
- Marriott, D., Pampanin, S., Bull, D., and Palermo, A. (2008) Dynamic testing of precast, post-tensioned rocking wall systems with alternative dissipating solutions. *Bulletin of the New Zealand Society for Earthquake Engineering*, **41**(2), 90-103.

- Marriot, D. (2009) The development of high-performance post-tensioned rocking systems for the seismic design of structure, PhD Thesis. University of Canterbury.
- McKenna, F., Fenves, G., and Scott, M. (2000) Open system for earthquake engineering simulation. University of California, Berkeley, CA.
- Nakaki, S. D., Stanton, J. F., and Sritharan, S. (1999) An overview of the PRESSS five-story precast test building. *PCI Journal*; **44**(2) 26-39.
- Nicknam, A. and Filiatrault, A. (2012) Seismic design and testing of propped rocking wall systems. *Proceedings of the 15th World Conference on Earthquake Engineering (15WCEE)*, Lisbon, Portugal.
- NZS 3101-06 (2006) Concrete structures standards. Standards New Zealand, Wellington, New Zealand.
- Otani, S. (1974) SAKE, A computer program for inelastic response of R/C framed to earthquakes. Report UILU-Eng-74-2029, University of Illinois, Urbana Champaign.
- Palermo, A. (2004) The use of controlled rocking in the seismic design of bridges. Technical University of Milan, Milan.
- Pampanin, S., Priestley, M. J. N., and Sritharan, S. (2001) Analytical Modelling of the Seismic Behavior of Precast Concrete Frames Designed with Ductile Connections. *Journal of Earthquake Engineering*; **5**(3) 329-367.
- Pampanin, S., Cattanach, A., and Haverland, G. (2010) PRESSS design handbook: seminar notes. Technical report, TR44, New Zealand Concrete Society, Auckland, N.Z.
- Pampanin, S., Kam W., Haverland, G., and Gardiner, S. (2011) Expectation Meets Reality: Seismic Performance of Post-Tensioned Precast Concrete Southern Cross Endoscopy Building During the 22nd Feb 2011 Christchurch Earthquake, NZ Concrete Industry Conference, Rotorua.
- Perez, F. J., Sause, R., Pessiki, S., and Lu L.W. (2002) Lateral load behavior of unbonded post-tensioned precast concrete walls. *Advances in Building Technology, Vols I and II proceedings*, ed. M. Anson, J.M. Ko, and E.S.S. Lam, Amsterdam: Elsevier Science Bv. 423-430.

- Perez, F. J., Pessiki, S., and Sause, R. (2004) Experimental and analytical lateral load response of unbonded post-tensioned precast concrete walls. ATLSS Report No. 04-11, Lehigh University, Bethlehem, PA.
- Priestley, M. and Tao, J. (1993) Seismic response of precast prestressed concrete frames with partially debonded tendons. *PCI Journal*, **38**(1): 58–69.
- Priestley, M. J. N. and MacRae, G. A. (1996) Seismic tests of precast beam-to-column joint subassemblages with unbonded tendons. *PCI Journal*, **41**(1): 64-80.
- Priestley, M. J. N., Sritharan, S., Conley, J. R., and Pampanin, S. (1999) Preliminary results and conclusions from the PRESSS five-story precast concrete test building. *PCI Journal*, **44**(6), 42-67.
- Prakash, V., Powell, G., and Campbell, S. (1993) DRAIN-2DX base program description and user guide. Technical report UCB/SEMM-93-17, University of California, Berkeley.
- Rahman, A. M. and Restrepo, J. I. (2000) Earthquake resistant precast concrete buildings: seismic performance of cantilever walls prestressed using unbonded tendons. Research Report 2000-5, University of Canterbury, Christchurch.
- Rahman, M. and Sritharan, S. (2006) An evaluation of force-based design vs. direct displacement-based design of jointed precast post-tensioned wall systems. *Earthquake Engineering and Engineering Vibration*, **5**(2): 285-296.
- Seismology Committee (1999) Recommended lateral force requirements and commentary (Blue book), Structural Engineers Association of California, SEAOC, Calif., 327–421.
- Schoettler, M. J., Belleri, A., Dichuan, Z., Restrepo, J. I., and Fleischman, R. B. (2009) Preliminary results of the shake-table testing for the development of a diaphragm seismic design methodology. *PCI Journal*; **54**(1): 100–124.
- Sritharan, S., Aaleti, S., Henry, R. S., Liu, K. Y., and Tsai, K. C. (2008) Introduction to PreWEC and key results of a proof of concept test. *M. J. Nigel Priestley Symposium*, North Tahoe, California, IUSS Press, Pavia, Italy, 95-106.

- Sritharan, S., Aaleti, S., Henry, R., Liu, K., and Tsai, K. (2015) Precast concrete wall with end columns (PreWEC) for earthquake resistant design. *Earthquake Engineering and Structural Dynamics*, **44**(12), 2075–2092.
- Stanton, J. F., Stone, W. C., and Cheok, G. S. (1997) A hybrid reinforced precast frame for all seismic regions. *PCI Journal*, **42**(2): 20-32.
- Stone, W. C., Cheok, G. S., and Stanton, J. F. (1995) Performance of hybrid moment-resisting precast beam-column concrete connections subjected to cyclic loading. *ACI Structural Journal*, **92**(2): 229.
- Shultz, A. E. and Magana, R. A. (1996) Seismic behavior of connections in precast concrete walls. *Mete A. Sozen Symposium*, ACI SP 162, American Concrete Institute, Farmington Hills, MI.
- Twigden, K. M. and Henry, R.S. (2015) Experimental response and design of O-connectors for rocking wall systems. *Journal of Structures*, **44**(3), 261-271.
- Twigden, K. M. (2016) Dynamic response of unbonded post-tensioned concrete walls for seismic resilient structures, PhD Thesis. University of Auckland.
- Watkins, J., Henry, R., and Sritharan, S. (2013) Computational modelling of self-centering precast concrete walls. *Proceedings of the 4th ECCOMAS Thematic Conference on Computational Methods in Structural Dynamics and Earthquake Engineering*, Kos Island, Greece.

CHAPTER 3
SINGLE PRECAST CONCRETE ROCKING WALLS AS EARTHQUAKE
FORCE-RESISTING ELEMENTS

A paper submitted to the Journal of Earthquake Engineering and Structural Dynamics

Maryam Nazari, Sri Sritharan, and Sriram Aaleti

3.1. Abstract

Numerous Precast concrete walls with unbonded post-tensioning (PT) provide a simple self-centering system. Yet, its application in seismic regions is not permitted as it is assumed to have no energy dissipation through a hysteretic mechanism. These walls, however, dissipate energy imparted to them due to the wall impacting the foundation during rocking and limited hysteretic action resulting from concrete nonlinearity. The energy dissipated due to rocking was ignored in previous experimental studies because they were conducted primarily using quasi-static loading. Relying only on limited energy dissipation, a shake table study was conducted on four Single Rocking Walls (SRWs) using multiple-level earthquake input motions. All walls generally performed satisfactorily up to the design-level earthquakes when their performance was assessed in terms of the maximum transient drift, maximum absolute acceleration, and residual drift. However, for the maximum considered earthquakes, the walls often showed higher than the permissible drifts. Combining the experimental results with an analytical investigation, it is shown that SRWs can be designed as earthquake force-resisting elements to produce satisfactory performance under design-level and higher intensity earthquake motions.

Keywords: rocking wall, precast concrete, unbonded post-tensioning, shake table testing, seismic design, performance-based evaluation

3.2. Introduction

Investigations into improving seismic performance of precast concrete structures were initiated during the 1990's with the PREcast Seismic Structural Systems (PRESSSS) program (Priestley et al. 1999). In one of the earlier studies carried out in this program, Priestley and Tao (1993) suggested the use of applying post-tensioning (PT) tendons to tie precast components in building frames. Within the second phase of this program, researchers at Lehigh University analytically investigated this concept for precast concrete walls (Kurama et al. 1999). The unbonded post-tensioning connection (as shown in Figure 3-1a) enables the self-centering behavior for these walls following a base excitation, since the PT tendons are designed to remain elastic when the wall uplifts at the base and elongates the tendon (Figure 3-1b). For a moment demand at the wall base resulting from an earthquake excitation, a compressive force develops at the wall toe to balance the PT force, providing the resisting moment (Figure 3-1c). Stress distribution over a contact length at the rocking interface gives rise to this resultant force.

The overall lateral resistance behavior of these self-centering walls is generally idealized with a bilinear elastic hysteresis rule (Kurama et al. 1999). However, a small amount of hysteretic energy dissipation may occur primarily due to material nonlinearity of concrete at wall toes as well as the PT tendons if they experience yielding. Perez et al. (2004) observed this limited hysteresis action through monotonic and cyclic testing of five precast concrete walls. Apart from the inherent viscous damping of the system, some energy dissipation can also take place due to the wall toe

impacting on top of the footing. This form of damping was not captured in previous studies when quasi-static load was used (e.g., Perez et al. 2004).

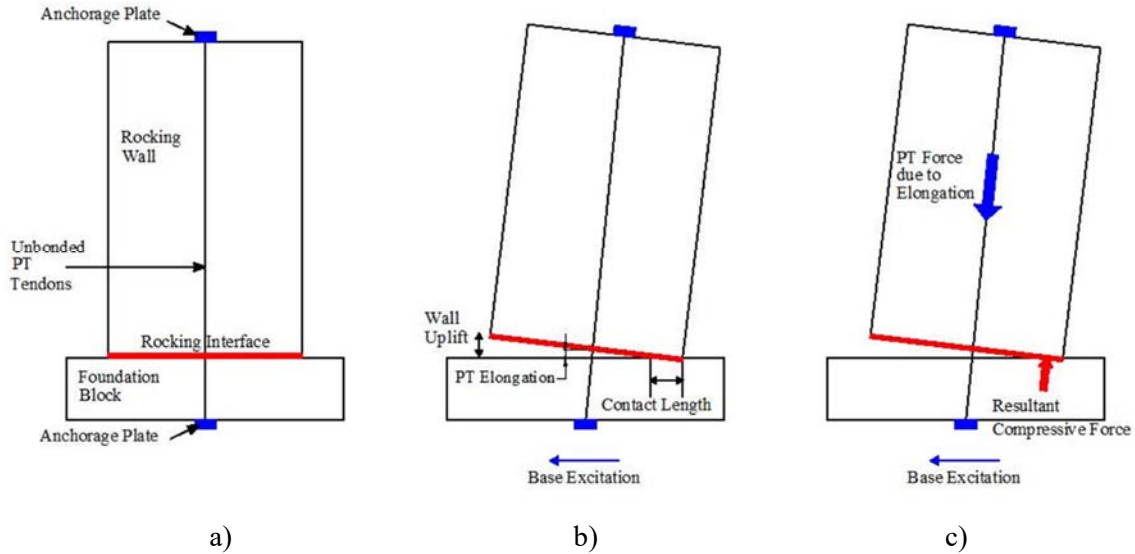


Figure 3-1. (a) Precast concrete wall with unbonded PT (b) wall uplift due to base excitation, and (c) moment resisting mechanism during rocking

To overcome the low energy dissipation capacity of Single Rocking Walls (SRWs), several self-centering wall systems with supplementary energy dissipating elements have been developed (e.g., Priestley et al. 1999; Rahman and Restrepo 2000; Sritharan et al. 2015). Based on the experimental findings from these systems, acceptance criteria for special concrete walls were established in ACI ITG-5.1 (2008). In this document, the relative energy dissipation ratio (β_h), a measure of the hysteretic damping of the system, is required to be at least 12.5%. This ratio, which corresponds to an equivalent viscous damping of about 8%, is expected to be provided through hysteretic energy dissipating elements. This requirement prevents the use of SRWs in high seismic zones.

In 2008, Marriot et al. (2008) conducted a series of shake table tests on a total of five post-tensioned walls, which included one single precast wall and four walls with different configurations of external energy dissipaters. Using a near-field and a far-field design-level earthquake excitation, the performance of these test walls was examined. All walls, including the SRW, provided satisfactory response with the maximum drift reaching a value less than the target drift of 1.5%. However, a total damping ratio in the order of 1 to 3% was reported for the SRW, through a free vibration testing. This paper investigates the acceptability of SRWs in seismic design using shake table testing. Four unbonded post-tensioned precast Single Rocking Walls were subjected to a series of earthquake excitations with varying intensities. Using the experimental data and results from an analytical study, different energy dissipation components of SRWs are first quantified. The performance of test walls is then evaluated based on multi-hazard acceptance criteria. Finally, improvising seismic design of SRWs is examined.

3.3. Experimental Program

3.3.1. Prototype structure

For this study, a six-story prototype office building was designed for a site class in Los Angeles, California (seismic zone 4 and soil type S_c). The typical plan view including the location of three SRWs and their dimensions are shown in Figure 3-2.

The prototype building was designed according to IBC (2009) and ASCE 7-05 (2005), resulting in each SRW to resist a base shear of 1895 kN (426 kip) and overturning moment of 30231 kN-m (22297 kip-ft) in the transverse direction.

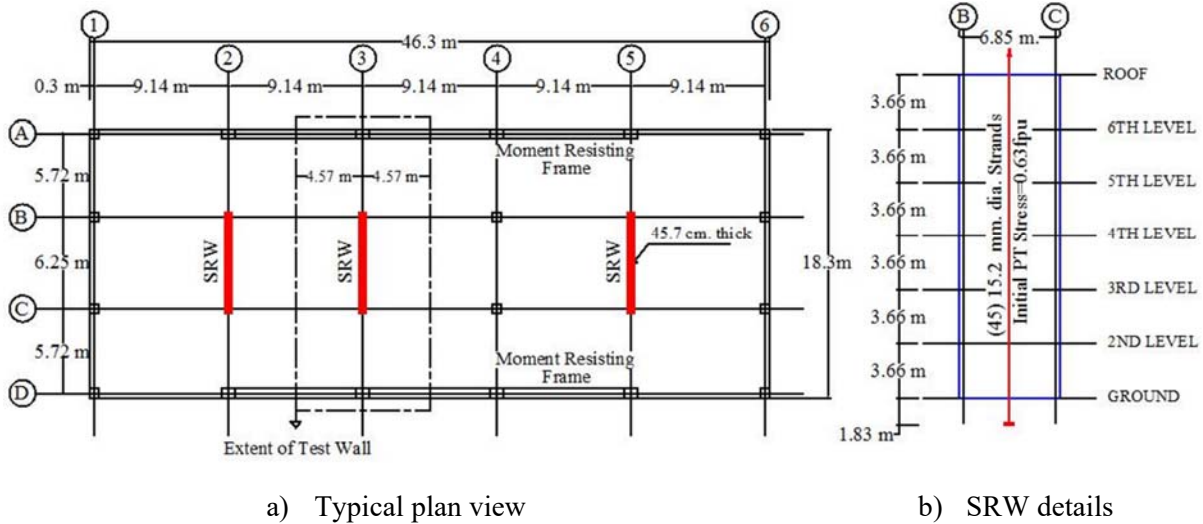


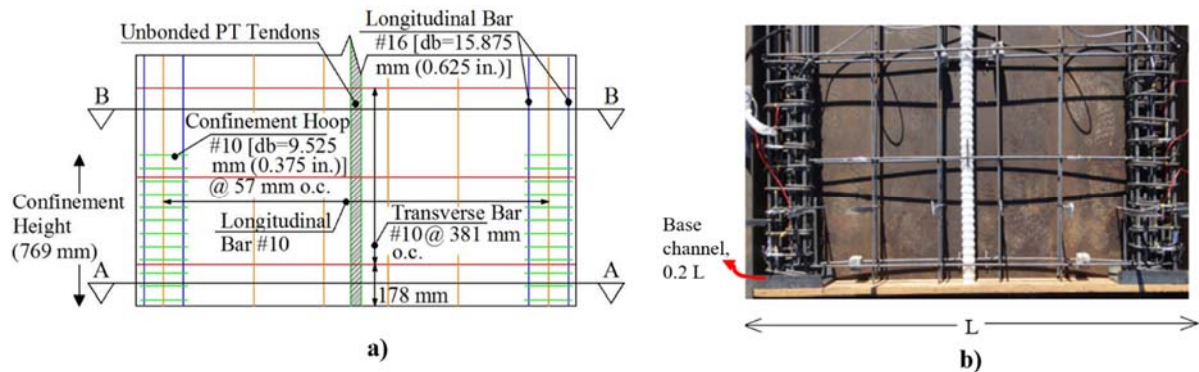
Figure 3-2. Details of the prototype building (1 m = 3.28 ft)

3.3.2. Test matrix

The test matrix included four SRWs, namely SRW1 through SRW4, at 5/18 scale of the prototype dimensions. To this end, the prototype SRW (as shown in Figure 3-2b) was simplified to an equivalent single degree of freedom (SDOF) system, with an effective height of 15.4 m (50.4 ft) and mass of 1170 kN.s²/m (6681 lb.s²/in), considering a linear rocking mode shape for the structure. SRW1 identically replicated the prototype wall and was 190.5 cm (6.25 ft) long, 487.7 cm (16 ft) tall and 12.7 cm (5 in.) thick, with a seismic mass of 25.1 kN.s²/m (143.2 lb.s²/in) located at the height of 4.27 m (14 ft). This wall was detailed according to the requirements of ACI 318-11 (2011), using a specified concrete strength of 41.4 MPa (6 ksi) and A706 Grade 60 reinforcement. As shown in Figure 3-3, the wall was reinforced only with the minimum amounts of longitudinal and transverse reinforcement. Following the ACI-ITG 5 guidelines (2008; 2009) and recommendations from Aaleti and Sritharan (2009), detailing also included confinement of a 76.9 cm (30.25 in.) long boundary element at each end of the wall, using No. 10 ($d_b = 9.525$ mm (0.375 in.), where d_b is the diameter of rebar) hoops with cross-ties spaced at 5.7 cm (2.25 in.). In

addition, the wall base corners were protected from experiencing any damage to cover concrete by placing a steel channel over $0.2L$ length, where L is the wall length (see Figure 3-3b). As recommended by ITG 5 (2008; 2009), prior to post-tensioning the wall, a steel fiber reinforced grout with a specified strength of 68.95 MPa (10 ksi) was placed as the interface material to ensure full rigid contact between the wall base and the foundation.

The Simplified Analysis (SA) method proposed by Aaleti and Sritharan (2009) was used as a tool to design the amount of PT in SRW1. In this method, the required area of tendons is determined based on moment equilibrium of forces acting on the wall base, using an equivalent stress block and a tri-linear approximation for estimating the neutral axis depth variation with wall base rotation without the need for iteration. Accordingly, 4-12.7 mm (0.5 in.) diameter PT tendons (a total area of 3.95 cm^2 (0.612 in^2)) along with initial prestressing stress of $0.57 f_{pu}$ (f_{pu} = tensile strength of tendon = 1862 MPa (270ksi)) was used to closely match the base shear and moment capacity of the scaled prototype wall (146 kN (33 kip) and 648 kN-m (478 kip-ft)) at 2% design drift.



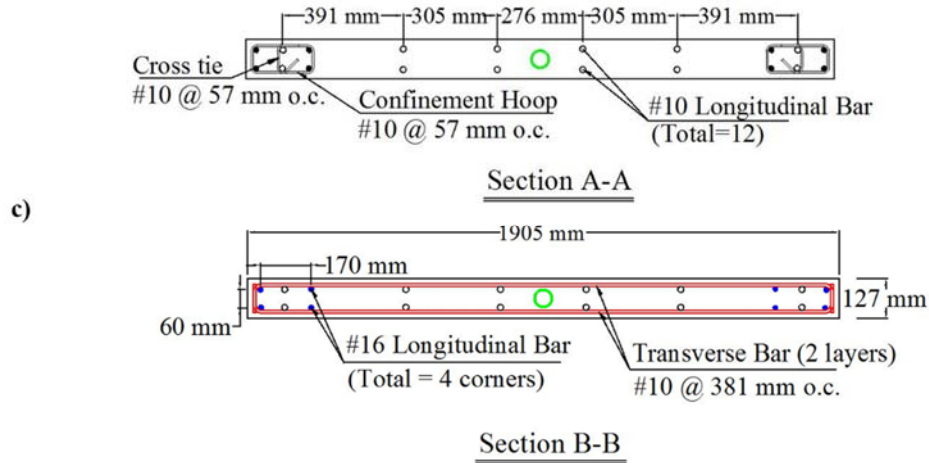


Figure 3-3. Elevation (a and b) and cross sections (c) of SRW1 (1 m = 3.28 ft)

Test units SRW2 through SRW4 were designed by varying the key design parameters such as: (i) the initial prestress force, P_i (initial stress, f_{pi} and total area of post-tensioning tendon, A_p), and (ii) base moment to base shear ratio (i.e., seismic height), which was reduced to 3.5 m (11.5 ft) for SRW4. Measured values of the target design parameters and the corresponding test wall capacities based on the SA method are shown in Table 3-1. As indicated in bold in Table 3-1, a 50% drop in the initial PT stress was experienced at an early stage of testing SRW1, due to unexpected response occurring during a harmonic excitation and causing the wall to experience 7.3% lateral drift. In addition, half of the PT tendons in the third and fourth test walls (SRW3 and SRW4) were eliminated toward the end of testing. This was to continue to evaluate the wall within the shake table capabilities; the reduced strength of these walls was comparable to that of SRW2.

Table 3-1. Test matrix (1 m = 3.28 ft; 1 ksi = 6.9 MPa; 1 kip = 4.45 kN)

Wall ID	Post-tensioning parameters					Shear resistance at 2% drift (kN) ^a
	No., dia.(cm) of PT tendon	Initial PT stress (f_{pi} , MPa), force (p_i , kN)		Concrete compressive stress (MPa)		
		Design	Measured	Design	Measured	
SRW1	4, 1.27	$0.57 f_{pu}$	$0.64 f_{pu}$	41.4	59.3	137/151
SRW1m		-	$0.3 f_{pu}$	-	59.3	104
SRW2	6, 1.27	$0.64 f_{pu}$	$0.5 f_{pu}$, 547	41.4	59.3	206/187
SRW3	6, 1.52	$0.64 f_{pu}$	$0.63 f_{pu}$	41.4	77.5	270/297
SRW3m	3, 1.52	-	$0.62 f_{pu}$	-	77.5	160
SRW4	6, 1.52	$0.64 f_{pu}$	$0.62 f_{pu}$	41.4	77.5	328/358
SRW4m	3, 1.52	-	$0.51 f_{pu}$	-	77.5	174

^a The SA method; using design/measured parameters.

^b SRW1m, SRW3m, and SRW4m; after 50% loss in the initial PT force of SRW1, SRW3, and SRW4.

Apart from studying the influence of design parameters, the test plan also investigated the impact of armoring the wall base using steel channels to minimize the extent of spalling of concrete at toe regions near the base. Channels were placed at the corners of SRW1 and SRW4 (see Figure 3-3b), while SRW3 and SRW2 were detailed with no channels and with channel for the entire wall length, respectively. As described by Sritharan et al. (2015), a 19.1 mm (3/4 in.) wide soft foam was glued right under the entire width of the wall ends to protect the cover from experiencing large compression forces and subsequent spalling.

3.3.3. Seismic test set-up and instrumentation

The set-up used for testing of SRWs at the NEES shake table facility of the University of Nevada at Reno (UNR) is shown in Figure 3-4. The inertia effect expected on the wall corresponded to a seismic weight of 267 kN (60 kip) at the model scale. This was generated using an external mass-rig system and applied through a pin-ended rigid link beam to the wall panel at

4.27 or 3.5 m (14 or 11.5 ft) effective seismic height of the test units. This mass is about 18% larger than that used in the prototype building, implying higher demand on the test walls. A detailed instrumentation, including load cells, direct current displacement transducers, krypton camera system (LED sensors), string potentiometers, strain gauges and accelerometers were used to capture wall behavior, including the change in the PT force. More information regarding the instrumentation layout can be found in Nazari et al. (2015).

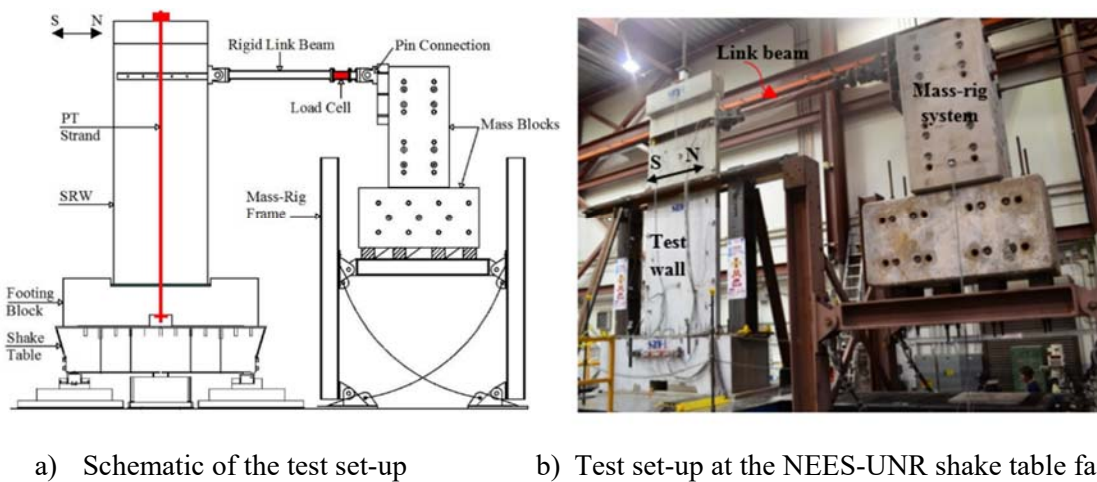


Figure 3-4. Experimental set-up used for the shake table testing

3.3.4. Load protocol

The performance of the SRWs was evaluated using a load protocol consisting of: i) ten earthquake records with different intensities, ii) harmonic motions, and iii) free vibration testing. Due to the space limitations, wall responses to earthquake loads are primarily presented here.

The selected motions were aimed to represent the following four seismic hazard levels: frequent (EQ-I), occasional (EQ-II), design-basis (DBE or EQ-III), and maximum considered events (MCE or EQ-IV). As presented by SEAOC seismology committee (1999), these hazard

levels are defined by five percent damped elastic acceleration response spectra, considering the prototype building location. For each hazard level, different types of ground motions (i.e., short vs. long- duration and far-field vs. near-field) were used, as summarized in Table 3-2. While the information provided in this table is at the prototype scale, the amplitude of all the motions was scaled up by $18/5$ and the time step was decreased by a factor of $5/18$ to satisfy the scale effects.

The first four motions in this table with “s” at the end of the ID of the input motions were short records in the range from 4 to 7 seconds. These are spectrum compatible motions of various intensities (EQ-I to EQ-IV), as used for the pseudo dynamic testing of the PRESS building (Priestley et al. 1999) and scaled following the recommendations of Rahman and Sritharan (2006). In addition, six long-duration recorded earthquakes were chosen, which included: i) IM-a, IM-b and IM-e, as used by Rahman and Sritharan (2006), ii) two recorded ground motions from recent earthquakes (Chile and Christchurch, New Zealand), and iii) Kobe-Takatori station, which was used in a rocking wall building test at the E-Defense facility (Tuna et al. 2012). Furthermore, some of the short-duration motions were repeated twice successively with sufficient time between the input motions to bring the test wall to rest prior to the second motion.

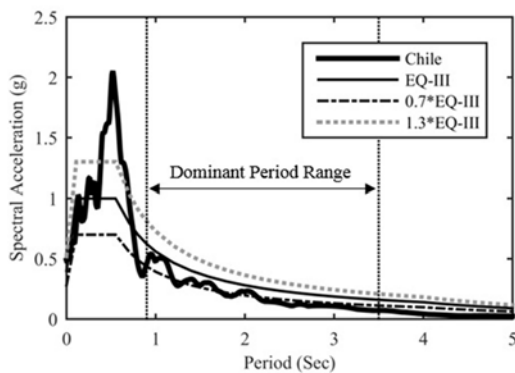
The scale factor for the long-duration motion, as noted in Table 3-2, was achieved such that the root mean square deviation (RMSD) of their spectral ordinates normalized by the mean of the target values of the selected spectrum, referred to as the coefficient of variation of RMSD, remains within $\pm 30\%$ over a selected period range (SEAOC 1999; Rahman and Sritharan 2006). This corresponded to 0.9 sec. to 3.5 sec and represented the elastic and effective periods of the prototype wall. The former is defined using the elastic stiffness of the system, which is based on the displacement at the onset of non-linear response. For the effective period calculations, a secant stiffness to the ultimate displacement capacity of the system at a lateral drift of 2% was used. This

procedure is illustrated in Figure 3-5a for the Chile ground motion, with the targeted hazard level of EQ-III. Accordingly, Figures 3-5b to 3-5d present the acceleration response spectra of the scaled input motions. The intensity of shake table-generated motions was estimated using the period range corresponding to each test wall.

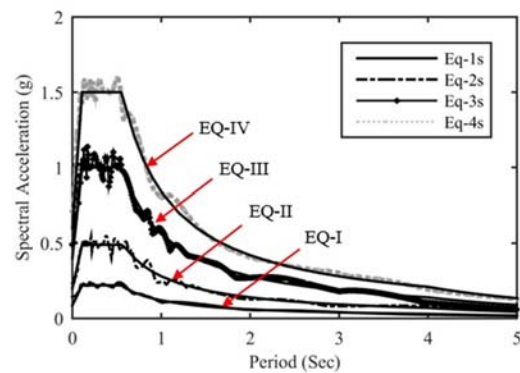
Table 3-2. List of input motions used for shake table testing of SRWs

ID	Earthquake name (Year), Station, FF/NF	Scale factor	Targeted hazard level	PGA (g) after applying the scale factor
Eq-1s	Hollister (1974), Gilroy Array#1, FF	0.67	EQ-I	0.14
Eq-2s	San Fernando (1971), Hollywood Storage, FF	1.00	EQ-II	0.23
Eq-3s	Imperial Valley (1940), Elcentro, FF	1.00	EQ-III	0.49
Eq-4s	Northridge (1994), Sylmar, NF	1.00	EQ-IV	0.71
IM-a	Morgan Hill (1984), Gilroy Array#6, NF	0.65	EQ-I	0.19
IM-b	Loma Prieta (1989), Saratoga Aloha Avenue, NF	0.64	EQ-II	0.32
IM-e	Kobe-Japan (1995), KJM, NF	0.94	EQ-III	0.56
NZ	New Zealand (2011), HVSC, NF	0.40	EQ-II	0.58
Chile	Chile (2010), Angol, FF	1.00	EQ-III	0.49
Takatori	Kobe-Japan (1995), Takatori, NF	0.60	EQ-IV	0.37

s = short-duration motion; NF = Near-Field motion; FF = Far-Field motion



a) Chile; response vs. target spectrum



b) Eq-1s to Eq-4s

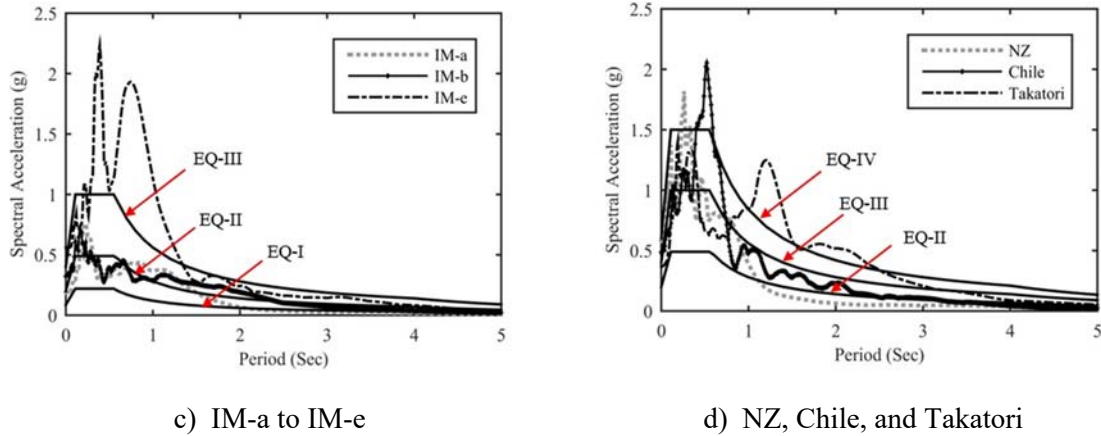


Figure 3-5. Spectral acceleration of scaled ground motions selected for the shake table testing

3.4. Analytical Model

As shown in Figure 3-6, the test walls were modeled in OpenSees (McKenna et al. 2000) as a SDOF system. In this model, a rigid lumped mass representing the inertia effect was concentrated at the effective seismic height of the system. The precast concrete wall was represented by an elastic beam column element, which was attached to the base through a zero-length rotational spring. The uniaxial SelfCentering material model available in OpenSees (McKenna et al. 2000) was used to simulate the moment-rotational characteristics of this spring. The flag-shaped hysteretic response of this material model facilitated capturing of the wall base moment resistance and its re-centering capability. Key properties for this uniaxial model, including the initial stiffness, yield force, and post-yield stiffness, were defined using the SA method (Aaleti and Sritharan 2009), which is subsequently shown in this paper to adequately capture the backbone curve of the rocking response of all test walls. For the flag-shaped hysteresis response, a beta factor of 0.2 (SRW2 with relatively no damage) or 0.3 (SRW1m, SRW3, and SRW4 with higher damage to the concrete) was assigned to represent the energy dissipation of the system as a ratio

of the yield force. This value was based on the limited hysteretic action observed during testing and corresponded to an average equivalent viscous damping ratio of 3.8% for the test walls.

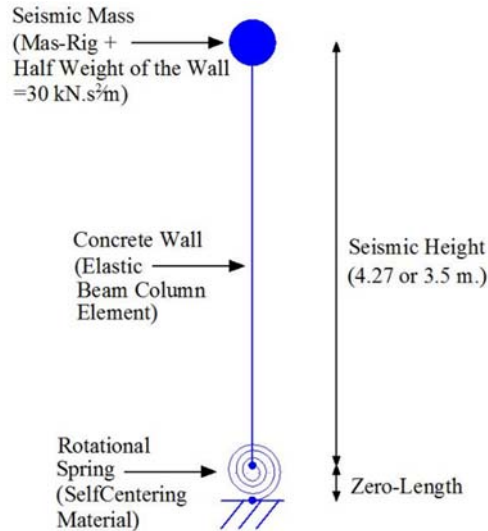


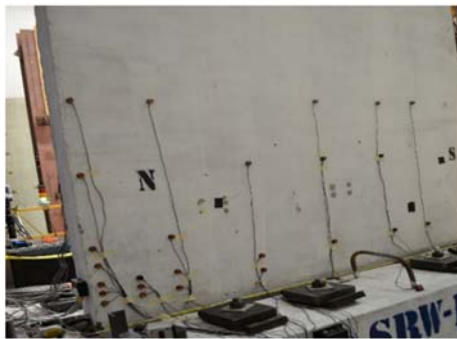
Figure 3-6. OpenSees model for a rocking wall (1 m = 3.28 ft; 1 kip = 4.45 kN)

3.5. Testing and Results

Each of the test walls was subjected to a total of 16 to 18 input motions. They included all 10 motions in Table 3-2 and other forms of selected motions from this table. These modifications were needed to: (i) investigate the wall performance at different intensities of motions than originally intended, by using additional scale factors (i.e., $0.8 \times \text{Eq-4s}$ representative of an EQ-III level earthquake), (ii) reduce their amplitude due to limitations of shake table capacities, or (iii) repeat a test (often with -1 as a scale factor). In some cases, the table-generated records were noticeably different from the input motions and thus they did not represent the targeted hazard level. Therefore, + or – signs were added to differentiate them (e.g., EQII⁺ and EQIII⁻). One unit of + or – sign was assigned when the coefficient of variation of the RMSD of the table accelerations deviated from the $\pm 30\%$ threshold with each additional 30%.

3.5.1. Observations

All single rocking walls performed satisfactorily and sustained negligible damage while subjected to EQ-I to EQ-III levels of input motions. Figure 3-7 shows undamaged state of the two test walls near the base after experiencing the EQ-III level motions. To illustrate the impact of using the base channels at the wall base, Figure 3-8 compares the damage to wall toe regions following the EQ-IV level motions. As shown in Figure 3-8a, SRW3 with no steel channel experienced some damage to the core concrete at both corners over a length of about 8 cm (3.15 in.) from the edge of the wall. However, SRW4 with the partial base armoring stayed undamaged for the entire length (see Figure 3-8b). With increase in drift, the extent of damage progressed further, as shown in Figure 3-8c for SRW3m. SRW4m also began to exhibit some distress to the cover concrete (Figure 3-8d) as the test progressed. When using the base channel for the entire wall length in SRW2, the extent of damage was significantly reduced even after the wall experienced a maximum drift of 5.4% during an EQ-IV level motion. When the walls displaced to higher drift levels, some prestress loss also occurred due to yielding of tendons, as they were designed to remain elastic up to a 2% lateral drift. Neither the PT loss nor the damage to the concrete affected the self-centering capability of the test walls during subsequent tests.



a) SRW1-a; IM-e



b) SRW4; 0.75×IM-e

Figure 3-7. Typical condition of wall base region after experiencing EQ-III level motions

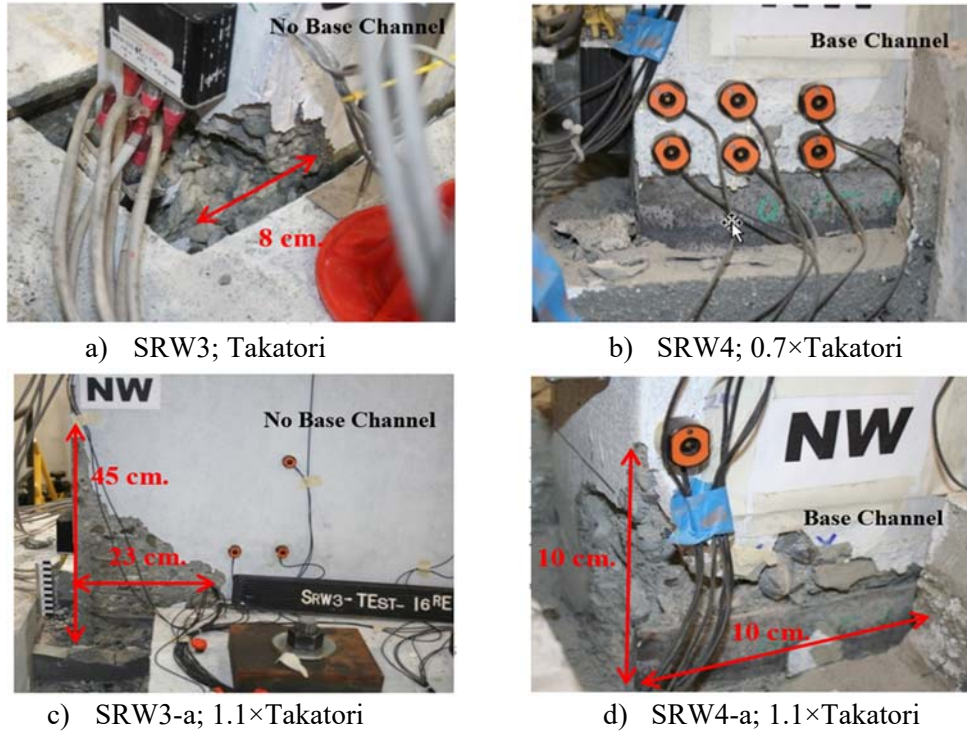


Figure 3-8. Impact of armoring the wall base using a steel channel as evidenced for EQ-IV level motions (1 m = 3.28 ft)

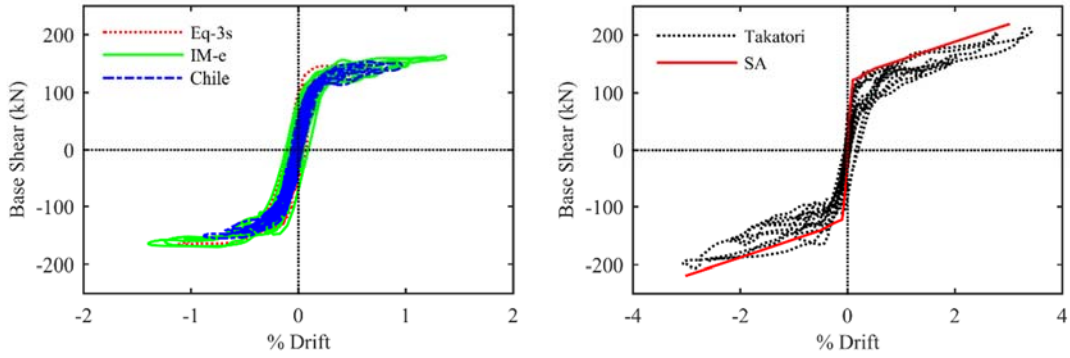
3.5.2. Characteristic response

Using measured data, typical SRW responses are presented together with the predicted responses obtained from the SA method (Aaleti and Sritharan 2009). Figure 3-9a shows the measured force-displacement responses of SRW2 when subjected to three EQ-III level motions. They produced comparable responses with the maximum drift in the range of 1 to 1.4%. Subsequently, the wall was subjected to Takatori earthquake representing an EQ-IV event and lost 14% of the initial prestress force as it experienced about 3.4% lateral drift. Figure 3-9b shows the corresponding response, which indicates relatively larger hysteresis loops than those shown in Figure 3-9a, due to yielding of the PT tendons. The variation of post-tensioning force is plotted in

Figure 3-9c as a function of wall lateral drift, which shows that the prestress loss occurred when the wall was subjected to an EQIV level excitation.

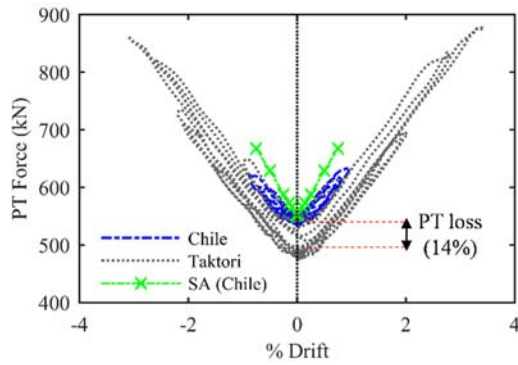
Figure 3-9d shows wall maximum uplift obtained from LED sensors during four input motions with different intensities. As seen for other rocking wall tests (Sritharan et al. 2015), a linear variation along the wall length, including over the compression zone, is seen. Increasing the intensity of the earthquakes from EQ-I to EQ-IV did not significantly change the contact length at the maximum drift. This is more clearly seen in Figure 3-9e, which depicts this quantity as a function of wall lateral drift at first peaks while subjected to four levels of ground motions. The variation of the maximum concrete strain recorded in the compression toe is plotted in Figure 3-9f. At the location of gauges, which is shown in this figure, the measured maximum strain of 3290 microstrain correlates with the undamaged state maintained for the confined concrete even after experiencing 4.3% lateral drift. The measured contact length and the maximum strain suggest that the wall would have experienced a maximum strain of 6900 microstrain at the extreme confined concrete fiber at the height of concrete gauge.

As seen in Figure 3-9, the SA method (Aaleti and Sritharan 2009) generally presents good estimates of the experimental captured data. The contact length was slightly underestimated by this method (see Figure 3-9e), resulting in higher tendon force, as depicted in Figure 3-9c. Repeating the initial prestress force with and without losses, estimated concrete strain in SRW2 shows good correlation with the measured values, as plotted in Figure 3-9f.

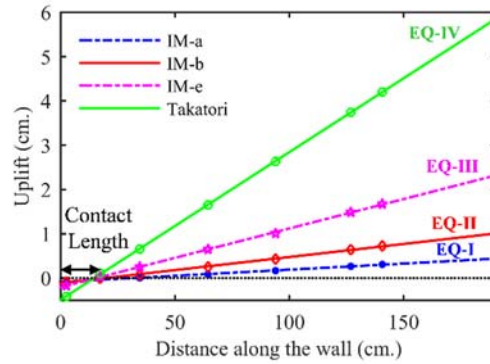


a) Lateral response; EQ-III level

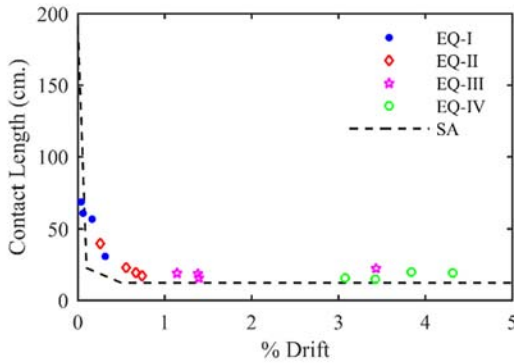
b) Lateral response; EQ-IV level



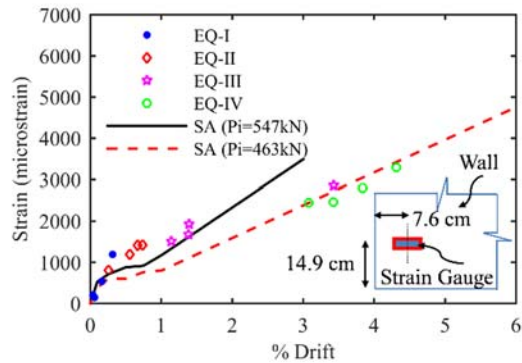
c) Variation of PT force; EQ-III and IV



d) Uplift along the wall length; EQ-I to IV



e) Contact length vs. drift; first peaks



f) Max. concrete strain vs. drift; first peaks

Figure 3-9. Global and local behavior of SRW2 using experimental data and the SA method
(1 m = 3.28 ft; 1 kip = 4.45 kN)

3.5.3. Influence of prestressing

The two most influencing parameters on the behavior of the SRWs are the initial prestressing force (P_i) and area of prestressing steel (A_p). The former primarily impacts the elastic stiffness while the latter influences the ultimate wall lateral resistance. Figure 3-10a shows the lateral responses of SRW2 when subjected to $1.4 \times \text{Takatori}$ and $1.8 \times \text{Takatori}$ motions. The initial prestressing force in the wall was 463 kN (104 kip) and 271 kN (61 kip), respectively, and this reduction was due to prestress loss occurring during previous ground motions. As shown in figure 3-10a, a lower initial post-tensioning force in SRW2 resulted in 52% reduction in the resistance of the system within its linear range. As expected, the ultimate lateral resistance of the wall remained unchanged. Figure 3-10b compares the lateral responses of SRW3 and SRW3m with initial prestressing force of 983 kN (221 kip) and 485 kN (109 kip), which was due to reducing the PT area from 8.4 cm^2 (1.3 in^2) to 4.2 cm^2 (0.65 in^2). As these walls were respectively subjected to Takatori and $1.1 \times \text{Takatori}$ motions, a lower ultimate lateral resistance of SRW3m, as well as a 53% reduction in the elastic stiffness was observed. As shown in Figure 3-10b, the ultimate wall lateral resistance was reduced from 273 kN (61 kip) to 148 kN (33 kip) at 2% lateral drift.

With an increase in the initial post-tensioning force, the decay of the SRW response was quicker and experienced less number of reversals. The lateral drift of SRW3 damped faster than SRW3m that had lower initial PT force, although they both experienced the same maximum lateral drift during Takatori motions (see Figure 3-10c). The same trend was observed for the angular velocity responses of SRW1m and SRW2 with initial PT force of 227 kN (51 kip) and 463 kN (104 kip) respectively for $0.8 \times \text{Eq-4s}$ motion (see Figure 3-10d).

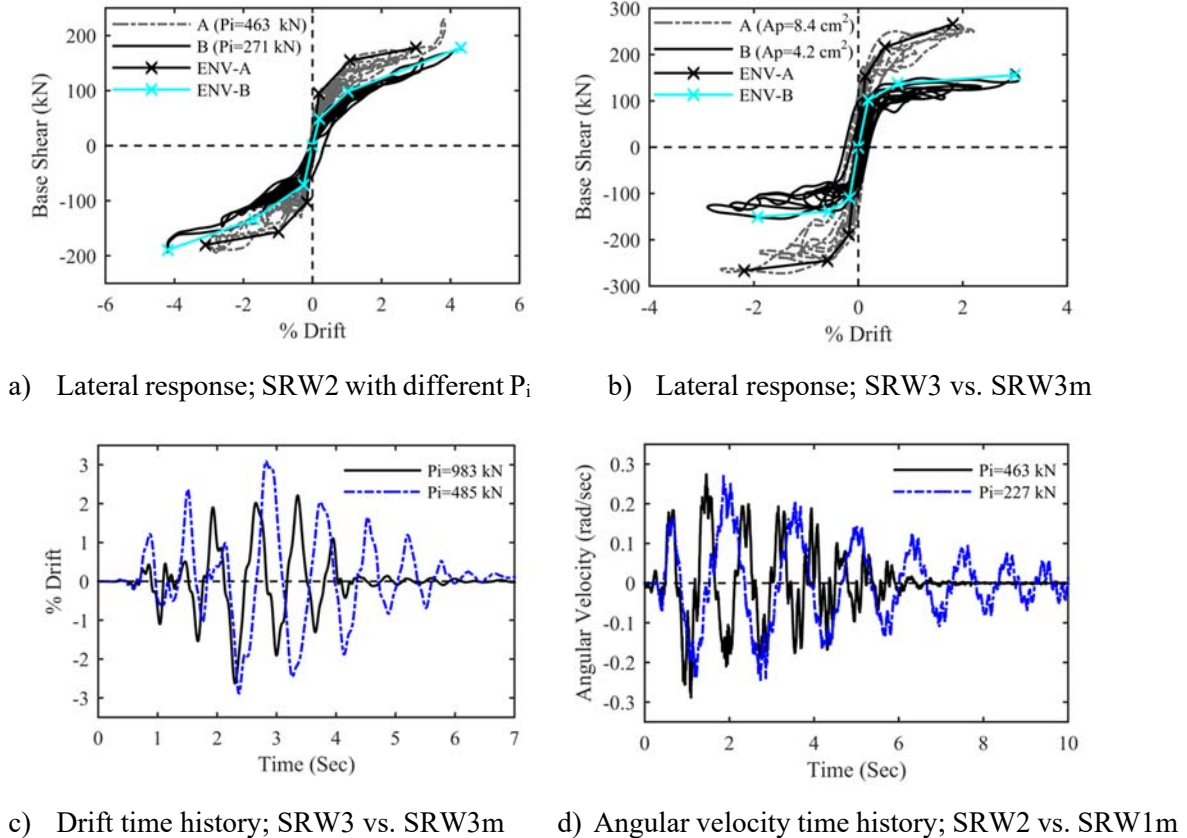


Figure 3-10. Influence of initial prestress force on the global behavior of test walls

(1 m = 3.28 ft; 1 kip = 4.45 kN)

3.5.4. Damping components

During an earthquake excitation, SRWs dissipate the seismic energy imparted to them through different mechanisms. They include hysteretic damping resulting from inelastic concrete strains developed in the wall toe regions especially at large drifts, inherent viscous damping, as well as energy dissipation due to impact. While the contribution of each mechanism is small, an appropriate estimate of the total damping encompassing all of the components has never been quantified using experimental data. Using responses of SRWs to different intensities of Eq-4s and

Takatori, this section quantifies the equivalent viscous damping ratios of SRWs corresponding to different energy dissipation mechanisms.

The Jacobsen's secant stiffness approach, as applied in the direct displacement-based design (DDBD) (Priestley 2000), was used to compute the equivalent viscous damping ratio due to hysteretic action (ξ_{hys}). This quantity was estimated from the area enclosed by each half-cycle of the lateral force-displacement hysteresis loops when the rocking walls underwent drifts between 1.4% and 2.6% during various earthquake excitations. This range includes the target design drift of 2% as the median value and focuses on damping that is more appropriate for moderate to large drifts. To create the experimental hysteretic loops, the lateral force was directly attained from the link beam force recorded by a load cell, which is approximated to be the inertia force provided by the external mass-rig (f_I) (Nazari et al. 2014). For the system to be in a state of equilibrium, f_I is considered to be balanced by the lateral restoring force (f_s) and the elastic viscous damping force (f_D). Therefore, this area-based damping ratio, shown in Figure 3-11a, represents a combination of the energy dissipation of the system due to both inelastic hysteretic action (ξ_{hys}) and inherent elastic viscous damping (ξ_{vis}). As seen in this figure, the estimated damping ratio is independent of the lateral drift and has an average value of 4.2% for SRW1m, SRW2, and SRW4. A higher average value of 7% was obtained for SRW3, which may be due to the unprotected wall base experiencing relatively more damage. Through cyclic analysis of a fiber based analytical model, Kurama (2002) established an equivalent damping of 3.8% (i.e., β_h value of 6%) for SRWs, which is comparable to the experimental results presented here.

Another source of elastic damping in SRWs results from the kinetic energy loss that occurs immediately before and immediately after an impact (ΔE_k). This is expressed by a coefficient of

restitution (c.o.r or r), which is defined as the square ratio of the exiting angular velocity to the approaching angular velocity of a rocking impact (Housner 1963). Housner (1963) introduced a constant c.o.r for free rocking models by defining a geometry dependent equation. This method predicts lower values of coefficient of restitution compared to the experimental data obtained from all test walls, as shown in Figure 3-11b for SRW2, which is consistent with findings of other researchers (e.g., Kalliontzis and Sritharan under review). Using the observed c.o.r, ΔE_k was quantified for the test walls during each impact. Figure 3-11c shows accumulated ΔE_k (i.e., $\Delta E_{k,ACC}$) for SRW1m during $0.8 \times \text{Eq-4s}$. Also included in this figure is the total energy dissipated by the link beam force to displace the wall during the impact duration (ΔE_{link}), which is negligible compared to $\Delta E_{k,ACC}$. This confirms that the calculations previously presented for the area-based damping ratio of test walls do not include the energy loss through impacts. To represent this energy dissipation component, $\Delta E_{k,ACC}$ was equated with a continuous viscous energy dissipation (E_{imp}) with damping ratio of ξ_{imp} (see Figure 3-11c). Use of this procedure for all test walls, excluding SRW3 with the maximum experienced damage, during a set of Takatori and Eq-4s motions with different intensities resulted in an average equivalent viscous damping ratio (ξ_{imp}) of 1.5%, as depicted in Figure 3-11d. The corresponding amount of damping, which is related to the secant stiffness of the system at 2% lateral drift, is in the range of 1 to 3% that was reported by Marriot et al. (2008) for the SRW. Adding the estimated ξ_{imp} , ξ_{hys} , and ξ_{is} resulted in an average total equivalent viscous damping ratio (ξ_{eq}) of 5.7% for the test walls during drift cycles of greater than 1%, as shown in Figure 3-11d. This figure also indicates that the contribution of damping due to impacts in the total energy dissipation of the rocking walls is less than 30%.

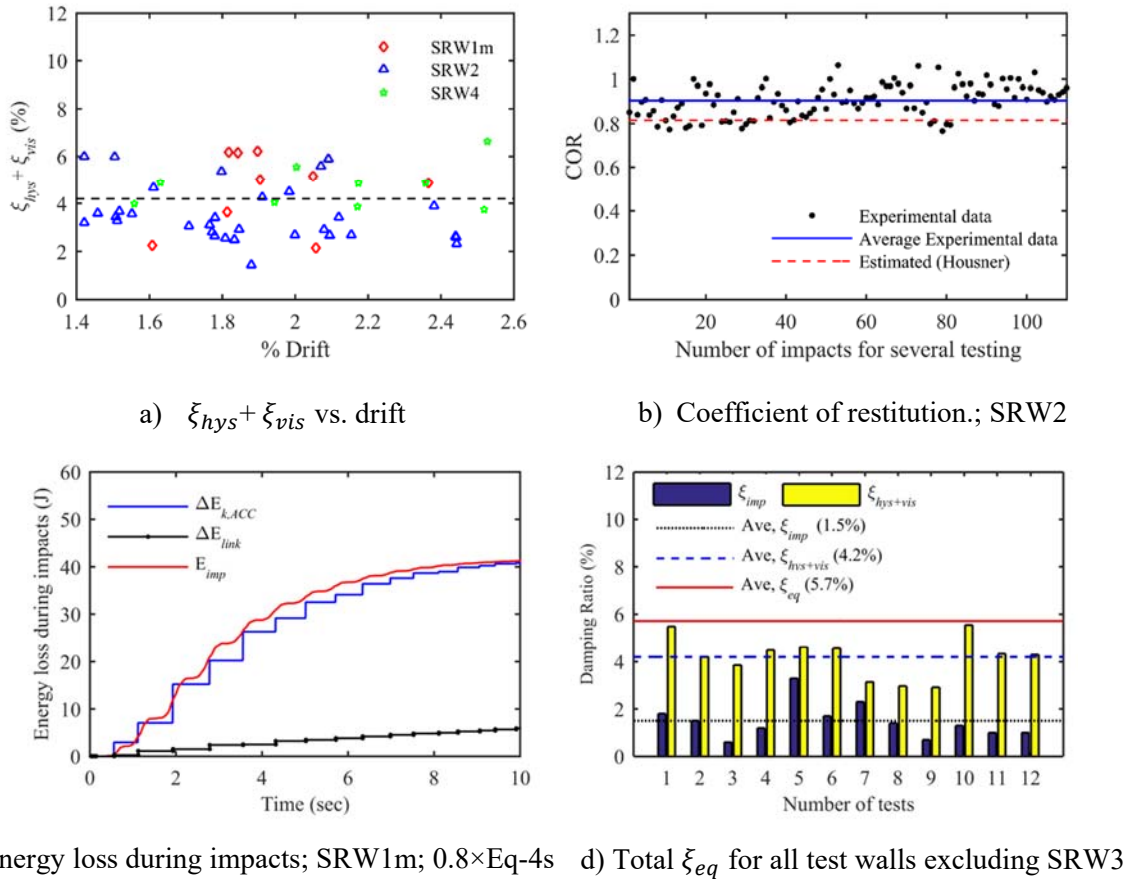


Figure 3-11. Estimation of equivalent viscous damping ratio of rocking walls using the experimental data

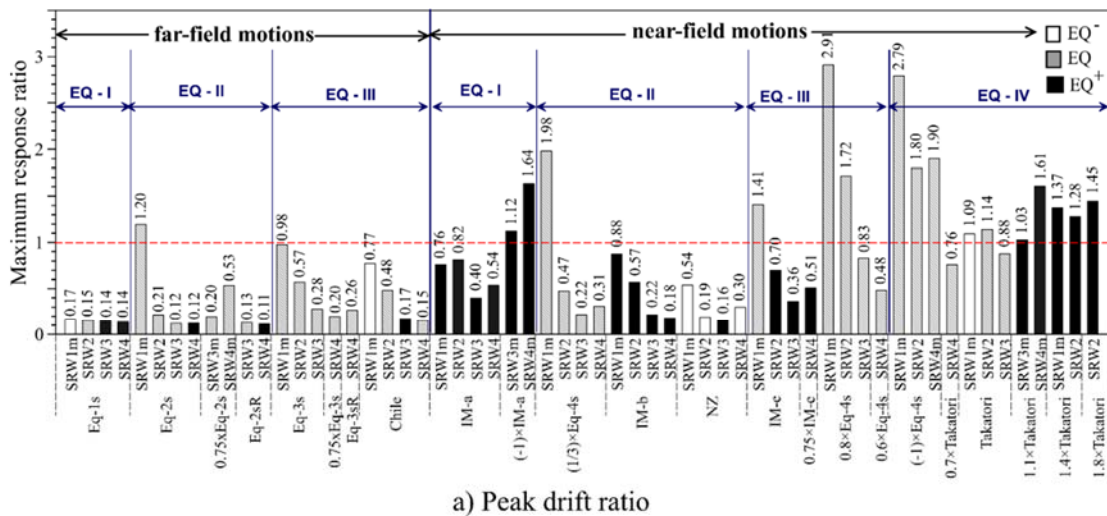
3.5.5. Performance-based seismic evaluation

Using the maximum lateral drift, maximum absolute acceleration, and residual drift as key variables, performance of all SRWs was evaluated using the measured responses from different earthquake motions. For this purpose, the acceptable performance limits for the aforementioned variables proposed by Rahman and Sritharan (2006) were used. Accordingly, the maximum permissible transient drifts for self-centering walls are: 0.4% (EQ-I), 1.2% (EQ-II), 2.0% (EQ-III), and 3.0% (EQ-IV); and the maximum permissible residual drifts are: 0.1% (EQ-I), 0.3% (EQ-II),

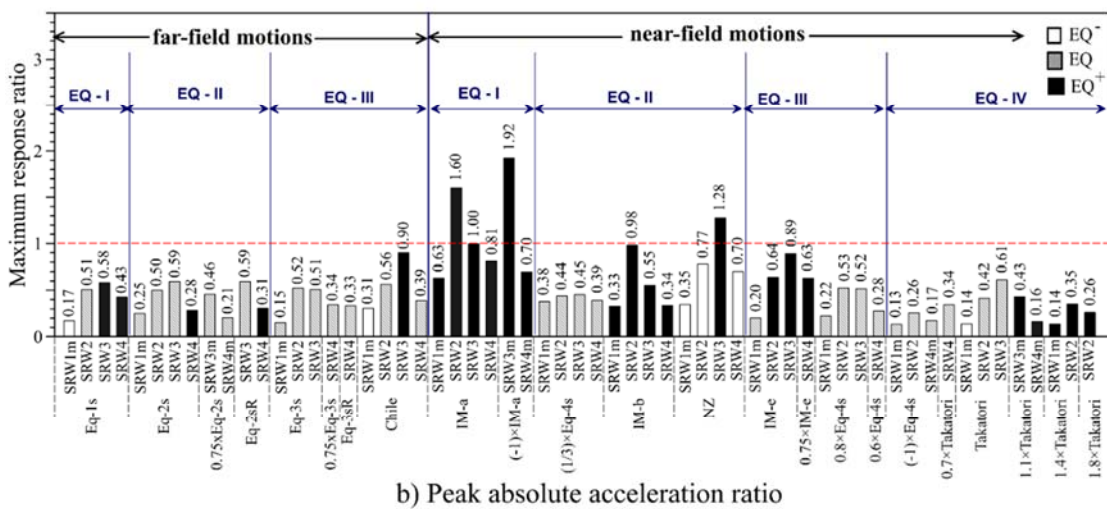
0.5% (EQ-III), and 0.75% (EQ-IV). Including the scale factor, the following acceleration limits were deformed: 0.954g (EQ-I), 2.117g (EQ-II), 4.32g (EQ-III), and 6.48g (EQ-IV). The results from this investigation are presented in Figure 3-12, which shows the ratio between the maximum wall demands to the allowable limits (i.e., the maximum response ratio). A value of above one for the ratio indicates that the particular criterion is not satisfied for a chosen input motion. Addition of “R” to the input motion represents a repeat of the same event (e.g., Eq-3s and Eq-3sR). To denote intensity level of the table acceleration, including + or – signs, different patterns on the column charts of Figure 3-12 are used.

As shown in Figure 3-12a, the near-field ground motions were generally more demanding on the test walls in terms of the lateral drift. This figure also presents reduced response of the rocking walls to the long-duration motions compared to the spectrum compatible short-duration motions with similar intensities. When subjected to EQ-I to EQ-III level motions, some walls responded with the maximum lateral drift beyond the allowable limit (see Figure 3-12a). They included: (i) SRW1m for EQ-II and EQ-III level motions, (ii) SRW2 for EQ-III level motions, and (iii) SRW3m and SRW4m during $-1 \times IM-a$ with an intensity of EQ-I⁺ (these two walls were not subjected to any EQ-III level motion). During the EQ-IV level near-field motions, only SRW3 and SRW4 with larger capacities experienced drift below the 3% allowable limit. Test walls were not subjected to any EQ-IV level far-field ground motion.

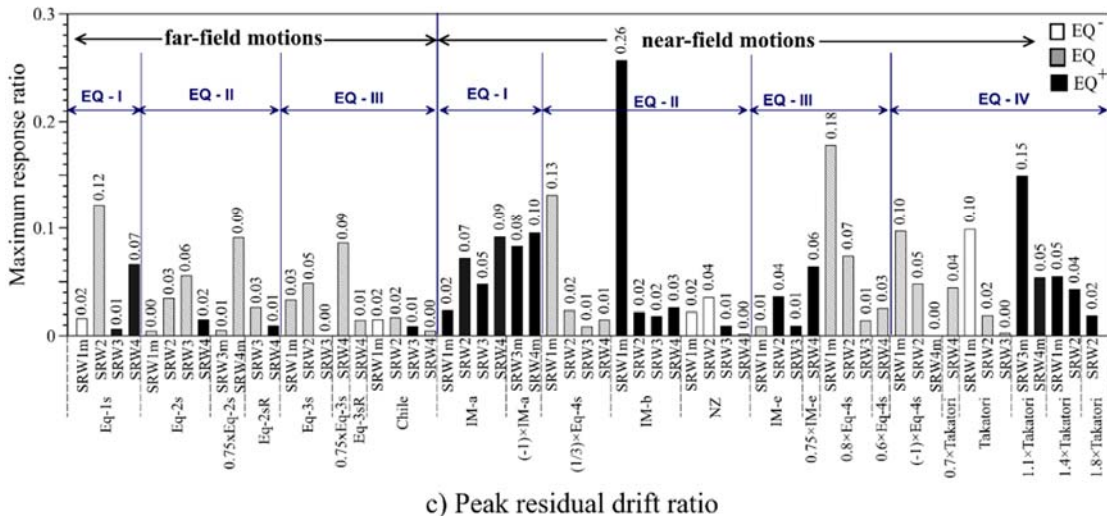
In terms of the maximum acceleration, all walls experienced acceptable values below the limits, except for some long-duration motions (see Figure 3-12b). In general, the maximum absolute acceleration of test walls which underwent larger drifts was smaller. Also as indicated in Figures 3-12c, all the rocking walls satisfactorily self-centered with negligible residual drift, even when they were subjected to the maximum considered earthquakes.



a) Peak drift ratio



b) Peak absolute acceleration ratio



c) Peak residual drift ratio

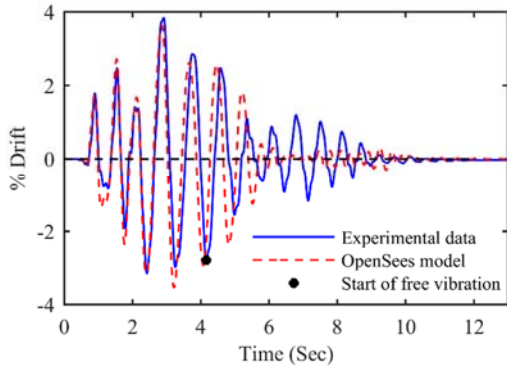
Figure 3-12. Ratio of the maximum wall demands to the allowable limits

3.6. Comparison with Analytical Results

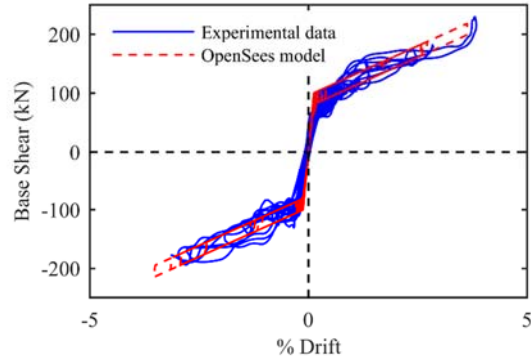
Results obtained from the analytical model and shake table testing were compared to validate the accuracy of the simple analytical model. For all analyses, the Newmark constant average acceleration solution method was used with an integration time step equal to the sampling rate (i.e., 0.00391 sec.). A 3% elastic viscous damping was included in the analysis to represent ξ_{imp} , using the tangent stiffness proportional Rayleigh damping in the model. According to the recommendations of Priestley and Calvi (2007), a modification factor of 2 was applied to the estimated ξ_{imp} of 1.5% to relate this secant stiffness based damping to a tangent stiffness based value. Figure 3-13a and Figure 3-13b, respectively, show the calculated lateral drift time history and the base shear-lateral drift response of SRW2 against the experimental measurements from the 1.4×Takatori EQ-IV event. As presented in these plots, good correlations are observed between the OpenSees analytical results and experimental data. As shown in Figure 3-13a, the peak drift response and its variation as a function of time were adequately captured using this model. Small differences between the experimental and theoretical period are seen, which is more apparent during the free vibration phase. The comparison presented in Figure 3-13b shows the elastic stiffness of the system was closely captured.

The calculated lateral drift time history responses of SRW1m to a set of EQ-I to EQ-IV motions (i.e., IM-a, NZ, Chile, and 1.4×Takatori) are plotted together with the test results in Figure 3-13c. This comparison shows that the model sufficiently captured the damage accumulation with the assumed hysteretic model. As shown in this figure, drift peaks are satisfactorily quantified. A similar comparison is also presented for the responses of SRW3 and SRW3m, SRW4 and SRW4m, when they were subjected to the EQ-IV level motions (see Figure 3-13d). As observed in these

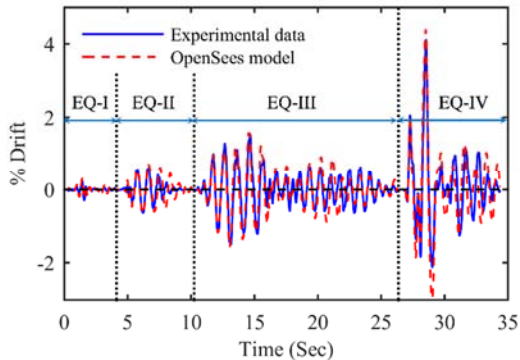
plots, the analytical peak lateral drifts compare well with the experimental results during the strong motions.



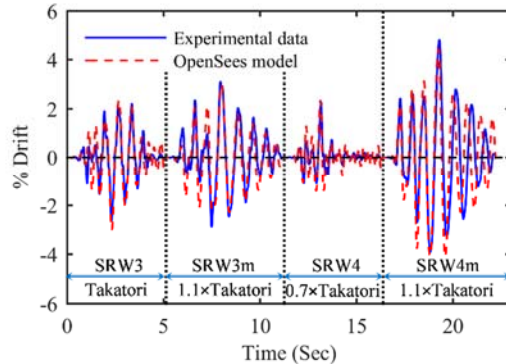
a) Drift time history; SRW2 (1.4×Takatori)



b) Lateral response; SRW2 (1.4×Takatori)



c) Drift time history; SRW1m
(Four levels of earthquakes)



d) Drift time history; SRW3 vs. SRW3m and
SRW4 vs. SRW4m (EQ-IV events)

Figure 3-13. Comparison between analytical results and experimental data (1 kip = 4.45 kN)

3.7. Use of SRW in Seismic Design

It was noted that SRWs are not commonly used in seismic design of buildings due to their low damping. In contrast, the shake table tests confirmed that they may be designed to produce satisfactory seismic response due to their ability to respond nonlinearly.

3.7.1. Base shear vs. damping

Recall that the larger mass than that used in designing the prototype building resulted in higher demand on the test walls. Subsequently, SRW2 closely provided shear capacity of the scaled prototype wall, whereas SRW3 and SRW4 had base shear resistance higher than SRW2. Therefore, to understand the feasibility of using SRWs with lower damping in seismic design, the basis of the DDBD approach as described by Priestley (2000) was used. In DDBD, the design base shear is obtained by multiplying the lateral displacement corresponding to a target design drift, which is typically taken as 2%, by the effective stiffness of the system. For the test walls, the effective mass = 29.6 kN.s²/m (0.169 kip.s²/in); the design displacement (Δ_d) = 8.54 cm (3.36 in.); and the base moment to base shear ratio (M/V) = 4.27 m (14 ft). Using this information, Figure 3-14a shows the estimated design base shear as a function of damping ratio. As indicated in this figure by a dashed line, SRW1 should provide damping ratio greater than 10.3% to maintain the maximum experienced drift of the system within the allowable limit during far-field events. Because of the lower energy dissipation capacity of SRWs, as represented by a damping ratio of 6%, the design base shear should be increased to 232 kN (52.2 kip) to ensure their satisfactory seismic performance (i.e., the dotted line in Figure 3-14a). Figure 3-14b, which compares the shear resistance of test walls at 2% drift with the corresponding DDBD values for near-field events, indicates the adequate design base shear of SRW3 and SRW4. This confirms the outcomes of seismic performance evaluation of test walls, as only these two test units satisfactorily performed in terms of allowable drift limit during DBE near-field motions.

It is concluded that SRWs designed with a larger shear force corresponding to their limited damping capacity can be applied in high seismic regions. The required base shear, as desired for design purposes, is estimated in the following section.

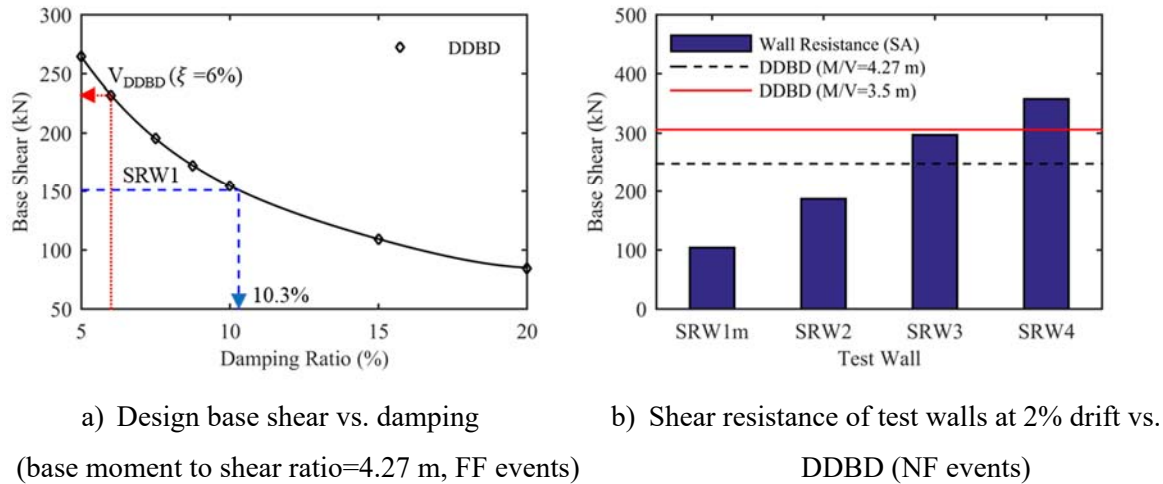


Figure 3-14. Assessment of shear resistance of test walls using DDBD approach
(1 kip = 4.45 kN; 1 m = 3.28 ft)

3.7.2. R-factor

Following a DDBD approach, it is shown in Figure 3-15a that the scaled prototype wall experiences a maximum drift of greater than 2% during DBE far-field events while it is designed with a strength reduction (or R) factor of 5, as applied for the traditional Cast-In-Place (CIP) walls. Consistent with the procedure described in the current design codes (SEAOC 1999), an R-factor of 3.7 is estimated to consider for nonlinear behavior of the rocking wall, as shown in Figure 3-15b. In this figure, the base shear forces corresponding to the elastic response of the system (V_e) and design-level (V_d) are respectively calculated from the FBD (i.e., IBC (2009) with $R=1$) and DDBD ($\xi_{eq}=6\%$) procedures. The elastic response displacement (Δ_e) of 4.6 cm (1.8 in.) is resulted from an elastic period of 0.9 sec, as estimated for the prototype system. The reductions due to over-strength is ignored in these calculations due to negligible second slope of the rocking system. Using the OpenSees model, satisfactory performance of the wall designed with the modified R-factor was indicated in terms of allowable drift during design-level earthquakes.

Accordingly, to account for the low damping capacity of SRWs, an R-factor of 3.5 is recommended to be used in the design. This results in a base shear of 1.4 times greater than that required for a CIP wall. Given that the CIP wall has an equivalent damping ratio of 18% (Priestley 2000) compared to about 6% for SRW, the increase in base shear for SRW is relatively modest. This is due to SRW responding nonlinearly beyond a lateral drift of about 0.3 to 0.5%.

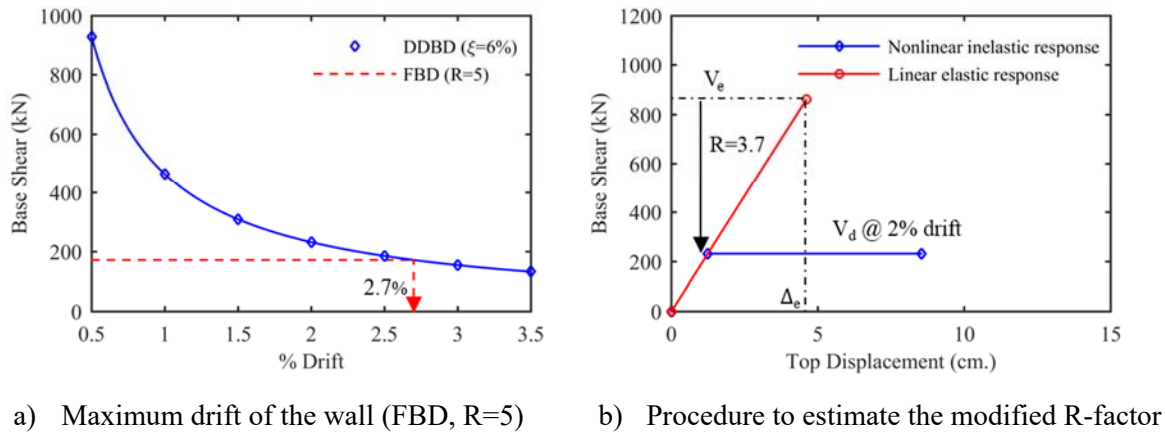


Figure 3-15. R-factor for design of the scaled prototype wall (FBD solution)

(1 m = 3.28 ft; 1 kip = 4.45 kN)

3.8. Conclusions

This paper presented the results from a series of shake table tests on four SRWs. The walls were designed with different amounts of post-tensioning steel and initial prestressing force, providing base shear resistance in the range of 137 kN (31 kip) to 328 kN (74 kip). The lowest amount of design base shear was chosen to closely match the capacity of a reference wall from a six story prototype building at 5/18 scale. Each SRW was subjected to a set of input motions representing different earthquake intensities. Although the walls were expected to have limited energy dissipation capacity, their performance was evaluated using criteria established for

traditional concrete walls with higher damping. The conclusions drawn from this study are presented below:

- 1- All SRWs showed satisfactory performance without experiencing visible damage up to the design-level earthquakes. Significant spalling of cover concrete occurred while they were subjected to the maximum considered input motions; however, the amount of damage was minimized due to the use of steel channels at the base of the walls.
- 2- All test walls re-centered with minimum residual drifts after four levels of earthquakes. Test results also showed that walls generally tend to attain the maximum absolute acceleration below the acceptable limits.
- 3- Based on the experimental observations, an average equivalent viscous damping ratio of 5.7% was established for SRWs. This damping includes 1.5% for the energy loss during impacts and 4.2% due to concrete nonlinearity as well as inherent material damping of the test units as they experience drifts between 1.4% and 2.6%.
- 4- While the damping ratio of SRWs is below 6%, it was shown that they can be designed to respond satisfactorily when an R-factor of 3.5 is used.
- 5- Results from the SA method [14] presented good estimates of the experimental characteristic responses of SRWs from shake table testing, including load-deformation behavior, variation of post-tensioning force, maximum concrete strain, and contact length. However, some overestimation of the PT force was obtained due to a lower prediction of the contact length.
- 6- Using a centerline OpenSees model, displacement time history and lateral load responses of SRWs were satisfactorily predicted during the strong portion of the motions at all intensity levels. A 3% tangent stiffness proportional elastic damping was used in these models to express the energy loss during impacts achieved from the experimental results.

3.9. Acknowledgments

The study reported in this paper was based upon the NEES Rocking Wall project supported by the National Science Foundation under Grant No. CMMI-1041650 and Dr. Joy Pauschke served as the program director for this grant. Any opinions, findings, and conclusions or recommendations expressed in this material are those of the authors and do not necessarily reflect the views of the National Science Foundation. All shake table tests were conducted using the NEES shared facility at the University of Nevada, Reno (UNR). The test units were donated by Clark Pacific and MidState Precast through coordination by PCI West. Materials provided by Sumiden Wire, GTI, Hayes Industries and help provided by ironworker local 118 with post-tensioning of specimens are also gratefully acknowledged.

3.10. References

- Aaleti, S. (2009) Behavior of rectangular concrete walls subjected to simulated seismic loading, PhD Thesis. Dept. of Civil, Construction and Environmental Engineering, Iowa State University, Ames, Iowa.
- Aaleti, S., and Sritharan, S. (2009) A simplified analysis method for characterizing unbonded post-tensioned precast wall systems. *Engineering Structures*, **31**(12), 2966–2975.
- ACI 318-11. (2011) Building code requirements for structural concrete. *ACI 318-11*, Farmington Hills, MI.
- ACI Innovation Task Group 5.1. (2008) Acceptance criteria for special unbonded post-tensioned precast structural walls based on validation testing and commentary. American Concrete Institute, Farmington Hills, MI.
- ACI Innovation Task Group 5.2. (2009) Requirements for design of a special unbonded post-tensioned precast shear wall satisfying ACI ITG-5.1 and commentary (ACI ITG-5.2). American Concrete Institute, Farmington Hills, MI.

- ASCE 7-05. (2005) Minimum design loads for buildings and other structures, ASCE/SEI 7-05.
- Housner, G. (1963) The behavior of inverted pendulum structures during earthquakes. *Bulletin of the Seismological Society of America*, **53**(2), 403–417.
- IBC I. (2009) International Code Council. International Building Code.
- Kalliontzis, D., Sritharan, S., and Schultz, A. (under review) Generalized formulation for coefficient of restitution of free rocking members, *Journal of Structural Engineering*.
- Kurama, Y., Sause, R., Pessiki, S., and Lu, L. (1999) Lateral load behavior and seismic design of unbonded post-tensioned precast concrete walls. *ACI Structural Journal*, **96**(4), 622–632.
- Kurama, Y. (2002) Hybrid post-tensioned precast concrete walls for use in seismic regions. *PCI Journal*, **47**(5), 36–59.
- Marriott, D., Pampanin, S., Bull, D., and Palermo, A. (2008) Dynamic testing of precast, post-tensioned rocking wall systems with alternative dissipating solutions. *Bulletin of the New Zealand Society for Earthquake Engineering*, **41**(2), 90–103.
- McKenna, F., Fenves, G., and Scott, M. (2000) Open system for earthquake engineering simulation. University of California, Berkeley, CA.
- Nazari, M., Aaleti, S., and Sritharan, S. (2015) Shake Table Testing of Single Rocking Walls @ UNR. *Network for Earthquake Engineering Simulation (distributor)*, doi: 10.4231/D3N29P75Z(SRW1), 10.4231/D3H98ZF0B(SRW2), 10.4231/D3CJ87M6Z (SRW3), and 10.4231/D37S7HT2T(SRW4).
- Nazari, M., Sritharan, S., and Aaleti, S. (2014) Shake table testing of unbonded post-tensioned precast concrete walls. *Proceedings of the 10th National Conference in Earthquake Engineering*, Earthquake Engineering Research Institute, Anchorage, AK.
- Perez, F., Pessiki, S., and Sause, R. (2004) Experimental and analytical lateral load response of unbonded post-tensioned precast concrete walls. ATLSS Report No. 04-11, Lehigh University, Bethlehem, PA.
- Priestley, M., and Tao, J. (1993) Seismic response of precast prestressed concrete frames with partially debonded tendons. *PCI Journal*, **38**(1), 58–69.
- Priestley, M. J. N., Sritharan, S., Conley, JR., and Pampanin, S. (1999) Preliminary results and

- conclusions from the PRESSS five-story precast concrete test building. *PCI Journal*, **44**(6), 42–67.
- Priestley, M. J. N. (2000) Performance Based Seismic Design. 12th World Conference on Earthquake Engineering, Auckland, New Zealand.
- Priestley, M., Calvi, G. M., and Kowalsky, M. J. (2007) Displacement-based seismic design of structures. *Building*, **23**(33), 1453-1460.
- Rahman, M., and Sritharan, S. (2006) An evaluation of force-based design vs. direct displacement-based design of jointed precast post-tensioned wall systems. *Earthquake Engineering and Engineering Vibration*, **5**(2), 285–296.
- Rahman, A. M. and Restrepo, J. I. (2000) Earthquake resistant precast concrete buildings: seismic performance of cantilever walls prestressed using unbonded tendons. Research Report 2000-5, University of Canterbury, Christchurch.
- Sritharan, S., Aaleti, S., Henry, R., Liu, K., and Tsai, K. (2015) Precast concrete wall with end columns (PreWEC) for earthquake resistant design. *Earthquake Engineering and Structural Dynamics*, **44**(12), 2075–2092.
- Seismology Committee. (1999) Recommended lateral force requirements and commentary (Blue book). Structural Engineers Association of California (SEAOC), California, USA.
- Tuna, Z., Gavridou, S., and Wallace, J. (2012) 2010 E-defense four-story reinforced concrete and post-tensioned buildings—preliminary comparative study of experimental and analytical results. *Proceedings of the 15th World Conference on Earthquake Engineering*, Lisbon, Portugal.

CHAPTER 4

DYNAMIC EVALUATION OF PREWEC SYSTEMS WITH VARYING HYSTERETIC ENERGY DISSIPATION

A paper to be submitted to the ASCE Journal of Structural Engineering

Maryam Nazari and Sri Sritharan

4.1. Abstract

Precast Wall with End Columns, known as the PreWEC, was developed as a solution for resisting earthquake lateral loads and validated using quasi-static testing. This paper presents a shake table investigation of this system, which evaluated the performance of four PreWECs with damping varying between 9 and 16%, using multiple-level earthquake input motions. Different amounts of lateral resistance were targeted for the four test units by varying key design parameters, including the post-tensioning area; location of the end columns; and number of the connectors joining the end columns to the wall panel. Results from this study (i) confirmed the ability of using PreWECs with different locations for the end columns; (ii) validated good seismic performance for all four systems in terms of the maximum transient drift, absolute acceleration, and residual drift; and (iii) enabled the strength reduction (R) factor of the PreWEC system to be expressed as a fraction of the available damping. Based on the test outcomes, a design procedure for PreWEC systems is also presented.

Keywords: Precast, Wall, PreWEC, unbonded post-tensioning, O-connector, hysteretic energy dissipation, shake table testing.

4.2. Introduction

To utilize precast concrete rocking walls cost effectively, PreWEC systems were developed by Sritharan et al. (2015). In these systems, special Oval-shaped connectors, or O-connectors, are placed between a Precast Wall panel and two End Columns, which provide supplementary hysteretic energy dissipation for the PreWEC. As outlined by these researchers, the columns may be positioned either at the end of the wall panel or on the sides of the panel near the wall toe. These columns may be designed to be as tall as the wall panel or shorter, depending on the need. When the PreWEC system is subjected to a lateral load, the wall panel and end columns experience a single crack opening at their bases, resulting in rocking response for these systems. The O-connectors, which are made from grade A50 steel plates, dissipate energy due to undergoing inelastic deformations resulting from the relative displacement between the column and wall panel along the column axial direction (Sritharan et al. 2015).

A large-scale quasi-static cyclic test and related analytical investigations of the behavior of PreWEC confirmed that this system complies with the criteria of ACI ITG-5.1 (2008), allowing it to be used in seismic design (Sritharan et al. 2015). Relying primarily on the large-scale quasi-static testing of different wall systems and limited analytical studies completed as of 1999 (e.g., Priestley et al. 1999; Stanton et al. 2002; and Kurama 2002), ACI ITG-5.1 (outlines seismic acceptance criteria for special unbonded post-tensioned precast concrete walls. The requirements of ACI ITG-5.1 include a minimum amount of hysteretic damping ratio of 8% for the post-tensioned systems to control their lateral displacements and decay of dynamic response following a major earthquake. This value has been questioned in a previous study that involved shake table testing of Single Rocking Walls (SRWs) without additional energy dissipaters (Nazari et al. 2016). This is because SRWs with almost 50% lower hysteretic damping compared to the amount

imposed by ACI ITG-5.1 satisfactorily performed during the design-level earthquakes. Therefore, it is of interest to determine the optimal amount of damping for the PreWEC systems to ensure their seismic response.

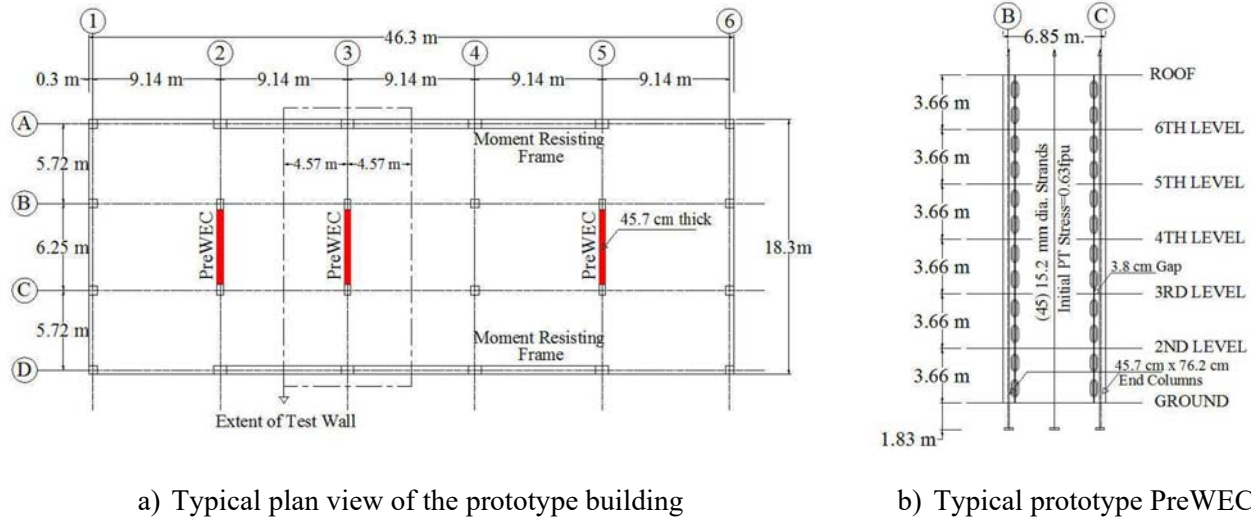
To investigate the performance of PreWECs under dynamic loading and evaluate the amount of required damping, a shake table test investigation was undertaken on four PreWEC systems using multiple-level earthquakes. These systems were designed with different amounts of initial Post-Tensioning (PT) force; hysteretic damping by varying the number and locations of O-connectors; and base moment to base shear ratio (i.e., seismic height), while satisfying the minimum requirements of ACI ITG-5.1 (2008). First, the shake table investigations began by presenting the experimental global and local seismic responses of rocking wall systems, including the variation of prestress force; equivalent damping ratio; and residual drift. The experimental data and results from a simplified analytical model were then used to conduct a performance-based seismic assessment of test units to ascertain the feasibility of using this new wall system in high seismic regions. Finally, a strength reduction (or R) factor suitable for force-based design of PreWEC systems was investigated, which can be adopted in ACI ITG-5.1.

4.3. Test Program

4.3.1. Prototype structure

In this study, 5/18-scale models of a PreWEC system designed for a six-story prototype office building in Los Angeles, California were experimentally investigated. Figures 4-1a and 4-1b show a typical plan view of the prototype structure, which includes the location of three PreWECs and their dimensions. The prototype building was designed according to IBC (2009)

and ASCE 7-05 (2005), resulting in each PreWEC to resist a base shear of 1895 kN (426 kip) and an overturning moment of 30231 kN-m (22297 kip-ft) in the transverse direction of the building.



a) Typical plan view of the prototype building

b) Typical prototype PreWEC

Figure 4-1. Details of the prototype building (1 m = 3.28 ft; 1 kip = 4.45 kN)

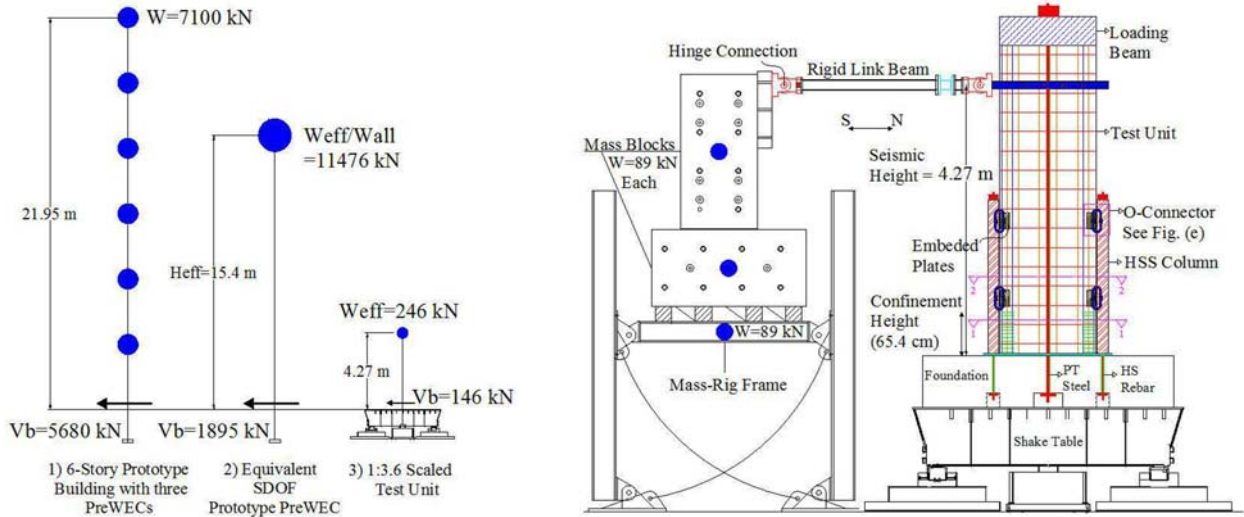
4.3.2. Test units

The test units were designed as a single degree of freedom (SDOF) system to capture the predominant rocking mode of the PreWEC system. Figure 4-2a displays two steps used to develop the scaled SDOF test unit. Table 4-1 summarizes the design parameters and capacities of the prototype PreWEC and the scaled test unit. Figure 4-2b shows a sketch of the test set-up at the NEES facility at the University of Nevada at Reno (UNR) which enabled application of the inertia effect at 4.27 m (14 ft) effective height of the test unit from a mass-rig system weighing 267 kN (60 kips). Assuming that the top half of the wall also induces the inertia effect, the total effective mass of the system is about 18% larger than that determined from the prototype building (see Figure 4-2a), implying higher shear demand on the scaled test unit as presented in Table 4-1.

Figure 4-2c shows reinforcement details of the scaled test unit according to the minimum requirements of ACI 318-11 (2011) using a specified concrete strength of 41.4 MPa (6 ksi) and A706 Grade 60 reinforcement. Following the ACI ITG-5 guidelines (2008; 2009) and recommendations from Aaleti and Sritharan (2009), confined boundary elements over a height of 65.4 cm (25.75 in.) were used at each end of the wall. Additionally, to provide a rigid rocking surface, a grout pad with a specified strength of 68.95 MPa (10 ksi) was placed as an interface material between the wall panel and foundation block (ACI ITG-5.1 2008; ACI ITG-5.2 2009). The Simplified Analysis (SA) method, proposed by Aaleti and Sritharan (2009), was used as a tool to design the wall post-tensioning and details of O-connectors. Accordingly, three-15.2 mm (0.6 in.) diameter PT tendons (a total area of 4.2 cm² (0.651 in²)) along with initial prestressing stress of 0.56 f_{pu} (f_{pu} = tensile strength of tendon = 1862 MPa (270ksi)) were used in the scaled test unit. A total of eight O-connectors were also placed between the wall and end columns for supplemental energy dissipation. The cyclic force-deformation properties of connectors were quantified using a test set-up, as shown in Figure 4-3a. Figure 4-3b presents the experimental response envelope of the connectors, which depicts the onset of yielding in addition to the ultimate fracture point, as noted in Table 4-1.

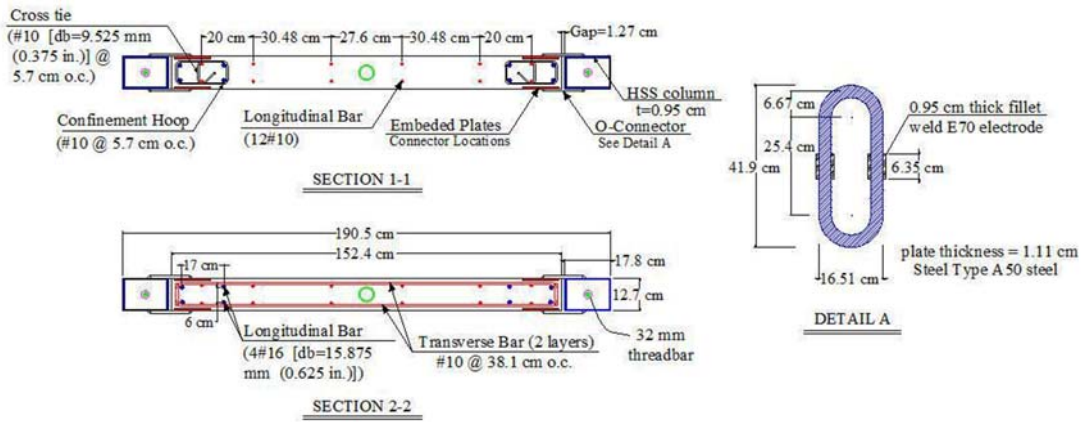
The test matrix included four PreWEC systems: namely PreWEC-1, PreWEC-2, PreWEC-s1, and PreWEC-s2, with PreWEC-2 representing the scaled wall summarized in Table 4-1. Other test units were detailed by changing the test parameters as follows: (i) the initial prestress force in the range of 440 kN (99 kips) to 830 kN (187 kips) by changing the initial stress and total area of PT tendons, (ii) damping ratios between 9 and 16% by varying the numbers of O-connectors, and (iii) base moment to base shear ratio of 3.5 m (11.5 ft) for PreWEC-1 and 4.27 m (14 ft) for the

rest of the test units. The measured values of key design variables and the corresponding estimated test unit capacities are provided in bold in Table 4-2.



a) Scaling prototype PreWEC to the test unit

b) Test set-up



c) Test unit details (cross-section of the wall panel and dimensions of the O-connectors)

Figure 4-2. Prototype building, details of the test unit and test set-up

(1 m = 3.28 ft; 1 kip = 4.45 kN)

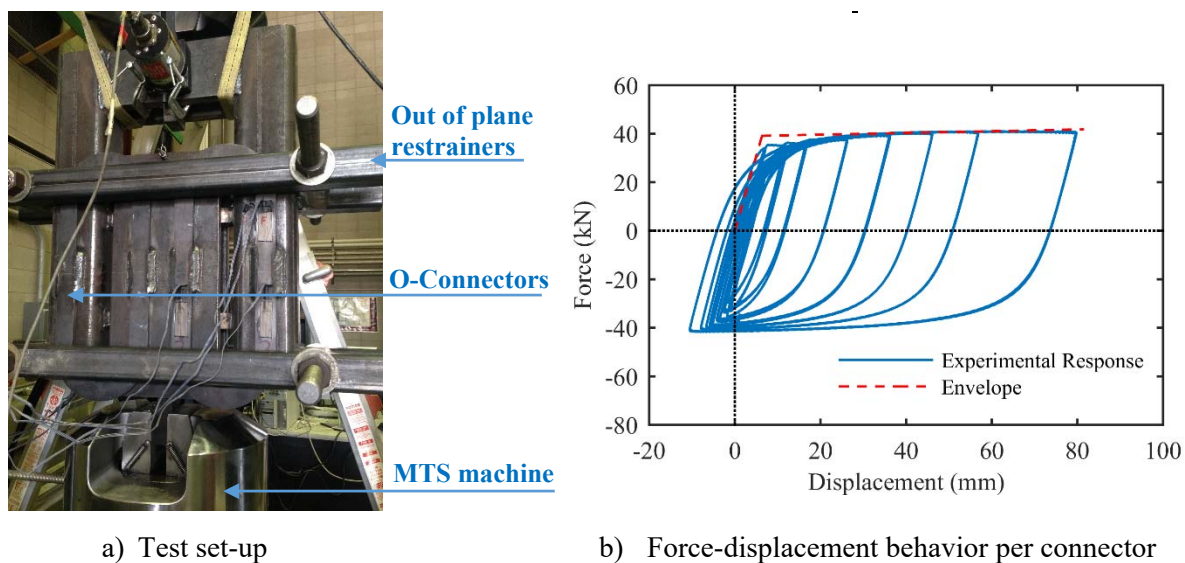


Figure 4-3. Testing of O-connectors and the cyclic response (1 m = 3.28 ft; 1 kip = 4.45 kN)

Table 4-1. Summary of design parameters and capacities for the prototype PreWEC and the scaled test unit (1 m = 3.28 ft; 1 kip = 4.45 kN)

Parameter		Prototype PreWEC		Scaled test unit	
		Wall panel	End column (concrete)	Wall panel	End column (HSS tube)
Dimension	Length (m)	5.25	0.76	1.52	0.18
	Thickness(m)	0.46	0.46	0.13	0.13
	Total length of the system (m)	6.85		1.91	
Post-tensioning parameters	Area (cm ²), A_{PT}	63	12.6	4.2	8.04 ^a
	Initial stress (MPa), f_{pi}	$0.63f_{pu}$	$0.8f_{pu}$	$0.56f_{pu}$	330 ^a
	Unbonded length (m)	23.8	23.8	6.43	3.3
O-connectors	Total number	48		8	
	Yield point: f_y, Δ_y (kN,mm)	-		39, 6.35	
	Ultimate point: f_u, Δ_u (kN,mm)	-		42, 81.3	
	@ 2% drift: $f_{2\%}, \Delta_{2\%}$ (kN,mm)	71.2, 101.6		40, 28.4	
Concrete compressive stress (MPa), f'_c		41.4	41.4	41.4	-
Design shear at 2% drift ratio (SA method)		1895 ^b		182	

^a 32 mm DYWIDAG threadbars tensioned to resist 1.5 times the max force of four connectors per joint.

^b This was increased to 2235 kN due to additional mass provided by the external mass-rig system.

Table 4-2. Test matrix (1 m = 3.28 ft; 1 kip = 4.45 kN; 1 ksi = 6.9 MPa)

Wall system ID	No.Conn ^a	Post-tensioning Parameters		Shear resistance at 2% drift ^b		
		No., dia.(cm), of PT tendon	Initial PT stress (f_{pi} , MPa)	Total (kN)	Wall Panel (%)	Connectors (%)
PreWEC-1	12	5, 1.52	1186 (0.64 f_{pu})/ 1233	349/ 372	64	36
PreWEC-2	8	3, 1.52	1048 (0.56 f_{pu})/ 996	182/ 183	59	41
PreWEC-s1	8	5, 1.52	1186 (0.64 f_{pu})/ 1169	290/ 312	81	19
PreWEC-s2	12	3, 1.52	1186 (0.64 f_{pu})/ 1186	243/ 254	63	37

^a Total number of O-connectors

^b SA method; using design/measured parameters.

Two different configurations of PreWEC systems were investigated. In PreWEC-1 and PreWEC-2, the end columns were positioned at the end of the wall panel whereas they were placed on the sides of the wall near the toe in PreWEC-s1 and PreWEC-s2. In the first two specimens, the length of the wall panel was decreased to 152.4 cm (5 ft) to keep the overall length of the system unchanged. Details of these two systems are presented in Figure 4-4. As shown in Figure 4-4a, each end column in PreWEC-1 and PreWEC-2 was clamped to the foundation using concentrated unbonded post-tensioning at the center of its section to resist against the force developing in the connectors. The columns in the PreWEC-s systems were anchored to the foundation using a pin connection, allowing them to freely rotate in-plane during lateral loading (see Figure 4-4b).

Apart from the design parameters summarized in Table 4-2, this study also indicated the effect of additional toe confinement on minimizing damage by casting steel channels into two precast test units. This armoring detail was used over a partial length (0.2L, where L is length of the wall) in both ends of PreWEC-s1 and over the full length in PreWEC-1. No armoring was considered for PreWEC-s2, similar to the scaled test unit (i.e., PreWEC-2). As discussed in Sritharan et al. (2015), a 19.1 mm (3/4 in.) wide soft foam was placed right under the concrete

cover to prevent the steel channels from deforming due to impacts and subsequent spalling of cover concrete of the wall panel.

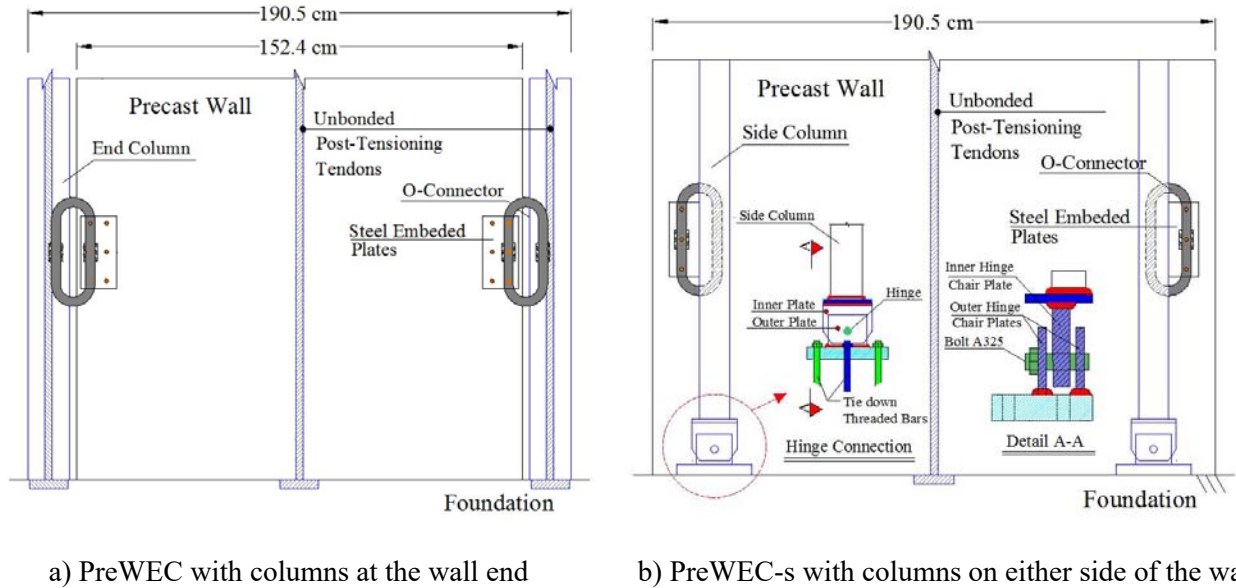
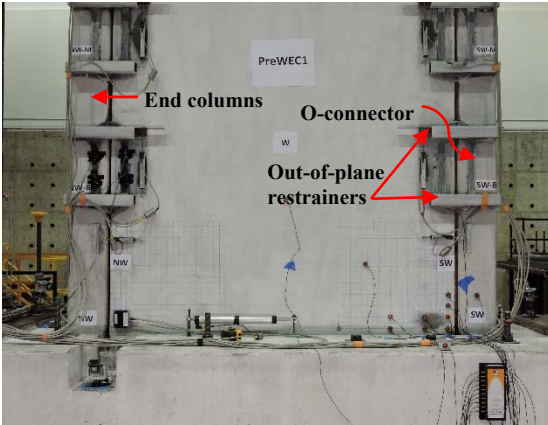


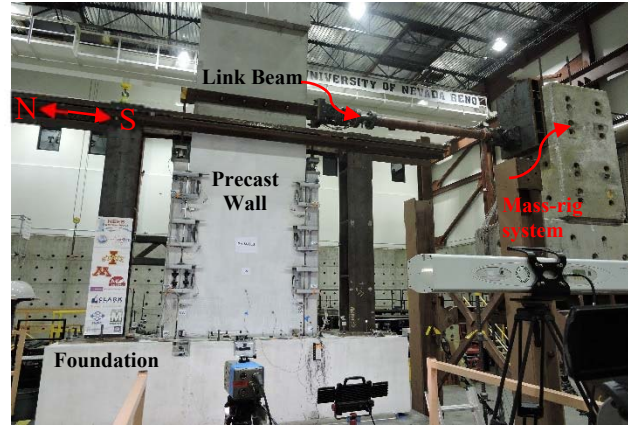
Figure 4-4. Configuration of PreWEC and PreWEC-s test units

4.3.3. Test set-up and loading protocol

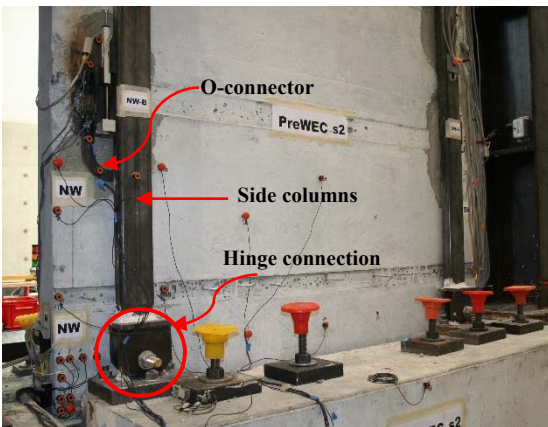
Figure 4-5 shows details of the shake table test set-up used for PreWEC and PreWEC-s systems. A detailed instrumentation was used to capture the wall behavior, including load cells, direct current displacement transducers, krypton camera system (LED sensors), string potentiometers, strain gauges and accelerometers. More details of the instrumentation scheme can be found in Nazari et al. (2015).



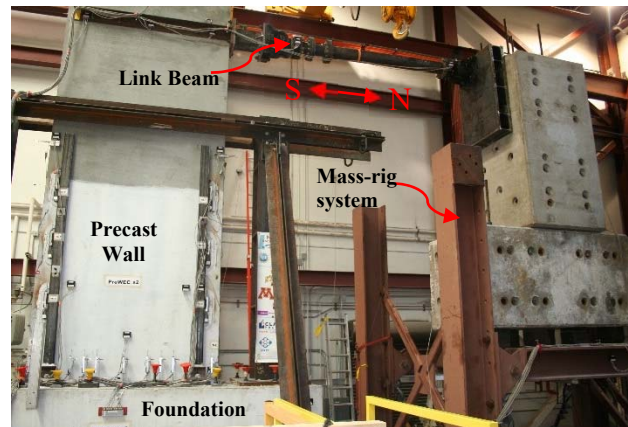
a) Details of a PreWEC system



b) Test set-up used for the PreWEC system



c) Details of a PreWEC-s system



d) Test set-up used for the PreWEC-s system

Figure 4-5. Experimental set-up used for the shake table testing

The loading protocol for dynamic testing of the units consisted of earthquake motions with different intensities, sinusoidal motions, and free vibration testing. Due to the space limitations, only wall responses to earthquake records are presented in this paper. The selected ground motions, as summarized in Table 4-3, were representative of four seismic hazard levels, EQ-I to EQ-IV, corresponding respectively to frequent events, occasional events, design-base earthquake (DBE) and maximum considered earthquakes (MCE). As summarized in Table 4-3, multiple-level ground motions consisted of short vs. long-duration and far-field (FF) vs. near-field (NF) earthquake

records. Since the information available in this table represents the motions for the prototype system, amplitude of all the records was scaled up by 18/5 and the time step was reduced by a factor of 5/18 to make the input motions compatible with the 5/18-scale of the test units.

Nazari et al. (2016) provides justification for the selection of the input motions and the scale factor presented in Table 4-3. All motions are based on recorded motions around the world with peak ground acceleration varying from 0.14 to 0.71g after applying the scale factor.

Table 4-3. List of ground motions

Input motion	Type of motion	Earthquake name (Year), Station, FF/NF	Scale factor	Targeted hazard level	PGA (g) after applying the scale factor
Short-duration					
Eq-1s	Spectrum compatible short duration motions used in PRESSS building (Priestley et al. 1999)	Hollister (1974), Gilroy Array#1, FF	0.67	EQ-I	0.14
Eq-2s		San Fernando (1971), Hollywood Storage, FF	1.00	EQ-II	0.23
Eq-3s		Imperial Valley (1940), Elcentro, FF	1.00	EQ-III	0.49
Eq-4s		Northridge (1994), Sylmar, NF	1.00	EQ-IV	0.71
Long-duration					
IM-a	Records recommended by Rahman and Sritharan (2006)	Morgan Hill (1984), Gilroy Array#6, NF	0.65	EQ-I	0.19
IM-b		Loma Prieta (1989), Saratoga Aloha Avenue, NF	0.64	EQ-II	0.32
IM-e		Kobe-Japan (1995), KJM, NF	0.94	EQ-III	0.56
NZ	Recordings from recent earthquakes	New Zealand (2011), HVSC, NF	0.40	EQ-II	0.58
Chile		Chile (2010), Angol, FF	1.00	EQ-III	0.49
Takatori	E-Defense test record (Tuna et al. 2012)	Kobe-Japan (1995), Takatori, NF	0.60	EQ-IV	0.37

Note: NF = near-field motion; FF = far-field motion

4.4. Analytical Modeling in OpenSees

A SDOF model, as shown in Figure 4-6, was developed in OpenSees (McKenna et al. 2000) for the test units, which included two zero-length rotational springs to connect an elastic beam-column element modelling the concrete wall panel to the base (See Figure 4-6a). The spring simulated by the uniaxial SelfCentering material model is available in OpenSees (McKenna et al. 2000) and was used to capture the moment resistance of the system provided by the wall post-tensioning as well as its re-centering capability. This was previously used to successfully model the moment-rotational characteristics of the SRWs (Nazari et al. Chapter 3). The second rotational spring at the base allowed for the resisting moment and hysteretic energy dissipation exhibited by PreWEC systems due to the use of the external steel O-connectors. This spring element used the Giuffre-Menegotto-Pinto material model, which is Steel02 in OpenSees to idealize moment rotation response of the connectors with an elasto-plastic material response. A number of parameters needed to be specified when modelling this spring, which included yielding and ultimate force-displacement properties of the connectors, as denoted in Table 4-1, in addition to the length of the moment lever arm between the connectors, as shown in Figure 4-6b. When the wall system rocks, the base rotational springs activate in parallel to take into account for the total resistance and energy dissipation of the system during rocking (see Figure 4-6b).

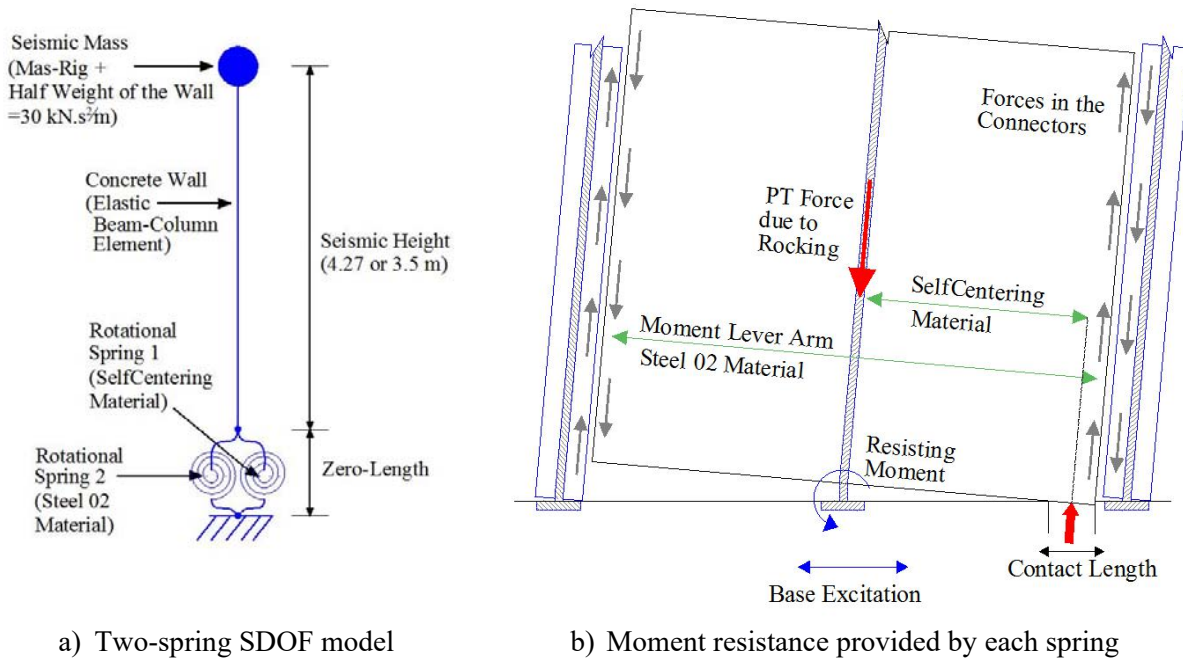


Figure 4-6. Opensees model for a PreWEC system (1 m = 3.28 ft; 1 kip = 4.45 kN)

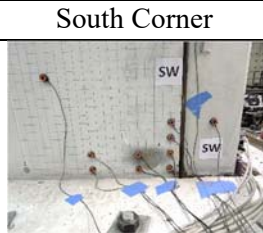











4.5. Test Observations and Key Results

A total of 18 to 30 input motions were applied to each test unit. Some of these input motions were generated using additional scale factors to the records summarized in Table 4-3. During testing, there were some differences between the actual table-generated ground motions and the intended records. Noticeable deviations of the shake table accelerations from the intended accelerations were differentiated by assigning + or – signs to the intensity level (e.g., EQI⁺, EQIII⁻). One unit of + and – sign were assigned when the RMSD of the spectral ordinates of the table-generated accelerations normalized by the mean of the target spectrum deviated by more than +30% and -30%, respectively.

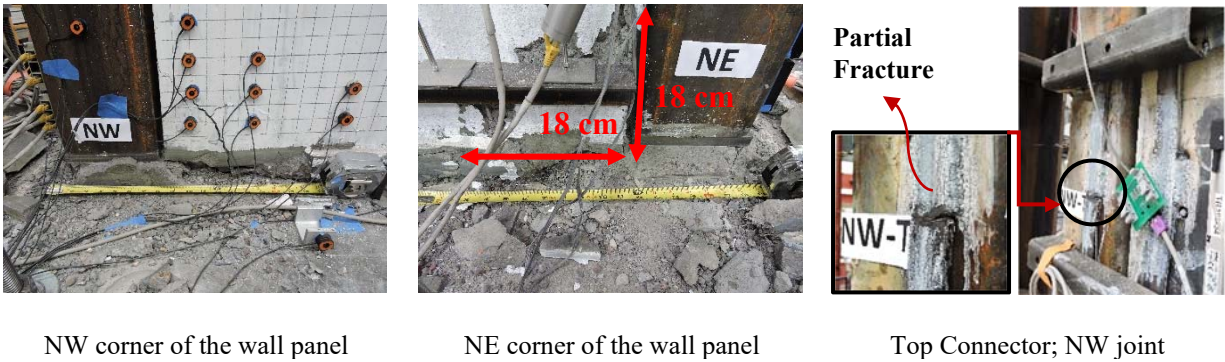
4.5.1. Test observations

All PreWEC systems performed well with minimal damage to the wall panels observed during EQ-I to EQ-III levels of input motions. As shown in Table 4-4, the damage to the PreWEC systems was limited to negligible spalling of cover concrete at the toes of the wall panel during a suite of EQ-III level seismic events. The extent of distress to the cover concrete progressed further as no base channel was used (e.g., PreWEC-s2 over a height of 28 cm (11 in.)). The onset of yielding of O-connectors was also observed while test units experienced a lateral drift of 0.6%.

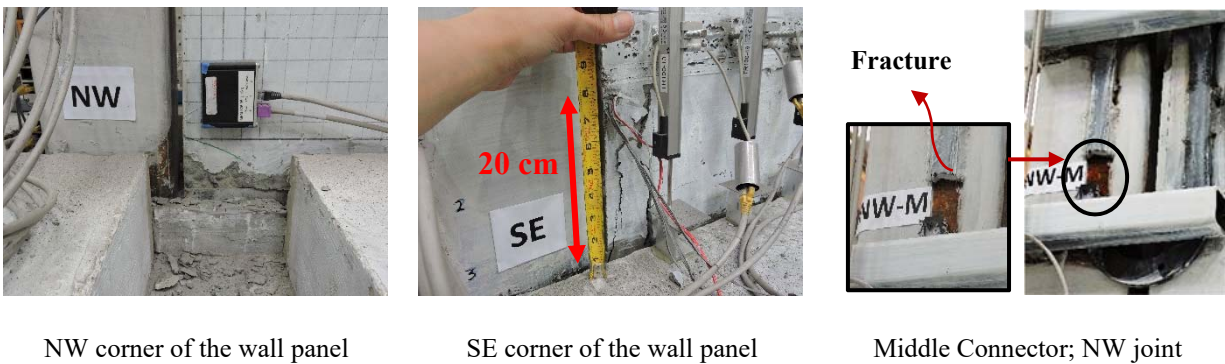
Table 4-4. Typical condition of the wall base region and connectors after experiencing EQ-III level motions (1 m = 3.28 ft)

Wall	Max Drift	South Corner	North Corner	Connector
PreWEC-1	1.9%			
PreWEC-2	2.2%			
PreWEC-s1	2.3%			
PreWEC-s2	2.3%			

As shown in Figure 4-7, the impact of wall base armoring on reducing damage was noticeable when PreWECs underwent larger drifts. As evidenced for EQ-IV level events, PreWEC-2 with no steel channel experienced some damage to the core concrete over a length of 18 cm (7 in.) from the edge of the wall (see Figure 4-7a) at 3.7% lateral drift; however, as shown in Figure 4-7b, PreWEC-1 with the base armoring along the wall length exhibited cracking and minor spalling of cover concrete over a height of 20 cm (8 in.) after experiencing maximum drift of 4.5%. Fracture of connectors and some yielding of post-tensioning tendons were also observed at this level.



a) PreWEC-2 without channels; max drift of 3.7% after an EQ-IV event



b) PreWEC-1 with channels; max drift of 4.5% after an EQ-IV event

Figure 4-7. Impact of armoring the wall base using a steel channel (1 m = 3.28 ft)

The testing was terminated with applying a set of EQ-III and EQ-IV level earthquakes to: (i) PreWEC-1 after fracture of about 67% of connectors as well as 14% loss of initial PT stress due to yielding of tendons, and (ii) PreWEC-s1 and PreWEC-s2 after loss of 20% and 23% of prestressing, respectively. The condition of the modified test units is denoted in this paper by adding “m” to the wall designation (e.g., PreWEC-1m). Neither the PT loss nor the fracture of connectors affected the self-centering capability of the PreWEC systems as they all experienced negligible amount of residual drift following earthquakes of different intensities. However, during 1.1×Takatori (i.e., representing an EQ-IV event), PreWEC-1m experienced additional local damage to the wall base, resulting in a residual drift of 2.35%.

4.5.2. Lateral load response

Using the measured data, the base shear-lateral drift responses of PreWEC units during an EQ-III level record (i.e., 0.8×Eq-4s) are compared in Figures 4-8a and 4-8b. As shown in Figure 4-8a, increasing the total number of connectors from eight in PreWEC-s1 to twelve in PreWEC-s2 resulted in larger hysteresis loops and consequently increased the amount of energy dissipation. Figure 4-8b shows greater ultimate resistance of PreWEC-s1 to PreWEC-2 due to a larger area of PT tendons as well as the increased length of the wall panel in the PreWEC-s system. Figure 4-8c presents the backbone responses of PreWEC-2 and PreWEC-s2 together with the response envelopes obtained from the SA method (Aaleti and Sritharan 2009). It can be seen that the SA method accurately captured the response envelope of PreWEC-2, but overestimated the same for PreWEC-s2. In PreWEC-s2, the connectors experienced lower relative displacement. Using the measured deformation of connectors, estimated response envelope of PreWEC-s2 shows good correlation with the observed data, as plotted in Figure 4-8d.

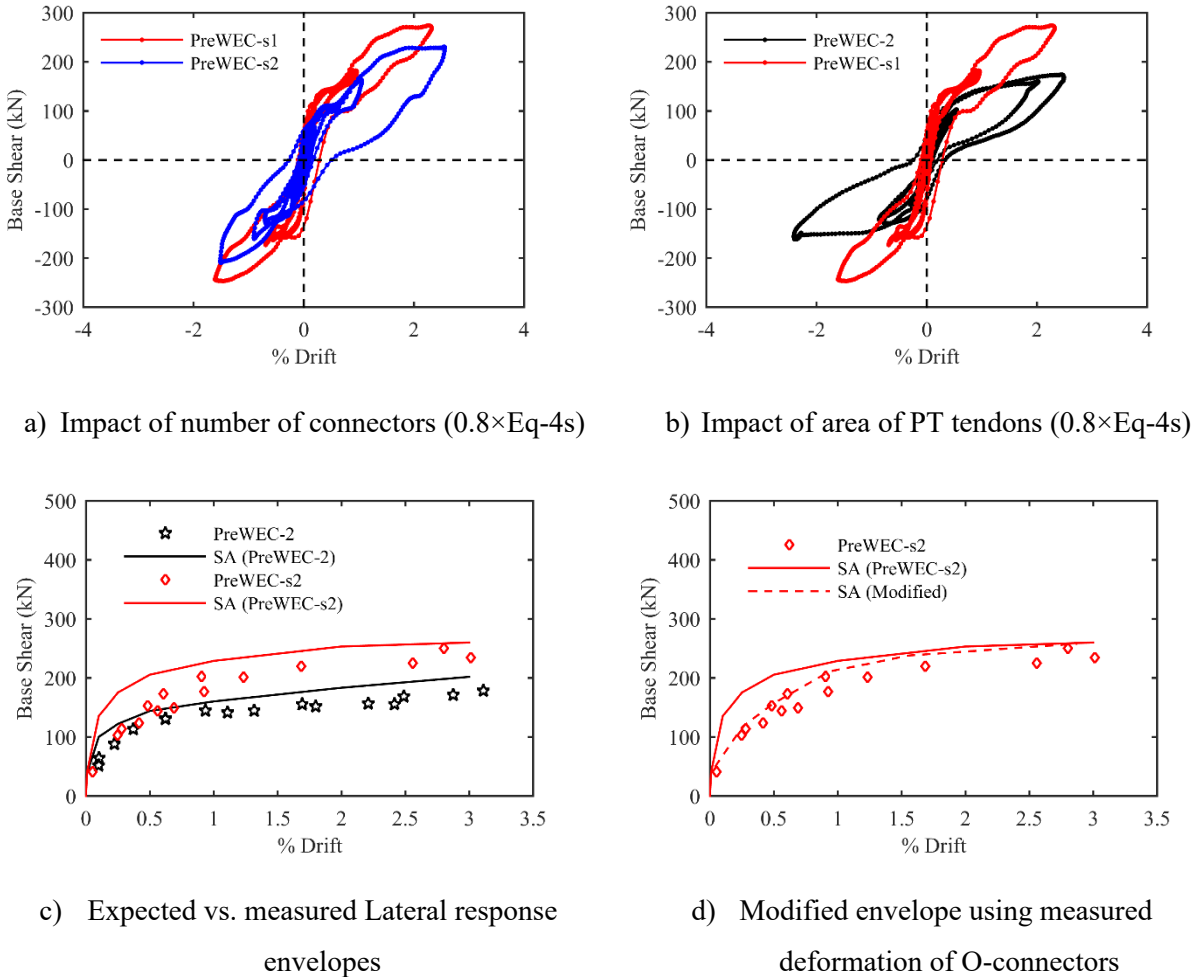
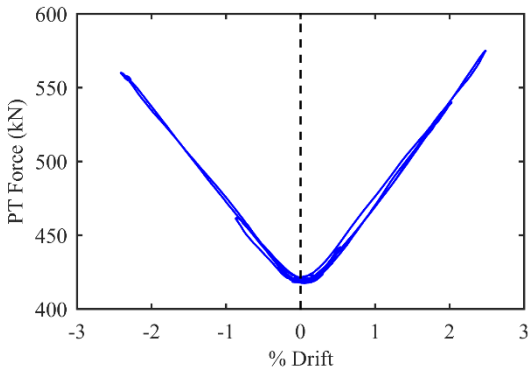


Figure 4-8. Lateral response of test units (1 kip = 4.45 kN)

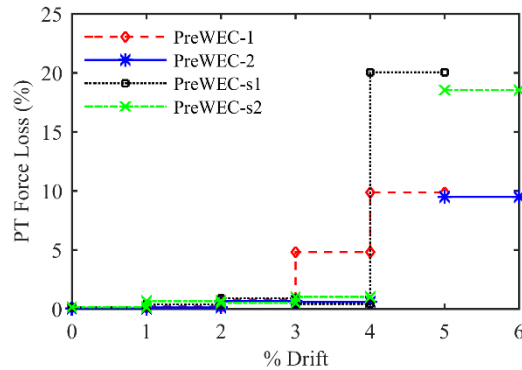
4.5.3. Post-tensioning behavior

The unbonded tendons remained elastic in all test units during four levels of earthquakes (e.g., PreWEC-2 during $0.8 \times \text{Eq-4s}$ as shown in Figure 4-9a). Figure 4-9b indicates average loss of the initial prestressing force under different range of drift levels. As presented in this figure, the PT tendons remained nearly elastic for lateral drifts less than 3%; however, PreWEC-s and PreWEC units experienced a maximum of 20% and 10% reduction in the PT force, respectively, after they underwent larger drifts during a set of sinusoidal excitations toward the end of testing.

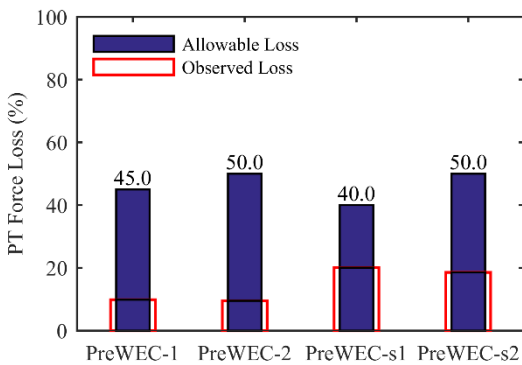
Some of the test units did not experience a certain amount of drift and as a result no data is reported for those units in this figure (e.g. PreWEC-s2 for a drift range of 4-5%). As shown in Figure 4-9c, the average observed PT loss in the PreWEC systems are lower than the permissible amount; this is anticipated following the SA method (Aaleti and Sritharan 2009) and may result in 20% drop in the shear resistance of the system at 2% lateral drift. Using the OpenSees model, dynamic analysis of the test units during EQ-III and EQ-IV level ground motions revealed a maximum of 10% increase in their average lateral drift as a result of this maximum allowed PT loss (see Figure 4-9d).



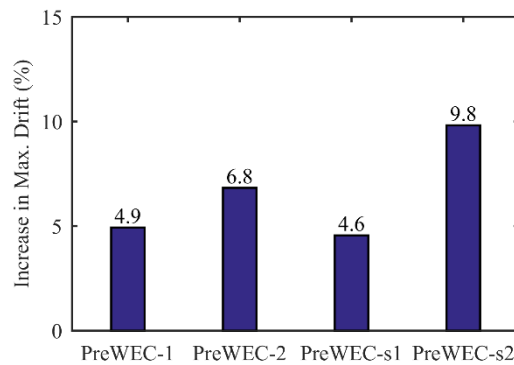
a) Variation of PT force vs lateral drift (PreWEC-2 during 0.8× Eq-4s)



b) Average of PT loss vs. range of drift



c) Allowable vs. observed PT loss

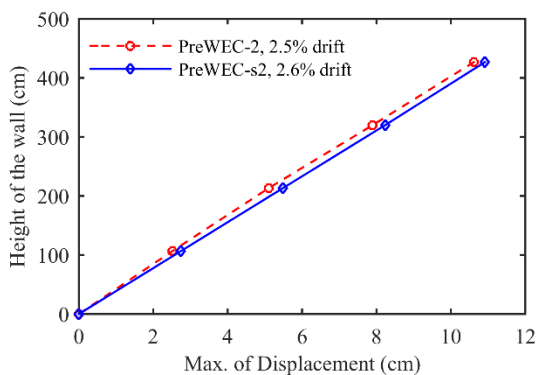


d) Increase in drift due to the allowable PT loss in PreWECs during strong motions

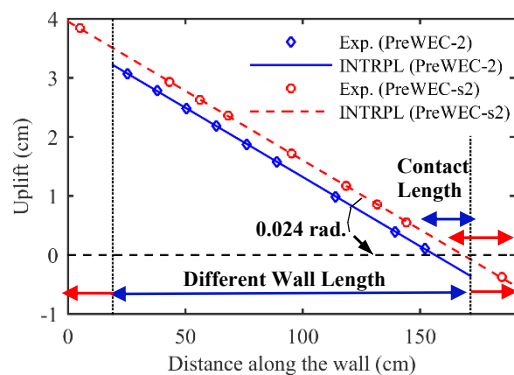
Figure 4-9. Post-tensioning force response: variation and loss vs. lateral drift (1 kip = 4.45 kN)

4.5.4. Wall uplift

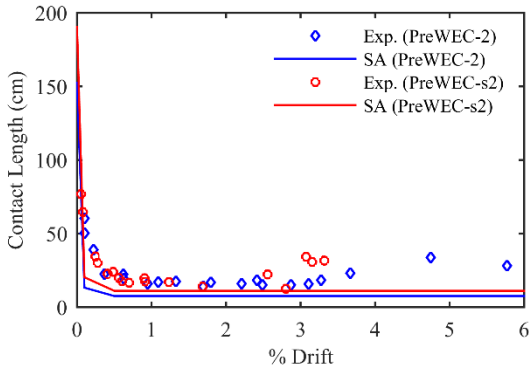
Figure 4-10a depicts linear distribution of deflection over the height of PreWEC-2 and PreWEC-s2 while these units experienced maximum rotation of 0.025 and 0.026 radians, respectively, during $0.8 \times \text{Eq-4s}$. This resulted in linear profile of the wall uplift, as closely captured in Figure 4-10b through interpolation on a data set measured by vertical displacement gauges along the base of the wall panels. Therefore, the wall uplift and the corresponding contact compression length primarily depend on the wall panel's rotation. Using the measured uplift profile, contact length of these units as a function of lateral drift at first peaks is presented in Figure 4-10c together with the predicted responses obtained from the SA method (Aaleti and Sritharan 2009). As depicted in this figure, slightly lower prediction of the contact length is observed for the wall panels which resulted in overestimation of their lateral resistance, as previously discussed. The observed difference increased for the drift levels greater than 3%, where wall toes experienced observable damage to the core concrete. The wall uplift response was also used to predict the vertical deformation of O-connectors, as shown in Figure 4-10d.



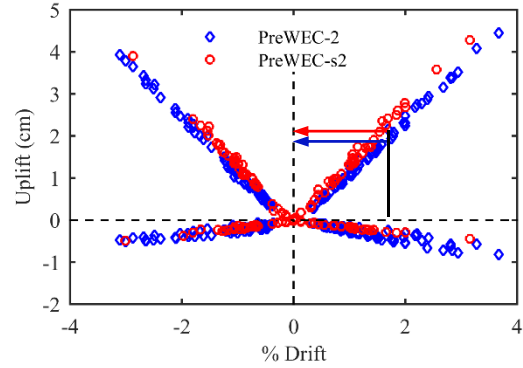
a) Deformation over height; $0.8 \times \text{Eq-4s}$



b) Uplift along the wall length; $0.8 \times \text{Eq-4s}$



c) Contact length vs. drift; first peaks

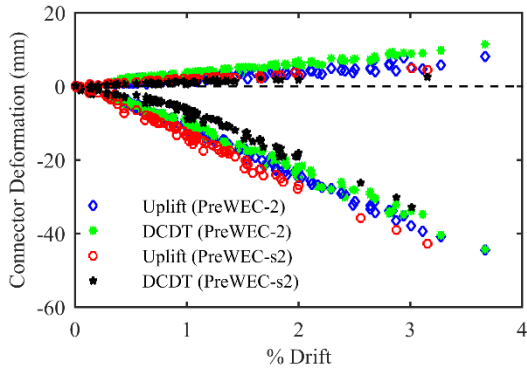


d) Wall uplift at the location of O-connectors

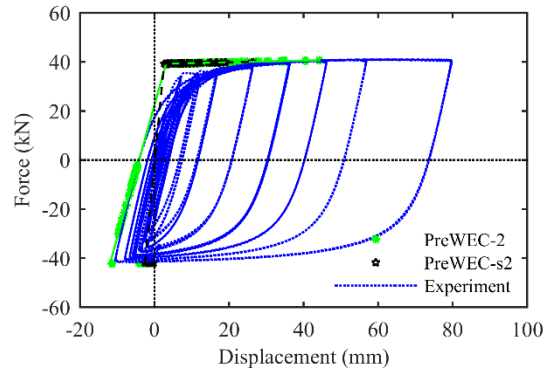
Figure 4-10. Deflected shape and wall uplift response (1 m = 3.28 ft)

4.5.5. Behavior of O-connector

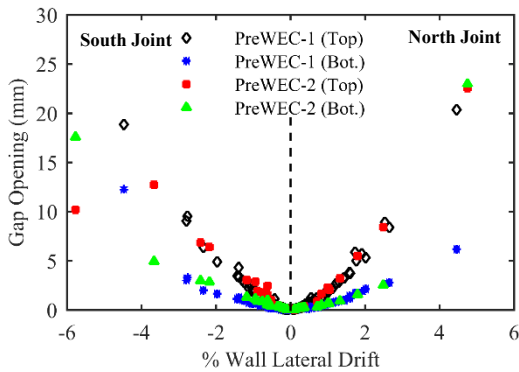
Figure 4-11a compares the measured deformation of O-connectors recorded through displacement gauges (DCDT) with the estimated data of Figure 4-10d for the two selected test units (i.e., PreWEC-2 and PreWEC-s2). According to this figure, O-connectors deformed about 10 mm (0.4 in.) less than expected in the PreWEC-s unit. It is likely this difference is resulted from the existent gap in the fabricated hinge connection at the base of side columns (see Figure 4-4b). Figure 4-11a also indicates lower compressive deformation of O-connectors in PreWECs-2, as they were placed at a location close to the neutral axis depth. As shown in Figure 4-11b, the observed response of O-connectors may result in smaller area-based energy dissipation capacity for the PreWEC-s test units. This could be revised by locating the O-connectors further from the contact length as well as modifying the hinge base connection.



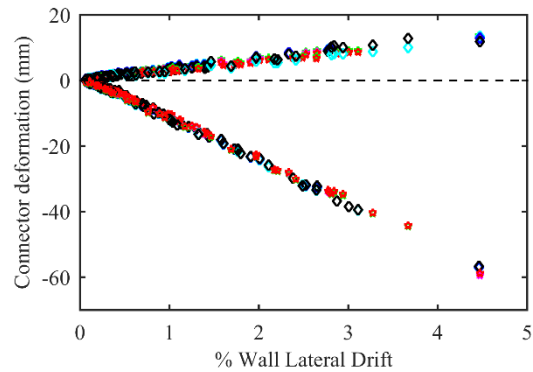
a) Average deformation of O-connectors



b) Force-deformation envelope



c) Gap opening over height of the trailing column for two PreWEC systems



d) Vertical deformation of O-connectors at different heights of two PreWEC units

Figure 4-11. Response of O-connectors (1 m = 3.28 ft; 1 kip = 4.45 kN)

4.5.6. Equivalent damping ratio

During an earthquake excitation, the seismic energy imparted to the PreWEC systems is dissipated through different mechanisms including: (i) the inherent elastic viscous damping of the system, (ii) the hysteretic damping due to inelastic deformations of O-connectors as well as material nonlinearity of concrete at wall toes, as shown in Figure 4-12a for PreWEC-s2 during $0.65 \times \text{Eq-4s}$, and (iii) the energy loss during impacts. The last two energy dissipating components were characterized with equivalent viscous damping ratios in this study as explained as follows.

Using the Jacobsen's secant stiffness approach, as applied in the direct displacement-based design (DDBD) (Priestley 2000), the equivalent viscous damping ratio of test units due to hysteretic action (ξ_{hys}) is plotted in Figure 12b, alongside $\pi \times \xi_{hys}$, which is defined by ACI ITG-5.1 (2008) to represent the relative energy dissipation ratio (β_h) of post-tensioned wall systems. Due to unsymmetrical nature of seismic loads, this approach was applied to each half-cycle of the hysteresis loops while test units were subjected to maximum displacement cycles during ground motions of different intensities. Adding the best fit curve through the experimental data points, as shown in Figure 4-12b, the hysteretic energy dissipation parameters (ξ_{hys} , β_h) at 2% design drift of the wall systems were estimated to be (14.6%, 0.46), (14.3%, 0.45), (7.7%, 0.24), and (14.4%, 0.45) for four test units, respectively. Since the link beam force was used to generate the experimental hysteresis loops, the estimated area-based damping quantity contains the inherent viscous damping (ξ_{vis}) as well.

The area enclosed by the force-deformation hysteresis loops of O-connectors was assessed to develop a simplified numerical equation for estimating the hysteretic damping ratio of the PreWEC system at D% drift level ($\xi_{hys,D\%}$), as shown below in Equation 4-1. This is based upon the assumption that the energy dissipation due to nonlinear behavior of concrete is negligible.

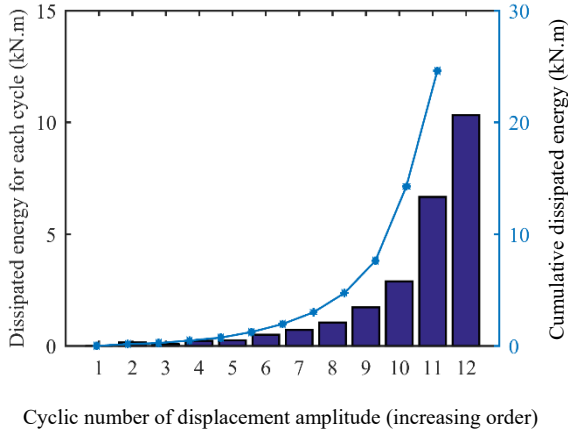
$$\xi_{hys,D\%} = \frac{1}{\pi} \frac{N_{conn.} \times F_{c,ave} \times (\Delta_{c,D\%} - \Delta_{c,y})}{V_{D\%} \times D\% \times H_s} \quad (\text{Equation 4-1})$$

where, $N_{conn.}$ is the total number of connectors, $V_{D\%}$ is the shear resistance of the PreWEC system at D% drift level, H_s is the seismic height and $F_{c,ave}$ is the average of connector forces at yield and certain drift level of the wall system (D%) with corresponding deformations of $\Delta_{c,y}$ and $\Delta_{c,D\%}$.

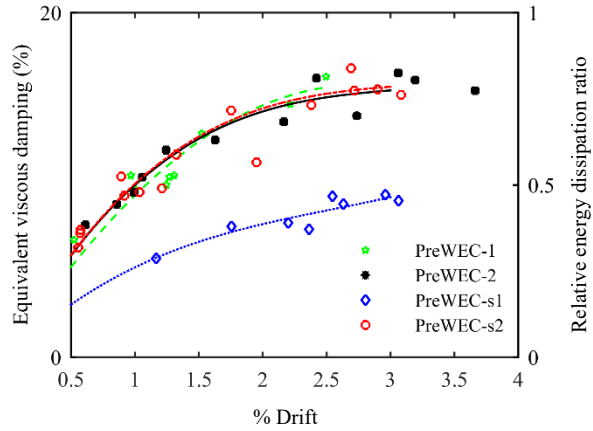
The results of a previous experimental investigation performed on SRWs (Nazari et al. 2016)

indicated an average of 4.2% equivalent viscous damping ratio due to concrete nonlinearity and inherent viscous damping of the system. Adding this amount to the results from Equation 4-1 resulted in a good estimate of the area-based damping of the system through the combined effects of viscous and hysteretic mechanisms. This is shown in Figure 4-12c by comparing the experimental damping with the total amount achieved from the numerical approach for the test units at 2% drift.

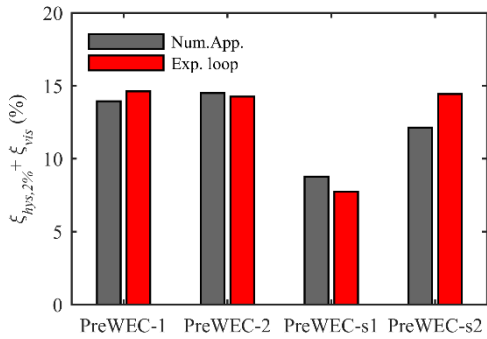
Another source of energy dissipation in PreWECs occurs in the form of kinetic energy loss through impacts of the rocking system on top of the foundation (Housner 1963). An equivalent viscous damping ratio due to impact (ξ_{imp}) was obtained in this study by equalizing the accumulative impact kinetic energy loss through testing ($\Delta E_{k,ACC}$) with a continuous viscous energy dissipation (E_{imp}). $\Delta E_{k,ACC}$ was determined by measuring the square ratio of the exiting to the approaching velocities of a rocking impact (Housner 1963). This was estimated for all test units during a set of Takatori and Eq-4s motions with different intensities and resulted in an average ξ_{imp} of 1% for the PreWEC systems, as depicted in Figure 4-12d. The corresponding amount of damping is related to the secant stiffness of the system at 2% lateral drift. Adding the estimated ξ_{imp} , ξ_{hys} , and ξ_{vis} resulted in an average total equivalent viscous damping ratio (ξ_{eq}) of 8.7% to 15.6% for the test wall systems.



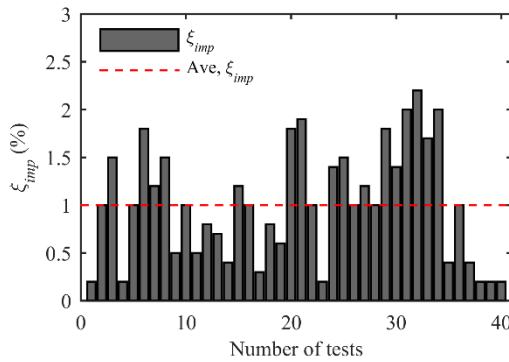
a) Hysteretic energy dissipation
(PreWEC-s2 during $0.65 \times E_q-4s$)



b) Measured area-based damping
($\xi_{hys} + \xi_{vis}$) vs. drift



c) Measured vs. approximated area-based
damping ratio at 2% drift



d) ξ_{imp} for test units during
multiple-level motions

Figure 4-12. Equivalent viscous damping ratio of test units (1 m = 3.28 ft; 1 kip = 4.45 kN)

4.5.7. Residual drift and self-centering capability

All test units self-centered with negligible residual drifts following multiple-level earthquake motions. Figure 4-13a presents the variation of average residual drift of the PreWEC systems (d_{res}) with different range of lateral drifts. As presented in this figure, a maximum d_{res} of 0.1% was recorded at the end of excitations which imposed a lateral drift range of 3-4% to the test units. According to Figure 4-13b, this amount is less than 30% of the maximum possible residual

drift (d_{RES}), as suggested for the self-centering systems by Henry (2011). d_{RES} is found by unloading from the maximum lateral displacement during the excitation. Residual drift of PreWEC-1m after the last EQ-IV level event (i.e., $1.1 \times$ Takatori) was not included in averaging the results presented in the plots of Figure 4-13.

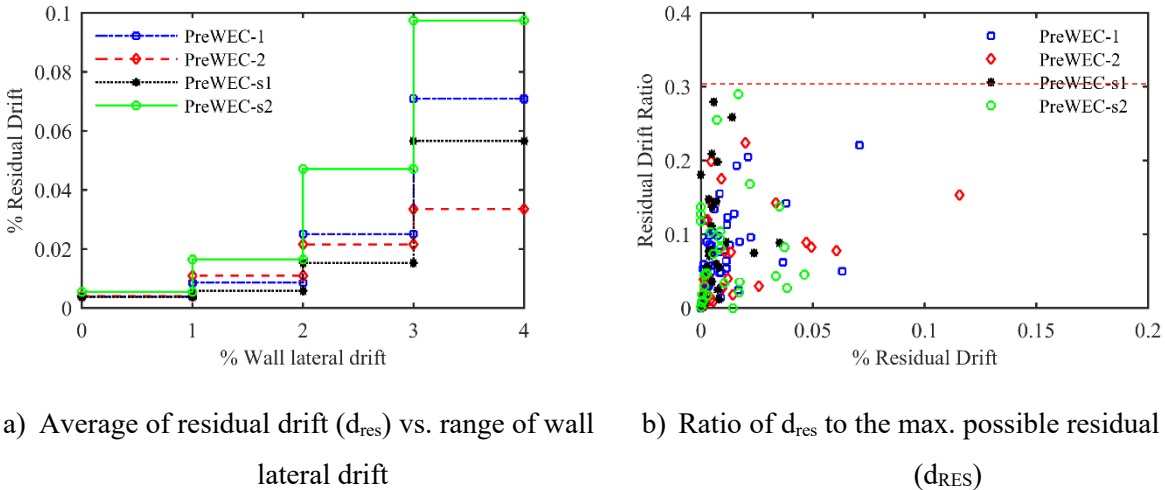


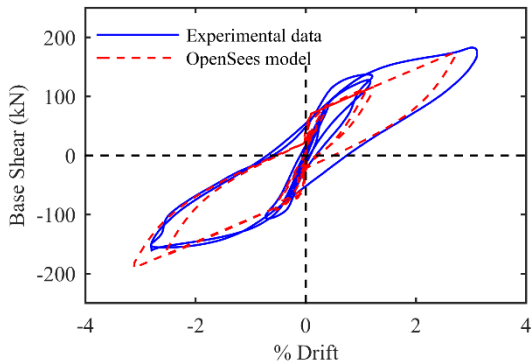
Figure 4-13. Residual drift of test units

4.6. Analytical Comparisons with Experimental Results

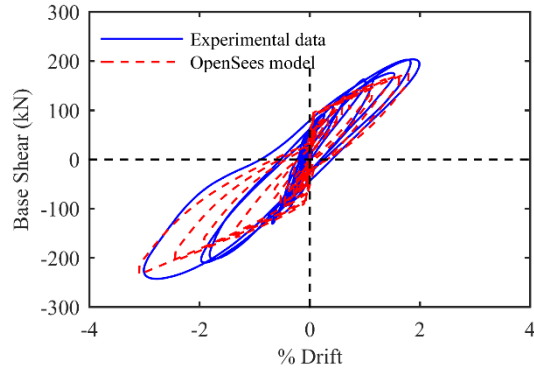
The analytical simulation of PreWEC systems was experimentally validated through the test data. Using the OpenSees model, a series of nonlinear time history analysis were performed applying the Newmark constant average acceleration solution method with an integration time step equal to the sampling rate (i.e., 0.00391 sec.). A Rayleigh damping model was used to introduce the elastic viscous damping of 2% in dynamic analysis. This is the tangent stiffness representation of the estimated damping of the test units due to impacts (see Figure 4-12d) (Priestley et al. 2007).

Figures 4-14a and 4-14b which present the calculated lateral load-drift hysteresis responses of two PreWEC test units against the test measurements during EQ-IV level motions show good

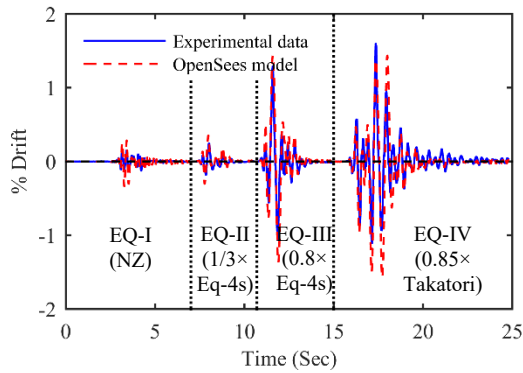
correlations between the OpenSees analytical results and experimental data. As presented in Figures 4-14c to 4-14f, while the predicted drift time history results of PreWEC systems obtained from the analytical model are comparable to that measured during the experimental tests, the peak of responses are excellently matched. Figures 4-14c and 4-14d ensure sufficiency of the assumed hysteretic model in capturing the damage accumulation by showing analytical responses of two PreWEC test units during a set of EQ-I to EQ-IV motions. Using this analytical model, the observed responses were accurately predictable during the strong motions, as shown in Figures 4-14e and 4-14f for two PreWEC-s test units.



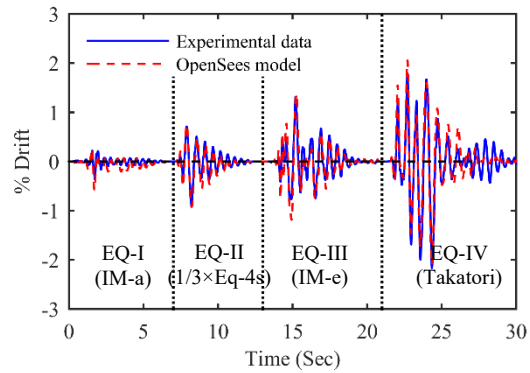
a) Lateral response; PreWEC-2 ($-1 \times \text{Eq-4s}$)



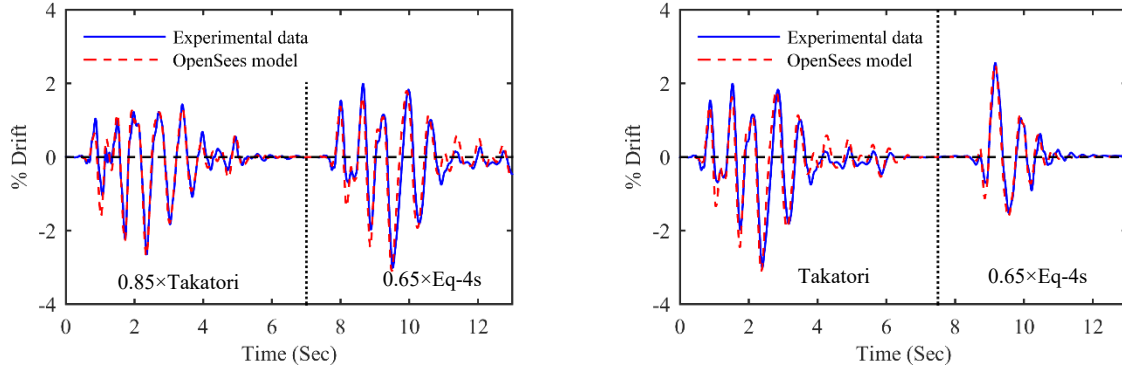
b) Lateral response; PreWEC-s2 (Takatori)



c) Drift time history response; PreWEC-1 (four levels of earthquakes)



d) Drift time history response; PreWEC-2 (four levels of earthquakes)



e) Drift time history response; PreWEC-s1 (EQ-IV events)

f) Drift time history response; PreWEC-s2 (EQ-IV events)

Figure 4-14. Comparison between analytical results and the experimental data
(1 kip = 4.45 kN)

4.7. Seismic Applicability of PreWEC Systems

4.7.1. Performance-based seismic assessment

In consistent with the acceptance criteria established by ACI ITG-5.1 (2008), the seismic performance of test units was evaluated using the shake table test results. As summarized in Table 4-5, these criteria are defined to: (i) assure the self-centering capability of the PreWEC system, (ii) avoid significant strength degradation of the system at large drifts, and (iii) verify an acceptable hysteresis behavior at the ultimate drift cycle of 3%. According to this table, all PreWEC systems fulfilled the mandatory seismic acceptance criteria outlined in this document and therefore could be designed as suitable solutions for regions with high seismicity.

Table 4-5. Seismic acceptance criteria of test units according to ACI ITG-5.1 (2008)

(1 m = 3.28 ft; 1 kip=4.45 kN)

Test unit	Section 7.1.2 ^a		Section 7.1.3 ^b	Section 7.1.4 ^c		
	PT force at $0.5 \times \Delta_T$ (kN)	$0.9 \times$ yield force (kN)		Δ_F	(1)	(2)
PreWEC-1	1005	< 1056	5.1%	0.46/0.49	22.2 > 5.3	0.97
Criteria	OK		OK	OK		
PreWEC-1m	844	< 1056	4.0%	0.22/0.22	12.3 > 2.8	1.00
Criteria	OK		OK	OK		
PreWEC-2	516	< 634	5.7%	0.45/0.49	8.9 > 2.0	0.15
Criteria	OK		OK	OK		
PreWEC-s1	992	< 1056	5.3%	0.24/0.29	14.4 > 3.7	0.41
Criteria	OK		OK	OK		
PreWEC-s1m	815	< 1056	5.3%	0.24/0.29	9.6 > 2.1	0.28
Criteria	OK		OK	OK		
PreWEC-s2	632	< 634	5.6%	0.45/0.49	11.3 > 2.6	1.25
Criteria	OK		OK	OK		
PreWEC-s2m	584	< 634	5.6%	0.45/0.49	6.4 > 1.6	1.46
Criteria	OK		OK	OK		

Note: An ultimate drift (Δ_T) of 3% was applied, according to section 5.4 of ACI ITG-5.1 [2].

^a PT force at $0.5 \times \Delta_T$ should be less than 0.9 times the measured yield force of the tendons at 1% elongation.

^b Δ_F is wall drift, where fracture of connectors happened. It should be greater than Δ_T . Also lateral force did not decrease with increasing drift ratio.

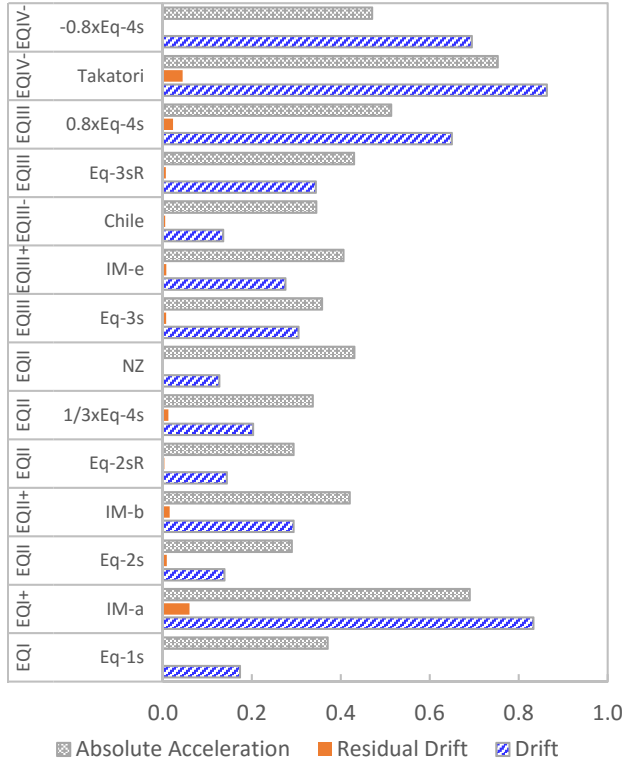
^c (1) β_h should be greater than 0.12, (2) Secant stiffness at $-1/10$ and $+1/10$ of Δ_T shall be not less than 0.1 times initial stiffness of the PreWEC, as defined in section 5.10, (3) Maximum shear-slip at Δ_T shall be less than 1.5 mm (0.06").

The seismic response of PreWECs was further studied in this paper using the measured maximum lateral drift (d_{max}), maximum absolute acceleration (a_{max}), and residual drift (d_{res}) of the test units from different earthquake motions. For this purpose, the recommendations of Rahman and Sritharan (2006) were used to select the permissible values of the aforementioned variables. Accordingly, the maximum response (d_{max} , a_{max} , d_{res}) of the test units at the reduced scale should

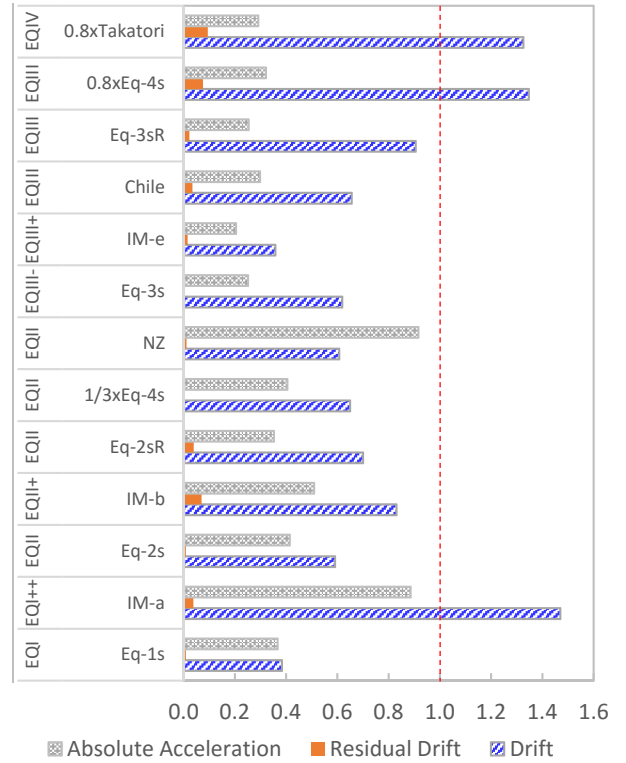
not exceed (0.4%, 0.954g, 0.1%), (1.2%, 2.117g, 0.3%), (2%, 4.32g, 0.5%), and (3%, 6.48g, 0.75%) during four seismic hazard levels of EQ-I to EQ-IV.

Ratio of the maximum observed responses to these permissible values were depicted in Figure 4-15 plots. A value of above one for the ratio indicates that the particular criterion is not satisfied for a particular input motion. The information provided in this figure includes the influence of + or – sign of hazard levels. As shown in Figure 4-15, test units generally displaced to larger drifts during near-field and short-duration motions. When subjected to EQ-I to EQ-III level motions, some PreWECs produced drift responses greater than the allowable limits. Except PreWEC-1m, which was tested with a lower shear resistance after fracture of 67% of connectors, the rest of these test units were subjected to earthquakes with greater intensities of EQI⁺ to EQIII⁺ (e.g., PreWEC-2 during 0.8×Eq-4s with an intensity of EQ-III⁺). The acceptable performance of these systems was arbitrated by comparing the maximum values of the lateral drift against the limiting values associated with hazard levels of EQ-II to EQ-IV. During the EQ-IV level near-field motions, PreWEC-2 and PreWEC-s2m with smaller shear resistance responded beyond the 3% allowable limit.

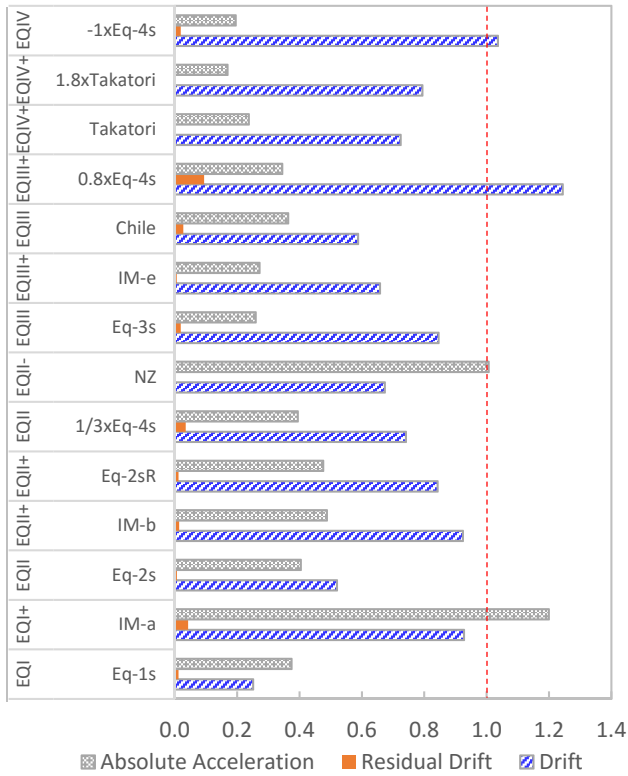
Excluding for some particular motions (e.g., IM-a with an intensity of EQ-I⁺⁺ and NZ), absolute acceleration of the test units was generally acceptable with sufficient margin of safety with respect to the permissible limits. Also, all the rocking systems satisfactorily self-centered with minimal residual drift after four levels of base excitations.



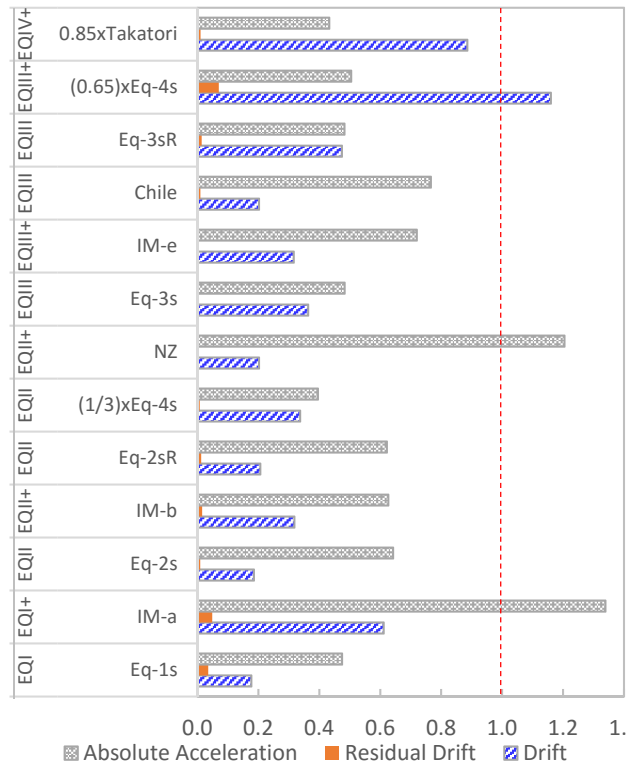
a) Response ratio of PreWEC-1



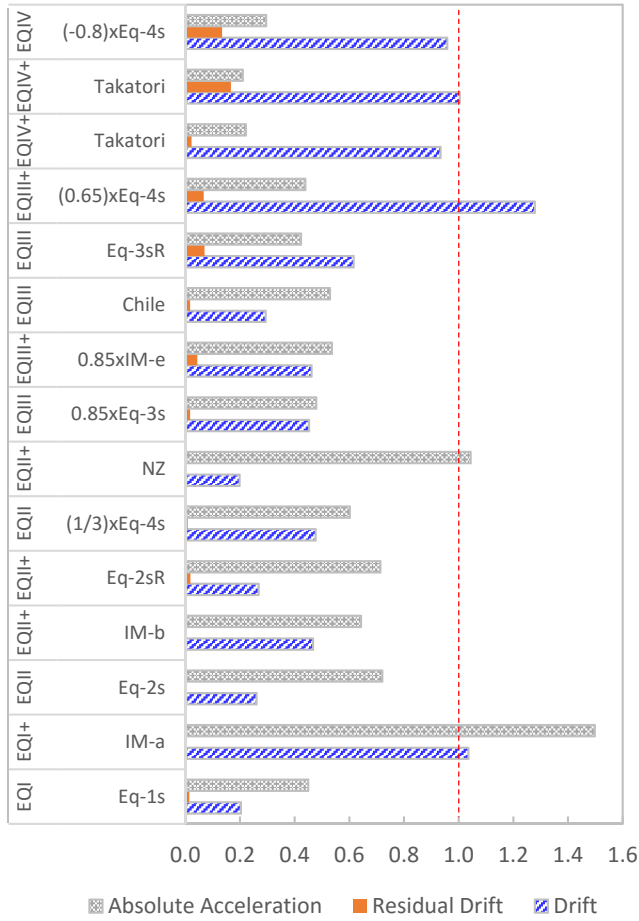
b) Response ratio of PreWEC-1m



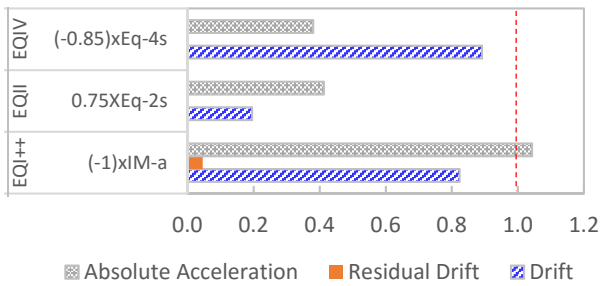
c) Response ratio of PreWEC-2



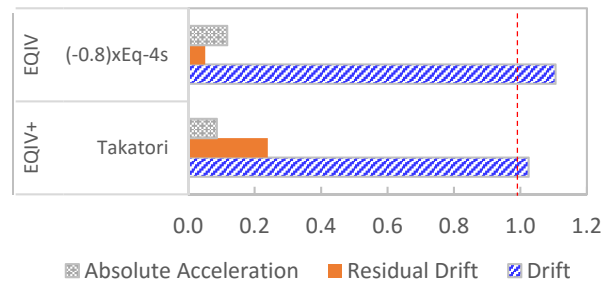
d) Response ratio of PreWEC-s1



e) Response ratio of PreWEC-s2



f) Response ratio of PreWEC-s1m



g) Response ratio of PreWEC-s2m

Figure 4-15. Ratio of the maximum system demands to the allowable limits

4.7.2. Shear resistance vs. damping

The shake table tests confirmed that lateral drift responses of PreWECs with smaller shear resistance may exceed the allowable limits during strong ground motions while they are designed to contain large energy dissipation capacity (i.e., β_h greater than 0.12). Therefore, to understand the feasibility of using PreWECs in seismic design practice, the concepts of the DDBD approach as described by Priestley (2000) was used. In this method, design shear forces are estimated by multiplying the lateral displacement corresponding to the target drift (i.e., 2% for EQ-III and 3% for EQ-IV level events) by the effective stiffness of the system which is a function of the damping. The design procedure is summarized in Table 4-6 for four test units.

Table 4-6. Design forces obtained from DDBD approach (Priestley 2000)

(1 m = 3.28 ft; 1 kips = 4.45 kN)

Test unit	ξ_{eq} , %		Δ_d , cm		T_e , sec. (FF/NF)		V_e , kN (FF/NF)	
	DBE	MCE	DBE	MCE	DBE	MCE	DBE	MCE
PreWEC-1	15.6	16.7	2.76	4.14	15.6	16.7	2.76	4.14
PreWEC-2	15.3	16.5	3.36	5.04	15.3	16.5	3.36	5.04
PreWEC-s1	8.7	10.3	3.36	5.04	8.7	10.3	3.36	5.04
PreWEC-s2	15.4	16.7	3.36	5.04	15.4	16.7	3.36	5.04

Measured and DDBD design shear forces of the PreWECs are compared in Figure 4-16 for near-field and far-field motions representing EQ-III and EQ-IV level earthquakes. This figure indicates the insufficient shear resistance of some test units, including PreWEC-1m for ground motions of earthquake levels EQ-III and EQ-IV in addition to PreWEC-2 and PreWEC-s2m during EQ-IV level near-field events. This confirms the outcomes of the seismic performance assessment of the test units, as previously presented in Figure 4-15.

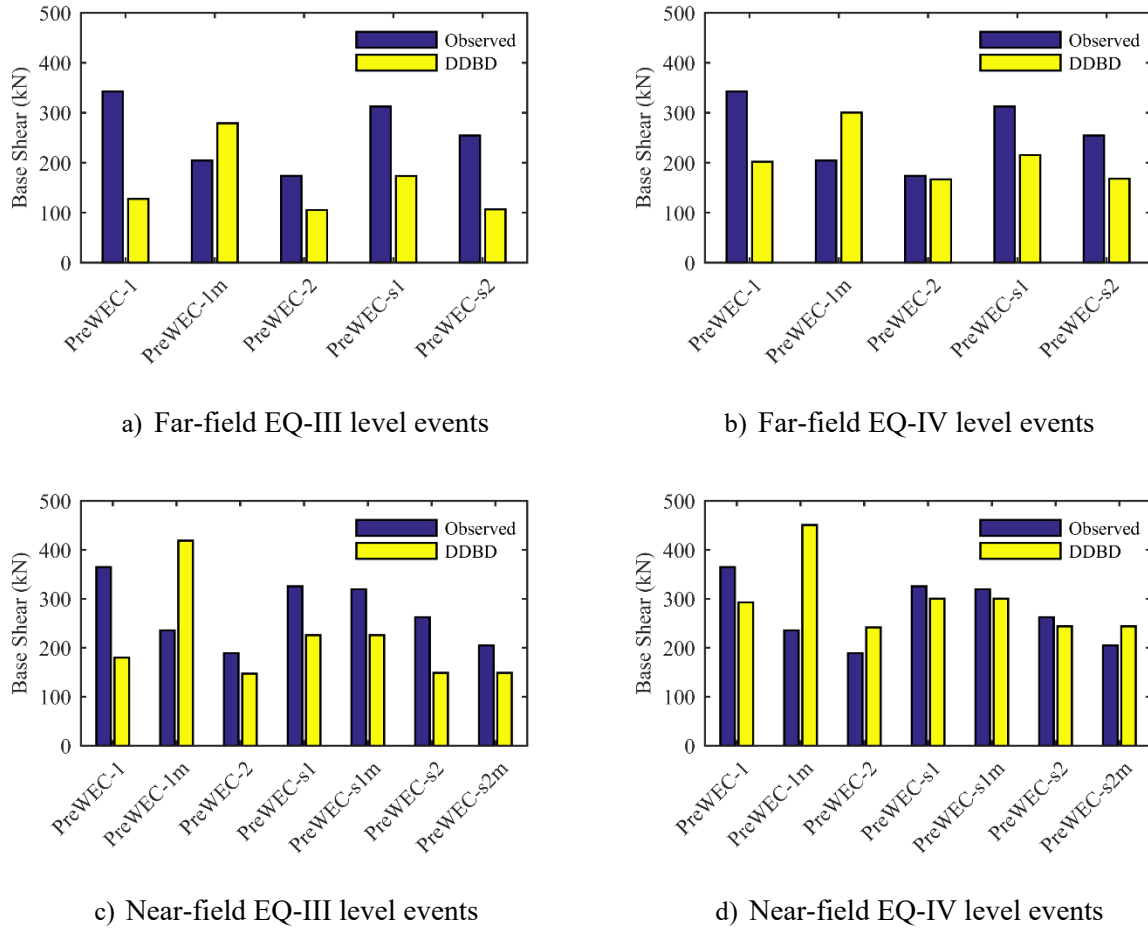


Figure 4-16. Observed vs. DDBD design shear forces of the test units (1 kip = 4.45 kN)

4.7.3. R-factor

Following a DDBD approach, it was shown that the test units designed with a shear resistance lower than that corresponding to their damping capacities were largely displaced during EQ-III and EQ-IV level motions; however, they met the seismic acceptance criteria of ACI ITG-5.1 (2008) (see Table 4-5). To estimate the design base shear of PreWEC systems following a Force-Based solution (FBD) as described in the current design codes, the strength reduction (or R) factor as a function of damping ratio is suggested and presented by Equation 4-2 for far-field motions:

$$R = 0.4648 \times \xi_{eq} + 0.9295 \quad (\text{Equation 4-2})$$

where R is the ratio of the base shear forces corresponding to the elastic response of the PreWEC system (i.e., from IBC (2009) with R=1) and the design-level; this is estimated for the selected damping ratio of the system following the DDBD procedure (see Figure 4-17).

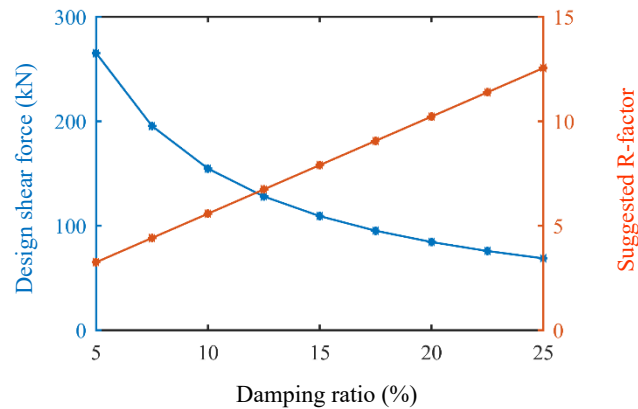


Figure 4-17. R-factors for design of the PreWEC systems with varying damping ratios
(1 kip = 4.45 kN)

4.7.4. Design recommendations

In addition to the requirements of ACI ITG-5.1 (2008), the following steps for seismic design of the PreWEC systems are suggested to limit their excessive displacement during design-level motions:

- Step 1: Establish a suitable hysteretic damping ratio (i.e., in the range of 10%-16%) at wall design drift ($\xi_{hys,D\%}$).
- Step 2: Estimate the appropriate amount of design shear force ($V_{D\%}$) either following a DDBD approach or FBD solution using an R-factor estimated from Equation 4-2.

- Step 3: Using the vertical uplift of the wall, estimate the expected deformation of O-connectors at design drift ($\Delta_{c,D\%}$). This is dependent on the wall panel length and the location of connectors.
- Step 4: Apply Equation 4-1 to estimate the required number of O-connectors ($N_{conn.}$). These elements are designed with the appropriate dimensions to obtain the required force-deformation capacities (Aaleti and Sritharan 2009). To consider for the energy dissipation due to concrete nonlinearity as well as damping due to impacts, an additional 5% damping ratio should be included while using this equation.
- Step 5: Use the SA method (Aaleti and Sritharan 2009) to design the post-tensioning parameters of the wall panel and the end columns, providing the required shear resistance ($V_{D\%}$) of the PreWEC. This is determined using moment equilibrium of forces acting on the base of the system, assuming the ultimate strength of the connectors and 95% of the yielding stress in PT tendons at the wall design drift (ACI ITG-5.1 2008; ACI ITG-521 2009).

The design procedure described above can be used to ensure acceptable performance of the PreWEC system during the maximum considered events. Accordingly, the design shear force ($V_{D\%}$) should be adjusted for an increased response spectra; however, R-factors can be still evaluated using the same equation.

4.8. Conclusions

This paper presented the results from a series of shake table tests on four PreWECs. They were designed with different amounts of prestressing force in the wall panel and end columns as well as O-connectors between these members, providing base shear resistance in the range of 182

kN (41 kip) to 349 kN (78 kip) and damping ratio varying from 8.7 to 15.6%. The lowest amount of design base shear was chosen to closely match the capacity of a PreWEC system from a six story prototype building at 5/18 scale. Although the test units were designed following the current criteria established for special unbonded post-tensioned precast concrete walls (ACI ITG-5.1 2008), their seismic response was evaluated during input motions of different seismic hazard levels to ensure viability of application of PreWECs in regions of high seismic risk. The conclusions drawn from this study are presented below:

- 1- All PreWECs showed satisfactory performance without experiencing visible damage up to the design-level earthquakes. Significant damage to both cover and core concrete occurred while they were subjected to the maximum considered input motions; however, the amount of damage was minimized due to the use of steel channels at the base of the walls.
- 2- The O-connectors satisfactorily provided the additional hysteretic energy dissipation by starting to yield at 0.6% wall drift. None of these elements fractured before the system displaced to 5% drift.
- 3- Based on the experimental observations, total equivalent viscous damping ratios of 8.7 to 15.6% were estimated for the test units. This damping includes 1% for the energy loss during impacts and 4.2% due to concrete nonlinearity as well as inherent material damping of the test units. Using the suggested equation in this paper, the additional hysteretic damping provided by O-connectors can be estimated as a function of the number and force-displacement characteristics of these elements as well as resistance of the PreWEC system at the design drift.
- 4- It was shown that PreWECs can be designed to respond satisfactorily in terms of lateral drift when R-factors corresponding to their damping ratios are used, as proposed in this paper.

- 5- Test results confirmed the re-centering capability of PreWEC systems with indicating negligible residual drifts after four levels of earthquakes. Test units also generally showed acceptable absolute acceleration below the permissible limits.
- 6- Results from the SA method (Aaleti and Sritharan 2009) presented good estimates of the experimental characteristic responses of PreWECs from shake table testing, including lateral response, variation of post-tensioning force, and contact length.
- 7- Using a centerline OpenSees model, displacement time history and lateral load responses of PreWECs were satisfactorily predicted at all intensity levels. A 2% tangent stiffness proportional elastic damping was used in these models to express the energy loss during impacts achieved from the experimental results.

4.9. Acknowledgements

The study reported in this paper was based upon the NEES Rocking Wall project supported by the National Science Foundation under Grant No. CMMI-1041650 and Dr. Joy Pauschke served as the program director for this grant. Any opinions, findings, and conclusions or recommendations expressed in this material are those of the authors and do not necessarily reflect the views of the National Science Foundation. All shake table tests were conducted using the NEES shared facility at the University of Nevada, Reno (UNR). The test units were donated by Clark Pacific and MidState Precast through coordination by PCI West. Materials provided by Sumiden Wire, GTI, Hayes Industries and help provided by ironworker local 118 with post-tensioning of specimens are also gratefully acknowledged.

4.10. References

- Aaleti, S. (2009) Behavior of rectangular concrete walls subjected to simulated seismic loading, PhD Thesis. Dept. of Civil, Construction and Environmental Engineering, Iowa State University, Ames, Iowa.
- Aaleti, S., and Sritharan, S. (2009) A simplified analysis method for characterizing unbonded post-tensioned precast wall systems. *Engineering Structures*, **31**(12), 2966–2975.
- ACI 318-11 (2011). Building code requirements for structural concrete. *ACI 318-11*, Farmington Hills, MI.
- ACI Innovation Task Group 5.1. (2008) Acceptance criteria for special unbonded post-tensioned precast structural walls based on validation testing and commentary. American Concrete Institute, Farmington Hills, MI.
- ACI Innovation Task Group 5.2. (2009) Requirements for design of a special unbonded post-tensioned precast shear wall satisfying ACI ITG-5.1 and commentary (ACI ITG-5.2). American Concrete Institute, Farmington Hills, MI.
- ASCE 7-05 (2005). Minimum design loads for buildings and other structures, ASCE/SEI 7-05.
- Henry, R. (2011) Self-centering Precast Concrete Walls for Buildings in Regions with Low to High Seismicity. PhD Thesis. Dept. of Civil and Environmental Engineering, The University of Auckland, Auckland, New Zealand.
- Housner, G. (1963) The behavior of inverted pendulum structures during earthquakes. *Bulletin of the Seismological Society of America*, **53**(2), 403–417.
- IBC I. (2009) International Code Council. International Building Code.
- Kurama, Y. (2002) Hybrid post-tensioned precast concrete walls for use in seismic regions. *PCI Journal*, **47**(5), 36–59.
- McKenna, F., Fenves, G., and Scott, M. (2000) Open system for earthquake engineering simulation. University of California, Berkeley, CA.
- Nazari, M., Aaleti, S., and Sritharan, S. (2015) Shake Table Testing of PreWEC @ UNR. *Network for Earthquake Engineering Simulation (distributor)*. doi: 10.4231/D3WM13V3P

(PreWEC-s1), and 10.4231/D3RV0D20F (PreWEC-s2).

- Nazari, M., Sritharan, S., and Aaleti, S. (under review) Single Precast Concrete Rocking Walls as Earthquake Force-resisting Elements. *Earthquake Engineering and Structural Dynamics*.
- Priestley, M.J.N., Sritharan, S., Conley, J.R., and Pampanin, S. (1999) Preliminary results and conclusions from the PRESSS five-story precast concrete test building. *PCI Journal*, **44**(6), 42–67.
- Priestley, M. J. N. (2000) Performance Based Seismic Design. 12th World Conference on Earthquake Engineering, Auckland, New Zealand.
- Priestley, M., Calvi, G.M., and Kowalsky, M.J. (2007) Displacement-based seismic design of structures. *Building*, **23**(33), 1453–1460.
- Rahman, M., and Sritharan, S. (2006) An evaluation of force-based design vs. direct displacement-based design of jointed precast post-tensioned wall systems. *Earthquake Engineering and Engineering Vibration*, **5**(2), 285–296.
- Seismology Committee. (1999) Recommended lateral force requirements and commentary (Blue book). Structural Engineers Association of California (SEAOC), California, USA.
- Sritharan, S., Aaleti, S., Henry, R., Liu, K., and Tsai, K. (2015) Precast concrete wall with end columns (PreWEC) for earthquake resistant design. *Earthquake Engineering and Structural Dynamics*, **44**(12), 2075–2092.
- Stanton, J.F., and Nakaki, S.D. (2002) Design Guidelines for Precast Concrete Seismic Structural Systems Unbonded Post-Tensioned Split Walls. PRESSS Report No. 01/03-09, Department of Civil Engineering, University of Washington, Seattle, WA.
- Tuna, Z., Gavridou, S., and Wallace, J. (2012) 2010 E-defense four-story reinforced concrete and post-tensioned buildings—preliminary comparative study of experimental and analytical results. *Proceedings of the 15th World Conference on Earthquake Engineering*, Lisbon, Portugal.

CHAPTER 5
INTERACTION OF DIFFERENT DAMPING COMPONENTS ON DYNAMIC
RESPONSE OF ROCKING WALLS

A paper to be submitted to the Journal of Engineering Structures

Maryam Nazari and Sri Sritharan

5.1. Abstract

Post-tensioned precast concrete rocking walls, as a seismic resilient system, dissipate energy imparted to them during an earthquake through the inherent viscous damping, radiation damping due to the wall impacting the foundation, and any available hysteretic damping. A shake table study on eight rocking wall units designed with different quantities of hysteretic damping ratio varying between 4 to 15%, generally demonstrated their satisfactory seismic performance during design-level and higher intensity earthquake motions. The test results confirmed lower participation of energy dissipation due to impacts as the hysteretic component increased. Larger hysteretic damping also led to greater reduction in the maximum drift of rocking walls as well as number of large drift cycles after the first peak of response. While larger displacement amplitude was achieved for the walls relying on lower hysteretic damping, it was shown that the duration of dynamic response of these walls was reduced by negative rate of input energy, which favorably removed a part of the seismic energy imparted to the system.

Keywords: unbonded post-tensioning, precast concrete wall, radiation damping, hysteretic energy dissipation, shake table testing, maximum seismic response

5.2. Introduction

Initiating with the idea of constructing seismic resilient precast structures in early 2000 (Priestley et al. 1999), Post-Tensioning (PT) tendons were used to tie precast concrete walls to the foundation (Kurama et al. 1999). When subjected to a lateral load, this connection allows for opening of mainly a single horizontal crack at the wall base and elongation of the PT tendons. As these lateral-resisting walls rock on top of the foundation under design-level earthquakes, the tendons will remain elastic enabling re-centering capability of the system. These Single precast Rocking Walls (SRWs) dissipate the energy imparted to them during an earthquake through sources of: (i) inherent viscous damping, (ii) radiation damping due to impacts of the rocking wall on top of the foundation (Housner 1963), and (iii) minor hysteretic damping as a result of concrete nonlinearity at wall toes and inelastic strains in PT tendons if they experience yielding during strong motions (Perez et al. 2004). Dependable seismic performance of SRWs in resisting the lateral forces exerted by major earthquakes is still debating. This is because of the uncertainty associated with the evaluation and performance of radiation damping in SRWs as well as negligible hysteretic energy dissipation capacity of these walls, which yet acknowledged to be the only reliable source of damping in structural systems. Due to this fact, special energy dissipating elements were designated to undergo inelastic deformations during rocking of the walls, which in turn properly dissipate the seismic energy from the structure (e.g., Priestley et al. 1999; Rahman and Restrepo 2000; Sritharan et al. 2015). Precast Wall with End Columns, known as the PreWEC, is one such system developed by Sritharan et al. (2015) by using a set of easily-replaceable steel Oval-shaped connectors, namely O-connectors. These special energy dissipating elements joining the wall panel with two end columns undergo the relative displacement as the system rocks.

Since the concept of self-centering precast concrete walls was recently applied in structural systems, their seismic performance was not much assessed by real earthquake events. Also, limited shake table investigations were conducted to evaluate the functionality of SRWs during major ground motions when compared to the emulated rocking systems designed with additional damping sources. Marriot et al. (2008) reported shake table tests on a SRW and four unbonded precast walls with alternative dissipating solutions, such as external viscous and hysteretic damping elements. Using a near-field and a far-field design-level and maximum considered earthquake, all test walls displayed excellent performance when their maximum responses were compared with the permissible limits; however, the SRW generally returned the largest peak displacement and acceleration. For the SRW, these researchers evaluated an equivalent viscous damping ratio of 1 to 3% due to all sources of energy dissipation in such systems (Marriot et al. 2008). Similar observations were reported by Twigden (2016) during snap-back testing of one SRW. As their reported damping ratio is about 1/6 of what generally recognized for conventional cast-in-place (CIP) concrete walls (Priestley 2002), the premise behind the survival of SRWs during strong ground motions is still questionable. Also, to the author's knowledge, no published data is available on quantification of different energy dissipation components of rocking walls both with and without external hysteretic dampers.

This paper presents experimental results from shake table testing of eight rocking walls, i.e., four SRWs and four PreWEC systems with different hysteretic energy dissipation capacity, to a total of ten multiple-intensity ground motions (Nazari et al. 2015). The conclusions from this study: (i) quantifies the participation of individual damping components of test units in energy dissipation of rocking systems, (ii) illustrates the impact of added hysteretic damping provided in PreWECs on their seismic response, such as peak value of drift as well as number of large drift

cycles afterwards, and (iii) puts forward the application of SRWs in seismic regions, relying on the reduced amount of absorbed seismic energy in these walls after they experienced large displacements resulting in their extended period of vibrations. This is shown to be mainly a consequence of removing a part of seismic energy from SRWs. The rest of seismic energy imparted to the system will be dissipated through available damping in these walls.

5.3. Energy Dissipation Mechanisms for Seismic Protection of Rocking Systems

During base excitation, with acceleration of \ddot{u}_g , the seismic input energy introduced to the system (E_I) is transferred into the kinetic energy (E_k) and consequently movement of the masses of the system. Within cycles of vibration, the generated kinetic energy is constantly converted into the recoverable elastic strain energy (E_{es}) and vice-versa. During this transition, some elastic energy loss will be induced because of several sources including the material nonlinearity prior to yielding (e.g., micro-cracking of concrete), friction, etc. This energy dissipation component is referred to as viscous damping (E_{vis}). Moreover, any inelastic deformation of structural elements within a cycle allows for extra energy dissipation in terms of the hysteretic strain energy (E_{hys}). The energy formulation of the system is obtained as follows:

$$\int M_s \ddot{u}(t) du + \int c \dot{u}(t) du + \int_0^{u_{es}} f_a(t) du + \int_{u_{es}}^{u_{hys}} f_a(t) du = - \int M_s \ddot{u}_g(t) du \quad (\text{Equation 5-1})$$

$$E_k(t) + E_{vis}(t) + E_{es}(t) + E_{hys}(t) = E_I(t) \quad (\text{Equation 5-2})$$

where M_s is the seismic mass displaced by u – consisting of elastic (u_{es}) and inelastic deformations (u_{hys}) of the system, c is the damping coefficient, and f_a is the nonlinear restoring forces generated by the hysteretic characteristics of structural elements. The energy balance

equation holds true that at any time t during ground motion duration $E_k(t) = E_{es}(t)$ and therefore the total input energy will be completely dissipated by viscous and hysteretic damping components such that $\sum_0^t E_I(t) = \sum_0^t E_{hys}(t) + \sum_0^t E_{vis}(t)$.

In rocking systems, the kinetic energy at the time of impact distorts the wall toe from its unstressed state and consequently is transformed into some elastic strain energy. A part of this internal energy is released, enabling the wall to bounce back and start rotating in the opposite direction. The rest, which is mostly defined in terms of the kinetic energy loss at the time of impact (ΔE_k) is radiated back into the foundation (Housner 1963). According to the rocking literature, this component, often referred to as radiation damping (E_{imp}), is the main source of energy dissipation in SRWs, as they are designed to remain elastic up to design drifts; however, small amounts of hysteretic damping is recognized mainly resulting from inelastic concrete strains developed in the wall toe regions as they strike the foundation during impacts (Perez et al. 2004). Additional hysteretic energy dissipation of rocking systems requires external dampers to be incorporated (e.g., Priestley et al. 1999; Rahman and Restrepo 2000; Sritharan et al. 2015).

Figure 5-1 shows different energy dissipation components associated with rocking of the wall systems. In this figure, $f_s(t)$ is the total resisting force of the system and equals to $c\dot{u}(t) + f_a(t)$. Therefore the corresponding energy term, $E_s(t)$, contains both $E_{hys}(t)$ and $E_{vis}(t)$. As shown in Equation 5-3, to have an exact estimation of radiation damping during base excitation, the observed kinetic energy loss – ΔE_k – was reduced from the instantaneous seismic energy transmitted to the system, as depicted in Figure 5-1. This is because impact occurs at very small rotations of the wall, where u is negligible, at which the seismic input energy will be altered to directly increase the kinetic energy of the system, while a part of that may be dissipated

due to impacts. This quantity is added up from the beginning of the record up to time t to measure the relevant component of energy dissipation – E_{imp} – and expressed as follows:

$$E_{imp}(t) = \sum_0^t [\Delta E_I - \Delta E_k]_{t=imp} = \sum_0^t [(\Delta E_I)_{t=imp} - (\frac{1}{2} \times M_s \times (\dot{u}_{after}^2 - \dot{u}_{before}^2))] \quad (Equation 5-3)$$

where $(\dot{u}_{after} - \dot{u}_{before})$ is the observed drop in the relative velocity of the rocking system during impacts.

Accordingly, Equation 5-4 includes all associated energy dissipation mechanisms to damp the seismic energy input into rocking wall systems. Regardless of their characteristics, the corresponding energy loss terms could be equalized with viscous damping ratios, as described in Nazari et al. (2016) (Chapters 3 and 4).

$$\sum_0^t E_I(t) = \sum_0^t E_{hys}(t) + \sum_0^t E_{vis}(t) + \sum_0^t [\Delta E_I - \Delta E_k]_{t=imp} \quad (Equation 5-4)$$

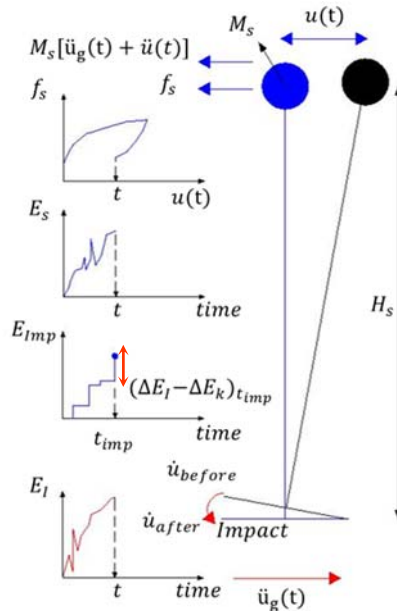
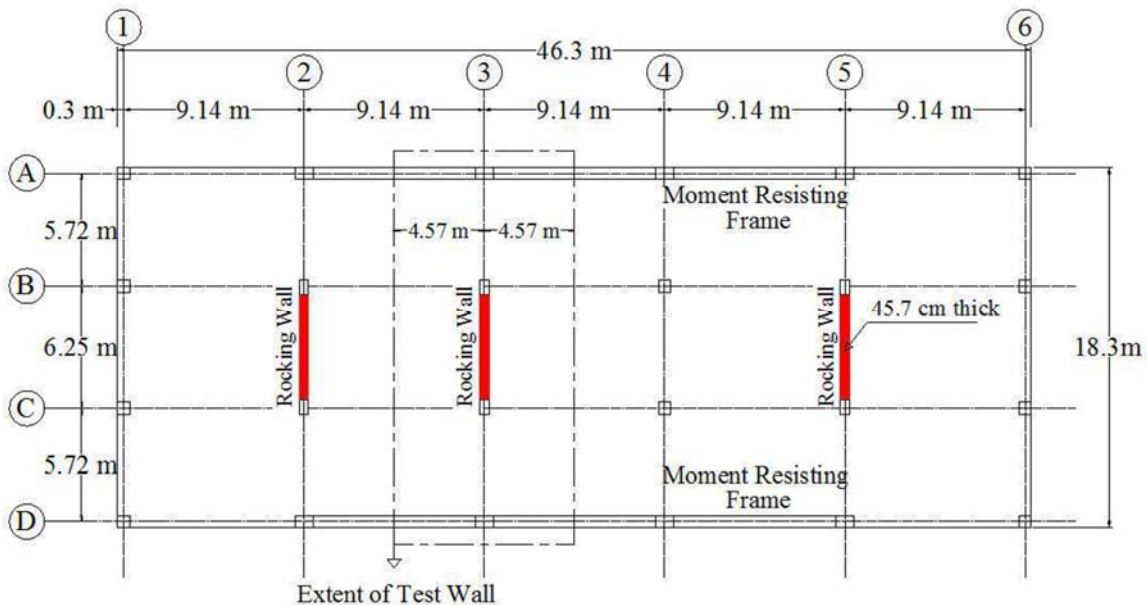


Figure 5-1. Rocking response and the associated energy terms

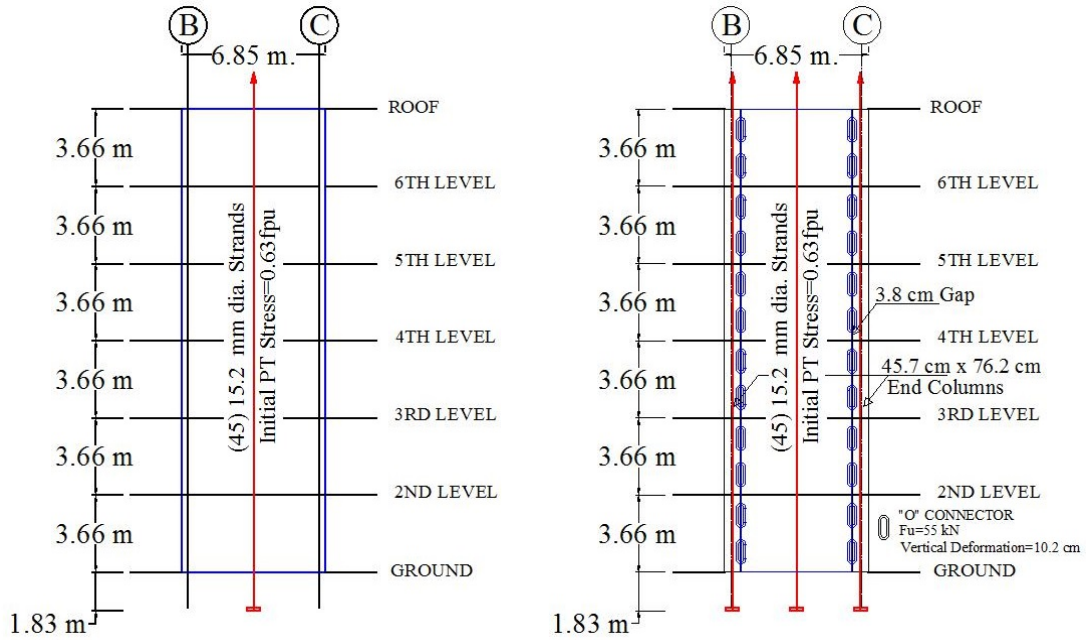
5.4. Summary of Experimental Investigation

Eight rocking units, consisting of four SRWs and four PreWEC systems were tested at the NEES shake table facility of the University of Nevada at Reno (UNR). They were 190.5 cm (6.25 ft) long, 487.7 cm (16 ft) tall and 12.7 cm (5 in) thick, representing a 5/18 scale model of a prototype rocking wall in a six-story office building designed for a location in Los Angeles, California. Figure 5-2 displays the typical plan view of the prototype structure including the location of three rocking walls and their dimension. Considering the predominant rocking mode of the prototype wall, it was simplified to an equivalent single degree of freedom (SDOF) system for the purpose of testing. The external mass-rig system used in the test set-up, as shown in Figure 5-3, facilitated application of the inertia effect from an effective weight of 267 kN (60 kips) at 4.27 m (14 ft) effective height of the SDOF test units. These wall systems were subjected to a set of scaled ground motions representing four seismic hazard levels of EQ-I to EQ-IV. EQ-III and EQ-IV levels respectively represent design-based (DBE) and maximum considered (MCE) earthquake events. As presented by SEOAC seismology committee (1999) these hazard levels are defined by five percent damped elastic acceleration response spectra. Table 5-1 lists the input motions consisting of: (i) four short-duration spectrum compatible motions, originating from the records developed for pseudo dynamic testing of the PRESSS building (Priestley et al. 1999), as shown in Figure 5-4a and (ii) a set of long-duration records scaled following the procedure presented in Figure 5-4b. According to this figure, the Root Mean Square Deviation (RMSD) of spectral ordinates of the scaled motion should lie between $\pm 30\%$ of the mean of the targeted hazard spectrum in the range of dominant period of the rocking system. While the information provided in Table 5-1 is at the prototype scale, the amplitude of all the motions was scaled up by 18/5 and the time step was decreased by a factor of 5/18 to satisfy the scale effects. The test matrix, as

detailed in Table 5-2, entails lateral resistance and equivalent viscous damping ratio of the test walls at 2% design drift as well as their maximum response ratios during EQ-III and EQ-IV hazard level motions normalized by the corresponding allowable limits; these limits are defined based on the recommendations of Rahman and Sritharan (2006) for different intensities of ground motions. Table 5-2 also presents four sets of test units – classified as groups A to D – with almost identical shear resistance. Results from this shake table study confirmed satisfactory seismic performance of the test units designed with shear forces corresponding to their energy dissipation capacities (e.g., SRW3 and PreWEC-s1). These forces were estimated using the relevant damping-dependent strength Reduction (or R) factors in a Force-Based Design (FBD) approach as described in Nazari et al. (2016). Damping ratio of the test units represents all energy loss terms as presented in Equation 5-4.

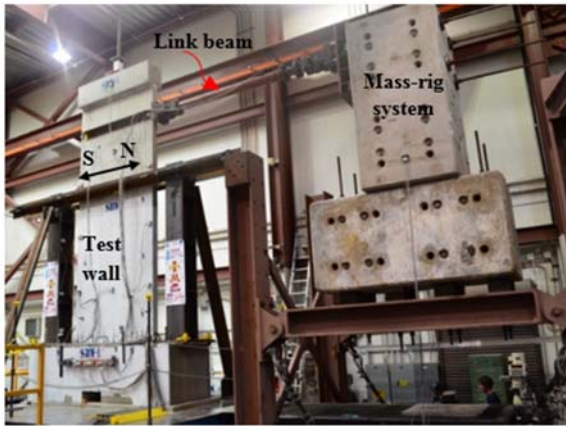


a) Typical plan view



b) SRW and PreWEC details

Figure 5-2. Details of the prototype building (1 m = 3.28 ft)



a) SRW



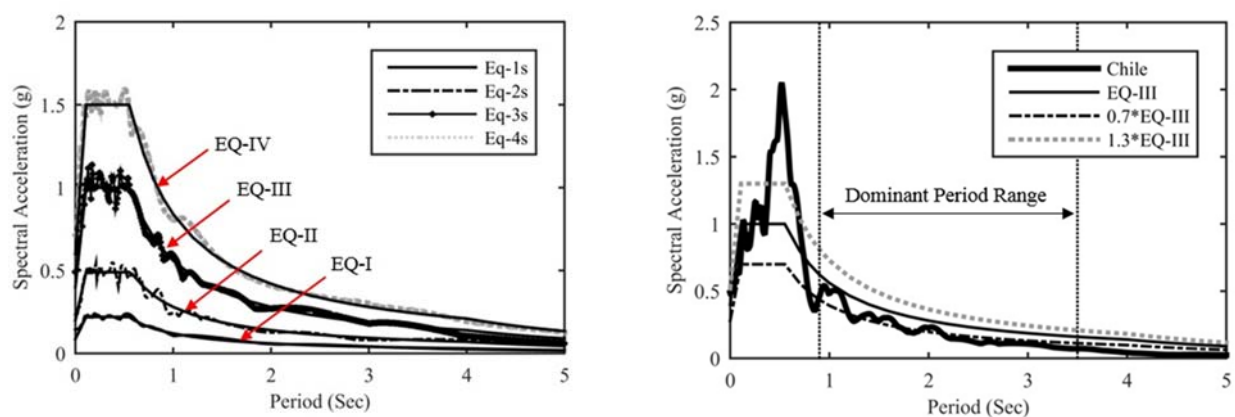
b) PreWEC

Figure 5-3. Experimental set-up used for the shake table testing

Table 5-1. List of ground motions

Input motion	Type of motion	Earthquake name (Year), Station, FF/NF	Scale factor	Targeted hazard level	PGA (g) after applying the scale factor
Eq-1s	Spectrum compatible used in PRESSS building (Priestley et al. 1999)	Hollister (1974), Gilroy Array#1, FF	0.67	EQ-I	0.14
Eq-2s		San Fernando (1971), Hollywood Storage, FF	1.00	EQ-II	0.23
Eq-3s		Imperial Valley (1940), Elcentro, FF	1.00	EQ-III	0.49
Eq-4s		Northridge (1994), Sylmar, NF	1.00	EQ-IV	0.71
IM-a	Rahman and Sritharan (2006)	Morgan Hill (1984), Gilroy Array#6, NF	0.65	EQ-I	0.19
IM-b		Loma Prieta (1989), Saratoga Aloha Avenue, NF	0.64	EQ-II	0.32
IM-e		Kobe-Japan (1995), KJM, NF	0.94	EQ-III	0.56
NZ	Recordings from the past earthquakes	New Zealand (2011), HVSC, NF	0.40	EQ-II	0.58
Chile		Chile (2010), Angol, FF	1.00	EQ-III	0.49
Takatori	E-Defense Test (Tuna et al. 2012)	Kobe-Japan (1995), Takatori, NF	0.60	EQ-IV	0.37

Note: s = short-duration motion; NF = near-field motion; FF = far-field motion



a) Short-duration spectrum compatible motions b) Scaled Chile, representing an EQ-III level event

Figure 5-4. Selected spectral acceleration of scaled ground motions

Table 5-2. Test matrix

Wall system ID	$V_{2\%}^a$ (kN)	Group (Ave. of $V_{2\%}$, kN)	Equivalent viscous damping ratio (%)		Maximum response ratio (drift, absolute acceleration, residual drift)	
			Hysteretic and viscous (E_s) at 2% drift	Impact (E_{imp})	DBE	MCE
SRW1	151	-	4.5	1.3	Not applied	Not applied
SRW1m	104	-			2.91, 0.31, 0.18	2.79, 0.14, 0.1
SRW2	187	A (175)	3.5	1.9	1.72, 0.64, 0.07	1.8, 0.42, 0.05
SRW3	297	B (297)	7.1	1.7	0.83, 0.9, 0.01	0.88, 0.61, 0.01
SRW3m	160	A (175)			Not applied	1.03, 0.43, 0.15
SRW4	358	C (365)	4.4	1.1	0.51, 0.63, 0.09	0.76, 0.34, 0.04
SRW4m	174	A (175)			Not applied	1.9, 0.17, 0.05
PreWEC-1	372	C (365)	14.6	1.5	0.65, 0.51, 0.02	0.86, 0.75, 0.04
PreWEC-1m	239	D (242)	4.2		1.35, 0.32, 0.08	1.33, 0.29, 0.09
PreWEC-2	183	A (175)	14.3	0.8	0.85, 0.36, 0.03	1.04, 0.24, 0.02
PreWEC-s1	312	B (297)	7.7	2.0	0.47, 0.77, 0.01	0.89, 0.43, 0.01
PreWEC-s1m	283	B (297)			Not applied	0.89, 0.38, 0.01
PreWEC-s2	254	D (242)	14.4	1.9	0.62, 0.54, 0.07	1.0, 0.3, 0.17
PreWEC-s2m	233	D (242)			Not applied	1.11, 0.12, 0.05

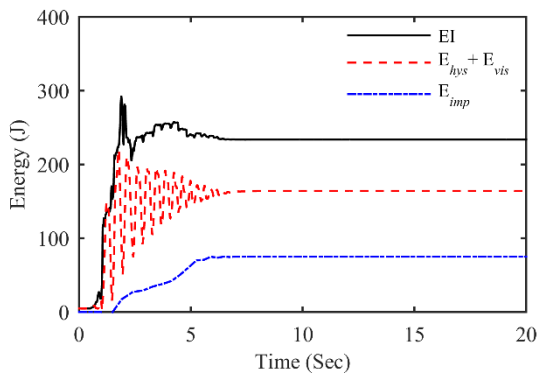
Note: Modified test units are denoted by adding “m” to their designation.

^a Shear resistance at 2% drift, using Simplified Analysis method (Aaleti and Sritharan 2009).

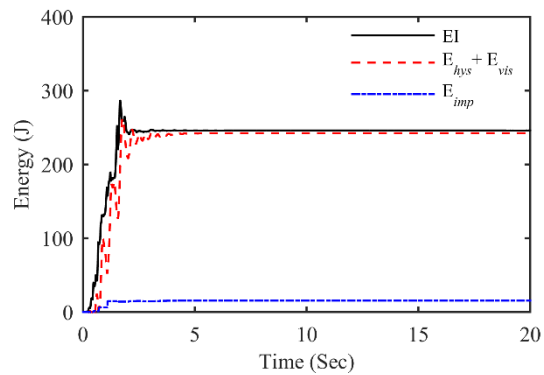
5.5. Participation of Different Energy Dissipation Components

Different damping components of the wall units were measured during experimental testing and their contribution in energy dissipation of SRWs and PreWECs were quantified and compared, as shown for the test units of group A in Figure 5-5. Figure 5-5a and 5-5b show the energy input and dissipation time-history responses of SRW2 and PreWEC-2 during $0.8 \times \text{Eq-4s}$ – representative of an EQ-III level earthquake. As shown in these figures, the SRW uses both radiation damping term as well as hysteretic and viscous components to dissipate the energy input into the system during base excitation; however, the PreWEC system mostly dissipates the seismic

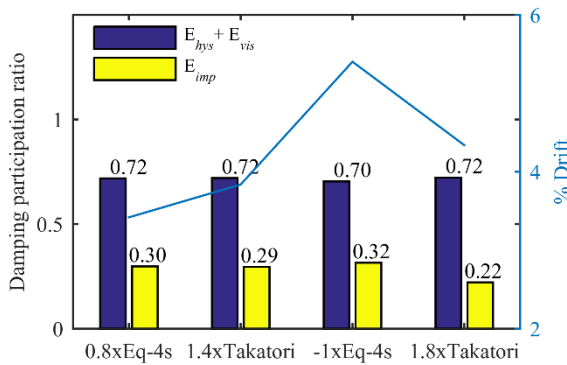
energy through hysteretic and viscous damping components. This is confirmed in Figure 5-5c and 5-5d by comparing the participation ratio of individual damping terms in energy dissipation of the rocking wall systems during a set of strong motions of hazard levels EQ-III and EQ-IV. Due to the noise of the experimental data, sum of the ratios is not an exact value of 1 in these plots. According to Figure 5-5c, contribution of radiation damping due to impacts in the total energy dissipation of the SRW is about 30%, as previously reported by the authors (Nazari et al. 2016). This amount is negligible for the PreWEC systems (see Figure 5-5d).



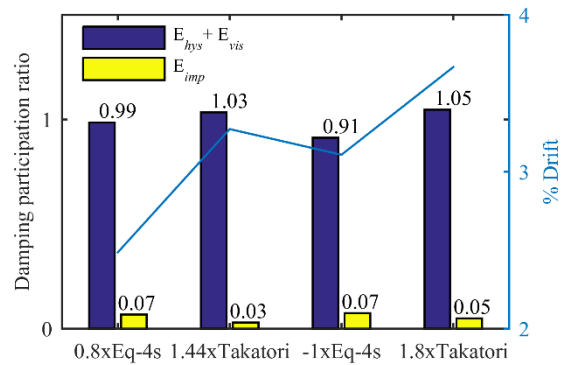
a) Energy terms; SRW2 during 0.8×Eq-4s



b) Energy terms; PreWEC-2 during 0.8×Eq-4s



c) Damping participation ratio;
SRW2 during EQ-III and EQ-IV events



d) Damping participation ratio;
PreWEC-2 during EQ-III and EQ-IV events

Figure 5-5. Participation of different damping terms to dissipate the seismic energy input into the rocking systems

5.6. Effect of Supplementary Hysteretic Dampers on Seismic Rocking Response

PreWEC allows for energy dissipation of the system greatly through inelastic hysteretic action of the O-connectors. SRW, on the other hand, incorporates the radiation damping to damp out a considerable amount of seismic input energy. Figure 5-6, which compares the drift time history response of rocking walls of group A during EQ-III and EQ-IV level earthquake excitations, indicates the influence of their dominant damping terms on the seismic response. According to these figures, PreWEC-2 with the added hysteretic energy dissipation compared to SRW2, experienced lower peak of drift during the input motion as well as faster decay of dynamic response after the table acceleration subdued. Forced and free phases of response are depicted in Figure 5-7 for SRW2 during $0.8 \times \text{Eq-4s}$.

During the excitation, additional hysteretic damping takes part into the energy dissipation of the PreWEC as the system completes the first cycle of motion with the maximum drift at which connectors start yielding; however, for a SRW, this form of energy dissipation resulting from concrete nonlinearity is limited and usually occurs at large drifts. Therefore, as outlined in Equation 5-2, greater recoverable strain energy (E_{es}) is needed to compensate the generated kinetic energy at any time during the earthquake. This requires the SRW to displace to a larger displacement compared to the PreWEC system.

The consequent larger initial energy content of SRW in the free vibration phase is gradually damped mainly due to radiation damping during impacts and negligible hysteretic energy dissipation. As shown in Figure 5-6, this results in more cycles of vibration with larger displacement response compared to the PreWEC system to come to rest. This figure also demonstrates longer rocking period of the SRW mostly after the strong portion of the motion, as

this variable is reliant on the displacement amplitude as well as the wall velocity after impacts (Housner 1963; Falcon et al. 1998). As subsequently shown in this paper, the extended period of vibrations will favorably assist in removal of a part of seismic energy from the SRW, after the wall experienced large displacements.

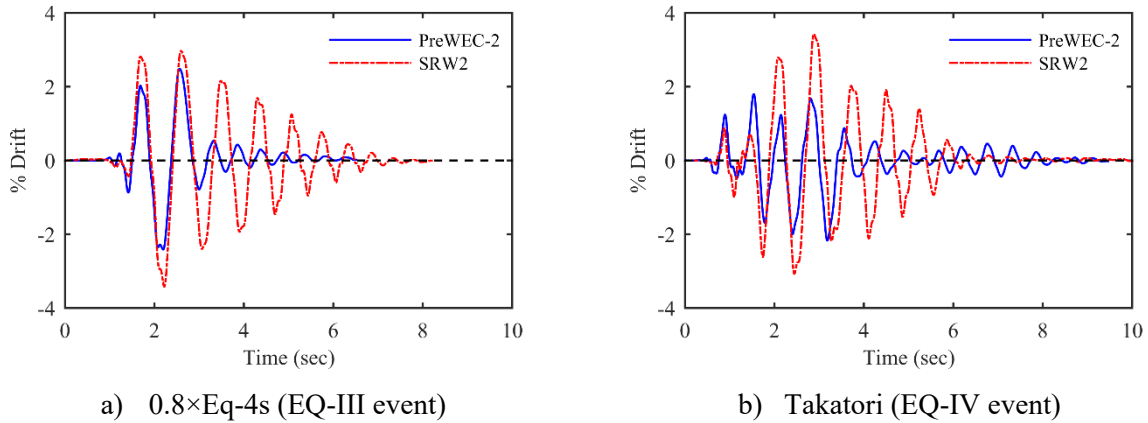


Figure 5-6. Time history drift response of SRW vs. PreWEC from group A

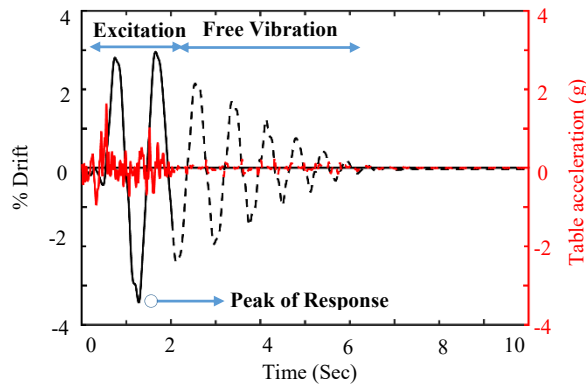


Figure 5-7. Forced and free phases of response of SRW2 during $0.8 \times \text{Eq-4s}$

5.6.1. Maximum of response

Impact of additional hysteretic damping on the maximum lateral drift is summarized in Figure 5-8 for rocking units of comparable lateral resistance, when subjected to earthquakes of all

intensities. Test units of each group are denoted by similar patterns on the column chart of Figure 5-8a. This figure shows a comparison of the equivalent viscous damping ratio of the test walls due to hysteretic and viscous mechanisms which varies from 3.5% for SRW2 to 14.6% for PreWEC-1. It can be observed that additional connectors in PreWECs increased total damping ratio of the rocking systems from a value of 1% for group B to about 10% for groups A and C. Figure 5-8b compares the maximum drift of SRWs against that of the PreWECs during earthquakes of different intensities. In this figure, values lie below the 45-degree line indicate reduction in the maximum drift of the PreWEC when compared to an identical SRW with a comparable resistance. The results confirmed that the drop in the peak drift of PreWECs generally occurred as these systems experienced larger displacements. This is attributed to the participation of O-connectors and thereby increasing the hysteretic damping in these rocking systems. As presented in Figure 5-8c, the average maximum drift of PreWEC system during applied ground motions divided by that of the SRW, namely the Normalized average maximum drift (D_N) of PreWEC, generally decreases with increasing their hysteretic damping ratio; this ratio is estimated based on their maximum experienced drift as presented in Nazari et al. (see Figure 4-12b). The average estimated level of hysteretic damping for SRWs is shown with a dashed vertical line in this figure. According to Figure 5-8c, using the connectors mostly leads to the reduction of maximum lateral drift in rocking systems (i.e., a value of below one for D_N) during the input motions with intensities greater than or equal to that of the design-level earthquake. PreWEC-s1 with the lowest level of hysteretic damping experienced larger drifts compared to the other PreWECs during multiple-level earthquake motions, as shown in Figure 5-8d.

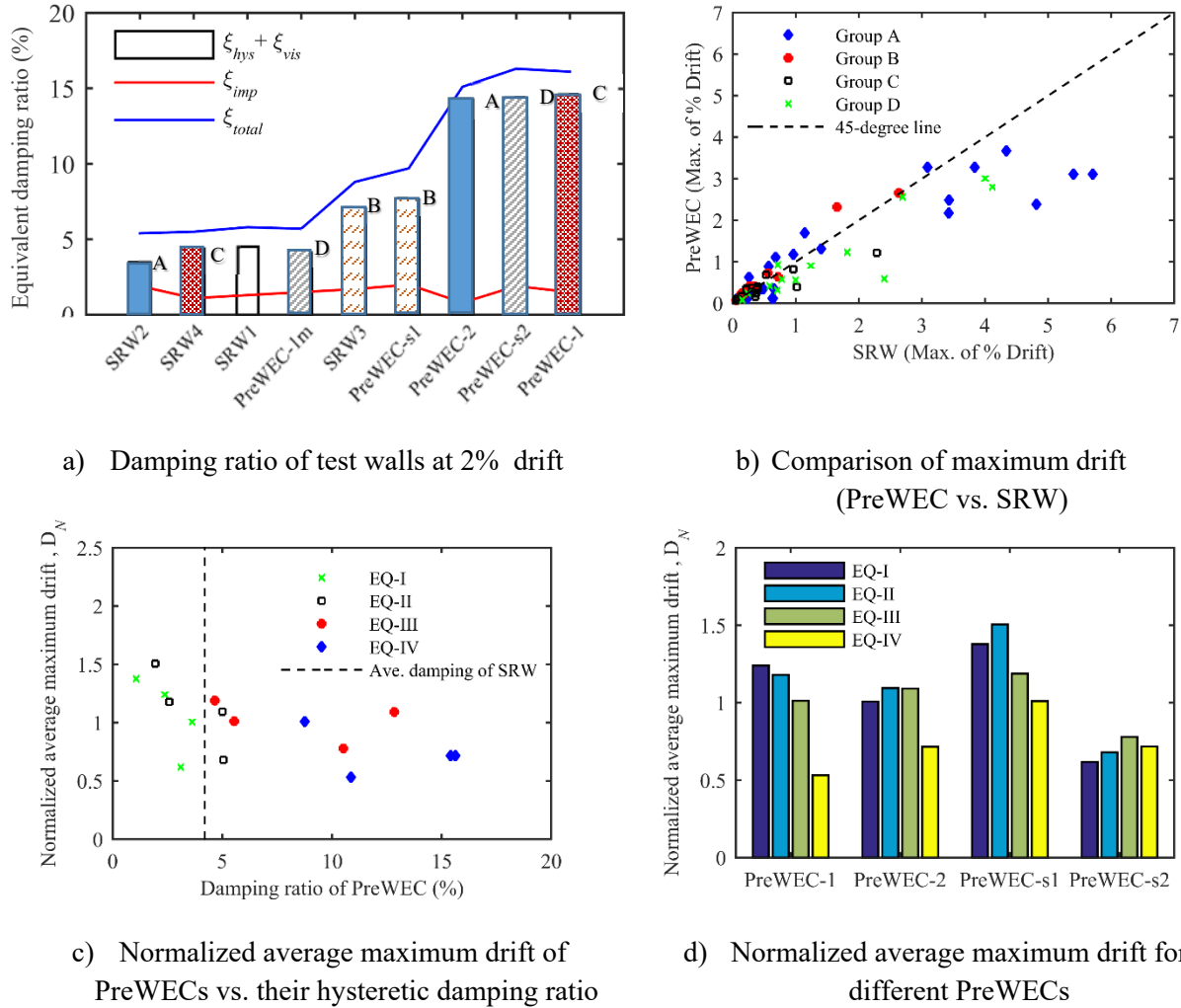


Figure 5-8. Impact of added hysteretic damping on the peak drift during multiple-level motions

5.6.2. Decay of response

The effect of additional hysteretic damping on decay of dynamic response is presented in Figure 5-9 by comparing the number of large peaks after the maximum drift of the identical SRWs and PreWECs. The horizontal axis in Figure 5-9 plots shows the amplitude of corresponding peaks during EQ-III and EQ-IV level motions normalized by the respective allowable limits, i.e., 2% and 3%. This ratio is referred to as the Normalized amplitude of drift peak (P_N). As seen in this figure,

the application of O-connectors in PreWECs can generally result in less number of cycles with large displacements after the peak (e.g., P_N greater than 0.4) indicating faster decay of dynamic response in these systems. The difference was not significant for the wall systems of group B, with almost identical equivalent damping ratios.

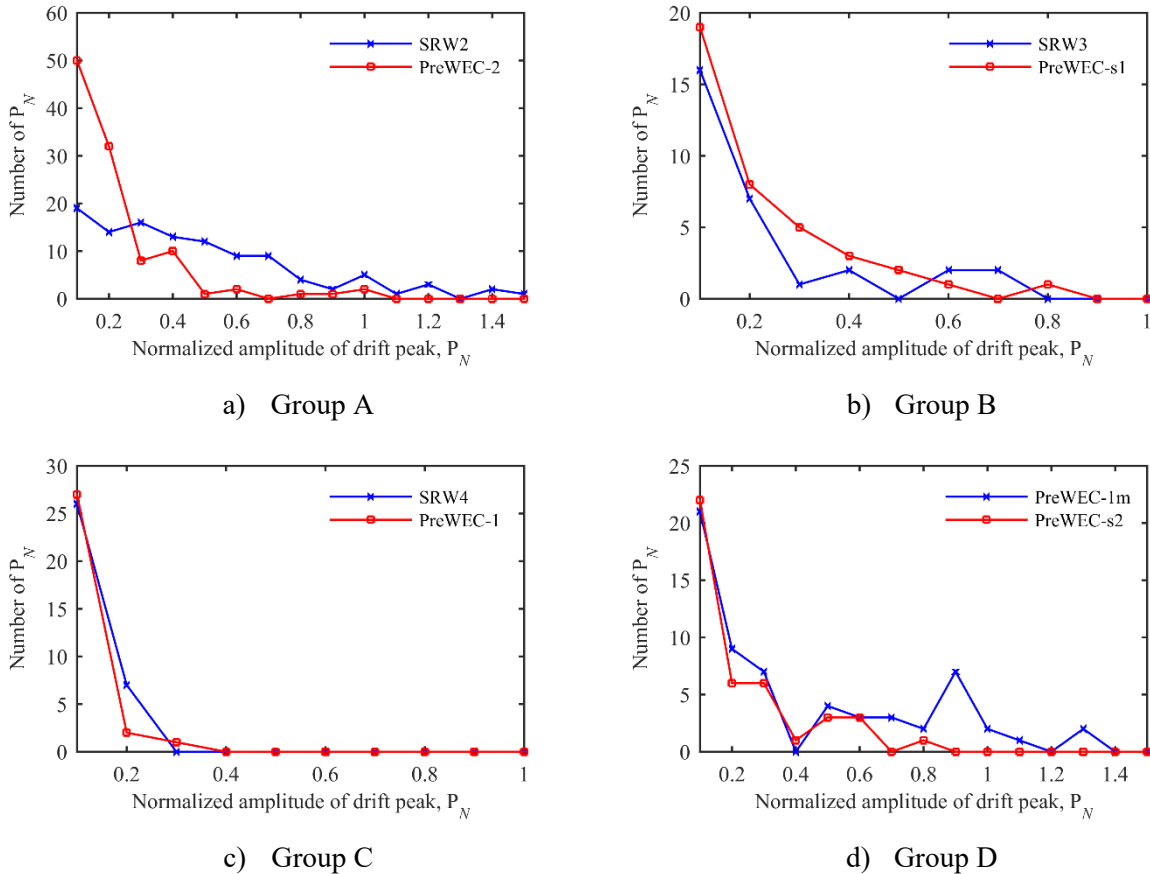


Figure 5-9. Impact of added hysteretic damping on decay of response for EQ-III and EQ-IV events

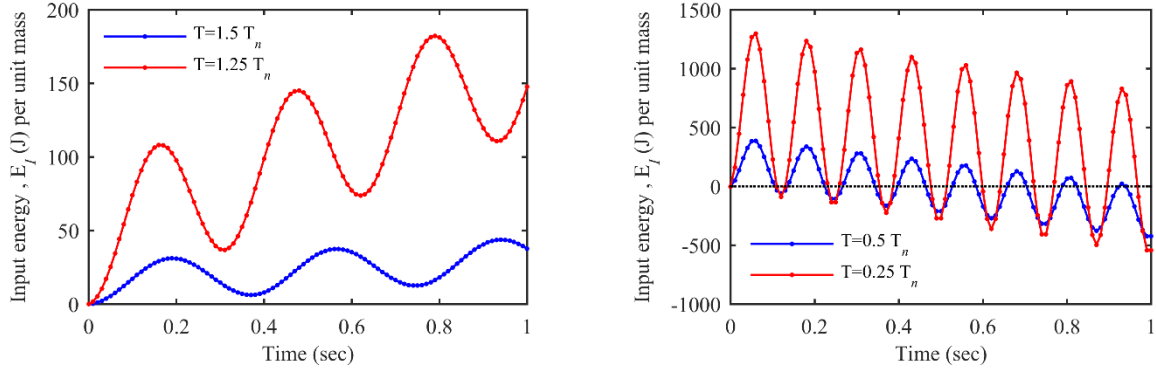
5.7. Single Rocking Walls with Limited Hysteretic Damping

To damp out the seismic input energy toward the end of the free vibration phase, SRWs are mostly prone to a gradual energy dissipation in the form of radiation damping within impact

durations in addition to some hysteretic and viscous damping. As the period of the wall exceeds the dominant period of the excitation, there will be a chance of removing some seismic energy from the system during cycles of vibrations. This fact, which was initially addressed in a study by DeJong (2012), is revealed here to be the most probable cause that SRWs with limited hysteretic energy dissipation can come to rest several seconds after strong excitations stopped.

5.7.1. Rate of input energy input into a SDOF system

As shown in Figure 5-1, the input energy – E_I – may fluctuate throughout the time history while generally increasing. This is because of either positive or negative rate of seismic energy – ΔE_I – as it is added to the system or removed. Negative rate of input energy due to ground motion occurs following the relative movement of the rocking wall and the foundation and results in removing some of the seismic energy at the end of the vibration cycles. According to Equation 5-1, this situation mathematically occurs as the ground acceleration (\ddot{u}_g) is of matching sign of the velocity response (du) of the system. To actualize the virtual meaning of negative energy rate, relative response of a SDOF system with viscous damping ratio of 3% to a sinusoidal harmonic motion with displacement profile of $u_g = \sin \omega t$ was investigated. Dominant period of the excitation, $\omega/2\pi$, was selected to be 0.25, 0.5, 1.25 and 1.5 times the natural period of this system (i.e., $T_n = 0.5$ sec). Figure 5-10 plots show the accumulated seismic input energy during these four harmonic motions per unit mass of the system. It is seen that within one second of the excitation, negative rate of seismic energy mostly occurs once duration of the ground motion impulse was smaller relative to the current period of the system – see Figure 5-10b.



a) Larger period of motion compared to SDOF

b) Shorter period of motion compared to SDOF

Figure 5-10. Energy input into a SDOF system during sinusoidal motions of different frequencies

5.7.2. Negative rate of energy input into SRWs

SRWs have a great chance to remove a part of the seismic energy from the system after experiencing large displacement response and consequently longer period of vibrations – as depicted in Figure 5-6 – compared to the dominant period of the applied ground motion. This is shown in Figure 5-11 by comparing the energy input into SRW2 and PreWEC-2 during $1.4 \times \text{Takatori}$. Figure 5-11a, which compares the time history of seismic energy imparted to these systems, indicates the lower total amount absorbed by the SRW beyond the strong portion of the motion; however, the PreWEC system was subjected to the almost identical motion (see Figure 5-11b).

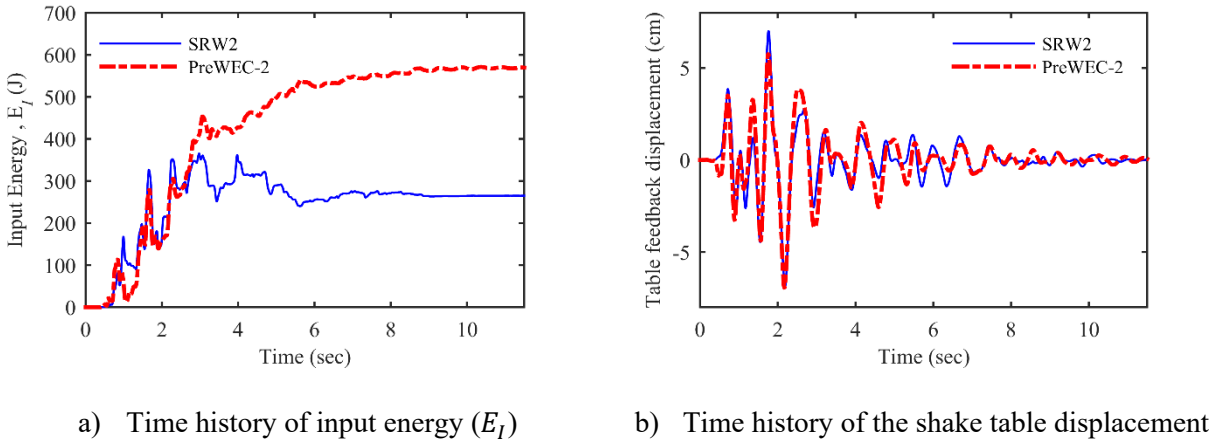
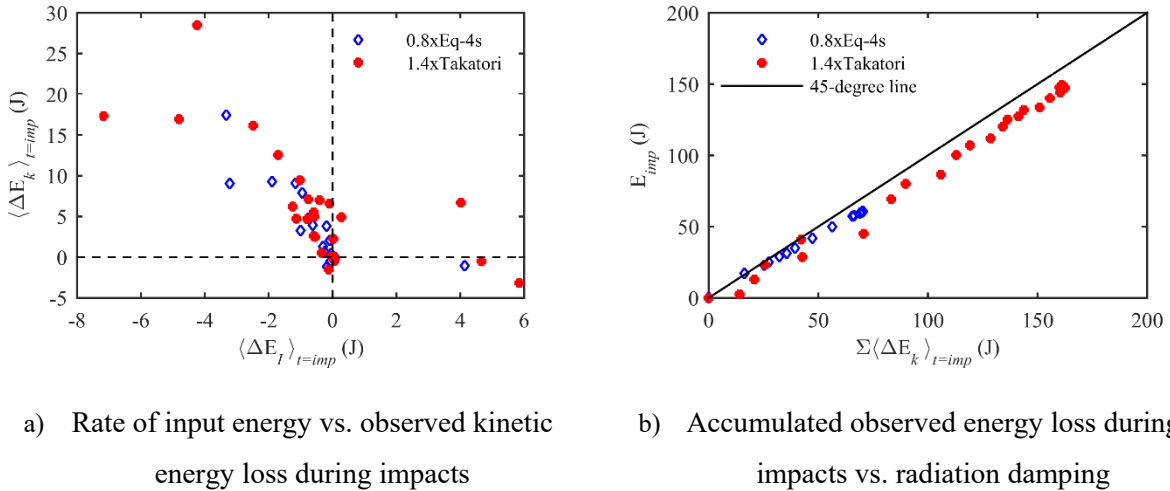


Figure 5-11. Rate of energy input into the rocking walls of group A during $1.4 \times$ Takatori

This is shown in Figure 5-12a, as $(\Delta E_I)_{t=imp}$ is plotted against the observed kinetic energy loss at the time of impact $(\Delta E_k)_{t=imp}$ during $0.8 \times$ Eq-4s – representing an EQ-III event – and $1.4 \times$ Takatori – representing an EQ-IV event. Figure 5-12b presents variation of the accumulated $(\Delta E_k)_{t=imp}$ over the duration of motion against the total amount of energy radiated back to the foundation, together with a 45-degree line. It can be seen that $\sum(\Delta E_k)_{t=imp}$ can approximately represent the amount of radiation damping – E_{imp} – while the wall rocks during base excitations. According to Figure 5-12 plots, an increased negative rate of input energy mostly occurring at the time of impacts, led to a larger observed kinetic energy loss and thereby greater amount of radiation damping. As a result, impacts of the SRWs on top of the foundation not only assist in energy dissipation of the wall, but also increase the chance of seismic energy removal from the system.



a) Rate of input energy vs. observed kinetic energy loss during impacts b) Accumulated observed energy loss during impacts vs. radiation damping

Figure 5-12. Negative rate of input energy at the time of impacts of SRW2

5.8. Conclusions

This paper quantified and compared different energy dissipation components of precast concrete rocking walls with and without additional hysteretic damping from the results of a series of shake table tests on a set of PreWECs and SRWs. These rocking wall systems dissipate the seismic input energy through: (i) hysteretic damping resulting from inelastic concrete strains developed in the wall toe regions especially at large drifts and deformation of O-connectors in PreWECs, (ii) inherent viscous damping, and (iii) radiation damping due to impacts. A summary of findings drawn from the study are presented:

- 1- Radiation damping of a rocking body during earthquake excitation was approximately estimated using the measured velocities of the system immediately before and immediately after an impact. The rate of energy transmitted to the rocking system during impacts, which was mostly negative, slightly affected the amount of observed kinetic energy loss at the time of impact.

- 2- Participation of radiation damping in energy dissipation of SRWs was about 30%, while PreWECs dissipated a significant amount of the energy imparted to the structure during a large earthquake through hysteretic action of the O-connectors.
- 3- Yielding of connectors within the first few cycles of the motion resulted in lower peak drift response of PreWECs compared to SRWs. Right after the strong portion of the motion, SRWs gradually dissipated their large content of seismic energy through rocking of the wall on top of the foundation.
- 4- It was shown that the additional connectors attempted to reduce the maximum peak of the drift response in PreWECs, as these systems experienced strong motions of earthquake levels EQ-III and EQ-IV. PreWEC-s1 with the lowest amount of added hysteretic damping exhibited greater responses when subjected to earthquakes of all intensities.
- 5- During DBE and MCE events, the additional hysteretic damping generally resulted in faster decay of the drift response toward the end of the free vibration phase. It was found that the number of cycles with peaks greater than 40% of the allowable drift limits were reduced in PreWECs compared to the emulated SRWs.
- 6- It was concluded that while SRWs have limited hysteretic damping capacity, they absorbed lower amount of seismic energy as they rocked toward the end of the free vibration phase with an extended period compared to PreWECs. The growth in the rocking period, which occurred due to their larger displacement and velocity amplitude, was mainly responsible for favorable relative movement of the rocking wall and the foundation in which seismic energy was removed from the system. This study theoretically defined the aforementioned situation once the wall aligned itself with the shake table after the table slowed down to speed up in the opposite direction.

5.9. Acknowledgments

The study reported in this paper was based upon the NEES Rocking Wall project supported by the National Science Foundation under Grant No. CMMI-1041650 and Dr. Joy Pauschke served as the program director for this grant. Any opinions, findings, and conclusions or recommendations expressed in this material are those of the authors and do not necessarily reflect the views of the National Science Foundation. All shake table tests were conducted using the NEES shared facility at the University of Nevada, Reno (UNR). The test units were donated by Clark Pacific and MidState Precast through coordination by PCI West. Materials provided by Sumiden Wire, GTI, Hayes Industries and help provided by ironworker local 118 with post-tensioning of specimens are also gratefully acknowledged.

5.10. References

- Aaleti, S., Sritharan, S. (2009) A simplified analysis method for characterizing unbonded post-tensioned precast wall systems. *Engineering Structures*, **31**(12), 2966–2975.
- Dejon, M. J. (2012) Amplification of rocking due to horizontal ground motion. *Earthquake Spectra*, **28**(4), 1405-1421.
- Falcon, E., Laroche, C., Fauve, S., and Coste, C. (1998) Behavior of one inelastic ball bouncing repeatedly off the ground. *The European Phys. J. B*, **3**(1), 45-57.
- Housner, G. (1963) The behavior of inverted pendulum structures during earthquakes. *Bulletin of the Seismological Society of America*, **53**(2), 403–417.
- Kurama, Y., Sause, R., Pessiki, S., and Lu, L. (1999) Lateral load behavior and seismic design of unbonded post-tensioned precast concrete walls. *ACI Structural Journal*, **96**(4), 622–632.
- Marriott, D., Pampanin, S., Bull, D., and Palermo, A. (2008) Dynamic testing of precast, post-tensioned rocking wall systems with alternative dissipating solutions. *Bulletin of the New Zealand Society for Earthquake Engineering*, **41**(2), 90–103.
- Nazari, M., Aaleti, S., and Sritharan, S. (2015) Shake Table Testing of Single Rocking Walls and

PreWECs @ UNR. *Network for Earthquake Engineering Simulation (distributor)*. doi: 10.4231/D3N29P75Z (SRW1), 10.4231/D3H98ZF0B (SRW2), 10.4231/D3CJ87M6Z (SRW3), 10.4231/D37S7HT2T(SRW4), 10.4231/D3WM13V3P (PreWEC-s1), and 10.4231/D3RV0D20F (PreWEC-s2).

Nazari, M., Sritharan, S., and Aaleti, S. (under review) Single Precast Concrete Rocking Walls as Earthquake Force-resisting Elements. *Earthquake Engineering and Structural Dynamics*.

Perez, F., Pessiki, S., and Sause, R. (2004) Experimental and analytical lateral load response of unbonded post-tensioned precast concrete walls. ATLSS Report No. 04-11, Lehigh University, Bethlehem, PA.

Priestley, M. J. N., Sritharan, S., Conley, J.R., and Pampanin, S. (1999) Preliminary results and conclusions from the PRESSS five-story precast concrete test building. *PCI Journal*, **44**(6), 42–67.

Priestley, M. (2002) Direct displacement-based design of precast/prestressed concrete buildings. *PCI Journal*, **47**(6), 66–79.

Rahman, M., and Sritharan, S. (2006) An evaluation of force-based design vs. direct displacement-based design of jointed precast post-tensioned wall systems. *Earthquake Engineering and Engineering Vibration*, **5**(2), 285–296.

Rahman, A. M. and Restrepo, J. I. (2000) Earthquake resistant precast concrete buildings: seismic performance of cantilever walls prestressed using unbonded tendons. Research Report 2000-5, University of Canterbury, Christchurch.

Seismology Committee. (1999) Recommended lateral force requirements and commentary (Blue book). Structural Engineers Association of California (SEAOC), California, USA.

Sritharan, S., Aaleti, S., Henry, R., Liu, K., and Tsai, K. (2015) Precast concrete wall with end columns (PreWEC) for earthquake resistant design. *Earthquake Engineering and Structural Dynamics*, **44**(12), 2075–2092.

Tuna, Z., Gavridou, S., and Wallace, J. (2012) 2010 E-defense four-story reinforced concrete and post-tensioned buildings—preliminary comparative study of experimental and analytical results. *Proceedings of the 15th World Conference on Earthquake Engineering*, Lisbon, Portugal.

Twigden, K. M. (2016) Dynamic response of unbonded post-tensioned concrete walls for seismic resilient structures, PhD Thesis. University of Auckland

CHAPTER 6
STRENGTH REDUCTION FACTORS FOR SEISMIC DESIGN OF PRECAST
CONCRETE ROCKING WALL SYSTEMS AND VERIFICATION

A paper to be submitted to the PCI Journal

Maryam Nazari and Sri Sritharan

6.1. Abstract

The current practice recommends a strength reduction (R) factor of 5 for designing the structures using precast concrete rocking walls. The unbonded post-tensioned Single Rocking Walls (SRWs) with negligible damping capacity, are often coupled with supplementary hysteretic energy dissipating elements. This paper recommends simplified expressions of R-factors suitable for their force-based design as a factor of damping. Using an experimentally validated analytical model, a parametric study was performed to investigate the seismic response of rocking wall systems designed for six, nine, and twelve story buildings with their damping ratios varying from 6% (i.e., for a SRW) to 18%. The robustness of the suggested R-factors was demonstrated as these systems satisfactorily conformed to performance-based objectives during design-based and maximum considered earthquake motions. The results of these analyses were also used to present a cost-effective design of precast concrete rocking walls for low to mid-rise buildings.

Keywords: rocking wall system, precast concrete, unbonded post-tensioning, numerical parametric study, seismic design, R-factor.

6.2. Introduction

Precast concrete rocking walls provide a self-centering system to ensure the resilient seismic performance of structures. The simplest form of such a system is the Single Rocking Wall (SRW) that is connected to the foundation using unbonded Post-Tensioning (PT) tendons (Kurama et al. 1999). To improve the energy dissipating ability and seismic performance, additional energy dissipating elements are designed for use in SRWs (e.g., Priestley et al. 1999; Rahman and Restrepo 2000; Sritharan et al. 2015). The Precast Wall with End Columns, namely PreWEC, is one such system developed by Sritharan et al. (2015), using a set of steel O-connectors as the external dampers. These connectors provide a wide range of damping capacities for the rocking wall system. SRWs and PreWECs can be designed to resist seismic loads by varying: (i) the initial stress and total area of PT tendons, and (ii) force in the connectors joining the end columns to the wall panel.

A review of the literature indicates that the majority of tests on different rocking wall systems have been conducted quasi-statically (e.g., Perez et al. 2004), which led to the limited investigation into their seismic design. Relying primarily on these experiments and limited analytical studies (e.g., Priestley et al. 1999; Stanton et al. 2002; and Kurama 2002), ACI ITG-5.1 (2008) was developed to outline seismic acceptance criteria for special unbonded post-tensioned precast concrete walls in regions of high seismicity. According to this guideline, the design elastic response acceleration as defined in ASCE 7-05 (2005) should be reduced by a constant strength Reduction (or R) factor of 5 or 6 for the rocking walls designed to be used respectively in bearing wall or building frame systems; this criterion does not account for the energy dissipating ability of the rocking structure.

To quantify damping capacities of SRWs and PreWECs and the related R-factors, a series of shake table tests were carried out by the authors on a total of eight post-tensioned walls (Nazari et al. 2015). These walls were subjected to a series of earthquake excitations with varying intensities and their performance was assessed in terms of the maximum transient drift, maximum absolute acceleration, and residual drift based on multi-hazard acceptance criteria (SEAOC 1999). It was indicated that the test walls responded satisfactorily when they were designed corresponding to their damping capacities following the basis of the Direct Displacement-Based Design (DDBD) approach (Priestley 2000). Simplified expressions were then suggested to compute R-factors for the Force-Based Design (FBD) of rocking walls both with and without additional hysteretic damping.

To establish appropriate design procedures for SRWs and PreWECs, the suggested R-factors were calibrated as part of this study using an experimentally validated model developed in OpenSees. Through this model, a series of six, nine, and twelve story buildings were subjected to nonlinear dynamic analyses using two sets of near-field (NF) and far-field (FF) ground motions, each representing design-based (DBE) and maximum considered (MCE) events. These multi-story buildings were designed with SRWs and PreWECs with different hysteretic energy dissipation capacity and consequent R-factors. Using acceptance criteria defined in terms of lateral drift, residual drift, and absolute acceleration, a multiple-level performance-based seismic evaluation was conducted to validate the modified design solutions for these buildings. A cost index was also developed to specify the most economical rocking wall option (i.e., SRW or PreWEC) for designing low to mid-rise buildings.

6.3. Rocking Wall Systems

SRWs are designed with unbonded PT tendons as the primary reinforcement across the connection interface between the wall and the foundation. Their limited energy dissipation capacity is mainly provided through impacts of the wall panel as it rocks on top of the foundation and material nonlinearity of concrete at wall toes. Thereby, researchers (e.g., Priestley et al. 1999; Rahman and Restrepo 2000; Sritharan et al. 2015) included supplementary hysteretic energy dissipaters in SRWs and developed rocking wall systems (e.g., PreWEC as presented by Sritharan et al. 2015). PreWEC consists of a SRW connected to two end columns, using special energy dissipating Oval-shaped connectors, namely O-connectors. Different configuration options of the PreWEC system is available as presented in Sritharan et al. (2015). Figure 6-1 compares detail of a SRW with a typical PreWEC system. Figure 6-2 presents the measured force-deformation response of a typical O-connector with the specified dimensions.

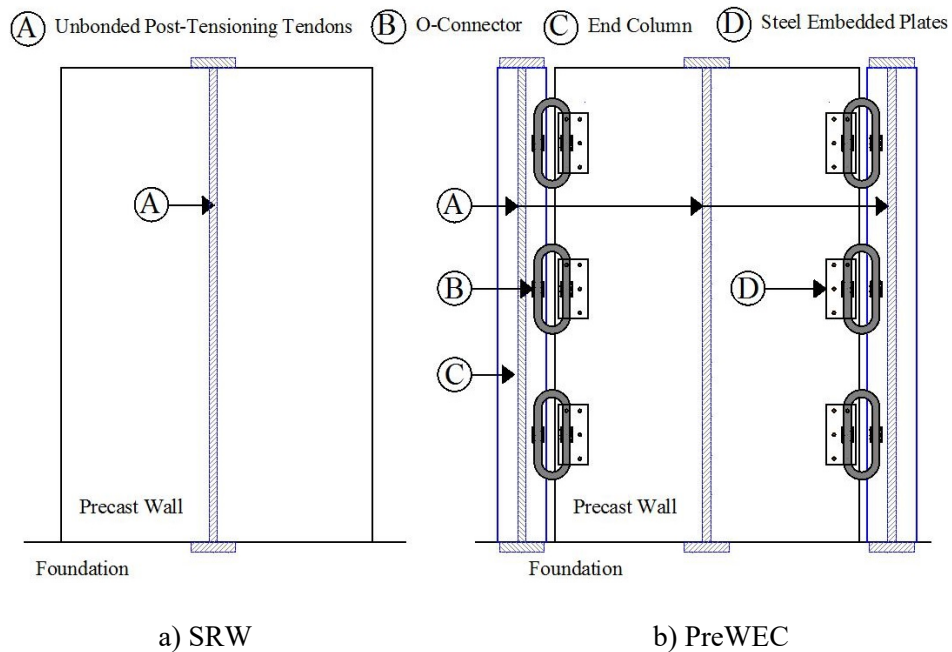


Figure 6-1. Rocking wall systems

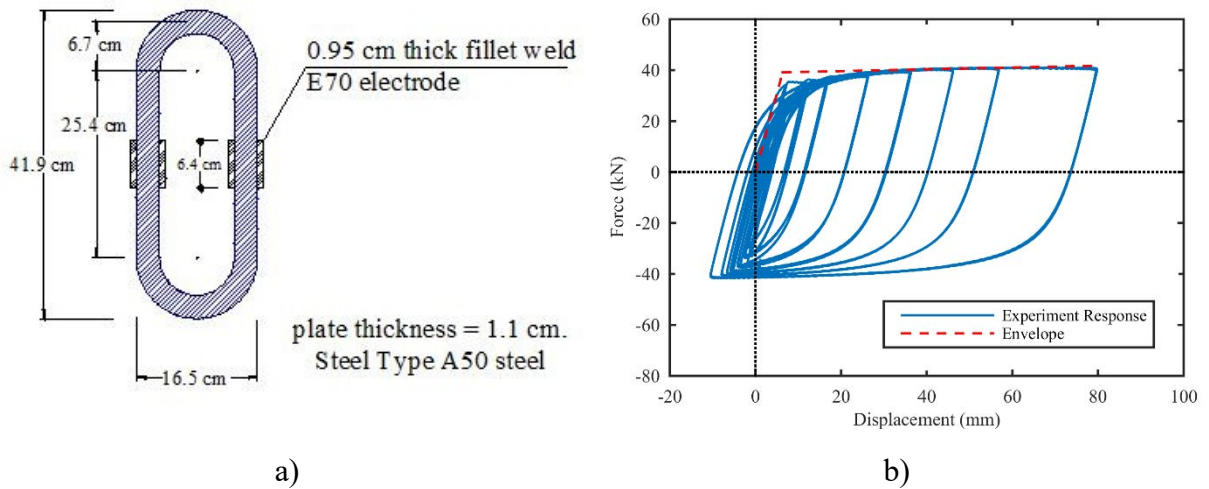


Figure 6-2. Dimensions (a) and corresponding force-displacement behavior (b) of an O-connector used in PreWEC (1 m = 3.28 ft; 1 kip = 4.45 kN)

6.4. Current Design Practice

Currently, ACI ITG 5.1 (2008) outlines acceptance criteria for rocking wall systems to be used in seismic regions. This document requires the application of supplementary energy dissipating elements in the system to provide a minimum hysteretic damping ratio of about 8%. This prevents the seismic application of SRWs.

Specific design provisions of the rocking wall systems satisfying ITG 5.1 is presented in ACI ITG 5.2 guideline (2009). This document covers the design procedures suitable for jointed (Priestley et al. 1999) and hybrid wall systems (Rahman and Restrepo 2000) based on experimental and analytical research. Some major design considerations of ITG 5.2 are summarized as follows:

- **Design drift:** A minimum height-length ratio of 0.5 is required (section 4.4.2). This ratio will determine the amount of the design drift following section 4.3.4.

- **Self-centering capability:** PT tendons should remain elastic till design drift (section 4.4.7). According to section 7.1.2 of ITG 5.1, the PT force should not exceed 90% of the strength of the tendons at 1% elongation, while the wall displaced to 3/4 the design displacement.
- **Area of PT tendons:** The required area of PT tendons is determined using moment equilibrium of forces acting on the wall base, assuming the ultimate strength of the connectors and 95% of the yielding stress in PT tendons at the design drift (section 6.4.1).
- **Initial prestressing:** Estimating the neutral axis depth of the wall at the design drift (see section 5.6.3.8) leads to establish the initial stress in PT tendons (section 6.4.4).
- **Design of supplementary damping devices:** Design requirements for O-connectors used in PreWEC systems are not covered in this guideline.

Nominal flexural strength: ϕ times the provided strength should resist a moment demand at the wall base resulting from a design-level earthquake excitation (section 5.6.2.1). The classical force-based approaches (e.g., IBC 2009 and ASCE7-05 2005) are used to estimate the required design moment. According to section R5.4 of ITG 5.1, an R-factor of 5 or 6 is used for the rocking walls designed respectively as bearing wall or building frame systems in the concrete structures.

- **Additional detailing:** Designing the confined boundary elements at the wall corners is required, satisfying the provisions of ACI 318-11 (2011) (section 5.6.3.6). Also, walls should be detailed with minimum amount of shear stirrups and longitudinal reinforcement, as suggested by this code.

6.5. Recommended New R-factors

Following the current design practice (IBC 2009; ASCE 7-05 2005), R-factors are used to reduce linear elastic design forces of structures to account for their hysteretic energy dissipation. For the rocking wall systems, an R-factor of 5, as used for the conventional concrete shear walls, is considered when these walls are used in a bearing wall system (ACI ITG-5.1 2008); however, this value does not reflect their actual energy dissipation capacity. The results from an experimental shake table study conducted on eight rocking walls (Nazari et al. 2015) were used to establish R-factors for such systems as a function of their total equivalent viscous damping ratio, as presented by Equations 6-1a and 6-1b. Using these equations for seismic design of rocking wall systems during far-field (FF) and near-field (NF) ground motions results in buildings that are capable of achieving the basic seismic performance objectives as defined by SEAOC seismology committee (1999).

$$R = 0.4648 \times \xi_{eq} + 0.9295 ; \text{ FF records} \quad (\text{Equation 6-1a})$$

$$R = 0.1547 \times \xi_{eq} + 2.6503 ; \text{ NF records} \quad (\text{Equation 6-1b})$$

where, R = response reduction factor and ξ_{eq} = total equivalent viscous damping ratio, in percent, at the design drift level.

As outlined through this shake table study, ξ_{eq} consisting of: (i) 4.2% equivalent viscous damping ratio of the walls due to the material nonlinearity of concrete at wall toes and inherent viscous damping of the system, (ii) 1% and 1.5% damping due to impacts for PreWECs and SRWs, respectively, and (iii) the additional equivalent viscous damping ratio of PreWEC systems due to

hysteretic action of O-connectors; following equation was suggested to correlate this damping component with the response characteristics of O-connectors (as presented in Chapter 4).

$$\xi_{hys,D\%} = \frac{1}{\pi} \frac{N_{conn.} \times F_{c,ave} \times (\Delta_{c,D\%} - \Delta_{c,y})}{V_{D\%} \times D\% \times H_s} \quad (\text{Equation 6-2})$$

where, $\xi_{hys,D\%}$ = damping ratio due to hysteretic action of O-connectors at $D\%$ design drift level of the system, $N_{conn.}$ = total number of connectors, $V_{D\%}$ = shear resistance of the system at $D\%$ design drift level, H_s = seismic height (moment to base shear ratio), and $F_{c,ave}$ = average of connector forces at yield and $D\%$ design drift level of the wall with corresponding deformations of $\Delta_{c,y}$ and $\Delta_{c,D\%}$.

Any given range of $\xi_{hys,D\%}$ could be used for designing the PreWECs and the R-factor changes accordingly. This allows for more flexibility in the design of rocking wall systems. According to Equations 6-1a and 6-1b, SRWs could be designed with an R-factor of about 3.5, regardless of their limited damping ratio of less than 6%. Although design forces of SRWs are expected to be greater than those for PreWECs, the proposed approach in this study presents different design solutions to apply rocking wall systems in the structures. This is ignored in current design criteria of ITG 5 (2008; 2009).

6.6. Proposed Design Approach

In addition to the requirements of ITG 5 guidelines (2008; 2009), the following steps are recommended for design of the rocking wall systems, including SRWs and PreWECs:

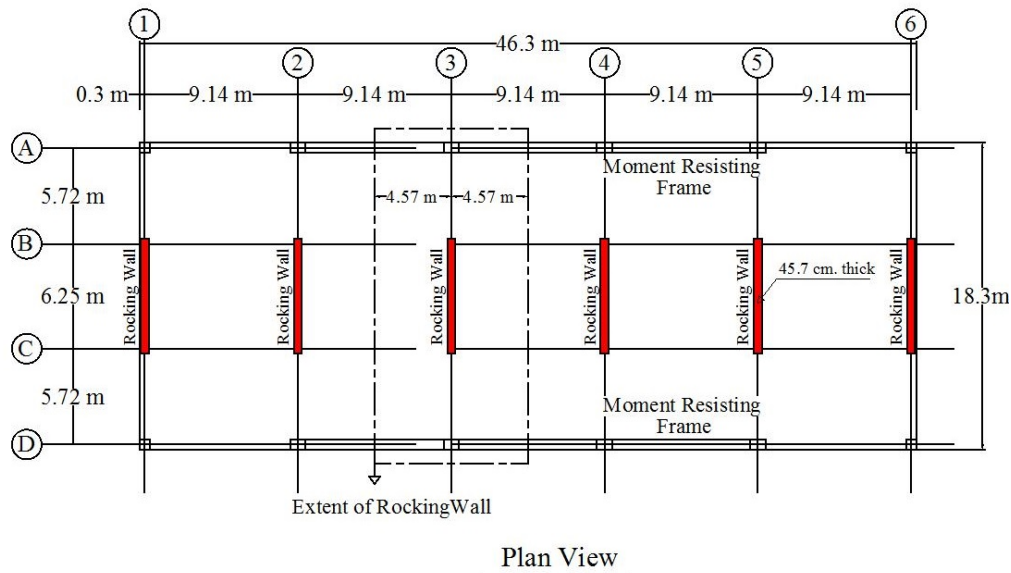
- For a PreWEC system:

1. Establish a suitable damping ratio at the wall design drift (i.e., in the range of 10% to 16%).
 2. Locate the O-connectors with respect to the wall length and find out their expected deformation when the wall displaced to its design displacement.
 3. Following the recommendation of Aaleti and Sritharan (2009) and Twigden and Henry (2016), estimate dimensions of the O-connectors to obtain their force-deformation properties at the onset of yielding as well as the ultimate fracture point.
- Following the current force-based design practice, estimate the design force of rocking wall systems corresponding to their damping capacity. Equation 6-1a and Equation 6-1b are used to estimate the corresponding R-factor. Alternatively, a DDBD approach can be used to estimate the design forces (Priestley 2000).
 - For a PreWEC system:
 - 1- Apply Equation 6-2 to estimate the required number of O-connectors.
 - 2- The initial stress and area of PT tendons for clamping the end columns to the foundation is designed to resist 1.4 times the ultimate force of connectors per joint. Self-weight of the columns and any applied gravity load may be considered as the additional prestressing force.
 - Estimate the initial stress and area of PT tendons in the wall panel. If gravity loads are designed to transfer to the foundation through the wall panels, the initial prestressing force could be reduced.

6.7. Parametric Study

6.7.1. Design of the buildings

Six, nine, and twelve story buildings were designed for a location in California (i.e., seismic zone 4 and soil type S_C). The typical plan view of the buildings is shown in Figure 6-3. As highlighted in red in this figure, a maximum of six rocking walls (i.e., SRW or PreWEC) were used as seismic resisting systems of these buildings in the orthogonal direction. These walls were designed in accordance with the proposed design approach to withstand design-based as well as maximum considered earthquake events. Responses of the buildings to NF and FF ground motions were also investigated in this study while these wall systems were designed with the appropriate R-factors (see Equations 6-1a and 6-1b). Considering different intensity levels of NF and FF events, representing DBE and MCE motions, four different design details were presented for each case study, as summarized in Tables 6-1 and 6-2.



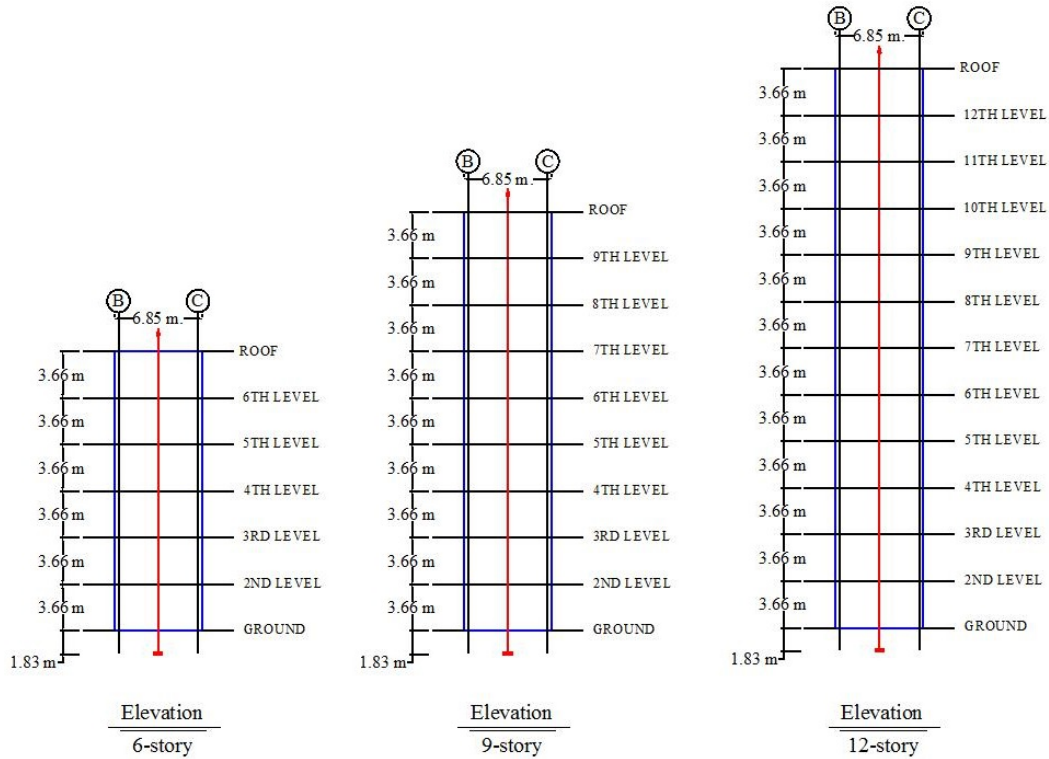


Figure 6-3. Plan view and elevations of the buildings (1 m = 3.28 ft)

The procedure for design of the buildings with SRWs and PreWECs is explained in the following sections.

6.7.2. Example of design of the buildings with SRWs

Due to low energy dissipation capacity of SRWs, using this option resulted in large design forces of the buildings, as presented in Table 6-1. The building designation in this table refers to the type of the rocking wall and number of the stories (e.g., SRW6 is a six-story building with SRWs as the lateral resisting elements). To resist the earthquake loading, buildings were designed with four to six SRWs. As shown in Table 6-1, area of PT tendons and initial prestressing varies from 78.4 cm^2 (12.15 in^2) and $0.65f_{pu}$ to 224 cm^2 (34.72 in^2) and $0.75f_{pu}$; where f_{pu} = tensile

strength of strand = 1862 MPa (270ksi). The required design parameters are estimated as explained in the previous sections and presented below for SRW6 during FF-DBE events:

- Dimensions:

Wall height= 2195 cm (864 in.); Wall length= 686 cm (270 in.); Wall thickness=46 cm (18 in.); Length of PT tendons= 2377 cm (936 in.)

- Design drift:

1- ITG 5.1 (2008), 5.4: Ultimate drift: $\min \{0.8 \times (2195/686) + 0.5, 3\} = 3\%$

2- ITG 5.2 (2009), 4.3.4: Design drift: $(2/3) \times 3 = 2\%$

- Damping ratio and corresponding R-factor for FF events:

$\xi_{eq} = 6\%$; Recall from Equation (6-1a); $R = 0.4648 \times \xi_{eq} + 0.9295 = 3.7$

- Design force for the six-story building (ASCE 07-05 2005):

$C_s = 0.234$; $V = 9972$ kN (2241 kips) resisted by four SRWs

$V = 2493$ kN (560 kips) per wall

- Gravity load transferred through the SRW: $P_D = 4159$ kN (935 kips)

- Required area of the PT tendons (A_p) and the initial prestressing stress (f_{pi}), using moment equilibrium of forces acting on the wall base.

$A_p = 78.4$ cm² (12.15 in.²); $f_{pi} = 1210$ MPa (175.5 ksi)

- Check the self-centering capability:

1- PT force at 1.5% drift: $P_{1.5\%} = 12006$ kN (2699 kips)

ITG 5.1 (2008), 7.1.2: $12006 \times 10^3 / 7840 < 0.9 \times 1770$

2- Contact length at design drift: $C_{2\%} = 84$ cm (33 in.)

$$\text{ITG 5.2 (2009), 4.4.7: } 1210 + 196500 \times 0.02 \times (686/2 - 84) / 2377 < f_{py} = 1675 \text{ MPa}$$

6.7.3. Example of design of the buildings with PreWECs

PreWECs with total equivalent viscous damping ratios (ξ_{eq}) of 13% and 18% were also used for resisting seismic loads of the multi-story buildings. The n-story building designed with such wall systems named either PreWECn-13 or PreWECn-18, depending on the energy dissipation capacity of the system. According to Table 6-2a, these systems could be designed with lower amount of PT tendons compared to the SRWs, as they use additional O-connectors to limit the structural response. Therefore, area of PT tendons and initial prestressing varies from 4.2 cm² (0.65 in²) and 0.6 f_{pu} to 140 cm² (21.7 in²) and 0.75 f_{pu} . Table 6-2b presents the design details of end columns and O-connectors. For PreWECn-13 and PreWECn-18 buildings, four and six connectors were used per floor, respectively, to join the wall panel with either of the end columns; however, they were increased to eight connectors for two PreWECn-18 case studies (see Table 6-2b). Force-deformation properties of different types of connectors, namely connectors A to D, are summarized in Table 6-2c. The required design parameters are estimated as explained in the previous sections and presented below for PreWEC9-13 during the NF-DBE events:

- Dimensions:

Wall panel: height=3292 cm (1296 in.); length=533 cm (210 in.); thickness=46 cm (18 in.);

Length of PT tendons= 3475 cm (1368 in.)

End columns: height= 3292 cm (1296 in.); length=76 cm (30 in.); thickness=46 cm (18 in.); Length of PT tendons= 3475 cm (1368 in.)

- Design drift:

1- ITG 5.1 (2008), 5.4: Ultimate drift: $\min \{0.8 \times (3292/533) + 0.5, 3\} = 3\%$

2- ITG 5.2 (2009), 4.3.4: Design drift: $(2/3) \times 3 = 2\%$

- Damping ratio (expected) and corresponding R-factor for NF events:

$$\xi_{eq} = 13\%; \text{ Recall from Equation (6-1b); } R = 0.1547 \times \xi_{eq} + 2.6503 = 4.7$$

- Details of O-connectors:

Use four O-connector Type A per joint per floor (see Table 6-2c).

- Design force for the six-story building (ASCE 07-05 2005)

$$C_s = 0.138; V = 8801 \text{ kN (1979 kips) resisted by five PreWECs}$$

$$V = 1760 \text{ kN (396 kips) per wall}$$

- End columns: Required area of the post-tensioning tendon ($A_{p,col}$) and the initial prestressing ($f_{pi,col}$) to resist the ultimate force of connectors:

$$A_{p,col} = 25.2 \text{ cm}^2 (3.91 \text{ in.}^2); f_{pi,col} = 1582 \text{ MPa (230 ksi) per end column}$$

$$0.7 \times (2.52 \times 1582 + 23.6 \times (32.92 \times 0.76 \times 0.46)) > 36 \times 80.1 \text{ kips}$$

- Gravity load transferred through the wall panel: $P_D = 6236 \text{ kN (1402 kips)}$

- Wall panel: Required area of the post-tensioning tendon (A_p) and the initial prestressing (f_{pi}), using moment equilibrium of forces acting on the wall base.

$$A_p = 63 \text{ cm}^2 (9.8 \text{ in.}^2); f_{pi} = 1303 \text{ MPa (189 ksi)}$$

- Check the self-centering capability:

1- PT force at 1.5% drift: $P_{1.5\%} = 9207 \text{ kN (2070 kips)}$

$$\text{ITG 5.1 (2008), 7.1.2: } 9207 \times 10^3 / 6300 < 0.9 \times 1770$$

2- Contact length at design drift: $C_{2\%} = 80 \text{ cm (31.5 in.)}$

ITG 5.2 (2009), 4.4.7: $1303 + 196500 \times 0.02 \times (533/2 - 80) / 3475 < f_{py} = 1675 \text{ MPa}$

- Estimate the equivalent viscous damping ratio due to deformation of O-connectors:

1- Using Equation (6-2);

$$\xi_{hys,D\%} = \frac{1}{\pi} \times \frac{2 \times 36 \times 0.5 \times (78 + 75.6) \times (5.7 - 0.64)}{1760 \times 0.02 \times 3292}$$

$$= 7.7\%$$

$$\xi_{eq} = 7.7 \text{ (O-connector)} + 4.2 \text{ (material nonlinearity of concrete)} + 1 \text{ (impact)} = 12.9 \cong 13$$

6.8. Selection and Scaling of Ground Motions

The buildings for this case study were subjected to a set of ground motion records, as presented in FEMA P695 (2009). Subsequently, a total of 35 earthquakes corresponding to site class C were selected for this study. As summarized in Table 6-3, this record set includes ten FF and twenty-five NF records. These records were scaled to represent EQ-III and EQ-IV seismic hazard levels, representing DBE and MCE events.

As presented by SEAOC guideline (1999) and in consistent with the requirements of ASCE7-05 (2005), these hazard levels are defined by five percent damped elastic acceleration response spectra with equivalent peak ground accelerations of 1 g (i.e., EQ-III) and 1.5 g (i.e., EQ-IV), considering the building location. The scale factors, as noted in Table 6-3, were achieved for each ground motion such that the root mean square deviation (RMSD) of their spectral ordinates remains within $\pm 30\%$ of the mean of the targeted hazard spectrum within a dominant period range of the rocking wall system (i.e., 0.5 to 5 sec. for the case-study buildings). The detailed procedure is described in Nazari et al. (2016).

Table 6-1. Design of the buildings with SRWs (1 m = 3.28 ft; 1 ksi = 6.9 MPa; 1 kip = 4.45 kN)

Building ID	R	#SRWs	Design force per wall; $V_{D\%}$ (kN)				Area of PT tendon (A_p , cm ²) / Initial PT stress (f_{pi} , MPa)			
	(FF/NF)	(DBE/MCE)	FF-DBE	NF-DBE	FF-MCE	NF-MCE	FF-DBE	NF-DBE	FF-MCE	NF-MCE
SRW6	3.7/3.6	4/6	2493	2590	2493	2590	78 / 0.65 f_{pu} ¹	84 / 0.65 f_{pu}	91 / 0.65 f_{pu}	98 / 0.65 f_{pu}
SRW9		4/6	2758	2866	2758	2866	196 / 0.7 f_{pu}	203 / 0.75 f_{pu}	217 / 0.7 f_{pu}	224 / 0.75 f_{pu}
SRW12		6/- ²	1976	2053	2964	3080	175 / 0.75 f_{pu}	189 / 0.75 f_{pu}	-	-

¹ f_{pu} = tensile strength of PT tendon = 1862 MPa (270ksi)

² Maximum number of SRWs (i.e., six) was not adequate to design the twelve-story building for MCE events.

Table 6-2a. Design of the buildings with PreWECs – Wall panel (1 m = 3.28 ft; 1 ksi = 6.9 MPa; 1 kip = 4.45 kN)

Building ID	R	#PreWECs		Design force per wall; $V_{D\%}$ (kN)				Area of PT tendon (A_p , cm ²) / Initial PT stress (f_{pi} , MPa)			
		(DBE/MCE)		FF-DBE	NF-DBE	FF-MCE	NF-MCE	FF-DBE	NF-DBE	FF-MCE	NF-MCE
	FF	NF									
PreWEC6-13	7.0/4.7	3/4	4/6	1772	1988	1994	1988	35 / 0.65 f_{pu} ¹	49 / 0.65 f_{pu}	49 / 0.65 f_{pu}	63 / 0.65 f_{pu}
PreWEC9-13		3/5	5/6	1962	1760	1765	2200	84 / 0.75 f_{pu}	63 / 0.7 f_{pu}	63 / 0.7 f_{pu}	140 / 0.75 f_{pu}
PreWEC12-13		4/5	5/- ²	1581	1892	1897	2364	63 / 0.75 f_{pu}	137 / 0.75 f_{pu}	137 / 0.75 f_{pu}	-
PreWEC6-18	9.3/5.4	3/4	4/6	1329	1705	1496	1705	4 / 0.6 f_{pu}	17 / 0.65 f_{pu}	7 / 0.6 f_{pu}	32 / 0.6 f_{pu}
PreWEC9-18		3/5	5/6	1471	1510	1324	1887	11 / 0.6 f_{pu}	14 / 0.65 f_{pu}	7 / 0.6 f_{pu}	53 / 0.75 f_{pu}
PreWEC12-18		3/5	5/6	1581	1622	1423	2028	36 / 0.75 f_{pu}	42 / 0.75 f_{pu}	17 / 0.6 f_{pu}	102 / 0.75 f_{pu}

¹ f_{pu} = tensile strength of PT tendon = 1862 MPa (270ksi)

² Maximum number of PreWECs with 13% damping was not adequate to design the twelve-story building for NF-MCE events.

Table 6-2b. Design of the buildings with PreWECs – connectors and end columns (1 m = 3.28 ft; 1 ksi = 6.9 MPa)

Building ID	Type and number of connectors per joint per floor / total damping ratio (%)				Area of PT tendon ($A_{p,col}$, cm^2) / Initial PT stress ($f_{pi,col}$, MPa)			
	FF-DBE	NF-DBE	FF-MCE	NF-MCE	FF-DBE	NF-DBE	FF-MCE	NF-MCE
PreWEC6-13	A4 / 12.9	A4 / 12.1	A4 / 12.1	C4 / 12.5	17 / $0.85f_{pu}$			17 / $0.85f_{pu}$
PreWEC9-13	A4 / 12.0	A4 / 12.8	A4 / 12.8	C4 / 11.7	25 / $0.85f_{pu}$			35 / $0.85f_{pu}$
PreWEC12-13	A4 / 13.6	A4 / 12.4	A4 / 12.4	-	35 / $0.85f_{pu}$			-
PreWEC6-18	B6 / 17.8	B6 / 17.8	B6 / 17.4	D6 / 16.5	25 / $0.8f_{pu}$			25 / $0.8f_{pu}$
PreWEC9-18	B6 / 17.5	B6 / 17.2	B6 / 17.9	D8 / 18.1	38 / $0.8f_{pu}$			46 / $0.85f_{pu}$
PreWEC12-18	B6 / 16.6	B6 / 16.4	B6 / 17.8	D8 / 17.2	49 / $0.8f_{pu}$			62 / $0.85f_{pu}$

Table 6-2c. Design of the buildings with PreWECs – force deformation properties of O-connectors (1 m = 3.28 ft; 1 kip = 4.45 kN)

Connector ID	Force (kN)		Deformation (cm)	
	Yield	Ultimate	Yield	Ultimate
A	75.6	80.1	0.64	10.2
B	64.5	71.2	0.38	10.2
C	77.8	80.1	0.25	10.2
D	68.9	71.2	0.25	10.2

Table 6-3. List of input motions used for analysis of the buildings (FEMA P695 2009)

Earthquake				Scale Factor (DBE)		Scale Factor (MCE)	
Name (Year, Station)	Component 1	Component 2	PGA _{max} (g)	Comp. 1	Comp. 2	Comp. 1	Comp. 2
Far-Field (FF) ground motions							
Hector Mine (1999, Hector)	HEC000	HEC090	0.34	1.70	1.30	2.50	1.80
Kobe, Japan (1995, Nishi-Akashi)	NIS000	NIS090	0.51	1.33	1.20	2.00	2.00
Kocaeli, Turkey (1999, Arcelik)	ARC000	ARC090	0.22	4.50	-	6.00	-
Manjil, Iran (1990, Abbar)	ABBAR--L	ABBAR--T	0.51	1.30	0.85	2.00	1.40
Chi-Chi, Taiwan (1999, TCU045)	TCU045-E	TCU045-N	0.51	2.00	1.50	2.50	2.10
Friuli, Italy (1976, Tolmezzo)	A-TMZ000	A-TMZ270	0.35	2.90	-	4.00	-
Near-Field (NF) ground motions							
Loma Prieta (1989, Saratoga – Aloha)	STG_038	STG_128	0.38	1.00	1.60	1.50	2.30
Cape Mendocino (1992, Petrolia)	PET_260	PET_350	0.63	-	0.60	-	0.90
Landers (1992, Lucerne)	LCN_239	LCN_329	0.79	0.75	1.70	1.20	2.50
Northridge-01 (1994, Sylmar)	SYL_032	SYL_122	0.73	0.75	0.55	1.00	0.70
Chi-Chi, Taiwan (1999, TCU102)	TCU102_278	TCU102_008	0.29	0.65	0.65	1.20	1.10
Gazli, USSR (1976, Karakyr)	GAZ_177	GAZ_267	0.71	0.85	0.90	1.10	1.40
Nahanni, Canada (1985, Site 1)	S1_070	S1_160	1.18	1.60	1.65	2.30	2.50
Nahanni, Canada(1985, Site 2)	S2_070	S2_160	0.45	3.00	2.00	4.50	2.90
Loma Prieta (1989, BRAN)	BRN_038	BRN_128	0.64	1.15	-	1.50	-
Loma Prieta (1989, Corralitos)	CLS_038	CLS_128	0.51	1.30	-	2.00	-
Cape Mendocino (1992, Cape Men.)	CPM_260	CPM_350	1.43	0.70	1.45	1.00	2.30
Northridge-01 (1994, LA)	0637_032	0637_122	0.73	-	0.70	-	1.10
Chi-Chi, Taiwan (1999, TCU067)	TCU067_285	TCU067_015	0.56	0.75	0.75	1.10	1.20
Chi-Chi, Taiwan (1999,TCU084)	TCU084_271	TCU084_001	1.16	0.80	-	1.20	-
Denali, Alaska (2002,TAPS Sta.#10)	ps10_199	ps10_289	0.33	0.55	0.90	0.80	1.30

Figures 6-4a and 6-4b present the acceleration response spectra of the scaled records, including FF and NF events, which represent DBE and MCE events, respectively.

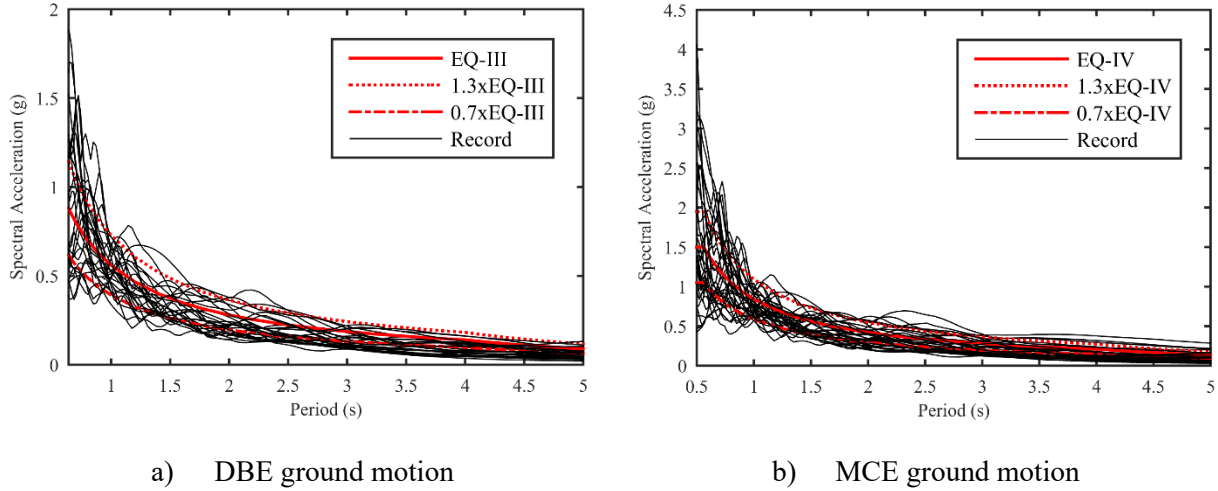


Figure 6-4. Spectral acceleration of scaled NF and FF ground motions selected for analysis

6.9. Analytical Model

An experimentally validated analytical model in OpenSees (McKenna et al. 2000) is used to compare the maximum responses of the buildings. This is a simplified single degree of freedom (SDOF) model of rocking wall systems, considering a linear rocking mode shape for the structure. Calculations for the effective mass (m_{eff}) and height (H_{eff}) of the substitute SDOF model for the six-story building with four SRWs is presented below. In the following equations, m_i and Δ_i present mass and displacement of each floor in the n-story building.

$$H_{eff} = \frac{\sum_{i=1}^n (m_i \Delta_i^2)}{\sum_{i=1}^n (m_i \Delta_i)} / 0.02 = 0.722 \times H_n = 0.722 \times 6 \times 3.66 = 15.86 \text{ m (52 ft)}$$

$$m_{eff/Wall} = \frac{\sum_{i=1}^n (m_i \Delta_i)}{0.02 \times H_{eff}} / 4 = 4.85 \times m_i / 4 = 4.85 \times 847.3 \times 8.38 / 4 = 8609 \text{ kN (1935 kip)}$$

Details of the OpenSees model is presented in Figure 6-5. As shown in this figure, the seismic mass of m_{eff} is on top of an elastic beam column element with a height of H_{eff} representing the precast concrete wall. This element is attached to the foundation using a zero-length rotational spring system, consisting of: (i) a SelfCentering material model (McKenna et al. 2000) to capture the wall base moment resistance and its re-centering capability as well as concrete nonlinearity, and (ii) an Steel02 material model (McKenna et al. 2000) to represent the moment resistance and hysteretic energy dissipation capacity of O-connector. These two springs perform in parallel to model the PreWEC; however, response of SRW is achieved by using only the former spring. More information about the material models are available in Nazari et al. (2016).

The experimental lateral drift time history responses of SRW and PreWEC test units from the shake table investigations (Nazari et al. 2015) were compared to the amount calculated using the OpenSees model. This comparison, as presented in Figure 6-6, confirmed the accuracy of this model in capturing the peak of lateral drift responses.

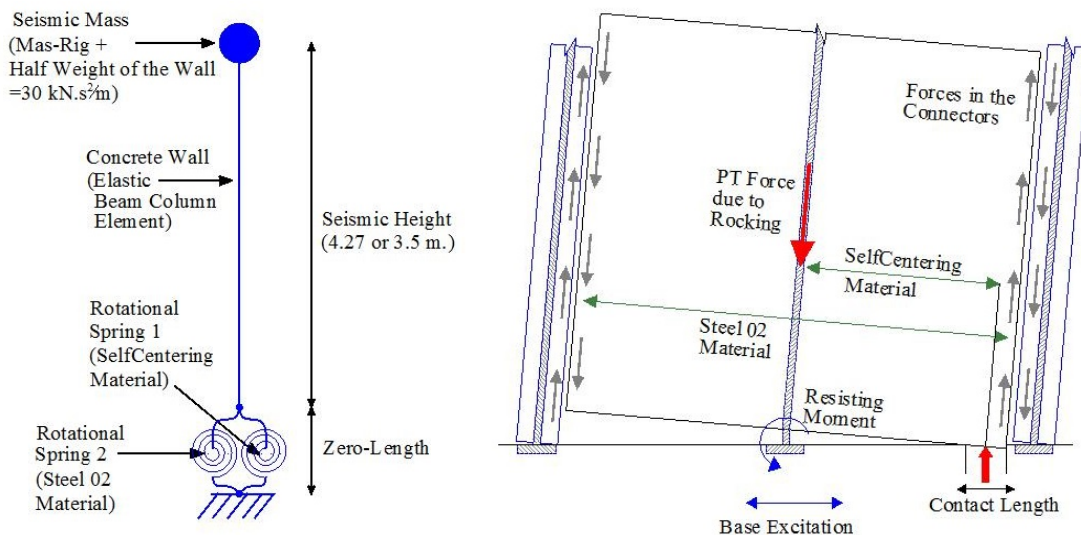
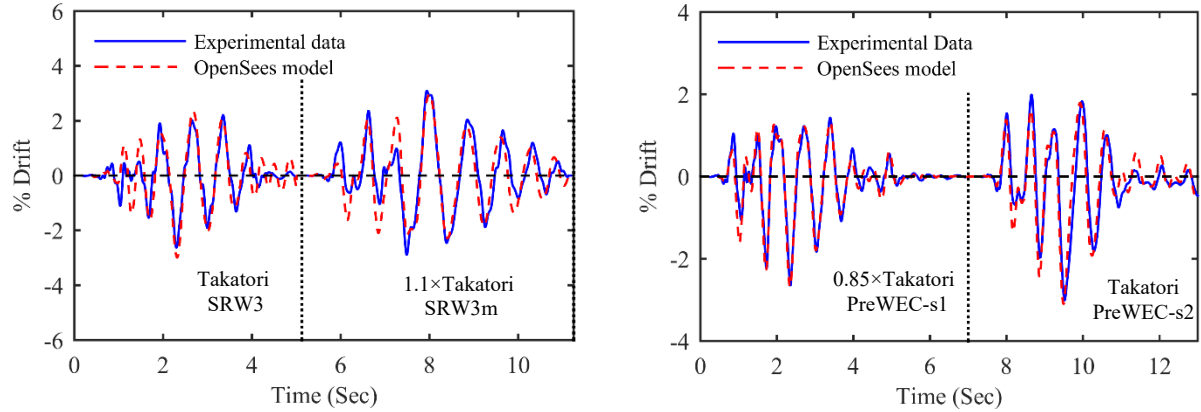


Figure 6-5. OpenSees model for a rocking wall (1 m = 3.28 ft; 1 kip = 4.45 kN)



a) lateral drift time history response; SRW

b) lateral drift time history response; PreWEC

Figure 6-6. Experimental verification of the analytical results (Nazari et al. 2016)

6.10. Dynamic Results

Using the OpenSees model, dynamic analysis of the rocking wall systems was run for each of the designs listed in Tables 6-1 and 6-2 and individual ground motions of Table 6-3 to give the maximum responses for the case-study buildings. For all analyses, the Newmark constant average acceleration solution method was used with an integration time step of 0.005 to 0.02 sec. (i.e., time step of the ground motions). 2 and 3% elastic viscous damping ratios were included in the analysis of PreWECs and SRWs, respectively, using the tangent stiffness proportional Rayleigh damping in the model.

6.10.1. Lateral drift

The ratio of the resulting maximum lateral drift to the acceptable performance limits proposed by Rahman and Sritharan (2006) were computed for all case studies. This ratio, namely d_{max} , is plotted in Figures 6-7a and 6-7b for six and twelve story buildings during FF and NF

design-level ground motions, respectively. 2 and 3% maximum permissible transient drifts were selected for these self-centering wall systems during DBE and MCE records (Rahman and Sritharan 2006). As shown in these figures, the proposed design approach led to satisfactory performance of rocking systems in terms of the maximum drift with generally sufficient margin of safety with respect to the selected permissible limits. Similar results were observed for all other case studies.

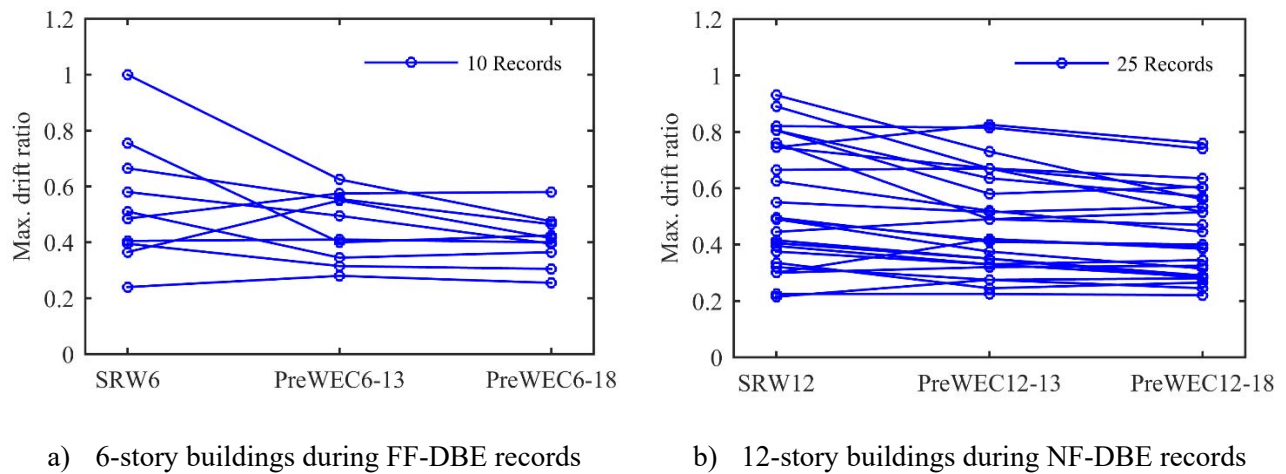
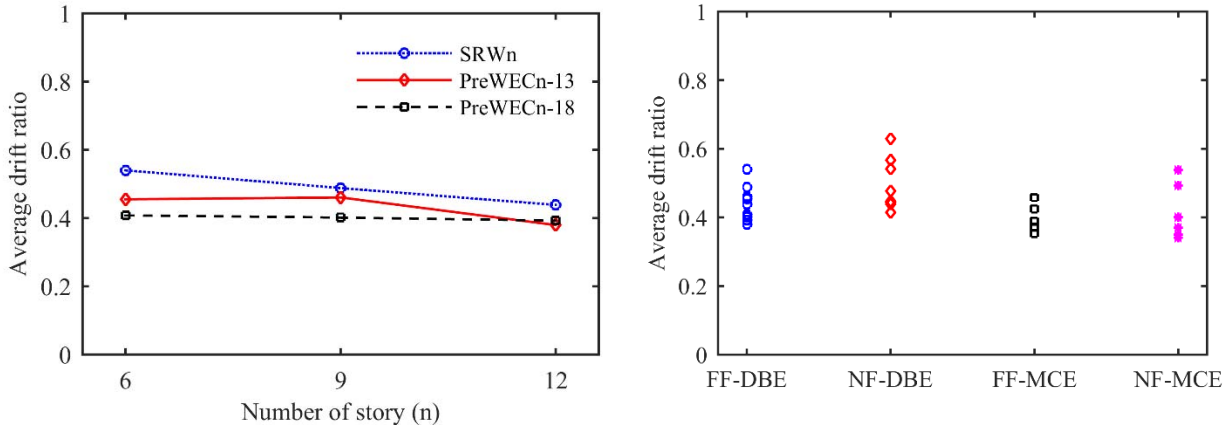


Figure 6-7. Ratio of the maximum drift to the allowable limit (d_{max})

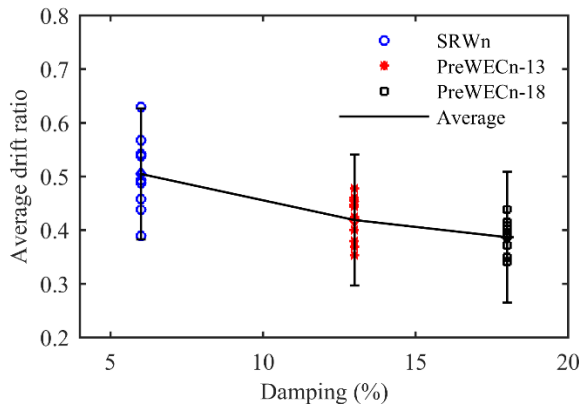
The average drift ratio (d_{ave}) of each building to different NF and FF ground motions of DBE and MCE was then estimated (e.g., d_{ave} of SRW6 during FF-DBE ground motions is average of the d_{max} of the building during ten FF records representing DBE events). Figure 6-8a shows correlations between d_{ave} of the buildings during FF-DBE records and height of the buildings. It was identified that the shorter buildings achieved relatively larger transient drifts compared to the taller buildings. Figure 6-8b presents variation in the d_{ave} of the buildings during different types of motions (i.e., NF and FF) representing DBE and MCE events. Accordingly, relatively greater drift responses were observed during NF records. As shown in Figure 6-8a and Figure 6-8b,

susceptibility of d_{ave} to the height of the building as well as the applied ground motion is relatively small. Figure 6-8c illustrates variation of d_{ave} as a function of damping ratios of the buildings. Each data point in this figure is d_{ave} of the building with $n=6, 9, \text{ or } 12$, during ground motions with a specific type and intensity (i.e., FF and DBE).



a) d_{ave} vs. height of the building (FF-DBE)

b) d_{ave} vs. type and intensity of the motion



c) d_{ave} vs. damping. Error bars represent ± 2 standard errors of the mean, the 95% confidence interval

Figure 6-8. Average ratio of the maximum drift to the allowable limit

As presented in Figure 6-8c, maximum drift response of structures generally decreased with increasing the damping ratio from 6% for SRWs to 18% for PreWEC systems. As shown in

this figure, a response ratio of less than 0.5 is observed in PreWECs even after these systems were designed with an increased R-factor ranging from 5 to 9 following the proposed approach. Figure 6-9, which compares the drift time history response of buildings designed with SRWs and PreWECs during two DBE records, indicates the effect of the additional hysteretic damping on faster decay of dynamic response.

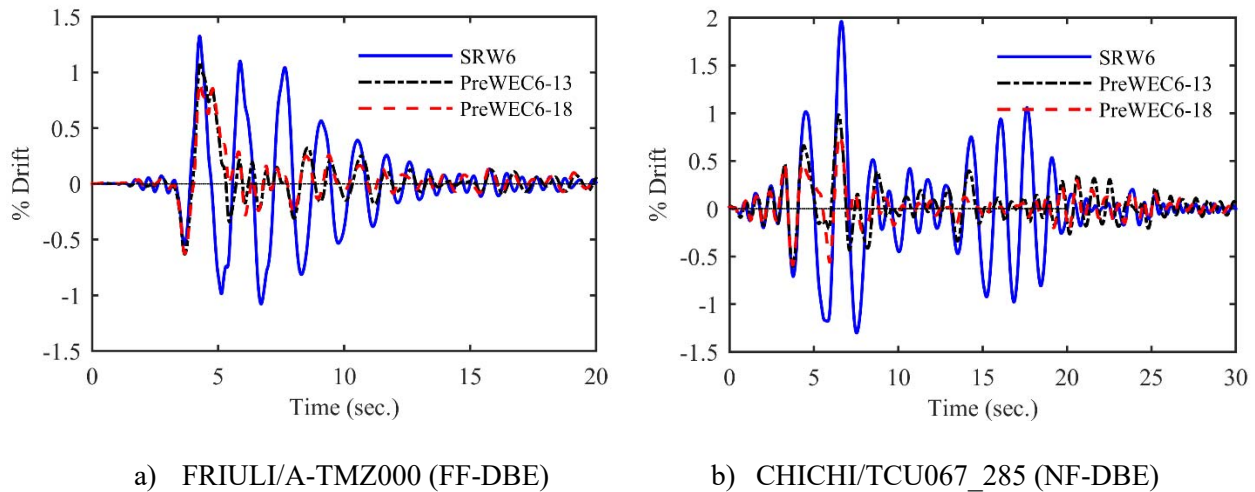


Figure 6-9. Impact of additional hysteretic damping on the drift time history response

6.10.2. Absolute acceleration and residual drift

The maximum absolute acceleration (a_{max}) and residual drift (d_r) ratios of the buildings are also shown in Figure 6-10 as a function of their damping ratios. According to Rahman and Sritharan (2006), the allowable limits for these responses are considered to be (1.2g, 0.5%) and (1.8g, 0.75%) for DBE and MCE events, respectively. These figures present the average of response ratios of the buildings during all ground motions, as previously presented for estimating d_{ave} in Figure 6-8 plots.

As shown in Figure 6-10a, all buildings generally tended to attain the maximum absolute acceleration below the acceptable limits. This figure also indicates that the average of a_{max} was relatively independent of the damping ratio of the system; however, it was generally greater as the building responded to the NF records. Figure 6-10b confirms the re-centering capability of the rocking structures with indicating negligible residual drifts of the buildings after DBE and MCE events.

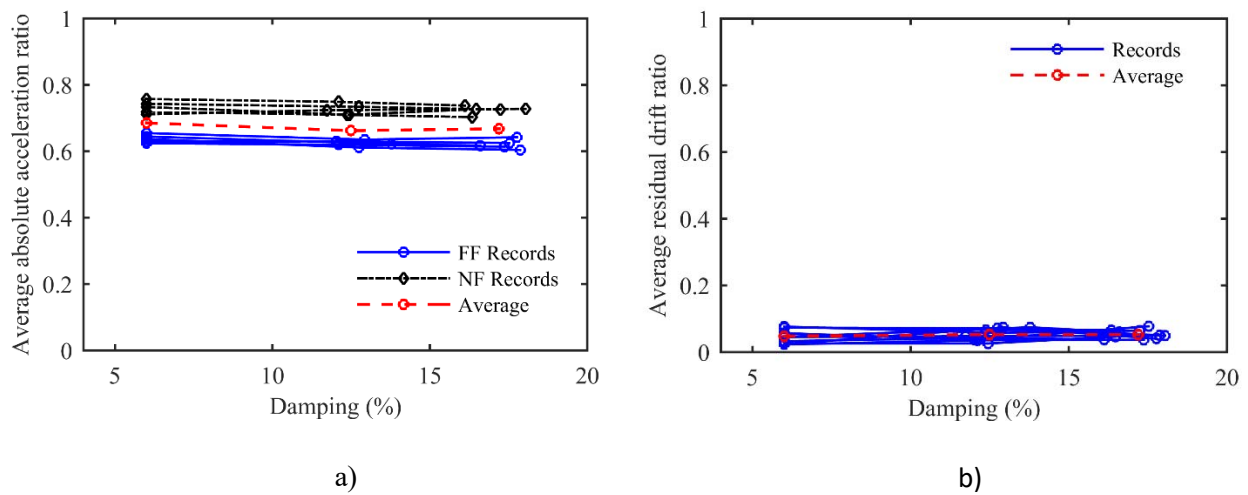


Figure 6-10. Average ratio of the maximum absolute acceleration (a) and residual drift (b) to the allowable limits

6.11. Cost-effective Design of Rocking Wall Systems

A cost index has been defined to highlight the cost estimates of the buildings in this case study. This cost index reflects the price of post-tensioning for the wall panels and end columns as well as the O-connectors and presented by Equation 6-3. Geometry of the precast concrete panels (i.e., wall and end columns) remained slightly unchanged between SRWs and PreWECs, thereby the concrete cost estimate is ignored in this equation.

$$P_{cost} = N_{wall} \times [(\alpha + \beta) \times (PT_{L,W} + PT_{L,col}) + \gamma N_{conn.} + P_{embeds} + P_{crane}]$$

(Equation 6-3)

where, P_{cost} = cost index, N_{wall} = number of wall systems per building, α and β = cost of material and labor for post-tensioning, i.e., \$0.59 and \$0.2 per foot for 15.2 mm (0.6 in.) diameter tendons, respectively, $PT_{L,W}$ and $PT_{L,col}$ = Length of PT tendons in the wall panel and end columns, γ = cost of material for O-connectors, i.e., \$20 per connector, $N_{conn.}$ = Number of connectors per wall, P_{embeds} = installation cost for member bracing and embeds, P_{crane} = crane charges, using a Manitowoc 16000 crane with a unit price of \$4,600 per day (e.g., six PreWECs and SRWs in a six-story building are picked in six and two days, respectively).

Figure 6-11 plots present variation of the normalized P_{cost} for all buildings during different types and intensity levels of ground motions. The minimum value of one in these figures is related to the most economical design option for each building, where the most expensive one is shown by a maximum value of two. As presented in these plots, PreWECs with additional hysteretic damping were generally the most economical design options; however, assemblage of the wall panel and end columns as well as the O-connectors in these systems led to higher installation costs compared to SRWs. For this comparative cost study, SRW12 and PreWEC12-13 were designed with seven walls to be used during MCE records (see Figure 6-11b and Figure 6-11d).

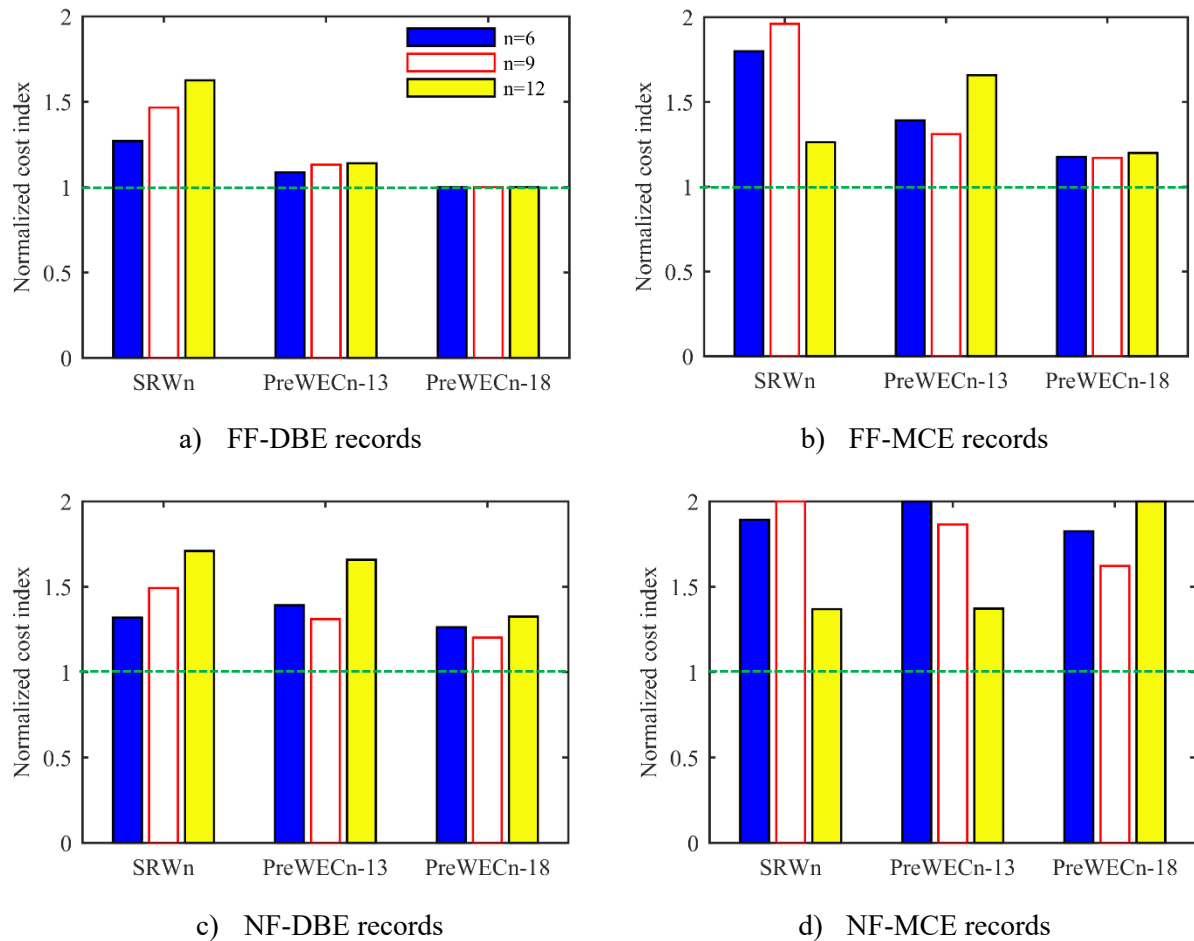


Figure 6-11. Normalized cost index for different case studies

6.12. Conclusions

An analytical parametric study was conducted in this paper to verify a set of new strength reduction (or R) factors suggested for designing the precast concrete rocking walls with and without additional hysteretic damping through a series of shake table tests. Using an experimentally validated OpenSees model, six, nine, and twelve story buildings with identical plan view were subjected to a set of scaled near-field and far-field ground motions representing the design-level and maximum considered events. They were designed to resist lateral forces in the

transverse direction of the building using rocking wall systems with different R-factors corresponding to their damping ratios varying from 6% (i.e., for a SRW) to 18% (i.e., for a PreWEC). Using the dynamic analysis results and criteria established for performance-based seismic evaluation of rocking walls, the following conclusions were drawn:

- 1- The seismic performance of the rocking structures designed with the new set of R-factors satisfied the performance limits of the maximum lateral drift, residual drifts and maximum floor acceleration for design-level and higher intensity near-field and far-field earthquake motions.
- 2- It was shown that PreWECs with larger additional hysteretic damping generally experienced lower maximum drifts with sufficient margin of safety with respect to the permissible limits. SRWs with the least amount of energy dissipation capacity responded satisfactorily as designed with the corresponding suggested R-factor.
- 3- Drift ratios (i.e., the maximum drift divided by the permissible value) generally decreased with increasing hysteretic damping ratios of the rocking buildings of different height for all levels of applied ground motions. The additional hysteretic damping also attempted for quicker decay of the building response.
- 4- The absolute acceleration ratios were mostly unchanged for all buildings while slightly increased as they were subjected to the near-field motions.
- 5- All buildings were self-centered with negligible residual drift ratios of lower than 0.1, after DBE and MCE ground motions.
- 6- Comparing the cost estimates of different buildings in this case study, it was concluded that PreWECs are generally the most economical rocking systems to be used in the design of low to mid-rise buildings.

6.13. Acknowledgments

The study reported in this paper was based upon the NEES Rocking Wall project supported by the National Science Foundation under Grant No. CMMI-1041650 and Dr. Joy Pauschke served as the program director for this grant. Any opinions, findings, and conclusions or recommendations expressed in this material are those of the authors and do not necessarily reflect the views of the National Science Foundation. All shake table tests were conducted using the NEES shared facility at the University of Nevada, Reno (UNR). The test units were donated by Clark Pacific and MidState Precast through coordination by PCI West. Materials provided by Sumiden Wire, GTI, Hayes Industries and help provided by ironworker local 118 with post-tensioning of specimens are also gratefully acknowledged.

6.14. References

- Aaleti, S. (2009) Behavior of rectangular concrete walls subjected to simulated seismic loading, PhD Thesis. Dept. of Civil, Construction and Environmental Engineering, Iowa State University, Ames, Iowa.
- Aaleti, S., and Sritharan, S. (2009) A simplified analysis method for characterizing unbonded post-tensioned precast wall systems. *Engineering Structures*, **31**(12), 2966–2975.
- ACI 318-11. (2011) Building code requirements for structural concrete. *ACI 318-11*, Farmington Hills, MI.
- ACI Innovation Task Group 5.1. (2008) Acceptance criteria for special unbonded post-tensioned precast structural walls based on validation testing and commentary. American Concrete Institute, Farmington Hills, MI.
- ACI Innovation Task Group 5.2. (2009) Requirements for design of a special unbonded post-tensioned precast shear wall satisfying ACI ITG-5.1 and commentary (ACI ITG-5.2). American Concrete Institute, Farmington Hills, MI.

- ASCE 7-05. (2005) Minimum design loads for buildings and other structures, ASCE/SEI 7-05.
- FEMA P695. (2009) Quantification of building seismic performance factors. Rep. FEMA P695, Federal Emergency Management Agency, Washington, D.C.
- IBC I. (2009) International Code Council. International Building Code.
- Kurama, Y., Sause, R., Pessiki, S., and Lu, L. (1999) Lateral load behavior and seismic design of unbonded post-tensioned precast concrete walls. *ACI Structural Journal*, **96**(4), 622–632.
- Kurama, Y. (2002) Hybrid post-tensioned precast concrete walls for use in seismic regions. *PCI Journal*, **47**(5), 36–59.
- McKenna, F., Fenves, G., and Scott, M. (2000) Open system for earthquake engineering simulation. University of California, Berkeley, CA.
- Nazari, M., Aaleti, S., and Sritharan, S. (2015) Shake Table Testing of Single Rocking Walls and PreWECs @ UNR. *Network for Earthquake Engineering Simulation (distributor)*. doi: 10.4231/D3N29P75Z (SRW1), 10.4231/D3H98ZF0B (SRW2), 10.4231/D3CJ87M6Z (SRW3), 10.4231/D37S7HT2T(SRW4), 10.4231/D3WM13V3P (PreWEC-s1), and 10.4231/D3RV0D20F (PreWEC-s2).
- Nazari, M., Sritharan, S., and Aaleti, S. (2014) Shake table testing of unbonded post-tensioned precast concrete walls. *Proceedings of the 10th National Conference in Earthquake Engineering*, Earthquake Engineering Research Institute, Anchorage, AK.
- Nazari, M., Sritharan, S., and Aaleti, S. (under review) Single Precast Concrete Rocking Walls as Earthquake Force-resisting Elements. *Earthquake Engineering and Structural Dynamics*.
- Nazari, M., and Sritharan, S. (to be submitted) Dynamic evaluation of PreWEC systems with varying hysteretic energy dissipation. *Journal of Structural Engineering*.
- Priestley, M. J. N., Sritharan, S., Conley, JR., and Pampanin, S. (1999) Preliminary results and conclusions from the PRESSS five-story precast concrete test building. *PCI Journal*, **44**(6), 42–67.
- Priestley, M. J. N. (2000) Performance Based Seismic Design. 12th World Conference on Earthquake Engineering, Auckland, New Zealand.
- Rahman, M., and Sritharan, S. (2006) An evaluation of force-based design vs. direct displacement-

based design of jointed precast post-tensioned wall systems. *Earthquake Engineering and Engineering Vibration*, **5**(2), 285–296.

Rahman, A. M. and Restrepo, J. I. (2000) Earthquake resistant precast concrete buildings: seismic performance of cantilever walls prestressed using unbonded tendons. Research Report 2000-5, University of Canterbury, Christchurch.

Sritharan, S., Aaleti, S., Henry, R., Liu, K., and Tsai, K. (2015) Precast concrete wall with end columns (PreWEC) for earthquake resistant design. *Earthquake Engineering and Structural Dynamics*, **44**(12), 2075–2092.

Seismology Committee. (1999) Recommended lateral force requirements and commentary (Blue book). Structural Engineers Association of California (SEAOC), California, USA.

Twigden, K. M. and Henry, R.S. (2015) Experimental response and design of O-connectors for rocking wall systems. *Journal of Structures*, **44**(3), 261-271.

CHAPTER 7

CONCLUSIONS AND RECOMMENDATIONS

7.1. Introduction

Seismic resilient buildings have been the focus of many recent research studies. In precast structures, alternative technologies have been consequently developed using unbonded Post-Tensioning (PT) to ensure life safety, as well as functionality of the structure, with minimal damage and residual drifts following a major earthquake. The unbonded post-tensioned Single Rocking Walls (SRWs) are the simplest form of these lateral resisting systems. With all the research efforts mainly contributing to investigation of the global behavior of the SRWs (e.g., Kurama et al. 1999), the ability of these walls to dissipate the energy imparted to the structure during a large earthquake had not been fully confirmed through dynamic testing. Due to a lack of understanding and uncertainty about their seismic performance, several self-centering wall systems with supplementary energy dissipating elements were developed, including Precast Walls with End Columns (PreWECs).

The primary aim of this study was to develop a deeper understanding of the seismic performance of the unbonded post-tensioned walls both with and without external energy dissipaters (i.e., PreWECs and SRWs) during earthquakes of varying intensities. One of the knowledge gaps in the field that this research targeted involved verifying the energy dissipation capacity of these walls and explaining how the damping affects the walls' seismic responses. Consequently, this work demanded the recommendation of a promising design procedure to secure acceptable seismic responses of SRWs and PreWECs below the allowable limits, as defined for

the design-level, and maximum considered earthquake events. This study also set out to determine whether unbonded post-tensioned precast concrete rocking walls without (i.e, SRWs) or those with additional energy dissipaters (e.g., PreWECs) are the most economical options to be used for designing damage-controlled buildings of different heights.

This chapter provides an overview of the work presented in the preceding chapters, and is followed by conclusions derived from multiple studies. Lastly, recommendations for future research will be described.

7.2. Summary of Results and Conclusions

Chapter 2 is a comprehensive literature review surveying all previous studies on topics related to the research presented herein, including experimental and numerical investigations of SRWs and other alternative precast post-tensioned walls with additional hysteretic dampers. This chapter starts with a brief description of the development of precast walls since their first application in the early 1990's (Kurama et al. 1999). As SRWs were conceived to have negligible damping, mainly provided through impacts of the rocking wall on top of the foundation, these walls were not tested for any seismic loading earlier than 2008 (Marriot et al. 2008). Meanwhile, SRWs were equipped with external dampers designed to yield in shear or flexure to provide additional hysteretic damping for the wall system. The work done by many researchers, along with their observations and comments regarding the application of rocking walls both with and without external dampers in seismic regions, is presented in this chapter. A few quasi-static tests performed on SRWs (e.g., Perez et al. 2004) indicated their negligible hysteretic energy dissipation due to spalling of cover concrete at wall toes during rocking of the wall on top of the foundation; this was reported to have occurred in addition to the damping due to impacts. Although different energy

dissipation components of SRWs have not been thoroughly quantified yet, some shake table studies were performed on SRWs (e.g., Marriot et al. 2008; Twigden 2016) with the purpose of evaluating their seismic performance. Among different alternatives to increasing the hysteretic energy dissipating capacity of SRWs, PreWECs were introduced (Sritharan et al. 2015). Through a large-scale quasi-static testing on PreWECs, it was shown that the damage could be kept localized in some easily-replaceable damage-absorbent connectors added to this wall system. In addition, superior performance of PreWECs compared to an identical cast-in-place concrete shear wall was studied (Sritharan et al. 2015).

Besides experimental studies, Chapter 2 also reviewed several analytical studies that predicted the dynamic response of precast walls with unbonded post-tensioning in an effort to better understand the applied damping components valid for these walls. Finally, the current design standards available worldwide, which provide recommendations for the seismic design of unbonded post-tensioned precast concrete rocking walls, were presented. A number of applications of these systems in the real-world (e.g., Paramount building in the U.S. 2002; Southern Cross Hospital in New Zealand 2011) indicates the continued need for more comprehensive research on seismic performance assessment of precast post-tensioned wall systems, their energy dissipation capacity, and specific seismic design procedures. To achieve these goals, three phases of shake table tests were performed in this study on a total of eight SRWs and PreWECs.

In Chapter 3, the results from a series of shake table tests on four SRWs subjected to a series of earthquake excitations with varying intensities were presented. The walls were designed with different shear resistance where the lowest amount was chosen to closely match the capacity of a reference wall from a six-story prototype building at 5/18 scale, designed following the current approach. This prospective study was designed to first investigate the global and local seismic

response of single unbonded post-tensioned walls with different design parameters, such as the area of PT tendons, initial prestressing, and the moment to base shear ratio. The experimental test data was then used to validate a Simplified Analysis (SA) method (Aaleti and Sritharan 2009) for the design of unbonded post-tensioned walls as well as a simplified analytical model developed in OpenSees (McKenna et al. 2000) for predicting their dynamic response.

The seismic performance of these test walls was then compared with multiple-level acceptance criteria to ensure whether the basic seismic objectives were satisfied as they were subjected to ground motions of varying intensities. To determine the optimal design shear for these SRWs, their energy dissipation capacity was estimated using the experimental data. For this purpose, an equivalent viscous energy dissipation ratio representing all damping components of SRWs, including damping due to impacts and hysteretic damping resulting from the nonlinearity of concrete at wall toes, was estimated and applied in the Direct Displacement-Based Design approach (DDBD) (Priestley 2000). Accordingly, an appropriate strength Reduction (or R) factor was proposed for SRWs for the first time to ensure their satisfactory seismic performance if they are selected to be used in regions with high seismic risk.

Following the same approach presented in Chapter 3, the feasibility of applying four PreWEC systems with different shear resistance and additional hysteretic energy dissipating capacity during earthquakes of differing intensities was evaluated in Chapter 4. The analytical model of SRWs was updated and improved to take into consideration the additional damping and resistance provided by the O-connectors. Two equations were developed in order to improvise the seismic design procedure; the first was an experimentally verified equation created to estimate the total equivalent viscous damping ratio of PreWECs with different amounts of O-connectors and post-tensioning. The second equation created in this study suggested that the linear seismic design

force of PreWECs be decreased based on their damping capacities, in order to achieve the appropriate R-factor for these systems.

Chapter 5 combined the experimental results on seismic behavior of SRWs and PreWECs presented in the two preceding chapters. This chapter systematically examined the participation of different energy dissipation terms in dynamic decay of response for unbonded post-tensioned walls both with and without additional hysteretic dampers. It also investigated the influence of this additional damping on the peak of lateral drift response as well as its attempt to reduce the number of large peaks after the maximum drift. Finally, larger period of SRWs compared to the dominant period of the excitation was found to be the source of a reduced amount of seismic energy imparted to such systems as compared to similar PreWECs.

The experimentally verified analytical models of Chapters 3 and 4 were used to numerically assess the dynamic response of buildings of different heights designed with precast rocking walls following the recommendations provided in these chapters. The specific objective of this extensive, numerically based case-study was to validate the previously proposed equations for calculating the strength reduction (or R) factor as a function of damping of the wall system. For this purpose, six, nine, and twelve story buildings with identical plan views were subjected to a set of scaled Near-Field (NF) and Far-Field (FF) ground motions representing the design-level and maximum considered events. These buildings were designed to resist lateral forces in the transverse direction of the building using rocking systems with diverse R-factors corresponding to their damping ratios varying from 6% (i.e., for a SRW) to 18% (i.e., for a PreWEC). A preliminary cost analysis was also performed in this chapter to pave the way for the designers to choose the most economical rocking wall system for buildings of different heights to achieve both a seismic-resilient and cost-effective lateral load resisting system.

Based on the experimental and analytical investigation of multiple precast rocking wall systems conducted in this research, the following conclusions were derived:

1- Seismic performance and design recommendations for SRWs

Within the shake table studies conducted on SRWs, several conclusions were produced that highlighted damping capacity and relevant design forces of these walls for their implementation in regions of high seismicity. The main results covered in this chapter are presented as follows:

- All SRWs showed satisfactory performance with negligible damage limited to minor cracking and spalling of concrete in the compressive toe region up to the design-level earthquakes. The extent of damage was increased while SRWs were subjected to the maximum considered input motions; however, the amount of damage was minimized due to the use of steel channels at the base of the walls. These steel channels were placed at either corners of the wall over $0.2L$ length, where L is the wall length, or the entire length of the wall.
- Results from the Simplified Analysis (SA) method (Aaleti and Sritharan 2009) presented good estimates of the experimental characteristic responses of SRWs from shake table testing, including load-deformation behavior, variation of post-tensioning force, maximum concrete strain, and contact length. However, some overestimation of the PT force was obtained due to a lower prediction of the contact length.
- Shake table test results indicated self-centering behavior of SRWs with minimal residual drift of the walls following four levels of earthquakes. Test results also showed that walls generally tended to attain the maximum absolute acceleration below the acceptable limits. The ground

motions with larger content in high frequency cycles generally forced the rocking wall to accelerate with a higher rate compared to other motions with the same intensity.

- Based on the experimental observations, an average equivalent viscous damping ratio of 5.7% was established for SRWs. This damping includes 1.5% for the energy loss during impacts and 4.2% due to concrete nonlinearity as well as inherent material damping of the test units as they experience drifts between 1.4% and 2.6%. Participation of damping due to impacts on energy dissipation of SRWs was approximated to be about 30%.
- The extent to which damping capacity of SRWs plays a role in their lateral drift response is highlighted, as it was shown that SRWs with different shear resistance responded differently during design-level ground motions. Experimental results indicated that SRWs can survive such large earthquakes with permissible drift ratios when they were designed following the Direct Displacement-Based Approach (DDBD) (Priestley 2000) and applying the 6% equivalent viscous damping ratio.
- Due to the ability of SRWs to respond nonlinearly, their linear elastic design force was reduced by a factor of 3.5 to attain a design value corresponding to their damping capacity, following a DDBD approach. Therefore, an R-factor of 3.5 was recommended for use in the design of SRWs following the Force-Based Design (FBD) methodologies applied in the current seismic codes (IBC 2015; ASCE 7-15 2015).
- Nonlinear time history analysis of SRWs was performed using a simplified lumped plasticity model. Validation of the analytical results with the available experimental test data confirmed the accuracy of this model in predicting the displacement time history and lateral load responses of SRWs during the strong portion of the motions at all intensity levels. Damping during impacts has been captured by applying 3% tangent stiffness proportional elastic

damping in this model. This value was selected based on the amount of equivalent viscous damping estimated from the experimental results to represent the observed relevant energy loss due to impacts. Since this damping component was not directly modeled and just equalized with an equivalent viscous damping ratio, the calculated period of the rocking wall within the free vibration phase was not completely matching the experimental observations.

2- Seismic performance and design recommendations for PreWEC systems:

After realizing the successful seismic performance of SRWs designed with shear forces following their limited damping capacity, the impact of additional energy dissipaters in reducing design forces of precast rocking walls was investigated. Accordingly, four PreWECs were subjected to different earthquakes, and it has been conclusively shown that:

- All PreWECs showed satisfactory performance without experiencing visible damage from the design-level earthquakes. Significant damage to both cover and core concrete occurred while they were subjected to the maximum considered input motions; however, the amount of damage was minimized due to the use of steel channels at the base of the walls. The intended yielding of O-connectors also occurred at 0.6% wall drift. None of these elements fractured before the system experienced 5% drift.
- A new configuration of PreWECs was tested using the columns (or connectors) at either side of the wall panel. Although the elongated wall length led to higher moment capacity of the system, it was shown that the location of O-connectors with respect to the contact length is crucial to providing similar damping capacity compared to the original PreWEC systems, where connectors were positioned adjacent to the wall panel.

- The impact of different design parameters on global and local response of PreWECs, including lateral response, variation of the PT force, contact length, response of the connectors, and the equivalent viscous damping was presented along with the calculated responses from the SA method (Aaleti and Sritharan 2009). Some overestimation of the lateral resistance was obtained using this method, due to a lower prediction of the contact length.
- Although fracture of connectors and yielding of PT tendons occurred at higher drifts, re-centering capability of PreWEC systems was maintained after four levels of earthquakes. Test units generally showed acceptable absolute acceleration below the permissible limits.
- Based on the experimental observations, the average equivalent viscous damping ratios of 8.7 to 15.6% were estimated for the test units. This damping includes 1% for the energy loss during impacts and 4.2% due to concrete nonlinearity as well as inherent material damping of the test units. Using a suggested equation in this study, the additional hysteretic damping provided by the O-connectors can be estimated as a function of the number and force-displacement characteristics of connectors as well as resistance of the PreWEC system at the design drift.
- It was shown that PreWECs can be designed to respond satisfactorily when R-factors corresponding to their damping ratios are used.
- Using a centerline OpenSees model, displacement time history and lateral load responses of PreWECs were satisfactorily predicted at all intensity levels. A 2% tangent stiffness proportional elastic damping was used in this model to express the energy loss during impacts achieved from the experimental results. It was observed that the simple modelling technique used to account for the impact damping, resulted in more accurate drift time history response of PreWECs compared to the SRWs. This could be because of the lower participation of

damping due to impacts, as the additional hysteretic dampers have been incorporated into the wall system.

3- Energy dissipation components and comparison of dynamic response of SRWs and PreWECs:

The influence of different energy dissipation components on response reduction of precast concrete walls was studied and results are presented as follows:

- Radiation damping of a rocking body during earthquake excitation was approximately estimated using the measured velocities of the system immediately before and immediately after an impact reduced from the instantaneous seismic energy transmitted to the system.
- Participation of radiation damping in energy dissipation of SRWs was about 30%, while PreWECs dissipated a significant amount of the energy imparted to the system during a large earthquake through hysteretic action of the O-connectors.
- Yielding of connectors within the first few cycles of the motion resulted in lower peak drift response of PreWECs compared to SRWs. Right after the strong portion of the motion, SRWs gradually dissipated a large amount of seismic energy mainly through rocking of the wall on top of the foundation.
- It was shown that the additional connectors attempted to reduce the maximum peak of the drift response in PreWECs, as these systems experienced strong motions of earthquake levels EQ-III and EQ-IV. PreWEC-s1 with the lowest amount of added hysteretic damping exhibited greater responses when being subjected to earthquakes of all intensities.
- During DBE and MCE events, the additional hysteretic damping generally resulted in faster decay of the drift response toward the end of the free vibration phase. It was found that the

number of cycles with peaks greater than 40% of the allowable drift limits were reduced in PreWECs compared to the emulated SRW.

- It was concluded that while SRWs have limited hysteretic damping capacity, they absorbed lower amount of seismic energy as they rocked toward the end of the free vibration phase with an extended period compared to the dominant period of excitation. The growth in the rocking period, which occurred due to their larger displacement and velocity amplitude, was mainly responsible for favorable relative movement of the rocking wall and the foundation in which seismic energy was removed from the system. Negative rate of input energy was also reported to occur at the time of impacts of SRWs.

4- Numerically based case study to examine the recommendations for the design of seismic-resilient and cost-effective precast rocking walls in concrete buildings:

When precast walls, with and without additional dampers, were designed following the recommendations of previous chapters, they were expected to respond below the allowable limits during the design-level earthquakes. The proposed design forces were achieved following the experimental results observed for eight test walls. To verify accuracy of this seismic design approach, the experimentally verified analytical model was used to calculate lateral drift, absolute acceleration, and residual drift of walls designed with the forces relevant to their damping capacities; these walls were used as lateral resisting elements of concrete buildings of different heights. Several conclusions were made and presented as follows:

- The seismic performance of the rocking structures designed with the new set of R-factors satisfied the performance limits of the maximum lateral drift, residual drifts, and maximum

floor acceleration for design-level and higher intensity near-field and far-field earthquake motions.

- It was shown that PreWECs with larger additional hysteretic damping generally experienced lower maximum drifts with a sufficient margin of safety with respect to the permissible limits. SRWs with the least amount of energy dissipation capacity responded satisfactorily as designed with the corresponding suggested R-factor.
- Drift ratios (i.e., the maximum drift divided by the permissible value) generally decreased with increasing hysteretic damping ratios of the rocking buildings of different heights for all levels of applied ground motions. The additional hysteretic damping also attempted for quicker decay of the building response.
- The absolute acceleration ratios were mostly unchanged for all buildings, but slightly increased as they were subjected to the near-field motions.
- All buildings were self-centered with negligible residual drift ratios of values lower than 0.1, after DBE and MCE ground motions.
- Comparing the cost estimates of different buildings in this case study, it was concluded that PreWECs are generally the most economical rocking wall systems to be used in the design of low to mid-rise buildings.

7.3. Recommended Research

Within the outcomes presented in this dissertation, several additional areas were identified, which require further investigation. A few recommendations for future study include:

- Extensive and detailed analytical building models capable of representing the rocking interface and the associated damping component should be created. The simplified single degree of freedom model presented in this study was sufficiently accurate for design purposes, however, this could be improved for further detailed investigations into the rocking response.
- Impact of large axial load (i.e., post-tensioning force or gravity load) on the behavior of these rocking wall systems should be investigated through an extended experimental study.
- Recommendations for the appropriate geometry of these walls, including, thickness, and height-to-length ratio, should be prescribed to allow for the intended rocking mode and avoid unexpected failure modes (e.g., lateral buckling of the walls).
- The out-of-plane resistance of these rocking walls during bi-directional ground motions requires further detailed study.
- A detailed and comprehensive loss assessment analysis should be performed to measure damage at various hazard levels and compare it with those estimated for the conventional ductile cast-in-place walls. This should include an estimation of the damage to both the structural and non-structural elements of a building.

7.4. References

- Aaleti, S., and Sritharan, S. (2009) A simplified analysis method for characterizing unbonded post-tensioned precast wall systems. *Engineering Structures*, **31**(12), 2966–2975.
- ASCE 7-15. (2015) Minimum design loads for buildings and other structures, ASCE/SEI 7-15.
- IBC I. (2015) International Code Council. International Building Code.
- Kurama, Y., Sause, R., Pessiki, S., and Lu, L. (1999) Lateral load behavior and seismic design of unbonded post-tensioned precast concrete walls. *ACI Structural Journal*, **96**(4), 622–632.
- Marriott, D., Pampanin, S., Bull, D., and Palermo, A. (2008) Dynamic testing of precast, post-

- tensioned rocking wall systems with alternative dissipating solutions. *Bulletin of the New Zealand Society for Earthquake Engineering*, **41**(2), 90–103.
- McKenna, F., Fenves, G., and Scott, M. (2000) Open system for earthquake engineering simulation. University of California, Berkeley, CA.
- Perez, F., Pessiki, S., and Sause, R. (2004) Experimental and analytical lateral load response of unbonded post-tensioned precast concrete walls. ATLSS Report No. 04-11, Lehigh University, Bethlehem, PA.
- Priestley, M. J. N., Sritharan, S., Conley, JR., and Pampanin, S. (1999) Preliminary results and conclusions from the PRESSS five-story precast concrete test building. *PCI Journal*, **44**(6), 42–67.
- Priestley, M. J. N. (2000) Performance Based Seismic Design. 12th World Conference on Earthquake Engineering, Auckland, New Zealand.
- Rahman, A. M. and Restrepo, J. I. (2000) Earthquake resistant precast concrete buildings: seismic performance of cantilever walls prestressed using unbonded tendons. Research Report 2000-5, University of Canterbury, Christchurch.
- Sritharan, S., Aaleti, S., Henry, R., Liu, K., and Tsai, K. (2015) Precast concrete wall with end columns (PreWEC) for earthquake resistant design. *Earthquake Engineering and Structural Dynamics*, **44**(12), 2075–2092.
- Twigden, K. M. (2016) Dynamic response of unbonded post-tensioned concrete walls for seismic resilient structures, PhD Thesis. University of Auckland.